



A BEAM FINITE ELEMENT MODEL INCLUDING WARPING

Application to the dynamic and static analysis of bridge decks

Diego Lisi

Tesi di laurea in Ingegneria Civile

Relatore: Prof. Pier Giorgio Malerba

Anno accademico 2011/2012

RIASSUNTO

Questa tesi si propone come obiettivo lo studio degli effetti dinamici e statici in travi continue con sezioni a parete sottile attraverso lo sviluppo di un modello a elementi finiti.

Quando una sezione in parete sottile soggetta a torsione è aperta la sua deformabilità è considerevolmente maggiore di quella di sezioni compatte e chiuse, per effetto della maggiore deformazione sezionale dovuta a questo tipo di sollecitazione, che ne determina un maggiore ingobbimento.

L'analisi esatta di travi a parete sottile considerando il fenomeno di ingobbimento è di complessa implementazione numerica, a causa dell' elevata esigenza computazionale delle soluzioni matematiche.

Le teorie classiche di travi sono analizzate inizialmente di modo che possa essere ottenuta una formulazione di equazioni governative in termini di spostamenti generalizzati. Si sono utilizzati i principi variazionali per determinare un modello approssimato e per caratterizzare un elemento finito di trave per l'analisi di sezioni in parete sottile.

In ambito statico, travi continue con asse rettilineo sono analizzate, mentre in dinamica le vibrazioni flessorio-torsionali di questi elementi sono investigate sia in regime libero sia forzato da un carico mobile concentrato. I risultati di queste analisi sono comparati con le soluzioni teoriche ottenute per elementi di trave.

L'obiettivo di questo elaborato è di proporre un modello generalizzato di trave per profili in parete sottile, utile per il progetto di ponti ferroviari realizzati nelle reti ad alta velocità. Un caso di studio di ponte a varie campate è illustrato per valutare il comportamento dinamica di differenti sezioni.

PAROLE CHIAVE: sezioni a parete sottile, impalcato da ponte, metodo degli elementi finiti, ingobbimento, elemento di trave, analisi dinamica, carichi mobili.

ABSTRACT

The present dissertation deals with the study of the dynamic and static effects on continuous beams of thin-walled cross-sections through the formulation of a finite element.

When a thin-walled cross-section of a beam structure has open profile the deformability greatly exceeds that of a compact section, because of to the out-of-plane deformations of this type of shapes when acted by torsion, being this effect due to the warping of the cross-section.

The exact analysis of thin walled beams considering the warping phenomena is usually difficult in its implementation by numerical codes for their mathematical solutions that are too complicated for routine calculations.

The classic beam theories are analyzed to obtain the set of equations governing the problem. The variational principles are used in order to obtain an approximation model and purpose a finite beam element for the analysis of thin-walled beams.

In static, straight and generally supported structures are analyzed, while in dynamic the torsional and lateral free-vibration and forced vibration is investigated. The results of the analysis and the compliance with the classic beam theory are discussed.

The aim of the work is to propose a generalized thin-walled beam model for the railway high-velocity bridge analysis and design. A simple numerical example of multi-span bridge is illustrated in order to evaluate the performance of different types of cross-sections when dynamic effects are considered.

KEYWORDS: thin-walled beams, bridge deck, finite element method, warping, beam element, dynamic analysis, moving load.

ACKNOWLEDGEMENTS

I would like to express my gratitude for all who contributed in a way or another in the accomplishment of this work.

Most importantly, I would like to thank my supervisors Pr. Francisco Virtuoso and Pr. Ricardo Vieira. Their helpful comments, advices, suggestions and contributions regarding all the critical aspects of my thesis have been very profitable over the last year.

I would thank all the colleagues of the Civil Engineering (DECivil) department for being extremely helpful and for creating a comfortable working environment. Their friendship has provided a real support.

Many thanks for my family: they made it possible for me to come to Lisbon.

Ringrazio in modo particolare la disponibilità e gentilezza del Prof. Pier Giorgio Malerba del Dipartimento di Ingegneria Strutturale, relatore al Politecnico di Milano del seguente elaborato.

INDEX

RIASSUNTO.....	iii
ABSTRACT.....	v
ACKNOWLEDGEMENTS.....	vii
1. INTRODUCTION.....	17
1.1. General introduction	17
1.2. Objectives of the work	17
1.3. Layout of the work.....	18
1.4. Original contributions of the present work.....	19
2. LITERATURE REVIEW AND BACKGROUND INFORMATION.....	21
2.1. Historical evolution of thin walled beam theories	21
2.2. Methods of analysis for thin walled beam structures.....	22
2.3. Lateral-torsional forced vibrations of thin walled beam structures	23
3. THIN-WALLED BEAMS EQUATIONS	25
3.1. Cross-section analysis.....	25
3.1.1. Kinematics and strains	25
3.1.2. Potential energy formulation	32
3.1.3. Elastic center and shear center	35
3.1.3. The direct method for the warping properties evaluation	37
3.1.4. A generalized method for the section properties evaluation.....	39
3.1.5. Kinetic energy formulation	53
3.2. Static analysis	54
3.2.1. Equilibrium and stresses.....	55
3.2.3. Basic load cases	60
3.3. Dynamic analysis.....	69
3.3.1. Equations of motion	69
3.3.2. Analysis of torsional free vibrations on thin-walled beams.....	73
4. FINITE ELEMENT APROXIMATION	77
4.1. Beam displacements discretization	78
4.1.1. Continuity.....	78
4.1.2. Approximation functions	79
4.2. The static formulation of the finite element	81
4.2.1. The formulation of a weak form for uncoupled torsion	81

4.2.2. The thin-walled beam element considering an additional DOF of warping.....	85
4.2.3. Selected load cases	93
4.3. The dynamic formulation of the finite element.....	110
4.3.1. The formulation of a weak form for the uncoupled torsion	110
4.3.2. The element mass matrix considering an additional DOF of warping.....	112
4.3.3. The undamped free-vibration.....	119
4.3.4. Examples.....	122
5. ANALYSIS OF DYNAMIC RESPONSE TO MOVING LOADS	133
5.1. The procedure of mode superposition	133
5.1.1. Uncoupled equations of motion with damping.....	134
5.1.2. Modal response to loading.....	135
5.2. Numerical modeling of dynamical response.....	136
5.2.1. Element property matrices.....	136
5.2.2. Time-stepping Newmark's method	138
5.3. Numerical example.....	139
5.3.1. Actions on the bridge and structural properties	139
5.3.2. Undamped free-vibration analysis.....	141
5.3.3. Forced-vibrations analysis and mode-superposition procedure.....	143
6. CONCLUSIONS AND FINITE DEVELOPMENTS.....	155
6.1. General remarks	155
6.1. Conclusions.....	155
6.2. Future developments	156
7. References	159
ANNEX 1.....	161

INDEX OF FIGURES

Figure 3.1 - Principal displacements and system coordinates of the beam.....	26
Figure 3.2 - Rotation of a I-Section around a general point P.....	26
Figure 3.3- Axial displacements of an I-Beam due to axial effect and bending for planes (x,y) and (x,z).....	27
Figure 3.4 - Vanishing of the shear strain of mid-surface (left) and distribution along the wall thickness for open cross-sections (right).	27
Figure 3.5 - Rotation of open cross-section.....	28
Figure 3.6 – Geometric interpretation of the sectorial coordinate.....	29
Figure 3.7 – Geometric interpretation of $h(s)$ and $h_s(s)$	31
Figure 3.8 – Open cross-section with N elements.	37
Figure 3.9 – Global reference axis and local axis of the element.	40
Figure 3.10 - Example of two-celled cross-section.	42
Figure 3.11 – Sketch of the three-branches open section.....	45
Figure 3.12 - Warping function distribution.....	46
Figure 3.13 – Sketch of the double-T bridge deck section.....	47
Figure 3.14 – Warping function distribution.....	48
Figure 3.15 – Box section of a bridge deck [m].....	49
Figure 3.16 - Warping function distribution.....	50
Figure 3.17 – Two-cells section of a bridge deck [m].	51
Figure 3.18 - Warping function distribution.....	53
Figure 3.19 – Generalized displacements of a C cross-section beam.....	59
Figure 3.20 – Forces in a C cross-section beam.....	59
Figure 3.21 – S-S beam ($L=2m$) acted upon uniform torque.....	62
Figure 3.22 - φ value of a S-S beam acted by uniform torque (analytical solution).....	63
Figure 3.23 – φ' value of a S-S beam acted by uniform torque (analytical solution).....	63
Figure 3.24 - $M\omega$ of a S-S beam acted by uniform torque (analytical solution).....	63
Figure 3.25 – Distribution of the torsion TS and T of a S-S beam acted by uniform torque (analytical solution).....	64
Figure 3.26 – S-S beam ($L=2m$) acted upon concentrated torque at midspan.....	64
Figure 3.27 – φ value of a S-S beam acted by concentrated torque (analytical solution).	65
Figure 3.28 – φ' value of a S-S beam acted by concentrated torque (analytical solution).	65
Figure 3.29 – $M\omega$ of a S-S beam acted by concentrated torque (analytical solution).	65
Figure 3.30 - Distribution of the torsion TS and T of a S-S beam acted by concentrated torque (anal. solution).	65
Figure 3.31 – Three continuous span beam acted by uniform torque at midspan.....	66
Figure 3.32 – φ value of a continuous three spans beam acted by uniform torque (analytical solution).....	67
Figure 3.33 – φ' value of a continuous three spans beam acted by uniform torque (analytical solution).	67
Figure 3.34– $M\omega$ of a continuous three spans beam acted by uniform torque (analytical solution).....	67
Figure 3.35 - Distribution of the torsion TS and T of a continuous three spans beam acted by uniform torque (analytical solution).....	68

Figure 3.36 – Distribution of the torsion $T\omega$ and T of a continuous three spans beam acted by uniform torque (analytical solution).	68
Figure 3.37 – Coupling between torsion and bending displacements for a C-beam.....	73
Figure 3.38 – Simply supported beam analyzed by (Gere, 1954).	74
Figure 3.39 – Values of the ratio r for the first 8 torsional vibration modes.....	75
Figure 4.1 – Degrees of freedom and shape functions of the two node elements.....	79
Figure 4.2 - Two-node Euler-Bernoulli element.	80
Figure 4.3 –Thin walled beam element subject to uncoupled torsion.	84
Figure 4.4 – Effects of the application of a general axial force on a thin walled beam (Cedolin, 1996).....	87
Figure 4.5 – Thin-walled C-beam element displacement referred to two axis.	91
Figure 4.6 –Thin-walled C-beam element displacements described by the elastic center axis.....	93
Figure 4.7 – Non-dimensional coordinate system.....	94
Figure 4.8 – φ value of a S-S beam acted by uniform torque (FEM solution).	95
Figure 4.9 – φ' value of a S-S beam acted by uniform torque (FEM solution).	95
Figure 4.10 - $M\omega$ of a S-S beam acted by uniform torque (FEM solution).	95
Figure 4.11 – Torsion T of a S-S beam acted by uniform torque (FEM solution).	95
Figure 4.12 – φ value of a S-S beam acted by concentrated torque (FEM solution).	96
Figure 4.13 – φ' value of a S-S beam acted by concentrated torque (FEM solution).	96
Figure 4.14- $M\omega$ of a S-S beam acted by concentrated torque (FEM solution).	96
Figure 4.15 - Torsion T of a S-S beam acted by concentrated torque (FEM solution).	97
Figure 4.16 – Coordinate system of the three continuous spans beam.	97
Figure 4.17 - φ value of a T-C-S beam acted by uniform torque (FEM solution).....	98
Figure 4.18 - φ' value of a T-C-S beam acted by uniform torque (FEM solution).	98
Figure 4.19 - $M\omega$ of a T-C-S beam acted by uniform torque (FEM solution).....	98
Figure 4.20 – Torsion T of a T-C-S beam acted by uniform torque (FEM solution).	99
Figure 4.21 – Convergence of the $M\omega$ value as function of the mesh refinement.	100
Figure 4.22 – ABAQUS element B310S and integration points for I-beam section.	100
Figure 4.23 - Longitudinal model of a bridge numerical example.	102
Figure 4.24 – Box-section of the bridge deck.	102
Figure 4.25 – Double-T section of the bridge deck.	102
Figure 4.26 – Lane model for general types of vertical loads.....	103
Figure 4.27 – Loading in the cross-section plane.	105
Figure 4.28 –Loading in the longitudinal direction.	105
Figure 4.29 – Coupling effect between torsion and transversal displacement.	105
Figure 4.30 – Displacements and rotation of the bridge model with double-T section (FEM model).....	106
Figure 4.31 – Shear force V_z and bending moment M_z along the elastic center axis.	107
Figure 4.32 – Torsion moment M_t and warping moment $M\omega$ along the elastic center axis.....	107
Figure 4.33 - Twist values along the beam axis for the double-T section and for the Box section.	108
Figure 4.34 – Saint Venant torsion contribution for the double-T section and for the Box section.	108
Figure 4.35 – Warping torsion influence in torsion response for different κ -values (FEM solution).	109

Figure 4.36 –Thin-walled C-beam element and uncoupled kinematic field.....	116
Figure 4.37 - Thin-walled C-beam element and coupled kinematic field.....	119
Figure 4.38 - Ratio r for 8 vibration modes in a S-S beam. Solution obtained by the presented model.....	124
Figure 4.39 - Ratio r for 8 vibration modes in a C-S beam. Solution obtained by the presented model.....	124
Figure 4.40 - Ratio r for 8 vibration modes in a C-C beam. Solution obtained by the presented model.....	124
Figure 4.41 - Influence of boundary conditions on the 1 st mode frequency.....	125
Figure 4.42 - Influence of boundary conditions on the 2 nd mode frequency.....	126
Figure 4.43- Influence of boundary conditions on the 3 rd mode frequency.....	126
Figure 4.44 - Influence of boundary conditions on the 4 th mode frequency.....	126
Figure 5.1 – Example of supported beam element acted by a constant and eccentric moving load.....	135
Figure 5.2 – Experimental values of the damping coefficient for different bridge spans. (Cunha, 2007).....	137
Figure 5.3 – Applied loads on a supported beam along x -direction.....	137
Figure 5.4 – Linear interpolation for the time intensity at time t	138
Figure 5.5 – Bridge layout of the cross-section and sketch of the actions considered.....	140
Figure 5.6 – Damping coefficients variation for the double-T bridge section.....	144
Figure 5.7 – Damping coefficients variation for the box girder bridge section.....	144
Figure 5.8 – Layout of the simply supported beam and moving load.....	145
Figure 5.9 – Mid-span dimensionless displacement comparison ($\alpha = 0.5$).....	146
Figure 5.10 – Mid-span dimensionless displacement comparison ($\alpha = 1$).....	146
Figure 5.11 – Mid-span dimensionless displacement comparison ($\alpha = 2$).....	146
Figure 5.12 - Mid-span dimensionless displacement comparison ($\alpha = 0.5, \beta = 0.1$).....	147
Figure 5.13 - Mid-span dimensionless displacement comparison ($\alpha = 1, \beta = 0.1$).....	147
Figure 5.14 - Mid-span dimensionless displacement comparison ($\alpha = 2, \beta = 0.1$).....	147
Figure 5.15 – Longitudinal beam-like model (a) and layout of the cross-section analyzed (b).....	148
Figure 5.16 – Dynamic influence lines of the displacement u_z at the section AA' (double-T section).....	149
Figure 5.17 - Dynamic influence lines of the twist φ at the section AA' (double-T section).....	149
Figure 5.18 - Dynamic influence lines of the displacement u_y at the section AA' (double-T section).....	150
Figure 5.19 - Dynamic influence lines of the displacement u_z at the section AA'(box girder section).....	150
Figure 5.20 - Dynamic influence lines of the twist φ at the section AA' (box girder section).....	151
Figure 5.21 - Dynamic influence lines of the displacement u_y at the section AA' (box girder section).....	151
Figure 5.22 – Displacement u_z for the two bridge sections analyzed (load speed: 420 km/h).....	151
Figure 5.23 – Horizontal displacements of the bridge cross-section(load speed: 420 km/h).....	152
Figure 5.24 - Twist of the bridge sections (load speed: 420 km/h).....	152
Figure 5.25 – Maximum vertical deflection of the section AA' for various speed values.....	153
Figure 5.26 – Maximum twist rotation of the section AA' for various speed values.....	153
Figure 5.27 – Displacement of the point P of the double-T section.....	154
Figure 5.28 – Dynamic influence line of the displacement u_zP	154
Figure A.0.1 – Cross-section layouts.....	161
Figure A.0.2 – Sectorial coordinate for the open and closed cross-sections.....	162
Figure A.0.3 – Cartesian coordinates referred to the elastic center.....	163

INDEX OF TABLES

Table 2.1 – Analogy between the theories of Vlasov and Bernoulli	21
Table 3.1 - Cross-Section parameters.	33
Table 3.2 – Beam loads per unit length.....	34
Table 3.3 - Section data input of the code assembled.....	45
Table 3.4 – Section data output of the code assembled.....	46
Table 3.5 - Section data input of the code assembled.....	47
Table 3.6 – Section data output of the code assembled.....	48
Table 3.7 - Section data input of the code assembled.....	49
Table 3.8 – Section data output of the code assembled.....	50
Table 3.9 - Section data input of the code assembled.....	51
Table 3.10 – Section data output of the code assembled.....	52
Table 3.11 – Equilibrium equations and boundary conditions.....	58
Table 3.12 - Cross-section layouts and position of the elastic and shear center.....	61
Table 3.13 – Boundary conditions for the three continuous spans beam.....	66
Table 3.14 – Dimensionless warping moment at supports.....	68
Table 3.15 – Characteristics of the beam element analyzed by (Gere, 1954).....	74
Table 4.1 – Smoothness of functions (Fish & Belytschko, 2007).....	78
Table 4.2 – Displacement field and approximation functions.....	85
Table 4.3 – Beam element displacements and corresponding axis of reference.....	90
Table 4.4 – Cross-section layout characteristics.....	94
Table 4.5 – Boundary conditions of the beam.....	94
Table 4.6 – FEM discretization for the continuous three spans beam.....	97
Table 4.7 – Boundary conditions of the three continuous spans beam.....	97
Table 4.8 – Decrease of the relative error of $M\omega/mL^2$ for different finite element meshes.....	99
Table 4.9 – Characteristics of the beam Elements loaded.....	101
Table 4.10 – Comparison of results between current model and ABAQUS element.....	101
Table 4.11 – Flexural characteristics of the bridge deck cross-sections.....	103
Table 4.12 – Section properties of the bridge cross-sections.....	104
Table 4.13 – Cross-section properties and torsion parameters.....	104
Table 4.14 – Boundary displacement fixed at nodes.....	106
Table 4.15 – Boundary conditions of the bar (S-S,C-S,C-C).....	123
Table 4.16 – Characteristics of the steel beam cross-section layout and bar length.....	127
Table 4.17 – Torsional vibration modes for a simply supported I-beam.....	128
Table 4.18 - Characteristics of the cross-section layout and span lengths.....	129
Table 4.19 - Torsional vibration modes for a three continuous spans I-beam.....	129
Table 4.20 – Characteristics of the cross-sections and structural systems compared.....	130
Table 4.21 – Mode vibration frequencies for the S-S beam and relative errors compared with ABAQUS.....	130
Table 4.22 – Mode vibration frequencies for the T-C-S beam and relative errors compared with ABABUS.....	130

Table 5.1 – General actions of the railway bridge	140
Table 5.2 – Undamped vibration modes and respective modal frequencies for the double-T bridge section.	141
Table 5.3 – Vibration modes for the double-T bridge section (frequencies in [Hz]).....	142
Table 5.4 – Undamped vibration modes and respective modal frequencies for the box bridge section.....	143
Table 5.5 – Rayleigh coefficients for the bridge cross-sections considered.....	144
Table 5.6 – Properties of the simply supported beam-like bridge discretization.....	145
Table 5.7 – Set of train velocities considered	148
Table 5.8 – Parameters considered for the numerical simulation of the current analysis.	149
Table 5.9 – Maximum displacement values for some characteristic velocities.....	153
Table 5.10 – Maximum twist values for some characteristic velocities.	153

1. INTRODUCTION

1.1. General introduction

Throughout history, thin walled structures become common construction elements. The reason for their extensive use is probably due to the trend of reducing the structural weight and to minimize building materials. This very natural optimization strategy constituted an important design principle for the realization of any type of structure.

For the large use of thin walled sections their behavior have been widely studied from many authors and the simplest way to consider these elements, when involved in frame structures analysis, is the adoption of longitudinal beam elements. This is possible whenever the response of slender elements is investigated, such as the analysis of steel structures, buildings, bridges or other complex structures.

The thin walled cross-sections appear in different forms, from simple hot rolled steel beams to the complex hull of a ship or the bridge deck shape. In all these cases the knowledge of flexural, axial and torsional response is essential for the analysis of the internal forces and the stress field acting on the sections.

The present analysis considers railway bridges with a cross-section that can be considered thin-walled. For these structures, the torsion has a very important role to investigate their structural response. It is well known that the torsional response of a thin-walled open section is very different from that of a compact or closed shaft. When the section of a bridge has an open profile the out-of-plane longitudinal deformations greatly exceed those of a closed section, either in a multicellular or in a monocellular type. This happens because of the physical behavior of this kind of shapes in their response to torsion solicitations: for this reason, in the field of bridges and advanced constructions, torsion is an important aspect to be considered in the design and the *warping* of the open sections cannot be neglected.

Warping introduces longitudinal strains as the section twists and significantly affects the torsional stiffness. In the case of thin-walled beams with open cross-section, the constraint of the axial warping strains provides the primary source of torsional stiffness.

1.2. Objectives of the work

The dynamic study of railway bridges has been greatly enhanced during the recent years: the means of transport are faster and heavier, while the structure over which they move are more slender and generally constituted by *thin-walled* cross sections.

This study presents a generalized beam model based on the FEM¹ technology for the static and dynamic analysis of thin-walled beams. According to the Euler-Bernoulli theory, six degrees of freedom for each end of the finite element are considered. A 7th degree of freedom will be considered in the finite element developed in order to describe the warping displacements.

¹ Finite element method

The consideration of the cross section warping is based on the Vlasov beam theory for thin walled open sections and extended to the closed thin-walled section by introducing a modified warping parameter according to the Benscoter theory.

In statics, straight and generally supported structures are analyzed, while in dynamics the torsional and lateral free and forced vibration analysis is presented. In the last part of the work an example of moving force acting eccentrically is presented, in order to evaluate the performance of this type of elements in bridge design.

The focus of the work is the analysis of double-T bridge open sections and box girder sections. An uncoupled flexural motion in the vertical plane and a coupled lateral-torsional vibration are studied showing the effect of the sectional properties on the mode frequencies. When forced vibration are considered, this work obtains dynamic influence lines for the twist rotation, the horizontal and vertical displacement of the midspan point for different train velocities, load magnitudes and eccentricity. The purpose is the formulation of a simple tool that enables the basic analysis of multi-span bridges through adequate beam models that consider the thin-walled open or closed section effects.

1.3. Layout of the work

In chapter 1 a general introduction to the current work is presented. The motivations and developments needed are illustrated considering the contribution of the thin walled beam elements to the civil engineering applications.

The chapter 2 proposes a general review of the thin-walled beam theories with particular attention to the torsion problem considering the different cross-section behaviors. A general survey summarizes also the application in dynamic analysis of these studies and the results obtained with the theoretical approach.

The chapter 3 presents the theory of thin-walled beams in statics and dynamics. Starting from the description of the beam element kinematics, the governing differential equations for thin-walled cross-sections are deduced by using the energetic approach. Several load cases are presented in static analysis considering the exact results, while in dynamics a torsional vibration analysis is presented.

The chapter 4 deals with the assembling of a finite beam element for the extensional, lateral and torsional analysis. The element property matrices are formulated from the thin-walled beam governing equations. The static analysis for some load cases are presented and the convergence of the element discretization is discussed. In dynamic the free-torsional vibration modes are presented for practical problems.

In chapter 5 a practical load case is developed. The aim of the study is the analysis of the bridge deck response to moving forces acting eccentrically along a multi-span longitudinal layout. The results obtained with the approximated method are compared with those of the theoretical analysis.

1.4. Original contributions of the present work

Thin-walled structures have gained a growing importance due to their efficiency in strength and cost and for this reason several applications in the high-speed railway bridges design have been recently developed. Many studies of bridge dynamic behavior have been performed using a so-called *macro-approach*. In this technique, the bridge system is discretized into a number of beam-column or grid elements and the focus is on forces rather than on stresses. The elements can be straight or curved and an analysis example is given by (Okeil & S., 2004). The method of analysis presented in this work is the space frame approach, which falls under the macromodel category.

The aim of this work is to develop a model for the static and dynamic analysis of one-dimensional straight beam structures with thin-walled cross-sections, extended for general conditions of supports and generalized applied loads. This type of element is suitable for the computer simulation of the results by the classic principles of the FEM technology.

The Vlasov's beam theory is adopted for the formulation, through the variational principles of a finite beam element with open cross-section. The polynomial Hermite's interpolation is used to obtain approximated results in static and dynamic analysis, using only one element type for open or closed cross-section. The only difference is that for the closed sections a warping function according to Bencoter's theory is considered.

In statics, examples of commonly loaded beams are studied and the exact solutions are approximated by means of an h refinement type of the element mesh.

In dynamics, the problem of free vibration is approached by modal analysis criteria for generally supported beams and a forced vibration numerical example is developed by using the mode superposition method (Clough & Penzien, 1982). The equation of motion are then integrated by the Newmark's step-by step method. The maximum values of displacement and rotation are found for common bridge deck cross-sections as a function of the train velocity and a series of dynamic influence lines are derived.

This kind of analysis, especially in dynamics, is useful for modeling straight beam structures and the consideration of thin-walled beam elements theory for illustrating open-section's response is a research field still in development, where the civil engineering recent means of analysis, such as the computer simulation of results, could develop a powerful contribution.

2. LITERATURE REVIEW AND BACKGROUND INFORMATION

The aim of this chapter is to synthesize and discuss the accredited knowledge established from the literature, related to the main concepts of the present work. The theory of thin-walled beam elements is presented in 2.1 with all the developments made. Then a survey of the FEM approximations studied for solving the static and dynamic problem of beam structures is also presented in 2.2 and 2.3. The chapter concludes with section 2.4 by highlighting the original contribution of this work to the overviewed research fields.

2.1. Historical evolution of thin walled beam theories

The behavior of thin-walled elements has been extensively studied by the theories of elastic beams. For arbitrary profiles, loading cases and boundary conditions, an important non uniform torsional warping occurs, hence the Saint Venant torsional theory, which is strictly restricted to uniform torsion with free warping of the cross-section, is no longer sufficient. A thin walled member resists to non uniform warping by both normal and shear stresses. If these stresses are important, an extended theory for non-homogeneous torsion is needed.

The general theory of thin-walled open cross-sections was developed in its final form by (Vlasov, 1961) where the non-uniform warping deformation effect is considered through the definition of a *sectorial coordinate*, while the transverse shear strain is neglected.

Thus, the sectorial coordinate is obtained by neglecting the transverse shear deformations through the wall thickness. The exact stress distribution is found by using Saint-Venant theory, but the beam equilibrium is ensured by introducing Vlasov bimoment. This is admissible for open cross-section but the theory becomes more complex when closed thin-walled section are considered, because the shear stresses are statically indeterminate.

In table 2.1 is shown the analogy between Vlasov theory and Bernoulli beam theory.

Table 2.1 – Analogy between the theories of Vlasov and Bernoulli.

Vlasov theory of non-uniform torsion	Correspondent of the Bernoulli beam theory
Warping moment	Bending moment
Warping torsion	Shear
Twist angle	Transversal displacement in the flexural plan
Twist gradient along the beam axis	Gradient of the transversal displacement
Warping function	Displacement distribution over the cross-section area

(Benscoter, 1954) introduced a new sectorial coordinate, where the shear transverse strains are no longer neglected and a fictitious shear deformation is introduced. Benscoter theory characterizes the warping degree of freedom by an independent function which is different from the gradient of the torsional angle.

All the cases in which uniform and non-uniform torsion are present represent the so called “mixed torsion problems”. Many other authors studied this kind of problem and with different approaches. When the hypothesis of cross section non-deformability is relaxed, additional modes called distortional modes are added to the classic ones describing the behavior of a thin-walled beams: tension/compression, bending and torsion. These additional modes are related to the in-plane deformation of a thin-walled cross section.

Important progress has been recently made by using different numerical methods: beam elements are defined using beam theory with a single warping function valid for arbitrary geometry of cross sections, without any distinction between open or closed profiles and without using sectorial coordinates. The results obtained have been compared for stability analysis of beams (Saadé, Espion, & Warzée, 2003).

2.2. Methods of analysis for thin walled beam structures

The analysis of thin-walled beam with arbitrary section are recently approached considering either the principle of virtual displacements or using variational principles. These methods are suitable for automatic computation of three-dimensional straight beam elements.

Different stiffness methods have been presented for closed cross-sections considering the Bescoter's assumption in the static (Prokić, 2002) and in dynamic (Prokić & Lukić, 2007) structural analysis. In this theory the function that defines warping intensity represents a new unknown that may be derived as a function of the angle of rotation of the profile. (Shakourzadeh, Guo, & Batoz, 1993) formulate a finite element for the static analysis of open and closed thin-walled sections, using the same initial assumptions. An exact hybrid element is formulated accounting the exact solution by non-polynomial interpolation functions.

In static analysis, the theories of bending and torsion are often compared in the literature by pointing out an analogy between Bernoulli bending theory and Vlasov torsional theory for open cross sections. (Kollbrunner & Basler, 1969) shows this analogy by analyzing commonly supported beams examples. All the internal forces in terms of warping moments refers to different cross-section types and the results are illustrated for different load cases, in order to establish a classification for some profiles and bridge sections.

In dynamics, one of the first works approaching the effect of warping on the mode frequency of vibration of I-beams have been performed by (Gere, 1954). This simple analysis dealt with the free-torsional vibrations of bars of thin-walled open sections for which the shear center and the elastic center coincide. The author, considering the Vlasov's assumptions, found the principal torsional frequencies and derived the mode shapes by solving exactly the differential equations for uncoupled mixed torsion.

Models treating the triply coupled vibration of open cross-sections have been considered: (Friborg, 1985) developed a numerical procedure which generates an exact dynamic stiffness matrix from the differential equations given by Vlasov. A static stiffness matrix, the associated consistent mass and geometric stiffness matrices may be established from the exact matrices. This work approach considers a model in which bending, torsion and axial effect are coupled and the shear axis does not coincide with the elastic center, as happens for arbitrary shape of cross-sections.

It may be said that these theories of thin-walled beams are labeled as exact and the solutions presented yield also exact results.

The computer simulation of results has an important rule today in defining approximated solutions. Starting from the variational principles, a general system of differential equations can be discretized directly by using the Galerkin method, based on the deflected shape. The displacement modes in bending and torsion are approximated by analytical functions and the solution depends on this choice.

2.3. Lateral-torsional forced vibrations of thin walled beam structures

Moving loads acting on elastic elements have a great effect in such structures composed by these elements, especially at high velocities. Their peculiar feature is that load functions generally vary in both time and space. This represents probably one of the original problems of structural dynamics in general.

In the present work, generally supported beam elements will be analyzed and only the case in which the load mass is small against the beam mass is considered. This problem have been studied from many authors, but the simple load case considered for the present study is a moving force with constant magnitude. (Fryba, 1999) shows the basic results obtained through the application of the method of integral transformations and then extends them to all cases of speed and viscous damping.

The number of works dealing with the combined lateral-torsional vibrations of beams under moving loads is relatively limited; although generally supported bridges with open monosymmetric cross-sections with two lanes are commonly used in the national road network of many countries, and are quite sensitive to the above type of motions. (Michaltos, Sarantithou, & Sophianopoulos, 2003) solved the coupled equations of motion derived from the application of an eccentric moving vertical load. The separation of variables method and harmonic functions for shape and amplitude are used as in the classic solutions of the problem.

3. THIN-WALLED BEAMS EQUATIONS

The thin-walled beam governing equations are derived in this chapter. The beam section can have a generic cross-section geometry, being adopted the most common layouts for civil engineering applications.

The properties of the cross-section are analyzed in section 3.1 with particular interest in define a displacement field for a beam element. The potential and kinetic energy of the beam will be obtained for this kind of elements in order to apply a variational approach for the complete formulation of the governing equations and the boundary conditions. The Euler-Bernoulli assumptions are taken into account and the contribution of the longitudinal displacement derived from the cross-section warping is considered.

Energy expressions for this kind of element are summarized in section 3.2 and 3.3 where a static and a dynamic analysis are followed by practical examples on load case studies, with particular attention in mixed torsion. In solving this practical problems the general solution for the mathematical problem is extended to a finite length bar and relative warping influence is set by means of different types of cross-section analyzed.

3.1. Cross-section analysis

The definition of the beam kinematics when subjected to axial effect, bending and torsion is essential to obtain the complete form of potential and kinetic energy of the beam. The expression of a displacement field will be totally described in section 3.1.1 where the generalized displacements are introduced for a one-dimensional beam element.

All the types of loading and boundary conditions are taken into account in order to obtain a complete formulation of the potential energy for each degree of freedom in 3.1.2.

The equations of section 3.2. are obtained considering as assumption that the displacement field depends from two special axes: the shear center axis and the elastic center axis, respectively. The position of these two points in the cross-section plan will be deduced in 3.1.3 for all general types of open and closed thin-walled section beams.

In 3.1.4 the kinetic energy is defined for the beam element in its complete form for all the generalized displacements.

3.1.1. Kinematics and strains

Prismatic thin-walled beams are considered straight and of constant cross-section. For convenience of notation a x-axis is defined parallel to the longitudinal direction of the beam, while the y-axis and z-axis describe the transversal plane of the cross-section. The corresponding displacement field adopted for the axial direction is u_x , while u_y and u_z are used for the cross-section's plane. Two dimensions are associated with the cross-section plane and a single dimension is used to describe the beam behavior along its axis. As shown in figure 3.1 for an I-beam, the whole element is represented by its generator line.

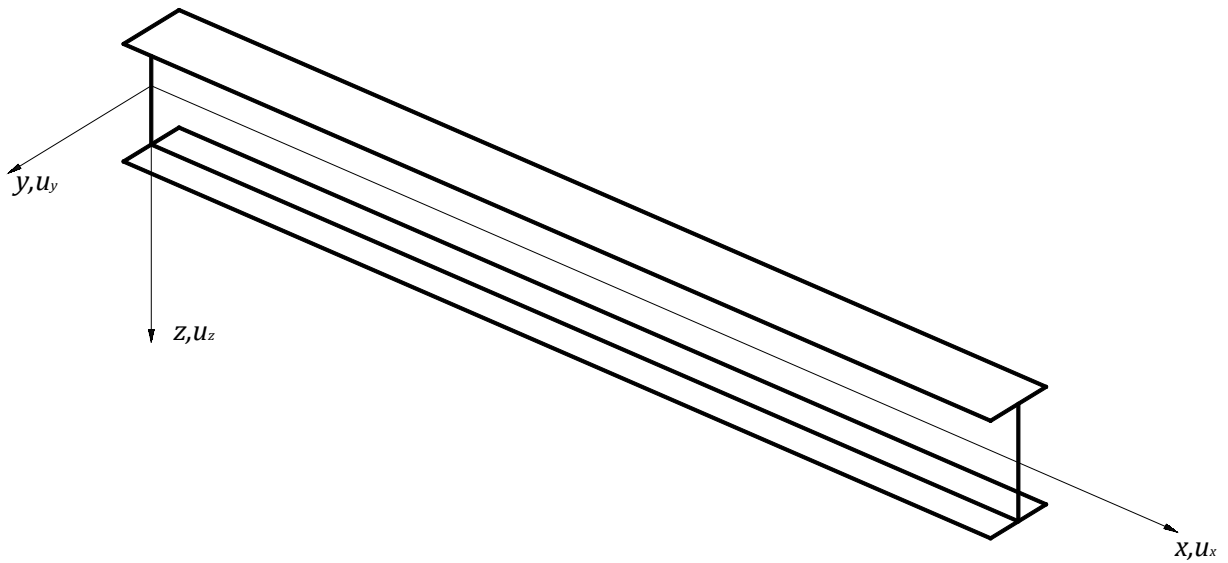


Figure 3.1 - Principal displacements and system coordinates of the beam.

In-plane displacements due to bending and torsion of the cross-section

The transverse displacement of a cross-section is described by two body translations ξ_y and ξ_z and a twist rotation φ around a generic point $P = (y_p, z_p)$ as illustrated in figure 3.2. The displacement components are given by

$$u_y = \xi_y - (z - z_p)\varphi \quad (3.1)$$

$$u_z = \xi_z + (y - y_p)\varphi \quad (3.2)$$

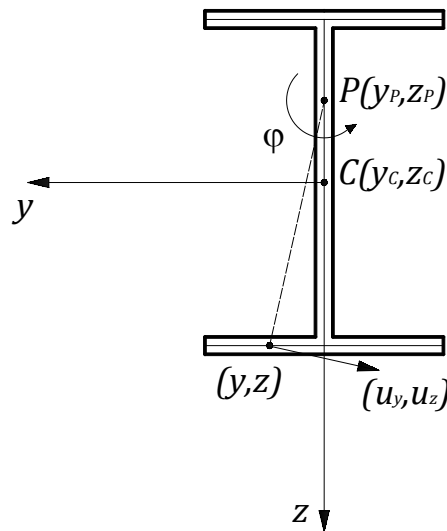


Figure 3.2 - Rotation of a I-Section around a general point P.

Axial displacements of the cross-section due to bending and axial translation

The axial displacement u_x is obtained from the linear combination of four components, one from a rigid body translation η (figure 3.3), two from rotation around lines such as the y and z - axis in the cross-section and finally one from warping.

The rotations of the cross-section, ϑ_y and ϑ_z , associated with the beam bending can be obtained according to the Bernoulli hypothesis as follows

$$\vartheta_y = \xi_y' \tag{3.3}$$

$$\vartheta_z = -\xi_z' \tag{3.4}$$

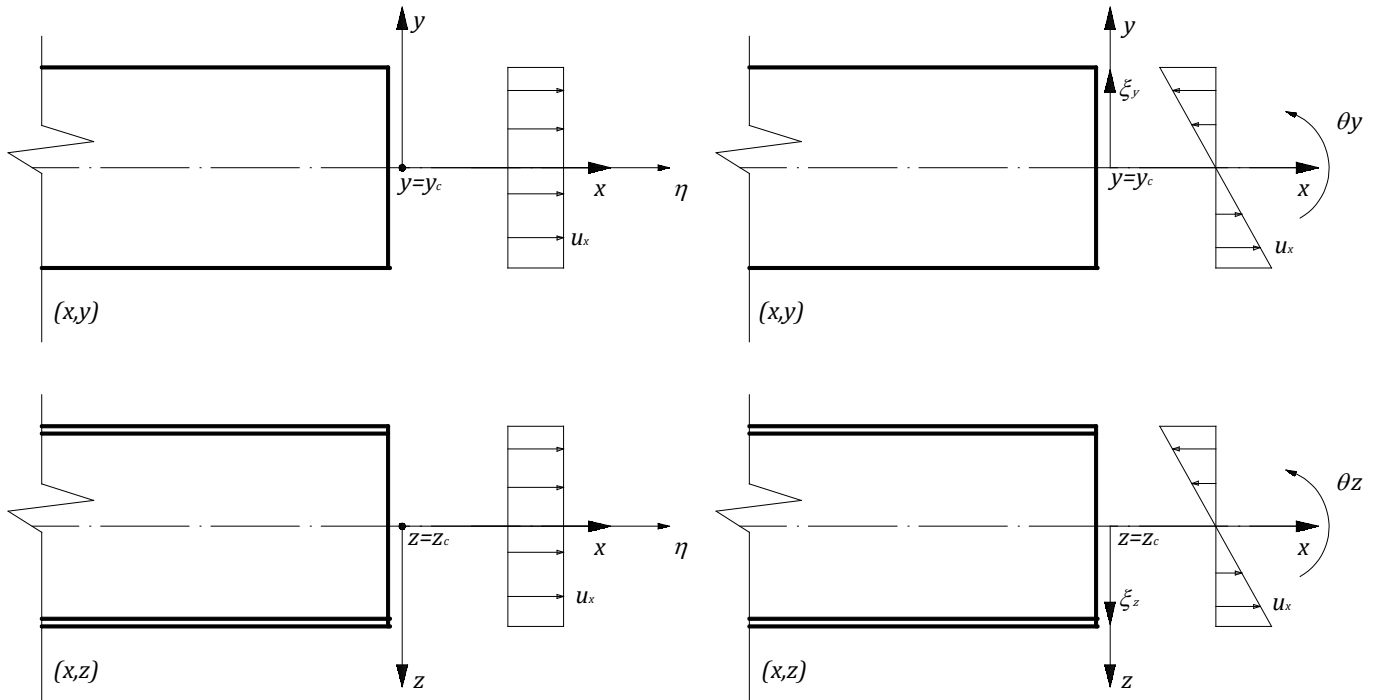


Figure 3.3- Axial displacements of an I-Beam due to axial effect and bending for planes (x,y) and (x,z) .

Torsion and warping of the cross-section

The warping of the cross-section introduces longitudinal out-of-plan displacements. In obtaining these displacements the Vlasov hypothesis that warping does not introduce any shear strain in the mid surface of the beam will be considered. This statement is illustrated in figure 3.4 showing the mid surface of an I-beam.

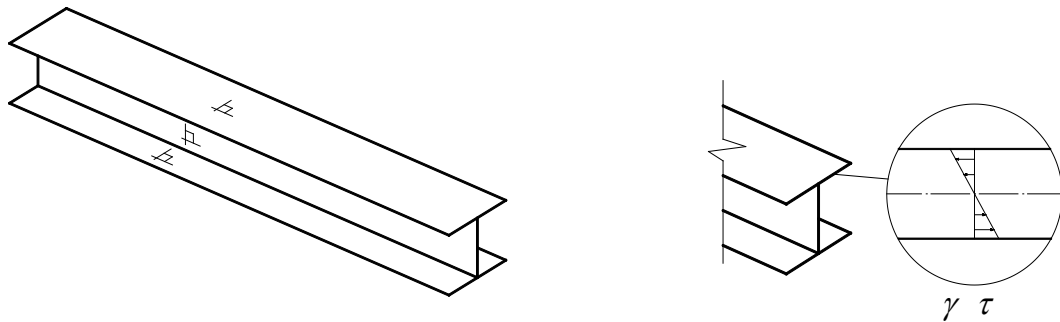


Figure 3.4 - Vanishing of the shear strain of mid-surface (left) and distribution along the wall thickness for open cross-sections (right).

This condition does not interfere with Saint Venant homogeneous torsion problem, that assume linear variation of stress τ_s and strain γ_s over the thickness (figure 3.4).

The vanishing shear strain condition in the mid-surface of the beam enables a direct determination of the cross-section warping function. When cross-sections twist, they are assumed to remain non-deformed in their own plane, so their displacements can be described by the axial component $u_x(s, x)$ and a rotation $\varphi(x)$ around a point P. The position on the centerline is described by the arc lengths, shown in figure 3.5, and the center of rotation is assumed to be known.

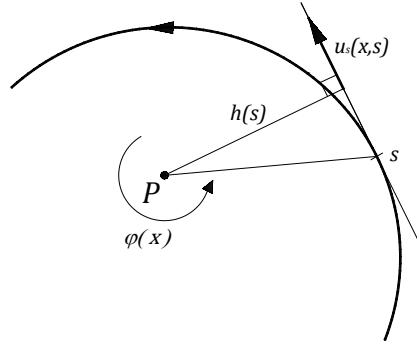


Figure 3.5 - Rotation of open cross-section.

The in-plane displacement u_s along the tangent at s can be written as

$$u_s(s, x) = h(s)\varphi(x) \quad (3.5)$$

The condition of no shear deformation is

$$\gamma(s, x) = \frac{\partial u_s}{\partial x} + \frac{\partial u_x}{\partial s} = 0 \quad (3.6)$$

That yields, substituting u_s , followed by integration with respect to s

$$u_x(s, x) = -\frac{\partial \varphi(x)}{\partial x} \int_s h(s) ds \quad (3.7)$$

Starting from the equation (3.7) a new quantity can be defined as *sectorial coordinate* and is

$$\int_s h(s) ds = \psi(s) \quad (3.8)$$

The interpretation of this function is discussed in the next two sections for an open and a closed cross-section, respectively.

Sectorial coordinate of an open cross-section

The sectorial coordinate $\int_s h(s) ds = \psi(s)$ defined by the equation (3.8) has a geometric interpretation for an open section. As shown in figure 3.6 it represents twice the area swept by a line from the center of rotation P to the generic point s on the midline of the section wall. Upon the integration on the total length of the arc $\psi(s) = 2A_s$.

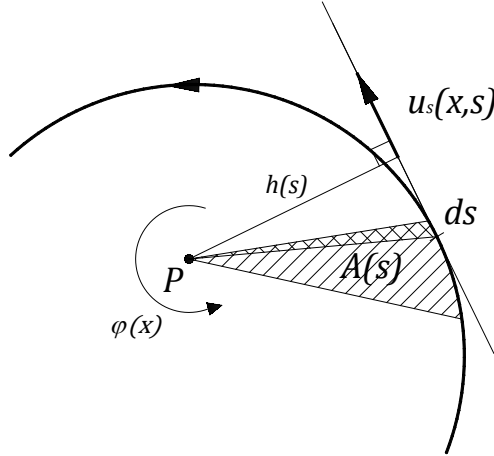


Figure 3.6 – Geometric interpretation of the sectorial coordinate.

Later will be discussed how to calculate the position of the center of rotation by means of its particular properties with respect to bending and axial displacements.

Sectorial coordinate for a closed thin-walled section

Vlasov theory is stated as applicable for closed cross-sections by combining the assumption of neglecting shear warping at midwalls for the calculation of profile warping function with Bencoter independent warping degree of freedom. Usually for a *closed section* the integral of the equation (3.8), extended to the entire perimeter, is most known in the following form

$$\oint h(s) ds = \psi(s) = 2A_s = \Omega \quad (3.9)$$

The shear distortion of the equation (3.6), if calculated for a closed section yields

$$\gamma(s, x) = \frac{\partial u_s}{\partial x} + \frac{\partial u_x}{\partial s} = \gamma_t \quad (3.10)$$

The value of the shear distortion is given by Bredt's formulae and gives

$$\gamma_t = \frac{T}{\Omega G t} \quad (3.11)$$

Substituting equations (3.5), (3.7) and (3.11) in equation (3.10) follows that

$$u_x(x = s) = u_x(x = 0) + \int_0^s \frac{T}{\Omega G t} ds - \varphi' \int_0^s h(s) ds \quad (3.12)$$

If the totality of the closed perimeter is considered in the integrals, it leads to

$$\oint \frac{T}{\Omega G t} ds = \varphi' \oint h(s) ds = \varphi' \Omega \quad (3.13)$$

Where Ω has been defined in (3.9). From (3.13) the *rate of twist* and the *torsional stiffness modulus* can be obtained as follows

$$\varphi' = \frac{T}{GK} \quad (3.14)$$

$$K = \frac{\Omega^2}{\oint \frac{ds}{t}} \quad (3.15)$$

Now a new sectorial coordinate can be calculated from (3.12) that leads to

$$u_x(x = s) = -\varphi' \psi(s) \quad (3.16)$$

where $\psi(s)$ is the coordinate defined as

$$\omega(s) = \psi(s) - \frac{\Omega}{\oint \frac{ds}{t}} \int_0^s \frac{ds}{t} + c_1 \quad (3.17)$$

in which c_1 can be obtained imposing as zero the axial virtual work $\oint \omega(s) t(s) ds = 0$. Note that this coordinate has been defined for the shear center but the same formulae obtained in the next are valid, because of the validity of the Vlasov theory.

Total axial displacements of the cross section

With all the contributions of the general displacements, the axial displacement of a thin-walled beam of open cross section is represented in the form

$$u_x(s, x) = \eta(x) - (y - y_c) \xi_y'(x) - (z - z_c) \xi_z'(x) - \omega(s) \varphi'(x) \quad (3.18)$$

The variation of u_x over the section is described by the classical Euler-Bernoulli assumption by means of $\eta(x)$, $\xi_y(x)$, $\xi_z(x)$, while the last term, composed by $\varphi(x)$, represents the displacement due to the warping of section. The equation (3.18) can be considered as an axial effect of the classic beam theory in which torsion is incorporated in a systematic way, including its non-homogeneous part.

Tangential shear strain over the cross-section

The complete form of the warping function can be found by imposing the shear strain value at the mid-surface of the beam wall. The displacement components of the equations (3.18) have been derived directly from the assumption of Vlasov's theory and implying

$$\gamma_y = \frac{\partial u_y}{\partial x} + \frac{\partial u_x}{\partial y} = \left(-(z - z_p) - \frac{\partial \omega}{\partial y} \right) \varphi' = 0 \Rightarrow \frac{\partial \omega}{\partial y} = -(z - z_p) \quad (3.19)$$

$$\gamma_z = \frac{\partial u_z}{\partial x} + \frac{\partial u_x}{\partial z} = \left((y - y_p) - \frac{\partial \omega}{\partial z} \right) \varphi' = 0 \Rightarrow \frac{\partial \omega}{\partial z} = (y - y_p) \quad (3.20)$$

Taking into account the definition of the tangent vector as

$$\mathbf{t} = \begin{bmatrix} t_1 \\ t_2 \end{bmatrix} = \begin{bmatrix} \frac{dy}{ds} \\ \frac{dz}{ds} \end{bmatrix} \quad (3.21)$$

the displacement derivatives relatively to the arc length s can now be calculated as follows

$$\frac{\partial \omega}{\partial s} = \frac{\partial \omega}{\partial y} t_1 + \frac{\partial \omega}{\partial z} t_2 = \frac{\partial \omega}{\partial y} \frac{dy}{ds} + \frac{\partial \omega}{\partial z} \frac{dz}{ds} = -(z - z_p) \frac{dy}{ds} + (y - y_p) \frac{dz}{ds} \quad (3.22)$$

where the components t_1, t_2 describe the tangent vector in the plane as shown in equation (3.21).

Considering the definition of the normal to the thin wall as

$$\mathbf{n} = \begin{bmatrix} n_1 \\ n_2 \end{bmatrix} = \begin{bmatrix} -\frac{dz}{ds} \\ \frac{dy}{ds} \end{bmatrix} \quad (3.23)$$

the projection h of the vector of coordinates $[(z - z_P), (y - y_P)]$ on the local normal (figure 3.7) can be identified in the equation (3.22). The relations obtained can be written as follows

$$\frac{\partial \omega}{\partial s} = h(s) \quad (3.24)$$

$$\frac{\partial \omega}{\partial n} = \frac{\partial \omega}{\partial y} n_1 + \frac{\partial \omega}{\partial z} n_2 = \frac{\partial \omega}{\partial z} \frac{dy}{ds} - \frac{\partial \omega}{\partial y} \frac{dz}{ds} = (y - y_P) \frac{dy}{ds} + (z - z_P) \frac{dz}{ds} \quad (3.25)$$

The parameter h_s identified in figure 3.7 is defined by the equation (3.25). In fact it leads to

$$h_s = (y - y_P) \frac{dy}{ds} + (z - z_P) \frac{dz}{ds} = \frac{\partial \omega}{\partial n} \quad (3.26)$$

which represents a linear variation of ω across the wall thickness, i.e.

$$\omega(s, n) = \omega_{n=0}(s) + h_s(s)n \quad (3.27)$$

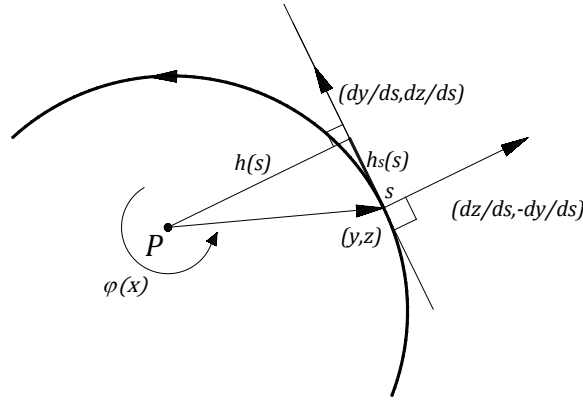


Figure 3.7 – Geometric interpretation of $h(s)$ and $h_s(s)$.

The distribution of the tangential shear strain component over the wall thickness can then be obtained as follows

$$\gamma = \frac{\partial u_s}{\partial x} + \frac{\partial u_x}{\partial s} = \frac{\partial}{\partial x} ((h + n)\varphi) + \frac{\partial}{\partial s} (-\omega\varphi') = 2n\varphi' \quad (3.28)$$

which corresponds to the linear variation of the Saint Venant shear strain for open thin-walled sections.

Axial strain over the cross-section

The strain component ε along the beam axis is obtained from the derivative of the axial displacement (3.18) as follows

$$\varepsilon = \eta'(x) - (y - y_c)\xi_y''(x) - (z - z_c)\xi_z''(x) - \omega(s)\varphi''(x) \quad (3.29)$$

3.1.2. Potential energy formulation

The potential energy is defined by two parts, the strain energy and the external work produced by the load. Two strain components are present in the current analysis, the normal axial strain ε and the Saint Venant shear strain γ . By applying Hooke's law is possible to obtain the corresponding axial and shear stresses

$$\text{Axial stress: } \sigma = E\varepsilon \quad (3.30)$$

$$\text{Shear stress: } \tau = G\gamma \quad (3.31)$$

where E is the module of elasticity and G is the shear modulus of the prescribed material, given by $G = \frac{E}{2(1+\nu)}$.

These two quantities are assumed to be constant along the bar length.

The elastic *strain energy* density per unit volume is obtained from the two components as follows

$$U = \frac{1}{2}E\varepsilon^2 + \frac{1}{2}G\gamma^2 \quad (3.32)$$

The load is given in terms of volume forces, so the *external work* per unit volume can be expressed as follows

$$W = p_x u_x + p_y u_y + p_z u_z = \mathbf{p} \cdot \mathbf{u} \quad (3.33)$$

being $\mathbf{p} = \begin{bmatrix} p_x \\ p_y \\ p_z \end{bmatrix}$ the vector of volume forces and $\mathbf{u} = \begin{bmatrix} u_x \\ u_y \\ u_z \end{bmatrix}$ the displacements vector considered.

Axial strain energy per unit length

The strain energy per unit length is obtained by integration of the equation (3.32) over the cross section area. The integration of the *axial* strain (3.29) gives the contribution

$$\begin{aligned} \frac{1}{2} \int_A E \varepsilon^2 dA &= \frac{1}{2} E \int_A [\eta'(x) - (y - y_c)\xi_y''(x) - (z - z_c)\xi_z''(x) - \omega(s)\varphi''(x)]^2 dA = \\ &= \frac{1}{2} E [\eta' \quad -\xi_y'' \quad -\xi_z'' \quad -\varphi''] \begin{bmatrix} A & S_y & S_z & S_\omega \\ S_y & I_{yy} & I_{yz} & I_{y\omega} \\ S_z & I_{zy} & I_{zz} & I_{z\omega} \\ S_\omega & I_{\omega y} & I_{\omega z} & I_{\omega\omega} \end{bmatrix} \begin{bmatrix} \eta' \\ -\xi_y'' \\ -\xi_z'' \\ -\varphi'' \end{bmatrix} \end{aligned} \quad (3.34)$$

This is the expression of the quadratic and symmetric mathematical energy density after integration over the transverse area. The vector $[\eta' \quad -\xi_y'' \quad -\xi_z'' \quad -\varphi'']$ represents the generalized strains, including axial, flexural and warping components. The terms in the matrix are obtained from integration over the area and represent the cross-section geometrical parameters. It is useful to specify that all the sectorial moments refers to the point P, which is generic. All these quantities are represented in the table 3.1.

Tangential strain energy per unit length

The Saint Venant shear strain energy contribution is obtained by the following integration

$$\frac{1}{2} \int G \gamma^2 dA = \frac{1}{2} \varphi' G K \varphi' \quad (3.35)$$

In table 3.1 are listed all the geometrical properties of the cross-sections.

Table 3.1 - Cross-Section parameters.

Quantities	Open Section	Closed Section
Area:	$A = \int_A dA$	$A = \oint_A dA$
Static moment:	$S_y = \int_A (y - y_c) dA$	$S_y = \oint_A (y - y_c) dA$
	$S_z = \int_A (z - z_c) dA$	$S_z = \oint_A (z - z_c) dA$
Moments of inertia:	$I_y = \int_A (y - y_c)^2 dA$	$I_y = \oint_A (y - y_c)^2 dA$
	$I_z = \int_A (z - z_c)^2 dA$	$I_z = \oint_A (z - z_c)^2 dA$
	$I_{yz} = \int_A (z - z_c)(y - y_c) dA = I_{zy}$	$I_{yz} = \oint_A (z - z_c)(y - y_c) dA = I_{zy}$
Sectorial moments:	$S_\omega = \int_A \omega(s) dA$	$S_\psi = \oint_A \psi(s) dA$
	$I_{y\omega} = \int_A (y - y_c) \omega(s) dA$	$I_{y\psi} = \oint_A (y - y_c) \psi(s) dA$
	$I_{z\omega} = \int_A (z - z_c) \omega(s) dA$	$I_{z\psi} = \oint_A (z - z_c) \psi(s) dA$
Warping constants	$I_{\omega\omega} = \int_A \omega(s)^2 dA$	$I_{\psi\psi} = \oint_A \psi(s)^2 dA$
Torsion parameter:	$K = \frac{1}{3} \int t^3 ds$	$K = \frac{\Omega^2}{\oint \frac{ds}{t}}$

External work per unit length

Integrating the equation (3.33) over the cross-section area the following expression is obtained

$$\int_A (p_x u_x + p_y u_y + p_z u_z) dA = q_x \eta + q_y \xi_y + q_z \xi_z + m_\varphi \varphi - m_y \xi'_y - m_z \xi'_z - b \varphi' \quad (3.36)$$

where the load is considered in terms of volume forces by means of p_x, p_y, p_z . Surface tractions and concentrated loads can be considered as limiting forms of volume forces.

All the beam loads are defined in table 3.2. Notice that for each generalized displacement $\eta, \xi_y, \xi_z, \varphi, \xi'_y, \xi'_z, \varphi'$ there is a beam load, as the boundary conditions imposed. These 7 displacement components are the degrees of freedom of thin-walled beam elements, so warping can be considered as an additional d.o.f. to the 6 of a simply one-dimensional beam in space.

Table 3.2 – Beam loads per unit length.

Quantities	Open Section	Closed Section
Axial load:	$q_x = \int_A p_x dA$	$q_x = \oint_A p_x dA$
Transverse load:	$q_y = \int_A p_y dA$	$q_y = \oint_A p_y dA$
	$q_z = \int_A p_z dA$	$q_z = \oint_A p_z dA$
Bending moment loads:	$m_y = \int_A p_x (y - y_c) dA$	$m_y = \oint_A p_x (y - y_c) dA$
	$m_z = \int_A p_x (z - z_c) dA$	$m_z = \oint_A p_x (z - z_c) dA$
Torsion moment load:	$m_\varphi = \int_A p_z (y - y_P) - p_y (z - z_P) dA$	$m_\varphi = \oint_A p_z (y - y_P) - p_y (z - z_P) dA$
Bimoment load:	$b = \int_A p_x \omega(s) dA$	$b = \oint_A p_x \psi(s) dA$

Total potential energy

The total potential energy of the beam element can now be defined by the total quantity V or by the unit length energy F , after the integration over the cross-section area. The strain energy component is composed by quadratic terms, while the applied load part is represented by linear terms. Thus, the following expressions are obtained

Total potential energy:

$$V = \int_V (U - W) dV = \int_V \left(\frac{1}{2} E \varepsilon^2 + \frac{1}{2} G \gamma^2 - (p_x u_x + p_y u_y + p_z u_z) \right) dV \quad (3.37)$$

Potential energy per unit length:

$$V = \int_L F(\eta, \eta', \varphi, \varphi', \varphi'', \xi_y, \xi_z, \xi'_y, \xi'_z, \xi''_y, \xi''_z) dx \quad (3.38)$$

where the functional F is defined by

$$\begin{aligned}
F & \left(\eta, \eta', \varphi, \varphi', \varphi'', \xi_y, \xi_z, \xi'_y, \xi'_z, \xi''_y, \xi''_z \right) = \\
& = \frac{1}{2} E \left(\eta' A \eta' - \eta' S_y \xi''_y - \eta' S_z \xi''_z - \eta' S_\omega \varphi'' \right. \\
& - \xi''_y S_y \eta' + \xi''_y I_y \xi''_y + \xi''_y I_{yz} \xi''_z + \xi''_y I_{y\omega} \varphi'' \\
& - \xi''_z S_z \eta' + \xi''_z I_{zy} \xi''_y + \xi''_z I_z \xi''_z + \xi''_z I_{z\omega} \varphi'' \\
& \left. - \varphi'' S_\omega \eta' + \varphi'' I_{y\omega} \xi''_y + \varphi'' I_{\omega z} \xi''_z + \varphi'' I_{\omega\omega} \varphi'' \right) \\
& + \frac{1}{2} \varphi' G K \varphi' - \left(q_x \eta + q_y \xi_y + q_z \xi_z + m_\varphi \varphi - m_y \xi'_y - m_z \xi'_z - b \varphi' \right)
\end{aligned} \tag{3.39}$$

In the next part will be specified a suitable choice of the elastic center (x_c, y_c) and of the center of rotation (x_p, y_p) in order to obtain considerable simplifications of the equation (3.39) in coupling terms outside the diagonal of matrix of (3.34).

3.1.3. Elastic center and shear center

The coupled terms that appear in the energy density F take into account the contribution of the different generalized displacements and represent the coupling between axial effect, bending and torsion, which implies, for example, that a solution involving flexural displacements will also activate torsion and extension of the beam. The coupling between *extension* and *bending* is eliminated for $S_y, S_z = 0$, while coupled effects in *extension* and *bending* with respect to *torsion* displacements are cancelled if $S_\omega, I_{y\omega}, I_{z\omega} = 0$.

The elimination of the static moments of Table 3.1 follows from the choice of the point (y_c, z_c) as defined below

$$y_c = \frac{1}{A} \int_A y \, dA \tag{3.40}$$

$$z_c = \frac{1}{A} \int_A z \, dA \tag{3.41}$$

This defines the elastic center of the cross-section for homogeneous cross-section of the beam.

In a similar way, the condition $S_\omega, I_{y\omega}, I_{z\omega} = 0$ implies no bending or axial effect when the cross-section twists. The *shear center* is defined by the property $I_{y\omega}, I_{z\omega} = 0$, while $S_\omega = 0$ is satisfied by including a suitable constant in the definition of the sectorial coordinate (3.8). The coordinates (y_a, z_a) of this point will be defined neglecting the shear strain at the mid surface and evaluating the difference between sectorial coordinates ω_a and ω_p as follows

$$\frac{\partial(\omega_a - \omega_p)}{\partial y} = -(z_p - z_a) \tag{3.42}$$

$$\frac{\partial(\omega_a - \omega_p)}{\partial z} = (y_p - y_a) \tag{3.43}$$

being (y_p, z_p) the coordinates of the generic point of rotation P that define the sectorial coordinate ω_p .

The assumption have been done considering *open sections*. For compact and hollow section the distortion is present because of the elastic shearing of the cross section and has to be accounted for its effect in the warping parameter. In the next an adapted warping coordinate $\psi(s)$ will be considered for closed sections according to (Benscoter, 1954).

Integration of the relations (3.42) and (3.43) gives the expression of ω_a

$$\omega_a(s) = \omega_p(s) + (z_a - z_p)(y - y_c) - (y_a - y_p)(z - z_c) - c \quad (3.44)$$

where the unknown constant c is obtained by substitution of the expression of ω_a into the condition $S_{\omega_a} = 0$.

The value of the constant is

$$c = \frac{1}{A} \int_A \omega_p(s) dA = \frac{S_{\omega_p}}{A} \quad (3.45)$$

The expression of $\omega_a(s)$ can now be substituted in the orthogonality conditions $I_{y\omega}, I_{z\omega} = 0$, allowing to obtain the following equations

$$I_{y\omega_p} + (z_a - z_p)I_y - (y_a - y_p)I_{zy} = 0 \quad (3.46)$$

$$I_{z\omega_p} + (z_a - z_p)I_{yz} - (y_a - y_p)I_z = 0 \quad (3.47)$$

Considering the equations (3.46) and (3.47) the coordinates of the shear center (y_a, z_a) are obtained as follows

$$\begin{bmatrix} y_a \\ z_a \end{bmatrix} = \begin{bmatrix} y_p \\ z_p \end{bmatrix} + \frac{1}{I_z I_y - I_{yz}^2} \begin{bmatrix} I_y & I_{yz} \\ I_{zy} & I_z \end{bmatrix} \begin{bmatrix} I_{z\omega_p} \\ -I_{y\omega_p} \end{bmatrix} \quad (3.48)$$

The torsion problem is uncoupled between the axial effect and the bending of the beam when (y_c, z_c) are the coordinates of the elastic center and (y_a, z_a) define the shear center. This uncoupling is convenient from the point of view of analysis and useful to describe the non-homogeneous torsion mechanics.

Transformation of sectorial coordinates

The warping coefficient of the generic cross-section may be obtained either from integration of the sectorial coordinate ω_a or by transformation of the sectorial coordinate in relation to the generic sectorial coordinate ω_p . The substitution of (3.44) and (3.45) in the definition of $I_{\omega\omega}^a$ leads to the following transformation formula:

$$I_{\omega\omega}^a = I_{\omega\omega}^p - \frac{S_{\omega_p}^2}{A} + \begin{bmatrix} y_a - y_p & z_a - z_p \end{bmatrix} \begin{bmatrix} I_z & -I_{zy} \\ -I_{yz} & I_y \end{bmatrix} \begin{bmatrix} y_a - y_p \\ z_a - z_p \end{bmatrix} \quad (3.49)$$

Notice that the sectorial parameter for a generic point P of the cross-section is always more than $I_{\omega\omega}^a$, which means that the sectorial parameter corresponding to the shear center is the principal sectorial coordinate.

3.1.4. The direct method for the warping properties evaluation

The method seen above for evaluating the warping properties of the cross-section involves a large number of steps in their calculation. Separate techniques are required for open, single-celled and multi-celled profiles, and arithmetical values are difficult to avoid. The aim of this section is to describe a method that allows to obtain the warping function and the location of the shear center in one step: for this reason the method is called “direct”. The warping constant is then easily evaluated by using the warping function distribution along the section profile. The method was developed by (Attard, 1987) and is independent of the choice of axes and it does not require the calculation of the location of the elastic center and the principal axes.

Open profiles

An open profile is considered, whose N elements and $N + 1$ nodes are numbered. An arrow in each element indicates which is the first joint i and the second joint k , and is known as connectivity of the element; an arbitrary set of coordinate can be set as shown in figure 3.8. The values of the warping function at the nodes and the shear center location are the unknown values required. Two sets of unknowns are now introduced, the *global* set and the *element* set, respectively, as follows:

$$\boldsymbol{\omega}_e = [\omega_{i1}, \omega_{k1}, \omega_{i2}, \omega_{k2}, \dots, \omega_{i5}, \omega_{k5}, x_M, y_M] \quad (3.50)$$

$$\boldsymbol{\omega}_g = [\omega_1, \omega_2, \omega_3, \dots, \omega_6, x_M, y_M] \quad (3.51)$$

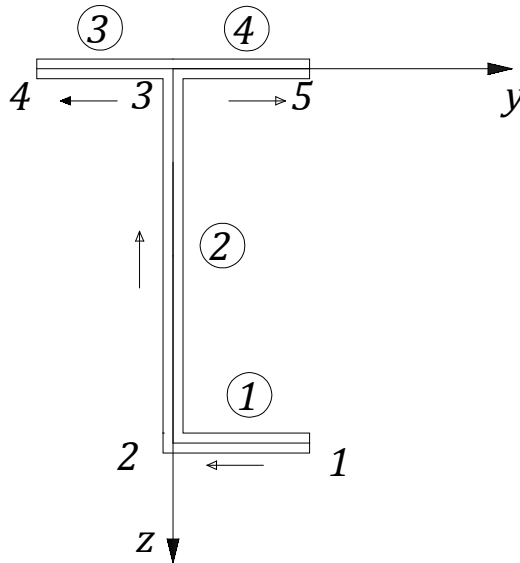


Figure 3.8 – Open cross-section with N elements.

Taking the pole at the shear center $A(y_a, z_a)$ the difference between ω_{in} and ω_{kn} of the element n is given by the Leibnitz formula (3.44), which is rearranged as follows for the generic element:

$$-\omega_{in} + \omega_{kn} + y_a(z_{kn} - z_{in}) - z_a(y_{kn} - y_{in}) = y_{in}(z_{kn} - z_{in}) - z_{in}(y_{kn} - y_{in}) \quad (3.52)$$

In an open profile with N elements this equation can be used for each element. Together they form the *element equation set*.

A further three equations are obtained because $S_\omega = 0$ and also $I_{y\omega}, I_{z\omega} = 0$ if the pole is located at the shear center A . These equations can be written in terms of the element unknowns which for the n th element are ω_{in} and ω_{kn} , in fact the elements are straight lines and therefore the warping function varies linearly between

adjacent nodal points. Thus, in addition to the set of element equation there is the following set of *property equations*:

$$\sum_{n=1}^N l_n t_n (\omega_{in} + \omega_{kn}) = 0 \quad (3.53)$$

$$\sum_{n=1}^N l_n t_n [\omega_{in} (2y_{in} + y_{kn}) + \omega_{kn} (y_{in} - 2y_{kn})] = 0 \quad (3.54)$$

$$\sum_{n=1}^N l_n t_n [\omega_{in} (2z_{in} + z_{kn}) + \omega_{kn} (z_{in} - 2z_{kn})] = 0 \quad (3.55)$$

where l_n and t_n are respectively the length and the thickness of the element.

The equations (3.52), (3.53), (3.54), (3.55) are therefore $(N + 3)$ equations in $(2N + 2)$ unknowns and can be written in a matrix form:

$$\mathbf{A} \{\boldsymbol{\omega}_e\} = \{\mathbf{R}\} \quad (3.56)$$

where the \mathbf{A} matrix, with dimensions $(N + 3) \times (2N + 2)$, and the \mathbf{R} vector, with $(N + 3)$ elements are written in the equation (3.57) for the cross-section in figure 3.8:

$$\begin{bmatrix} -1 & +1 & & & & & & & (z_{k1} - z_{i1}) & -(y_{k1} - y_{i1}) \\ & & -1 & +1 & & & & & (z_{k2} - z_{i2}) & -(y_{k2} - y_{i2}) \\ & & & & -1 & +1 & & & (z_{k3} - z_{i3}) & -(y_{k3} - y_{i3}) \\ & & & & & & -1 & +1 & (z_{k4} - z_{i4}) & -(y_{k4} - y_{i4}) \\ l_1 t_1 & l_1 t_1 & l_2 t_2 & l_2 t_2 & l_3 t_3 & l_3 t_3 & l_4 t_4 & l_4 t_4 & 0 & 0 \\ A_1 & B_1 & A_2 & B_2 & A_3 & B_3 & A_4 & B_4 & 0 & 0 \\ C_1 & D_1 & C_2 & D_2 & C_3 & D_3 & C_4 & D_4 & 0 & 0 \end{bmatrix} \begin{bmatrix} \omega_{i1} \\ \omega_{k1} \\ \omega_{i2} \\ \omega_{k2} \\ \omega_{i3} \\ \omega_{k3} \\ \omega_{i4} \\ \omega_{k4} \\ y_a \\ z_a \end{bmatrix} = \begin{bmatrix} y_{i1}(z_{k1} - z_{i1}) - z_{i1}(y_{k1} - y_{i1}) \\ y_{i2}(z_{k2} - z_{i2}) - z_{i2}(y_{k2} - y_{i2}) \\ y_{i3}(z_{k3} - z_{i3}) - z_{i3}(y_{k3} - y_{i3}) \\ y_{i4}(z_{k4} - z_{i4}) - z_{i4}(y_{k4} - y_{i4}) \\ 0 \\ 0 \\ 0 \end{bmatrix} \quad (3.57)$$

where:

$$A_n = l_n t_n (2y_{in} + y_{kn}) \quad (3.58)$$

$$B_n = l_n t_n (y_{in} + 2y_{kn}) \quad (3.59)$$

$$C_n = l_n t_n (2z_{in} + z_{kn}) \quad (3.60)$$

$$D_n = l_n t_n (z_{in} + 2z_{kn}) \quad (3.61)$$

In order to convert to global unknowns as in equation (3.51) a *connectivity matrix* \mathbf{C} can be used. Thus:

$$\{\boldsymbol{\omega}_e\} = \mathbf{C} \{\boldsymbol{\omega}_g\} \quad (3.62)$$

It has dimension $(2N + 2) \times (N + 3)$ and shows that $\omega_{i1} = \omega_1, \omega_{k1} = \omega_2, \text{etc.}$ For the example of figure 3.8 it has the following form:

$$\begin{bmatrix} \omega_{i1} \\ \omega_{k1} \\ \omega_{i2} \\ \omega_{k2} \\ \omega_{i3} \\ \omega_{k3} \\ \omega_{i4} \\ \omega_{k4} \\ y_a \\ z_a \end{bmatrix} = \begin{bmatrix} 1 & & & & & & & & & & \\ & 1 & & & & & & & & & \\ & & 1 & & & & & & & & \\ & & & 1 & & & & & & & \\ & & & & 1 & & & & & & \\ & & & & & 1 & & & & & \\ & & & & & & 1 & & & & \\ & & & & & & & 1 & & & \\ & & & & & & & & 1 & & \\ & & & & & & & & & 1 & \\ & & & & & & & & & & 1 \end{bmatrix} \begin{bmatrix} \omega_1 \\ \omega_2 \\ \omega_3 \\ \omega_4 \\ \omega_5 \\ y_a \\ z_a \end{bmatrix} \quad (3.63)$$

When \mathbf{A} and \mathbf{C} are multiplied the result is a square matrix \mathbf{B} whose dimensions are $(N + 3) \times (N + 3)$ and the equation (3.56) can be written as follows:

$$\mathbf{A} \{\omega_e\} = \mathbf{A} \mathbf{C} \{\omega_g\} = \mathbf{B} \{\omega_g\} = \{\mathbf{R}\} \quad (3.64)$$

And therefore:

$$\{\omega_g\} = \mathbf{B}^{-1} \{\mathbf{R}\} \quad (3.65)$$

Closed profiles

The above theory for open profile requires only two minor modifications before it can be applied to closed profiles. They are as follows:

- i) It is necessary to evaluate a constant ψ for each cell of the profile. In (Murray, 1984) it is shown how this may be done for both single-celled and multi-celled profiles and this aspect will be approached in the next section. For closed profiles the property equations remain unchanged while the element equation (3.52) of the element n is given by the algebraic equation:

$$-\omega_{in} + \omega_{kn} + y_a(z_{kn} - z_{in}) - z_a(y_{kn} - y_{in}) = y_{in}(z_{kn} - z_{in}) - z_{in}(y_{kn} - y_{in}) - \frac{\psi l_n}{t_n} \quad (3.66)$$

- ii) When writing down the element equations which are based upon the equation (3.98) it is necessary to omit one element from each cell. This is because the last element equation would only be a relationship between the values of the warping function at the first and at the last nodes, a relation which could be established from the three previous equations. However it is necessary to include these previously omitted element when the three property equations are considered.

3.1.5. A generalized method for the section properties evaluation

The purpose of this section is to introduce the theoretical basis for the implementation of a numerical code to evaluate the cross-section parameters, illustrated in table 3.1, for a thin-walled beam. The principal section parameters such as area, static and inertial moments are calculated by using the classical theory of structures, while for the calculus of the warping and torsional parameters a "direct approach" (Attard, 1987) is illustrated, in order to obtain a systematic method for the analysis of both open and closed profiles.

The method is independent of the choice of axes. The data input for code purposed is composed by the following dimensions:

- i) Number of the N joints of the cross-section;
- ii) Cross-section joint coordinates in the $(y-z)$ plan;
- iii) Number of the n elements connecting the joints;
- iv) Connectivity and thickness t_i of the elements.

Area, static and inertial moments

The i -element of a general cross-section, the global axis of reference (y, z) and the local axis (y', z') , (ξ, η) with the origin in the elastic center of the element are shown in figure 3.9. Taking into account the element length as l_i , the thickness as t_i , it is possible to calculate the total area of the profile as follows:

$$A = \sum_{i=1}^n A_i = \sum_{i=1}^n t_i l_i \quad (3.67)$$

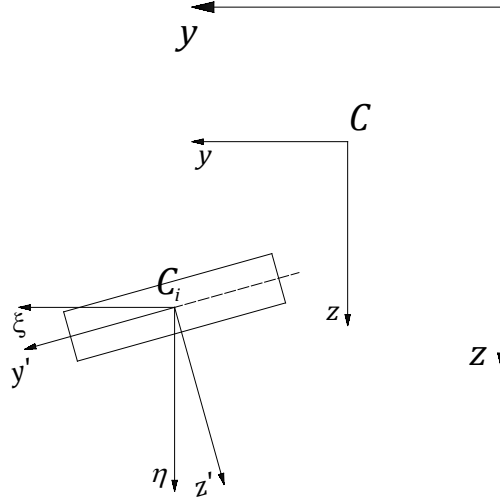


Figure 3.9 – Global reference axis and local axis of the element.

The elastic center coordinates (y_c, z_c) are calculated by introducing the static moments of the whole section:

$$S_y = \sum_{i=1}^n S_{yi} = \sum_{i=1}^n A_i z_{ci} \quad (3.68)$$

$$S_z = \sum_{i=1}^n S_{zi} = \sum_{i=1}^n A_i y_{ci} \quad (3.69)$$

being y_{ci} and z_{ci} the coordinates of the i -element and considering that:

$$y_c = \frac{S_z}{A} \quad (3.70)$$

$$z_c = \frac{S_y}{A} \quad (3.71)$$

Considering now the local axis reference (y'_{c_i}, z'_{c_i}) of the i -element, the inertia moments are:

$$J_{y'} = \frac{l_i t_i^3}{12} \quad (3.72)$$

$$J_{z'} = \frac{t_i l_i^3}{12} \quad (3.73)$$

with $J_{y'z'} = 0$. If the local reference considered is (ξ_{c_i}, η_{c_i}) the Mohr's circle has to be used in order to consider the rotation in the cross-section plan and the inertia moments are:

$$J_\xi = \frac{J_{y'} + J_{z'}}{2} + \frac{J_{y'} - J_{z'}}{2} \cos 2\alpha \quad (3.74)$$

$$J_\eta = \frac{J_{y'} + J_{z'}}{2} - \frac{J_{y'} - J_{z'}}{2} \cos 2\alpha \quad (3.75)$$

$$J_{\eta\xi} = -\frac{J_{y'} - J_{z'}}{2} \sin 2\alpha \quad (3.76)$$

Now the coordinate system with origin in the elastic center can be considered obtaining the inertia moment of the cross-section:

$$J_y = \sum_{i=1}^n [J_{\xi} + A_i(z_{ci} - z_c)^2] \quad (3.77)$$

$$J_z = \sum_{i=1}^n [J_{\eta} + A_i(y_{ci} - y_c)^2] \quad (3.78)$$

$$J_{yz} = \sum_{i=1}^n [J_{\xi} + A_i(y_{ci} - y_c)(z_{ci} - z_c)] \quad (3.79)$$

Torsional parameters of the cross section

The first step that is needed in order to calculate the torsional properties of a cross-section is the identification of the section type. In fact, for closed profiles, the modifications illustrated in the section 3.1.3 must be taken into account. If N_n and N_e are used to identify the number of the section nodes and the number of section elements, respectively, the following conditions define the section type:

$$\text{Open profile: } N_e = N_n - 1 \quad (3.80)$$

$$\text{Closed profile: } N_e > N_n - 1 \quad (3.81)$$

When the section type is identified by the computer code, it will be called an adequate subroutine which solves open or closed cross-sections. The solving method is illustrated below for open and closed sections, respectively.

Open profiles

The procedure for open profiles is widely described in the section 3.1.3 and it consists of solving the algebraic equations (3.66) considering all the elements of the cross-section. When the global unknowns are identified, they are used in order to obtain the warping parameter as follows:

$$I_{\omega\omega} = \frac{1}{3} \sum_{j=1}^{N_e} l_j t_j \left[(\omega_g(i))^2 + (\omega_g(i))(\omega_g(k)) + (\omega_g(k))^2 \right] \quad (3.82)$$

While the polar K is calculated by the sum over the cross-section elements:

$$K = \frac{1}{3} \sum_{j=1}^{N_e} l_j t_j^3 \quad (3.83)$$

Closed profiles

For closed cross-sections a value of ψ has to be calculated for each cell of the profile. The number of the cells N_a can be calculated as follows:

$$N_a = N_e - N_n + 1 \quad (3.84)$$

When the number of the cells is known, it must be established which elements compose each cell. The aim of the computer code can be divided in three principal steps:

- i) The creation of a matrix M_{glo} that contain for each column the number of the elements that identify the cell. This step will require an appropriate check of the elements for each cell.
- ii) The evaluation of the cellular parameters ψ by solving an algebraic equation.
- iii) The solution of the linear system governing the problem. The warping function distribution and the shear center location are completely defined at the end of this step.

The theoretical basis of this method have been introduced by (Murray, 1984). Each step will be shortly described below. For a detailed illustration of the computational approach, see (Manzoni, 2001) in the references.

Automatic check of the cross-section cells

A system for the automatic identification of the element that constitute a cell is to start with the first element and proceed with all the section elements in a clockwise direction, turning "on the right direction" each time that in a node are connected more than two elements. If along this path a joint connected by only one element is identified, the element counting back to a previous node and take another path. In a temporary vector are saved the external element identifier constituting the cell: this vector is named $V_{loc2,e}$. For the starting element e the orientation of the extreme joints must be defined in the clockwise direction.

In a second time for each element vector will correspond a nodal vector $V_{loc,e}$ that is useful to identify the nodes that connect only with an element.

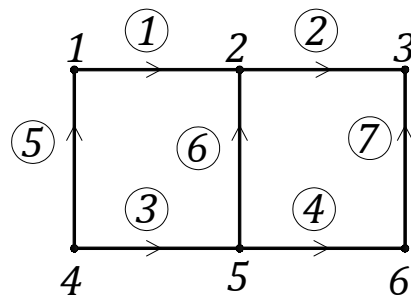


Figure 3.10 - Example of two-celled cross-section.

For the cross-section taken as example in figure 3.10 the vector $V_{loc,1}$ is [1 2 5 4 1], and the $V_{loc2,2}$ vector is [1 3 5 6]. Starting from the second element is $V_{loc,2} = [2 3 6 5 2]$ and $V_{loc2,2} = [2 4 6 7]$. So the matrix of the cells is the following:

$$M_{glo} = \begin{bmatrix} 1 & 2 \\ 3 & 4 \\ 5 & 6 \\ 6 & 7 \end{bmatrix} \quad (3.85)$$

Evaluation of the cell constants

For each cell with n elements and n nodes the area must be calculated as follows from the Gauss formulae:

$$A_{tot} = -\frac{1}{2} \sum_{j=1}^{n-1} [(y_j z_{j+1} - y_{j+1} z_j) - (y_1 z_{j+1} - y_{j+1} z_1) + (y_1 z_j - y_i z_1)] \quad (3.86)$$

The sign of the expression is due to the fact that the cell joints are disposed in the clockwise direction. The areas of the cells must be written in a vector \mathbf{S} . For a multi-cellular profile the N_a cell parameters can be calculated writing an equation for each i -element, so an algebraic system can be written as follows:

$$\mathbf{D}\{\boldsymbol{\psi}\} = \mathbf{2}\{\mathbf{S}\} \quad (3.87)$$

The matrix expression in (3.87) permits to obtain the N_a cell parameters ψ_i . The generic term of the square matrix \mathbf{D} , which has dimensions $(N_a \times N_a)$, is composed by the generic terms:

$$d_{i,i} = \sum_{j=1}^{n_i} \frac{l_j}{t_j} \quad (3.88)$$

$$d_{i,k} = -\sum_{j_c=1}^{n_{ck}} \frac{l_{j_c}}{t_{j_c}} \quad (i \neq k) \quad (3.89)$$

where:

- n_i is the number of the elements constituting the i cell;
- l_j and t_j are the length and the thickness, respectively, of the element for the i cell;
- n_{ck} represents the total element number that are common between the i cell and the k cell;
- l_{j_c} and t_{j_c} are the length and the thickness, respectively, of the common element j_c between the i cell and the k cell;

The generic term for the i cell of the \mathbf{S} vector, which has N_a elements, will be:

$$s_i = A_{tot,i} \quad (3.90)$$

Final solving of the equations

When the parameters of the system (3.87) have been calculated, it is possible to obtain the torsional parameter for the closed section as follows:

$$K = 2 \sum_{i=1}^{n_a} \psi_i A_i \quad (3.91)$$

The objective of the subroutine in this step is to assembly the matrices \mathbf{A} , \mathbf{C} and the vector \mathbf{R} , in order to solve the system (3.65) and determining the unknowns.

The matrix \mathbf{A} is assembled in two phases:

- i) in the first phase an element for each cell of the profile will be eliminated, obtaining at the end of this step an open profile. The elements deleted are written in a vector with N_a elements. The matrix \mathbf{A} , which has dimensions $(N_e - N_a + 3) \times (2(N_e - N_a) + 2)$ is assembled as seen for an open profile;
- ii) the second phase takes into account the modifications to the \mathbf{A} matrix due to the eliminated elements in the first step. For each deleted element the quantities of the equations (3.58),(3.59),(3.60),(3.61) are calculated and added to the 3 last rows of the \mathbf{A} matrix previously

defined, but only in the columns corresponding to the element joints that have a common node with the discarded element j_{sc} . This phase is needed in order to restore the property equations validity.

The matrix \mathbf{C} is assembled in the same way it was done for open profiles, but with the difference that, as happened for the matrix \mathbf{A} , the N_a elements j_{sc} that have been discarded don't have to be considered. Finally the matrix has dimensions $(2(N_e - N_a) + 2) \times (N_n + 2)$.

The vector \mathbf{R} is also assembled in two phases:

- i) In a first time the vector is written as illustrated in (3.57) for the open profiles, but discarding the j_{sc} elements;
- ii) in a second time the terms corresponding to the elements making part of a closed cell are corrected considering the cell parameters ψ_i . For each element considered, with the exception of the discarded elements, the following term is calculated:

$$r'_j = \psi_j \frac{l_j}{t_j} \quad (3.92)$$

and then subtracted to the correspondent term of the vector \mathbf{R} , which has $(N_e - N_a + 3)$ elements. If the corresponding element is clockwise directed, the term r'_j has to be add instead of subtracted. If the element belongs to two cells, the term r'_j is calculated as follows:

$$r'_j = \psi_{a1} \frac{l_j}{t_j} + \psi_{a2} \frac{l_j}{t_j} \quad (3.93)$$

being ψ_{a1} and ψ_{a2} the parameters of the two cells above mentioned.

When all the quantities are corrected the solving system can be developed numerically. Notice that this method permits the calculation of the warping parameter, as expressed by the (3.82), with respect to the shear center. If a warping parameter calculated with respect to another point located in the cross-section is needed, the transformation formulae (3.49) can be used.

Examples

Four examples will be illustrated in order to show the data input and output of the numerical code suggested for the section properties evaluation. The first two examples consider open section layouts, while the third and the last example are developed for closed section profiles.

Open section with three branches

The cross-section in figure 3.11 is considered, the data input for the computer code simulation are summarized by table 3.3.

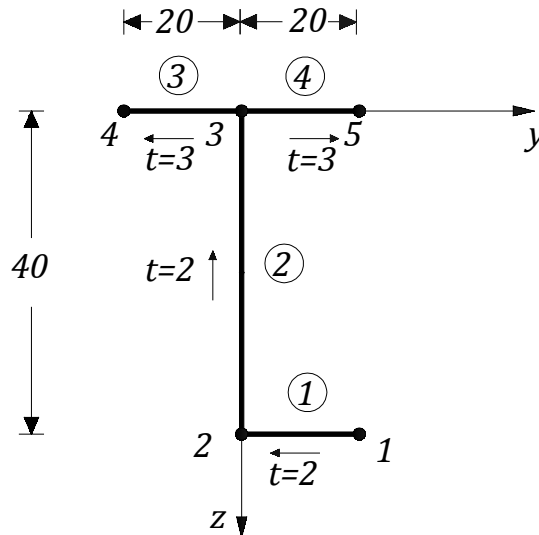


Figure 3.11 – Sketch of the three-branches open section.

Table 3.3 - Section data input of the code assembled.

Input data file: SECTION PROPERTIES	
NODES	ELEMENTS
5	4
1,20,40	1,1,2,2
2,0,40	2,2,3,2
3,0,0	3,3,4,3
4,-20,0	4,3,5,3
5,20,0	

The evaluation of the warping function along the cross-section profile involves the geometric matrix \mathbf{A} , the connectivity matrix \mathbf{C} and the \mathbf{R} vector, that are illustrated by (Attard, 1987) as reference for this example.

The results obtained are summarized in table 3.4. In figure 3.12 is shown the distribution of the warping function along the element walls.

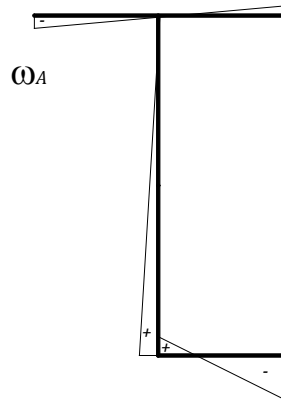


Figure 3.12 - Warping function distribution.

Table 3.4 – Section data output of the code assembled.

<i>Output data file: SECTION PROPERTIES [cm]</i>			
NODE	COORD. X	COORD. Y	TORSIONAL PROPERTIES OF THE SECTION:
1	20.0000	40.0000	Open profile
2	0.0000	40.0000	AK 520.000
3	0.0000	0.0000	I _{ww} 0.39153E+07
4	-20.0000	0.0000	
5	20.0000	0.0000	
NR.ELEMENTS= 4			OMEGA FUNCTION AT NODES:
ELEMENT	NODE 1	NODE 2	NODE OMEGA
1	1	2	1 -0.47059E+03
2	2	3	2 0.20706E+03
3	3	4	3 -0.18824E+02
4	3	5	4 -0.14118E+03
			5 0.10353E+03
PRINCIPAL PROPERTIES OF THE SECTION:			SHEAR CENTER COORDINATES:
AREA	240.0000		YA
YC	1.6667		-0.56471E+01
ZC	13.3333		ZA
AIY	64103.3333		0.61176E+01
AIZ	20693.3333		
AIYZ	10666.6667		

Double-T section of a bridge deck

The cross-section in figure 3.13 is considered. This is the cross-section that in the next chapters of the text will be considered as example of bridge deck's profile.

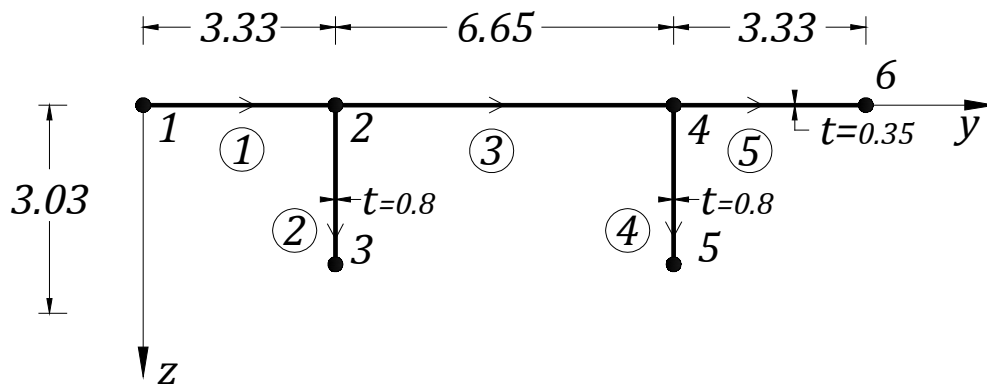


Figure 3.13 – Sketch of the double-T bridge deck section.

The data input for the computer code simulation are summarized by table 3.5.

Table 3.5 - Section data input of the code assembled.

<i>Input data file: SECTION PROPERTIES [m]</i>	
NODES	ELEMENTS
6	5
1,0,0	1,1,2,0.35
2,3.33,0	2,2,3,0.8
3,3.33,3.03	3,2,4,0.35
4,9.98,0	4,4,5,0.8
5,9.98,3.03	5,4,6,0.35
6,13.31,0	

The results obtained are summarized in table 3.6.

Table 3.6 – Section data output of the code assembled.

Output data file: SECTION PROPERTIES [m]			
NODE	COORD. X	COORD. Y	TORSIONAL PROPERTIES OF THE SECTION:
1	0.0000	0.0000	Open profile
2	3.3300	0.0000	AK 1.1647
3	3.3300	3.0300	I _{ww} 0.11014E+03
4	9.9800	0.0000	
5	9.9800	3.0300	
6	13.3100	0.0000	
NR.ELEMENTS= 5			OMEGA FUNCTION AT NODES:
ELEMENT	NODE 1	NODE 2	THICKNESS
1	1	2	0.35000E+00
2	2	3	0.80000E+00
3	2	4	0.35000E+00
4	4	5	0.80000E+00
5	4	6	0.35000E+00
PRINCIPAL PROPERTIES OF THE SECTION:			SHEAR CENTER COORDINATES:
AREA	9.5065		YA
YC	6.6550		0.6655E+01
ZC	0.7726		ZA
AIY	9.1618		-0.6636E+01
AIZ	122.3711		
AIYZ	0.0000		

In figure 3.14 is shown the distribution of the warping function along the element walls of the double-T section.

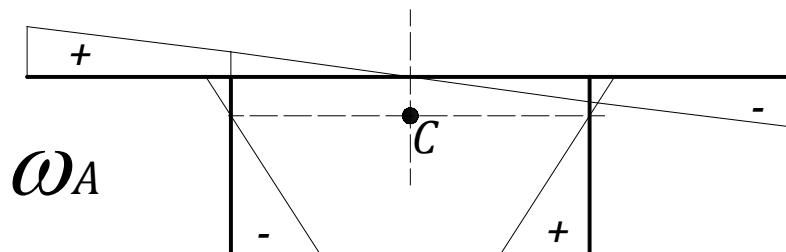


Figure 3.14 – Warping function distribution.

Box section of a bridge deck

A box section of a bridge deck is considered, as shown in figure 3.15. This is the box cross-section that in the next chapters of the text will be considered as example of bridge deck's profile.

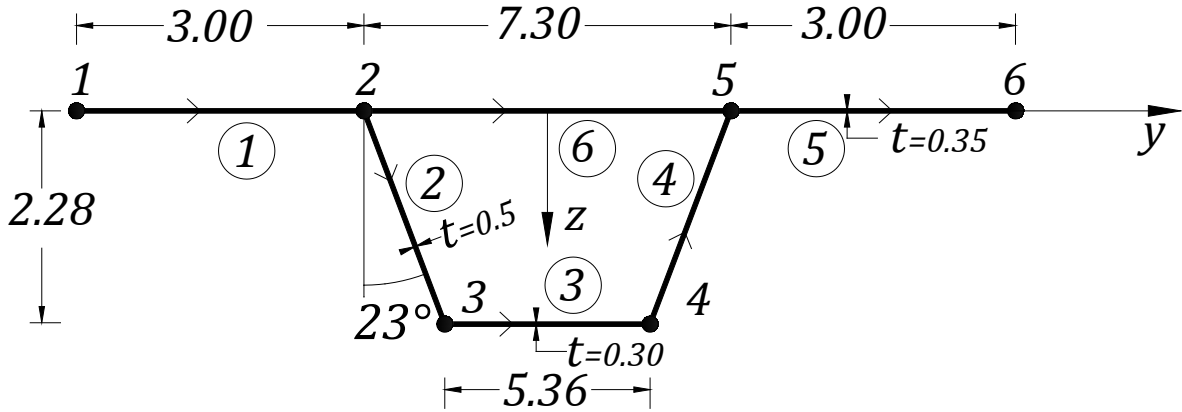


Figure 3.15 – Box section of a bridge deck [m].

The constant ψ for the closed cell is 0.5935 and the data input are shown in table 3.7.

Table 3.7 - Section data input of the code assembled.

<i>Input data file: SECTION PROPERTIES [m]</i>	
NODES	ELEMENTS
6	6
1,-6.65,0	1,1,2,0.35
2,-3.65,0	2,2,3,0.5
3,-2.68,2.28	3,3,4,0.3
4,2.68,2.28	4,4,5,0.5
5,3.65,0	5,5,6,0.35
6,6.65,0	6,2,5,0.35

The results obtained are summarized in table 3.8.

Table 3.8 – Section data output of the code assembled.

Output data file: SECTION PROPERTIES [m]			
NODE	COORD. X	COORD. Y	TORSIONAL PROPERTIES OF THE SECTION:
1	-6.6500	0.0000	Closed profile
2	-3.6500	0.0000	AK 17.1392
3	-2.6800	2.2800	I _{ww} 12.04
4	2.6800	2.2800	
5	3.6500	0.0000	
6	6.6500	0.0000	
NR.ELEMENTS= 6			OMEGA FUNCTION AT NODES:
ELEMENT	NODE 1	NODE 2	THICKNESS
1	1	2	0.35000E+00
2	2	3	0.50000E+00
3	3	4	0.30000E+00
4	4	5	0.50000E+00
5	5	6	0.35000E+00
6	2	5	0.35000E+00
PRINCIPAL PROPERTIES OF THE SECTION:			OMEGA
AREA	8.7412		1 -0.17140E+01
YC	6.6550		2 0.18514E+01
ZC	0.7428		3 -0.23766E+01
AIY	7.8350		4 0.23766E+01
AIZ	97.5001		5 -0.18514E+01
AIYZ	0.0000		6 0.17140E+01
PRINCIPAL PROPERTIES OF THE SECTION:			SHEAR CENTER COORDINATES:
			YA
			0.0000E+01
			ZA
			0.119E+01

In figure 3.16 is shown the distribution of the warping function along the element walls of the box section.

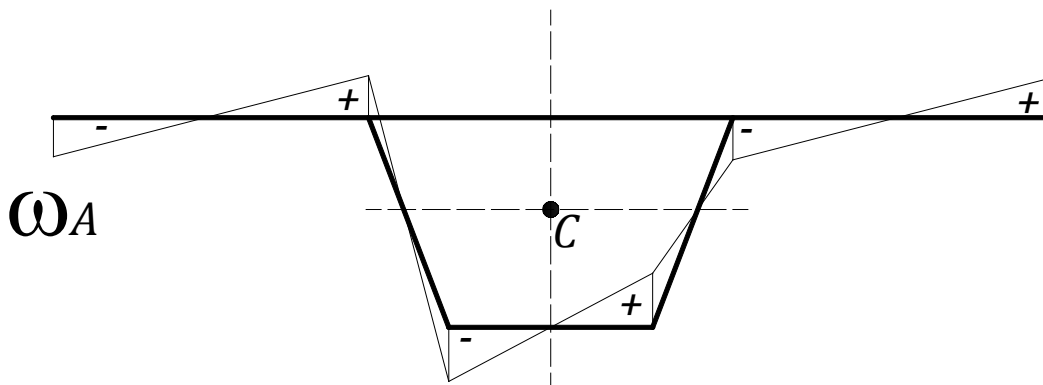


Figure 3.16 - Warping function distribution.

Two-boxes section of a bridge deck

A two-celled profile is considered in this example, as shown in figure 3.17.

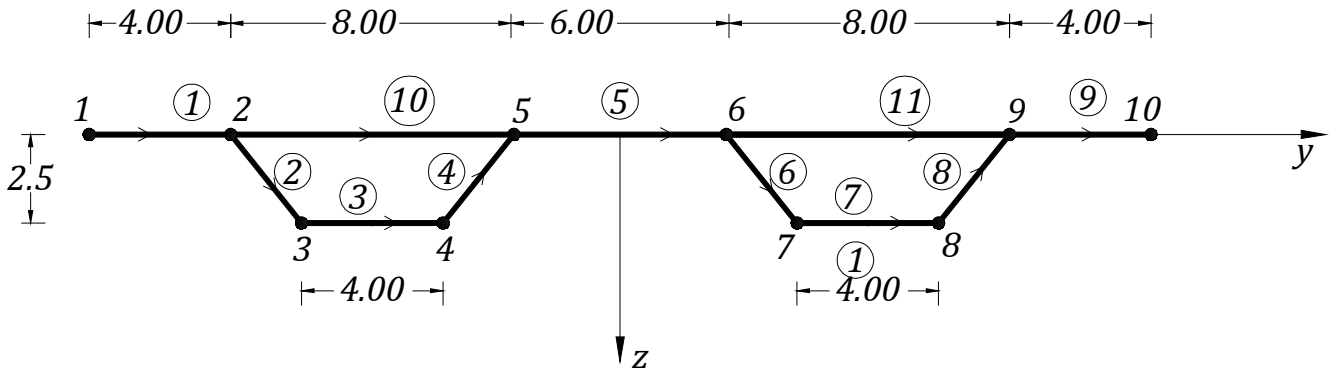


Figure 3.17 – Two-cells section of a bridge deck [m].

The constant ψ for the closed cell is calculated as 0.024452 and the data input are shown in table 3.9.

Table 3.9 - Section data input of the code assembled.

Input data file: SECTION PROPERTIES	
NODES	ELEMENTS
10	11
1,-15.00,0	1,1,2,0.015
2,-11.00,0	2,2,3,0.015
3,-9.00,2.50	3,3,4,0.015
4,-5.00,2.50	4,4,5,0.015
5,-3.00,0	5,5,6,0.015
6,3.00,0	6,6,7,0.015
7,5.00,2.50	7,7,8,0.015
8,9.00,2.50	8,8,9,0.015
9,11.00,0	9,9,10,0.015
10,15.00,0	10,2,5,0.015
	11,6,9,0.015

The results obtained are summarized in table 3.10.

Table 3.10 – Section data output of the code assembled.

<i>Output data file: SECTION PROPERTIES [m]</i>			
NODE	COORD. X	COORD. Y	TORSIONAL PROPERTIES OF THE SECTION:
1	-15.0000	0.0000	Closed profile
2	-11.0000	0.0000	AK 1.4672
3	-9.0000	2.5000	Iww 46.9586
4	-5.0000	2.5000	
5	-3.0000	0.0000	
6	3.0000	0.0000	
7	5.0000	2.5000	
8	9.0000	2.5000	
9	11.0000	0.0000	
10	15.0000	0.0000	
NR.ELEMENTS= 5			OMEGA FUNCTION AT NODES:
ELEMENT	NODE 1	NODE 2	THICKNESS
1	1	2	0.15000E-01
2	2	3	0.15000E-01
3	3	4	0.15000E-01
4	4	5	0.15000E-01
5	5	6	0.15000E-01
6	6	7	0.15000E-01
7	7	8	0.15000E-01
8	8	9	0.15000E-01
9	9	10	0.15000E-01
10	2	5	0.15000E-01
11	6	9	0.15000E-01
PRINCIPAL PROPERTIES OF THE SECTION:			SHEAR CENTER COORDINATES:
AREA	0.7621		YA
YC	0.0000		0.0000E+01
ZC	0.7087		ZA
AIY	0.7.674		0.04674E+01
AIZ	50.9955		
AIYZ	0.0000		

In figure 3.18 is shown the distribution of the warping function along the element walls of the two-boxes section.

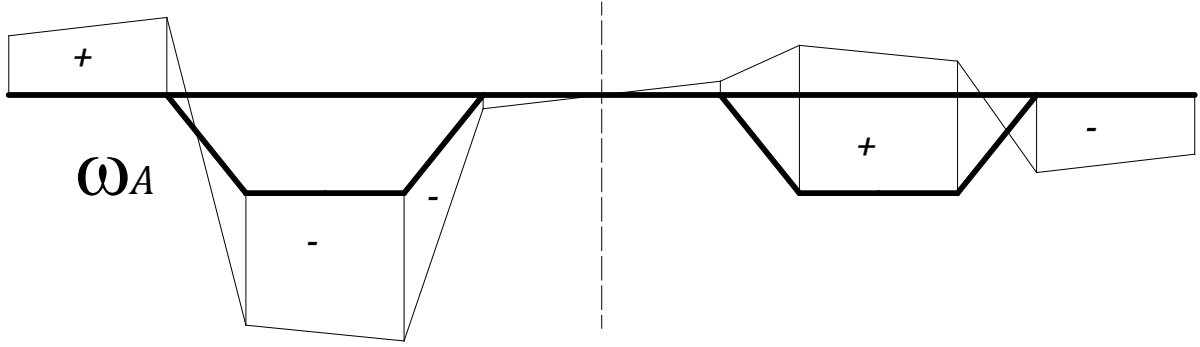


Figure 3.18 - Warping function distribution.

3.1.6. Kinetic energy formulation

The beam kinetic energy is defined as follows

$$T = \int_V \frac{1}{2} \dot{\mathbf{u}}^T \rho \dot{\mathbf{u}} dV \quad (3.94)$$

being the corresponding energy per unit volume defined as

$$\frac{1}{2} \dot{\mathbf{u}}^T \rho \dot{\mathbf{u}} = \frac{1}{2} \rho (\dot{u}_x^2 + \dot{u}_y^2 + \dot{u}_z^2) \quad (3.95)$$

The general expression per unit length is obtained by integration of (3.95) and substituting the velocities $\dot{u}_x, \dot{u}_y, \dot{u}_z$ from their definition in section 3.1.1. The dots define integration over the time t and $\rho [kg/m^3]$ is the mass per unit volume of the material.

Axial kinematic energy component

The axial component of the kinetic energy is defined as follows

$$\begin{aligned} \frac{1}{2} \rho (\dot{u}_x^2) &= \frac{1}{2} \rho \left(\dot{\eta} - (y - y_c) \dot{\xi}_y' - (z - z_c) \dot{\xi}_z' - \omega(s) \dot{\phi}' \right)^2 \\ &= \frac{1}{2} \rho (\dot{\eta}^2 - \dot{\eta} (y - y_c) \dot{\xi}_y' - \dot{\eta} (z - z_c) \dot{\xi}_z' - \dot{\eta} \omega(s) \dot{\phi}' \\ &\quad - (y - y_c) \dot{\xi}_y' \dot{\eta} + \left((y - y_c) \dot{\xi}_y' \right)^2 + (y - y_c) (z - z_c) \dot{\xi}_y' \dot{\xi}_z' + (y - y_c) \omega(s) \dot{\xi}_y' \dot{\phi}' \\ &\quad - (z - z_c) \dot{\xi}_z' \dot{\eta} + (z - z_c) (y - y_c) \dot{\xi}_z' \dot{\xi}_y' + \left((z - z_c) \dot{\xi}_z' \right)^2 + (z - z_c) \omega(s) \dot{\xi}_z' \dot{\phi}' \\ &\quad - \omega(s) \dot{\phi}' \dot{\eta} + \omega(s) (y - y_c) \dot{\phi}' \dot{\xi}_y' + \omega(s) (z - z_c) \dot{\phi}' \dot{\xi}_z' + (\omega(s) \dot{\phi}')^2) \end{aligned} \quad (3.96)$$

The axial kinetic energy is composed by the contribution of *extension*, *bending* and *torsion* given the warping of the cross-section.

In-plane kinematic energy components

Kinematic quantities u_y, u_z also generate kinetic energy contribution. If eq.(3.1) and eq.(3.2) are considered is possible to obtain

$$\frac{1}{2}\rho(u_y'^2 + u_z'^2) = \frac{1}{2}\rho \left(\xi_y'^2 - 2\xi_y'(z - z_P)\dot{\phi} + ((z - z_P)\dot{\phi})^2 + \xi_z'^2 + 2\xi_z'(y - y_P)\dot{\phi} + ((y - y_P)\dot{\phi})^2 \right) \quad (3.97)$$

In this part of the energy expression Saint Venant kinetic energy of shear is taken into account by the terms involving rigid rotation around the generic point P.

Total kinetic energy per unit length

The integration over the cross-section of the eq.(3.96) and (3.97) leads to the energy C per unit length of the beam, which allows to obtain the beam kinetic energy written as follows:

$$T = \int_0^L C(\dot{\eta}, \xi_y', \xi_z', \dot{\phi}, \xi_y'', \xi_z'', \dot{\phi}') dx \quad (3.98)$$

where

$$\begin{aligned} C(\dot{\eta}, \xi_y', \xi_z', \dot{\phi}, \xi_y'', \xi_z'', \dot{\phi}') = & \\ & \frac{1}{2}\rho(A\dot{\eta}^2 - S_y\dot{\eta}\xi_y'' - S_z\dot{\eta}\xi_z'' - S_\omega\dot{\eta}\dot{\phi}') \\ & - S_y\xi_y'\dot{\eta} + I_y\xi_y''^2 + I_{yz}\xi_y'\xi_z'' + I_{y\omega}\xi_y'\dot{\phi}' \\ & - S_z\xi_z'\dot{\eta} + I_{zy}\xi_z'\xi_y'' + I_z\xi_z''^2 + I_{z\omega}\xi_z'\dot{\phi}' \\ & - S_\omega\dot{\phi}'\dot{\eta} + I_{\omega y}\dot{\phi}'\xi_y'' + I_{\omega z}\dot{\phi}'\xi_z'' + I_{\omega\omega}\dot{\phi}'^2 \\ & + A\xi_y'^2 - 2\xi_y'S_z^P\dot{\phi} + I_z^P\dot{\phi}^2 \\ & + A\xi_z'^2 + 2\xi_z'S_y^P\dot{\phi} + I_y^P\dot{\phi}^2 \end{aligned} \quad (3.99)$$

Notice that in (3.99) all the coupling terms are considered. The geometric moments of inertia refer to the same generic point P . The uncoupling in terms of the kinetic energy defined in (3.99) is similar to the static case and corresponds to in-plane twist around the shear center while bending and axial effect are considered in relation to the elastic center.

3.2. Static analysis

In 3.1 the potential energy of a thin-walled beam of general cross-section was formulated and two particular points have been identified in the cross-section plan, the *elastic center* and the *shear center*. When the deformation of a beam is described considering these two points, axial effect, bending and torsion of the beam are uncoupled. In the following this uncoupled expression for the deformation field is adopted, in order to simplify the expression of equilibrium equations.

The equilibrium equations and corresponding static boundary conditions are derived in 3.2.1 for extension, bending and torsion considering the potential energy of the beam.

Solution of simple torsion problems are described for various load types and depending from the cross-section shape. The influence of warping is defined in terms of section stiffness showing differences between closed and open sections.

3.2.1. Equilibrium and stresses

The potential energy density per unit length is expressed in terms of the generalized displacements and their derivatives as already specified by the function $F(\eta, \eta', \varphi, \varphi', \varphi'', \xi_y, \xi_z, \xi'_y, \xi'_z, \xi''_y, \xi''_z)$. In eq.(3.39) a function of functions is called a *functional*, and the approach that will be used for developing the equilibrium equations is based on *variational principles*. The displacement functions will be obtained by examining how the functional varies as these functions change, taking into account infinitesimal variations. The solution for each generalized displacement satisfies the kinematic boundary conditions and gives the minimum value of $V(\eta, \eta', \varphi, \varphi', \varphi'', \xi_y, \xi_z, \xi'_y, \xi'_z, \xi''_y, \xi''_z)$. This is called the theorem of *minimum potential energy* and allows to obtain a set of differential equations, which correspond to the solution of the equilibrium in their *strong form*.

The potential energy will refer to the elastic center (y_c, z_c) and to the shear center (y_a, z_a) and is presented in its uncoupled form. Therefore, axial effect, bending and torsion can be treated separately, and all the coupling geometric quantities will vanish.

Axial effect

The generalized displacement $\eta(x)$ describe the axial extension of the beam. The associated potential energy is given by

$$V(\eta, \eta') = \int_0^L \left(\frac{1}{2} \eta' EA \eta' - q_x \eta \right) dx \quad (3.10)$$

The corresponding variation in the functional is denoted by $\delta V(\eta)$, which is defined by

$$\delta V(\eta) = V(\eta(x) + \delta\eta(x)) - V(\eta(x)) = \int_0^L (\eta' EA \delta\eta' - q_x \delta\eta) dx + \int_0^L \frac{1}{2} \delta\eta' EA \delta\eta' dx \quad (3.10)$$

The third term is a second order term and can be neglected because $\delta\eta$ is small. Thus the condition of minimum potential energy implies that $\delta V(\eta) = 0$, allowing to derive the following equation

$$\int_0^L (\eta' EA \delta\eta' - q_x \delta\eta) dx = 0 \quad (3.10)$$

At the minimum of $V(\eta)$ the first variation of the functional must vanish for the arbitrary variations $\delta\eta(x)$ that satisfy the kinematic boundary conditions. This is expressed as $\delta V(\eta) = 0$. The integral (3.102) is reformulated via integration by parts, whereby the derivative $\delta\eta'$ is integrated, and gives

$$\delta V(\eta) = [\eta' EA \delta\eta]_0^L - \int_0^L \delta\eta [(\eta' EA)' + q_x] dx = 0 \quad (3.10)$$

The first term in (3.103) is the boundary condition, defined for each end of the beam. The boundary forces satisfies the global equilibrium of the beam and thus $[\eta' EA \delta\eta]_0^L = 0$. In the integral, for arbitrary variations $\delta\eta(x)$ the term in brackets must vanish everywhere in order to verify the vanishing of δV . This allows to obtain the differential equation that corresponds to the extension equilibrium

$$\frac{d}{dx} \left(EA \frac{d\eta}{dx} \right) + q_x = 0 \quad (3.10)$$

The boundary terms are in the form of a product of the variation of the axial displacement $\delta\eta$ and a factor easily identified as the normal force

$$N = \int_A \sigma_x dA = EA \frac{d\eta}{dx} \quad (3.10 \quad 5)$$

When the normal force given by (3.105) is introduced into (3.104), the equilibrium equation for the extension is

$$\frac{dN}{dx} + q_x = 0 \quad (3.10 \quad 6)$$

This is the equilibrium equation for the beam extension problem, where the axial stiffness of the beam EA is supposed to be constant along the beam axis.

Bending

The bending problem is treated with the same approach. The only differences are that in this case there are two displacement components (ξ_y, ξ_z) and that also their second derivatives must be taken into account in the definition of the strain energy.

The associated potential energy is

$$V(\xi_\gamma, \xi_\gamma', \xi_\gamma'') = \int_0^L \left(\frac{1}{2} \xi''_\alpha EI_{\alpha\beta} \xi''_\beta - (q_\alpha \xi_\alpha - m_\alpha \xi'_\alpha) \right) dx \quad (3.10 \quad 7)$$

The use of the subscript γ in eq.(3.107) is to indicate the two components (ξ_y, ξ_z) and to avoid any relation to the subscripts α and β . The repeated subscripts α and β imply summation over $\alpha = y, z$ and $\beta = y, z$. This form is complete for the bending problem: simplifications of potential expression occur if the y, z axis are the principal axes with origin at the elastic center.

The first variation of $V(\xi_\gamma, \xi_\gamma', \xi_\gamma'')$ is the linear part of the difference $V(\xi_\gamma(x) + \delta\xi_\gamma(x)) - V(\xi_\gamma(x))$ and can be written as follows

$$\delta V(\xi_\gamma) = \int_0^L \left(\delta \xi''_\alpha EI_{\alpha\beta} \xi''_\beta - (-m_\alpha \delta \xi'_\alpha + q_\alpha \delta \xi_\alpha) \right) dx \quad (3.10 \quad 8)$$

The first term is integrated twice by parts and the second term is integrated once. The result is the following

$$\delta V(\xi_\gamma) = \left[\delta \xi'_\alpha (EI_{\alpha\beta} \xi''_\beta) - \delta \xi_\alpha (EI_{\alpha\beta} \xi''_\beta)' + \delta \xi_\alpha m_\alpha \right]_0^L + \int_0^L \delta \xi_\alpha \left((EI_{\alpha\beta} \xi''_\beta)'' - m_\alpha' - q_\alpha \right) dx \quad (3.10 \quad 9)$$

The stationarity condition imposes $\delta V(\xi_\gamma) = 0$ and implies that the factor $\delta \xi_\gamma = (\delta \xi_y, \delta \xi_z)$ must vanish identically over the length of the beam, therefore:

$$\frac{d^2}{dx^2} \left(EI_{\alpha\beta} \frac{d^2 \xi_\beta}{dx^2} \right) - \frac{dm_\alpha}{dx} - q_\alpha = 0, \quad \alpha = y, z \quad (3.11 \quad 0)$$

This differential equation represents the solution for the flexural problem in the principal direction. Note that eq. (3.110) is a vector equation with two components.

In this case the boundary terms in eq. (3.109) identify the bending moments M_α and the shear forces V_α , with their contribution to the virtual work by the rotations $-\delta \xi'_\alpha$ and the displacements $\delta \xi_\alpha$, respectively. Thus the first boundary term identifies the bending moments

$$M_\alpha = -EI_{\alpha\beta} \frac{d^2 \xi_\beta}{dx^2}, \quad \alpha = y, z \quad (3.11 \quad 1)$$

while the second and third boundary terms identify the shear forces

$$V_\alpha = -\frac{d}{dx}\left(EI_{\alpha\beta}\frac{d^2\xi_\beta}{dx^2}\right) + m_\alpha, \quad \alpha = y, z \quad (3.11 \quad 2)$$

Substituting the eq.(3.111) in the eq.(3.112) and then eq.(3.112) in eq.(3.110) the equilibrium equations of the bending problem are expressed in terms of statics as

$$V_\alpha = \frac{dM_\alpha}{dx} + m_\alpha, \quad \alpha = y, z \quad (3.11 \quad 3)$$

$$\frac{dV_\alpha}{dx} + q_\alpha = 0, \quad \alpha = y, z \quad (3.11 \quad 4)$$

Torsion

For the formulation of the equilibrium equations the torsion problem is described in terms of the angle of twist $\varphi(x)$ around the axis of the cross-section shear centers (y_α, z_α) . The potential energy expression leads to

$$V(\varphi, \varphi', \varphi'') = \int_0^L \frac{1}{2} (\varphi'' EI_{\omega\omega} \varphi'' + \varphi' GK \varphi' - (m_\varphi \varphi - b \varphi')) dx \quad (3.11 \quad 5)$$

being the first variation of $V(\varphi)$ written as follows

$$\delta V(\varphi) = \int_0^L (\delta \varphi'' EI_{\omega\omega} \varphi'' + \delta \varphi' GK \varphi' + b \delta \varphi' - m_\varphi \delta \varphi) dx \quad (3.11 \quad 6)$$

After the integration by parts the first variation takes the form

$$\begin{aligned} \delta V(\varphi) = & [\delta \varphi' (EI_{\omega\omega} \varphi'') - \delta \varphi (EI_{\omega\omega} \varphi'')]_0^L + \delta \varphi GK \varphi' + \delta \varphi b]_0^L \\ & + \int_0^L \delta \varphi ((EI_{\omega\omega} \varphi'')'' - (GK \varphi')' - b' - m_\varphi) dx \end{aligned} \quad (3.11 \quad 7)$$

The stationary condition implies the vanishing of the integral term in brackets of the equation (3.117) for arbitrary values of $\delta \varphi(x)$. This gives the differential equation of torsion

$$\frac{d^2}{dx^2} \left(EI_{\omega\omega} \frac{d^2 \varphi}{dx^2} \right) - \frac{d}{dx} \left(GK \frac{d\varphi}{dx} \right) - \frac{db}{dx} - m_\varphi = 0 \quad (3.11 \quad 8)$$

The boundary term in (3.117) multiplied by $-\delta \varphi'$ identifies the *bimoment* as

$$M_\omega = -EI_{\omega\omega} \frac{d^2 \varphi}{dx^2} \quad (3.11 \quad 9)$$

The *torsion moment* is obtained by taking into account all the terms in eq.(3.117) that correspond to the virtual work when multiplied by $\delta \varphi$

$$T = -\frac{d}{dx} \left(EI_{\omega\omega} \frac{d^2 \varphi}{dx^2} \right) + GK \frac{d\varphi}{dx} + b \quad (3.12 \quad 0)$$

Three contributions constitute the torsion moment: the *warping moment*, the *Saint Venant moment* and the externally applied distributed bimoment b :

$$\text{Warping torsion: } T_\omega = \frac{dM_\omega}{dx} = -\frac{d}{dx} \left(EI_{\omega\omega} \frac{d^2 \varphi}{dx^2} \right) \quad (3.12 \quad 1)$$

$$\text{Saint Venant torsion: } T_S = GK \frac{d\varphi}{dx} \quad (3.12 \quad 2)$$

Finally, substituting eq.(3.121) and eq.(3.122) in eq.(3.120) the torsion moment is

$$T = T_{\omega} + T_S + b \quad (3.123)$$

Substituting the eq.(3.120) in eq.(3.118) the second equilibrium equation for torsion is obtained

$$\frac{dT}{dx} + m_{\varphi} = 0 \quad (3.124)$$

Boundary conditions

The seven equilibrium equations have been defined considering extension, bending and torsion within the context of the theory of thin-walled beams. Seven boundary conditions, corresponding to the number of the degrees of freedom, are required for each end point of the beam for solving the static problem.

There are two basic forms of the boundary conditions. A *kinematic* boundary condition assigns a prescribed value to one of the seven general displacements. Alternatively a *static* boundary condition allows an arbitrary value of displacement but the corresponding static quantity must equal an external load at the same point.

In table 3.11 equilibrium equations obtained and boundary conditions quantities are shown for extension, bending and torsion.

Table 3.11 – Equilibrium equations and boundary conditions.

	Equation	Kinematic	Static
Extension	$\frac{dN}{dx} + q_x = 0$	η	N
Bending	$V_y = \frac{dM_y}{dx} + m_y$ $\frac{dV_y}{dx} + q_y = 0$	$\xi_y, -\xi'_y$	V_y, M_y
	$V_z = \frac{dM_z}{dx} + m_z$ $\frac{dV_z}{dx} + q_z = 0$	$\xi_z, -\xi'_z$	V_z, M_z
Torsion	$T = T_{\omega} + T_S + b$ $\frac{dT}{dx} + m_{\varphi} = 0$	φ, φ'	T, M_{ω}

Note that for non-symmetrical cross-sections the elastic center axis and shear center axis could not coincide. This means that the differential governing equations mentioned above are referred to two different x -axis. For example, in a C cross-section all the displacements and forces are illustrated in figure 3.19 and figure 3.20 where is shown that only the choice of two different axis serves to uncoupling the bending and the extension of the beam from its torsion behavior.

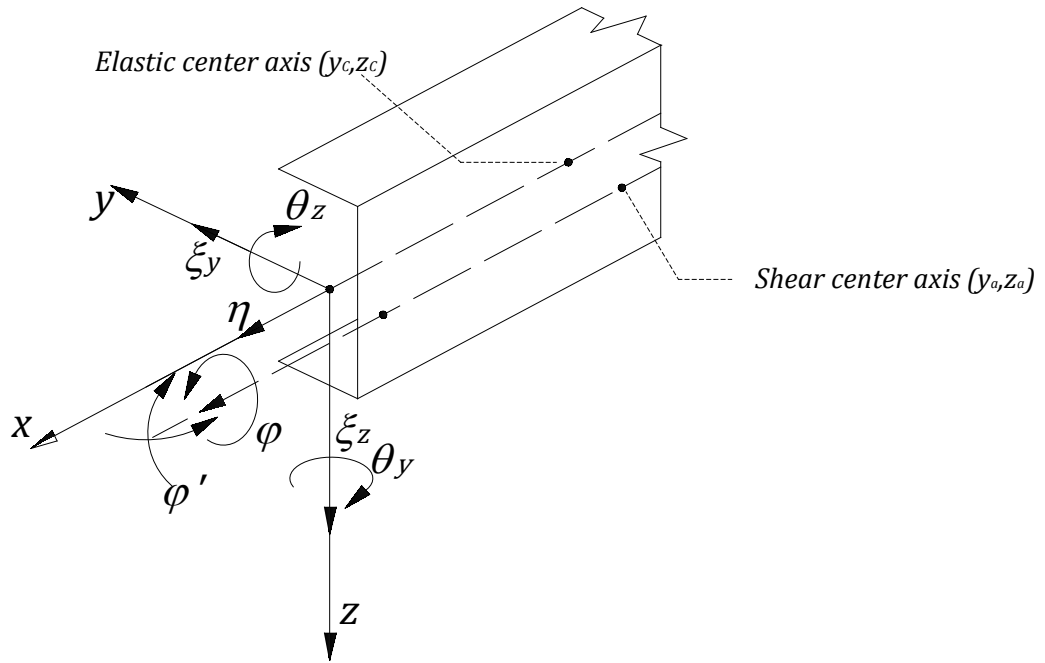


Figure 3.19 – Generalized displacements of a C cross-section beam.

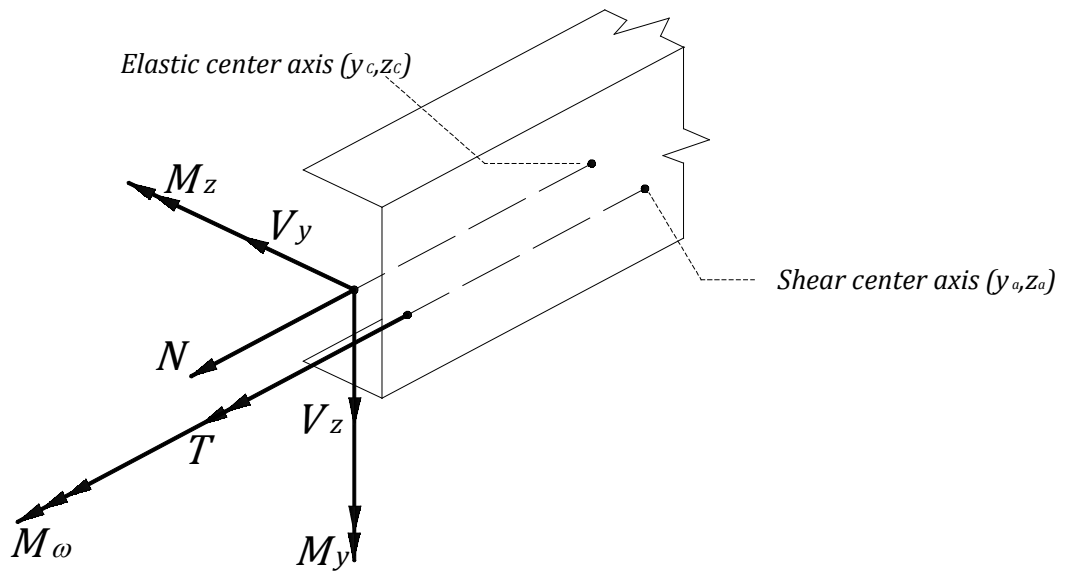


Figure 3.20 – Forces in a C cross-section beam.

3.2.3. Basic load cases

With the appropriate axes adopted for the decoupling of the equilibrium equations, extension, bending and torsion can be treated independently. The solutions techniques for Euler-Bernoulli theory applied on beams are assumed to be well known. Thus, only the non-homogeneous torsion problem is treated in this section and basic load cases are presented.

The general solution for the mathematical problem is extended to a finite length bar and is developed for solving practical problems of continuous beam spans by superposition of the particular and the general solution.

For each load case, the relative influence of warping is set by a particular parameter that is different for each different type of cross-section analyzed. Three common types of cross-section layouts are compared, in order to explore the main torsion stiffness of each one of these when loaded by torsion moments.

All the solutions presented are taken from (Kollbrunner & Basler, 1969).

Mixed-Torsion

The equation (3.118) is a differential equation of fourth order where the externally applied torque per unit length m is positive when applied in the positive φ -sense and no externally bimoment b is considered. Notice that the following theory is restricted to prismatic members so this linear differential equation is expressed for constant coefficients $EI_{\omega\omega}$ and GK . With this hypothesis, equation (3.118) can be written as follows

$$EI_{\omega\omega}\varphi^{iv} - GK\varphi'' = m \quad (3.125)$$

The solution for the homogeneous part of the differential equation (3.125) is of the form:

$$\varphi = C_1 + C_2 \frac{x}{d} + C_3 \sinh \beta \frac{x}{d} + C_4 \cosh \beta \frac{x}{d} \quad (3.126)$$

The C_1, C_2, C_3 and C_4 are the constants of integration that must be determined so as to satisfy the particular boundary conditions of the problem. For any beam there are two boundary conditions for each end, and with these four conditions it is possible to obtain the angle of twist of the bar at any cross-section along x direction.

Constant d is labelled the *torsion bending constant*, and could represent a “characteristic length”

$$d = \sqrt{\frac{EI_{\omega\omega}}{GK}} \quad (3.127)$$

If $x \ll d$ the influence of Saint Venant Torsion can be neglected because of the warping effect and eq.(3.126) becomes

$$\varphi = C_3 \sinh \beta \frac{x}{d} + C_4 \cosh \beta \frac{x}{d} \quad (3.128)$$

If $x \gg d$ Saint Venant strain is predominant on the cross section and the warping effect is negligible. So the expression of φ is composed only by the constant and linear term

$$\varphi = C_1 + C_2 \frac{x}{d} \quad (3.129)$$

Solution for a Bar of Finite Length L

It is appropriate for continuous bars to consider the solution of the angle of twist defined in terms of *hyperbolic functions*, with the coordinate x normalized by means of the bar length L . So the solution will be independent of the bar length and a new non-dimensional characteristic value is obtained

$$\kappa = \sqrt{\frac{GK \cdot L^2}{EI_{\omega\omega}}} \quad (3.130)$$

The differential equation (3.69) may be written in the following way

$$\varphi^{iv} - \frac{\kappa^2}{L^2} \varphi'' = \frac{m}{EI_{\omega\omega}} \quad (3.131)$$

Now it is useful to represent the solution in terms of a new non-dimensional and normalized coordinate $\xi = x/L$.

Considering a particular solution $\bar{\varphi}$ of the differential equation for each load case, the strain and the stresses could be written as follows

$$\text{Angle of twist } \varphi = C_1 + C_2\xi + C_3 \sinh \kappa\xi + C_4 \cosh \kappa\xi + \bar{\varphi} \quad (3.132)$$

$$\text{Angle of twist per unit length } \varphi' = C_2 \frac{1}{L} + C_3 \frac{\kappa}{L} \sinh \kappa\xi + C_4 \frac{\kappa}{L} \cosh \kappa\xi + \bar{\varphi}' \quad (3.133)$$

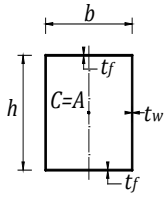
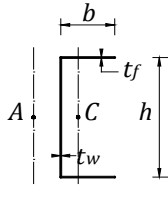
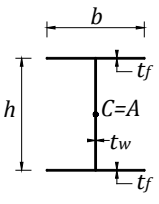
$$\text{Warping moment } M_{\omega} = -GK(C_3 \sinh \kappa\xi + C_4 \cosh \kappa\xi) - EI_{\omega\omega} \bar{\varphi}'' \quad (3.134)$$

$$\text{Torsional moment } T = GK \left(\frac{C_2}{L} + \bar{\varphi}' \right) - EI_{\omega\omega} \bar{\varphi}''' \quad (3.135)$$

Beam cross-sections

Solutions are obtained for three different sections, as shown in Table 3.12, where C is the elastic center and A the shear center

Table 3.12 - Cross-section layouts and position of the elastic and shear center.

			
$b[mm]$	100	100	170
$h[mm]$	360	360	360
$t_w[mm]$	14	14	8
$t_f[mm]$	14	14	12.7

Admitting a beam length of $L=2m$, a different value of the constant κ is obtained for each of the cross-sections analyzed:

- *Closed hollow section:* $b = 100mm$, $h = 360mm$, $t = t_w = t_f = 14mm$, $\kappa_{Hollow\ sec.} = 19.89$.
- *Channel cross Section:* $b = 100mm$, $h = 360mm$, $t = t_w = t_f = 14mm$, $\kappa_{C\ sec.} = 1.5$.
- *I cross Section:* $b = b_{f1} = b_{f2} = 170mm$, $t_f = 12.7mm$, $t_w = 8mm$, $\kappa_{I\ sec.} = 1.19$.

The constant κ is an index of the cross-section behavior with respect to the torsional stiffness. As $\kappa \gg 1$ for the closed hollow section, this means that the torsional response of this cross-section tends to pure Saint-Venant Torsion response. For the channel and I-section $d/L \approx 1$, both warping torsion and Saint Venant torsion have to be taken into account. The difference between a C and I-section is that the first one is mono-symmetric and the shear center does not coincide with the elastic center. In this case when a bending external load is acting on the beam the effect of torsion and bending are coupled. In fact for a C-section the boundary conditions for torsion are referred to the shear center axis. For I-section, the problem of torsion and bending could even be solved as uncoupled because of the coincidence of these two axes.

Boundary conditions

Three examples are presented for the analysis of the mixed torsion problem with different load cases.

Example 3.1: Simply supported beam acted by uniform torque

As first example of beam models the effect of a uniformly distributed torque m on a simply supported bar of length $L = 2m$ will be analyzed, as shown in figure 3.21. In the next S-S will denote a simply supported boundary conditions.

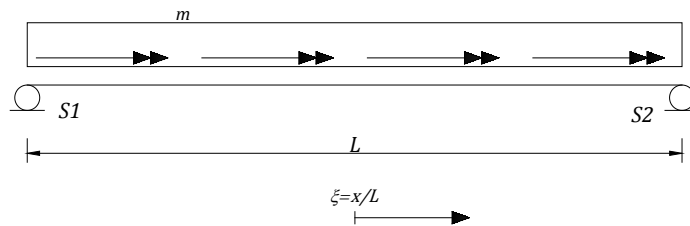


Figure 3.21 – S-S beam ($L=2m$) acted upon uniform torque.

A new coordinate system ξ is introduced by taking advantage of the symmetry of the problem. The coordinate ξ starts at the middle of the span and the solution can now be written in terms of a central coordinate system. The two supports at the ends cannot twist but warping is allowed. So the boundary conditions for each end support can be written as follows

$$S1 \begin{cases} \varphi\left(-\frac{1}{2}\right) = 0 \\ M_{\omega}\left(-\frac{1}{2}\right) = 0 \end{cases} \quad S2 \begin{cases} \varphi\left(+\frac{1}{2}\right) = 0 \\ M_{\omega}\left(+\frac{1}{2}\right) = 0 \end{cases} \quad (3.136)$$

For a load per unit length m the particular solution of the differential equation is $\bar{\varphi} = -\frac{m}{2} \frac{L^2}{GK} \xi^2$.

The normalized values of φ , φ' , M_{ω} and T for the closed, the channel and the I-section are shown in the figure 3.22, figure 3.23, figure 3.24, figure 3.25 for the simply supported beam.

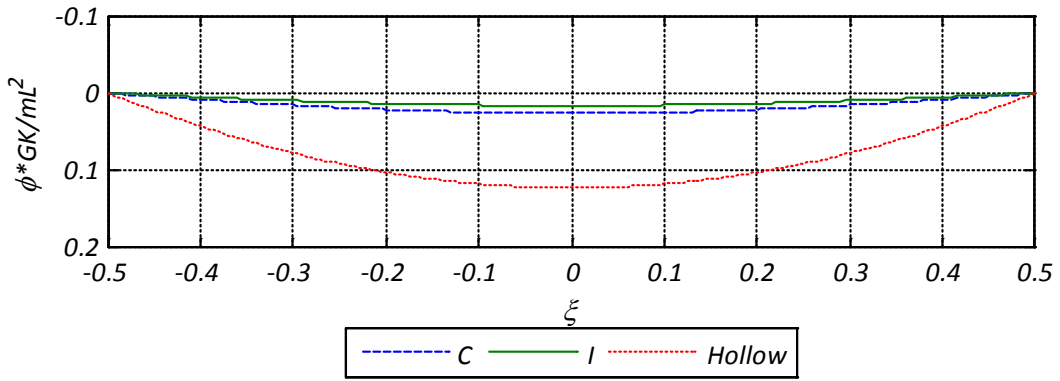


Figure 3.22 - ϕ value of a S-S² beam acted by uniform torque (analytical solution).

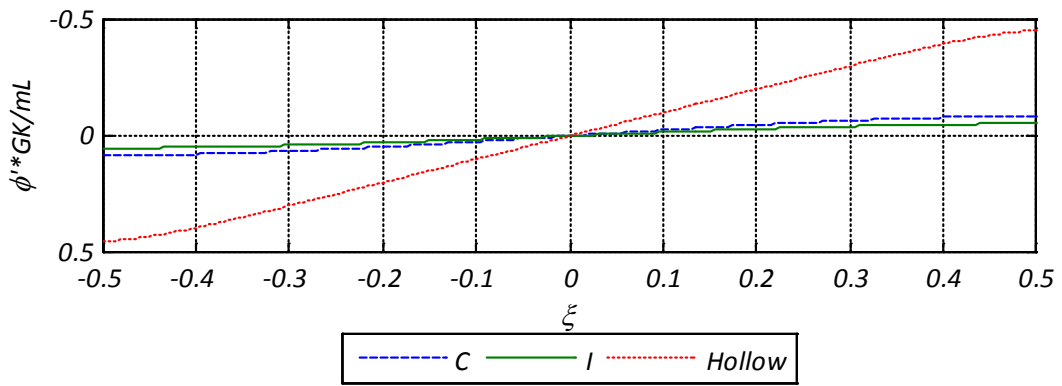


Figure 3.23 - ϕ' value of a S-S beam acted by uniform torque (analytical solution).

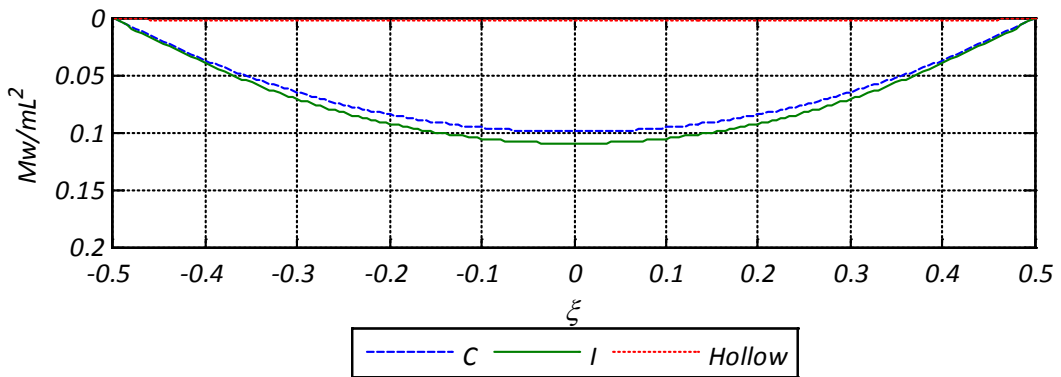


Figure 3.24 - M_ω of a S-S beam acted by uniform torque (analytical solution).

² Simply Supported

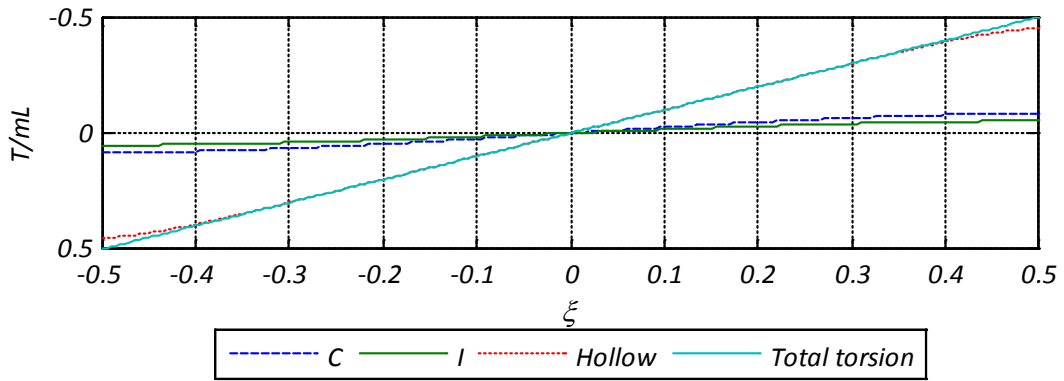


Figure 3.25 – Distribution of the torsion T_S and T of a S-S beam acted by uniform torque (analytical solution).

The normalized twist is proportional to the Saint Venant torsional stiffness GK and, as expectable, the twist of the hollow section achieves values much higher at midspan, while the torsion angle between the two open-sections is of the same order of magnitude (figure 3.22). Note that the first derivative of the twist angle is proportional to the Saint Venant torsion contribution: this means that the torsion moment T of the hollow beam is mainly composed by T_S (figure 3.23 and figure 3.25). On the other hand, the warping of the open sections gives higher values of the warping moments at the beam supports (figure 3.24), and the main torsion contribution of the I and C-beam is the T_ω .

Example 3.2: Simply supported beam acted by concentrated torque

In this example the static and kinematic quantities will be evaluated for a simply supported beam of $2m$ length acted by a concentrated torsional moment at midspan.

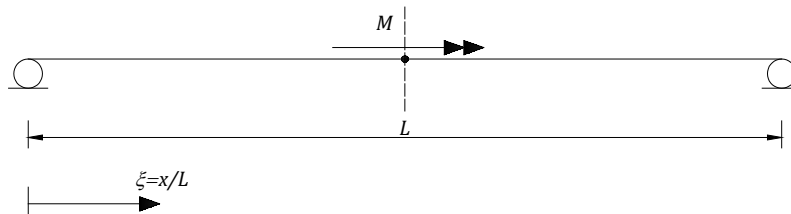


Figure 3.26 – S-S beam ($L=2m$) acted upon concentrated torque at midspan.

As in the example 3.1 the same boundary conditions (3.136) are defined for each end. For a concentrated torsional moment M acting at $\xi = \frac{1}{2} = \alpha$ the particular solution takes the form

$$\bar{\varphi}(\xi < \alpha) = 0 \tag{3.137}$$

$$\bar{\varphi}(\xi > \alpha) = \frac{ML}{GK} \left[\frac{1}{\kappa} \sinh \kappa \left(\xi - \frac{1}{2} \right) - \left(\xi - \frac{1}{2} \right) \right] \tag{3.138}$$

The results for the same types of section are shown in the figure 3.27, figure 3.28, figure 3.29 and figure 3.30 for the simply supported beam.

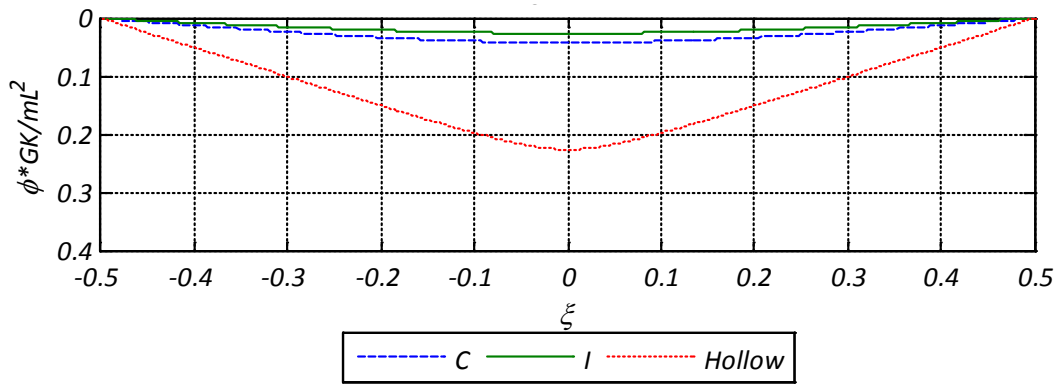


Figure 3.27 – ϕ value of a S-S beam acted by concentrated torque (analytical solution).

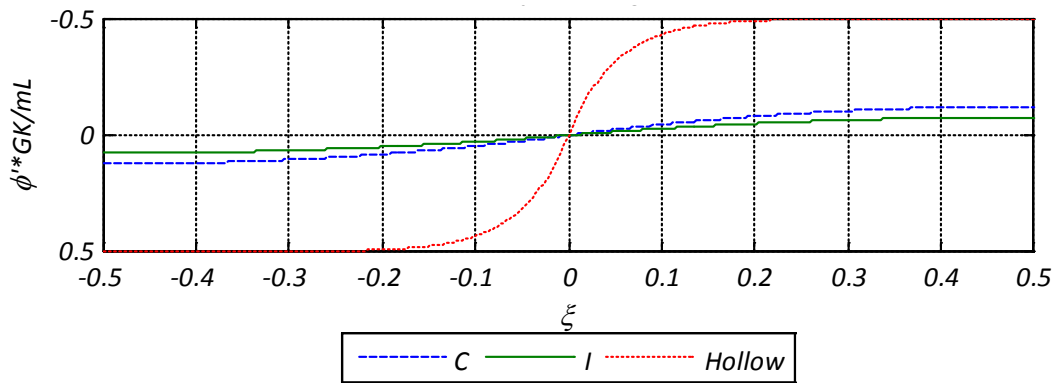


Figure 3.28 – ϕ' value of a S-S beam acted by concentrated torque (analytical solution).

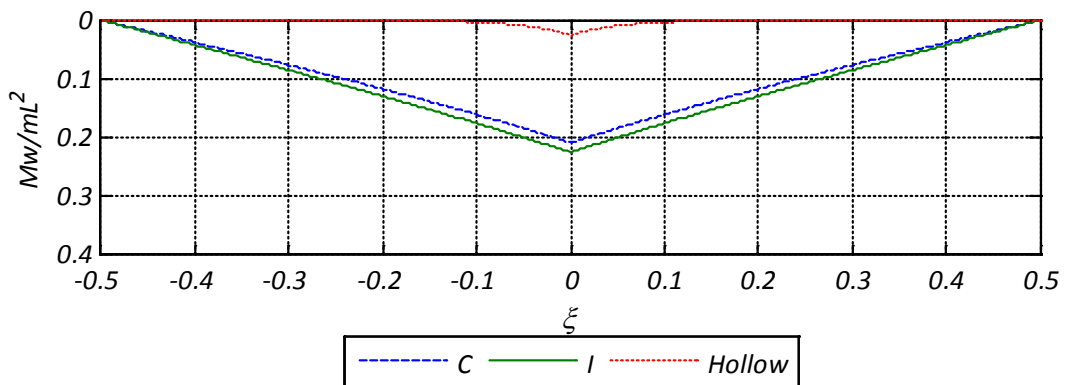


Figure 3.29 – M_w of a S-S beam acted by concentrated torque (analytical solution).

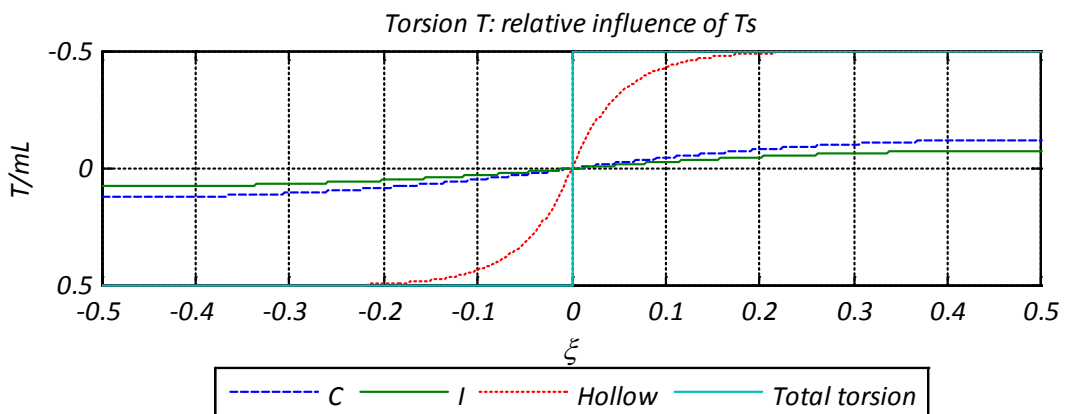


Figure 3.30 - Distribution of the torsion T_s and T of a S-S beam acted by concentrated torque (anal. solution).

The maximum value of the dimensionless twist for the open section beams is lower than the twist of the hollow section because the Saint Venant stiffness of these shapes is smaller (figure 3.27). The torsional response of the thin-walled open sections when acted by a concentrated torque at mid-span is similar to the bending response to a vertical concentrated load acting at the same point. In fact the table 2.1 shows that Vlasov theory assumptions for the mixed torsion for a thin walled open cross-section are similar to the Euler-Bernoulli bending behavior of a beam. This simple analogy explains the shape of the warping moment diagrams for the I and C-beam (see figure 3.29), while the warping torsion of the hollow-beam is negligible such shown in figure 3.30, where is illustrated the T_S influence on the total value of torsion.

Example 3.3: Three continuous spans acted by uniform torque

In this case a symmetric, three spans continuous beam with the central span acted upon a uniformly distributed torque m is analyzed as shown in figure 3.31

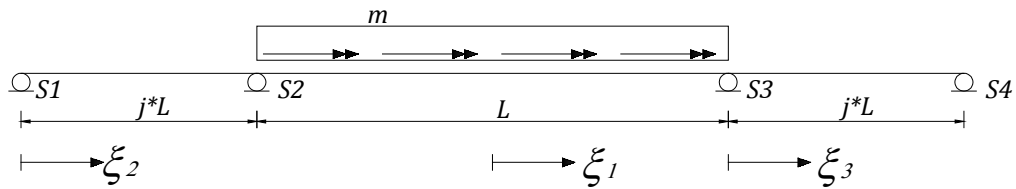


Figure 3.31 – Three continuous span beam acted by uniform torque at midspan.

Length span properties are also shown, where $L = 2m$ is the length of the central span and $j * L$ is the length of the lateral ones. The characteristic values are $\kappa = \sqrt{\frac{G * K * L^2}{E * \Gamma_{\omega\omega}}}$ for the central span and $\kappa_j = j * \kappa$ for the lateral spans (Kollbrunner & Basler, 1969).

The boundary conditions are summarized in table 3.13.

Table 3.13 – Boundary conditions for the three continuous spans beam.

Support	Static boundary prescribed	Kinematic boundary prescribed	
S1	$M_{\omega}(\xi_2 = 0) = 0$	$\varphi(\xi_2 = 0) = 0$	
S2	–	$\varphi(\xi_1 = -L/2) = 0$	$\varphi'(\xi_1 = -L/2) = \varphi'(\xi_2 = j * L)$
S3	–	$\varphi(\xi_1 = +L/2) = 0$	$\varphi'(\xi_1 = L/2) = \varphi'(\xi_2 = 0)$
S4	$M_{\omega}(\xi_3 = j * L) = 0$	$\varphi(\xi_3 = j * L) = 0$	

A new coordinate system ξ_i is introduced for each span as shown in figure 3.31.

The redundant warping moment called X at the supports fixes the torsion of the member and is

$$X = \frac{-\left(\frac{1}{2} - \left(\frac{1}{\kappa}\right) * \tanh\left(\frac{\kappa}{2}\right)\right)}{\left(\kappa * \frac{1}{\tanh(j * \kappa)} - \frac{1}{j} + (\kappa) * \tanh\left(\frac{\kappa}{2}\right)\right)} \quad (3.139)$$

Note that the equation (3.139) can be obtained by using the three moment equation for the continuous beam analysis.

As shown in the next figures with the plot of the solution, at the support sections ($\xi_1 = -0.5$ and $\xi_1 = +0.5$) the φ value is zero, and its first derivative is continuous. Mathematically, this means that the T_S function is not affected by jump discontinuities at the internal supports, while the M_{ω} function will present a kink at S1 and S2

because of the different values of the T_ω function on the left and the right side of the support. This case, as already mentioned, is comparable with the bending analysis results for the same continuous beam.

The results in terms of forces and displacements for the continuous three spans beam are shown in the figure 3.32, figure 3.33, Figure 3.34, figure 3.35.

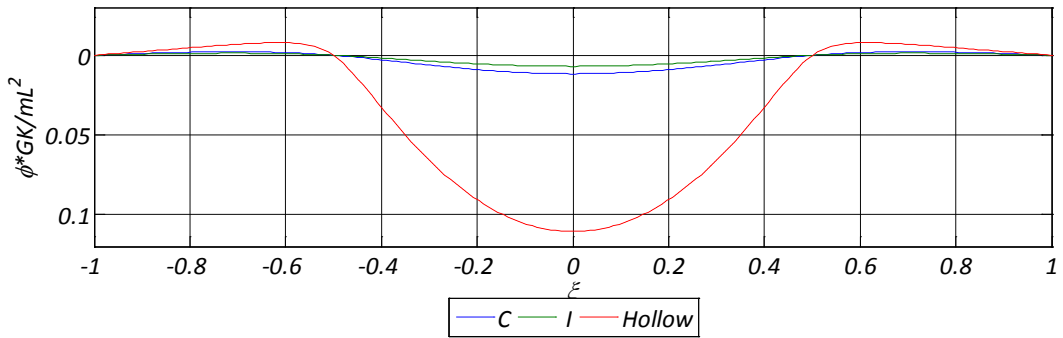


Figure 3.32 – ϕ value of a continuous three spans beam acted by uniform torque (analytical solution).

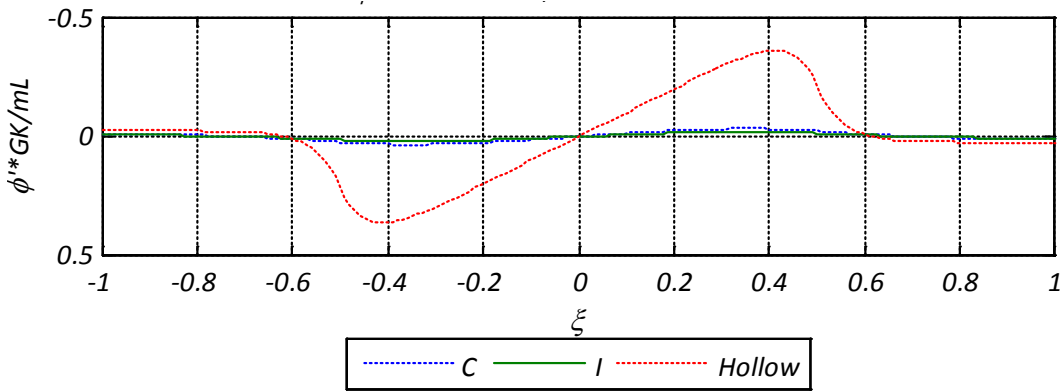


Figure 3.33 – ϕ' value of a continuous three spans beam acted by uniform torque (analytical solution).

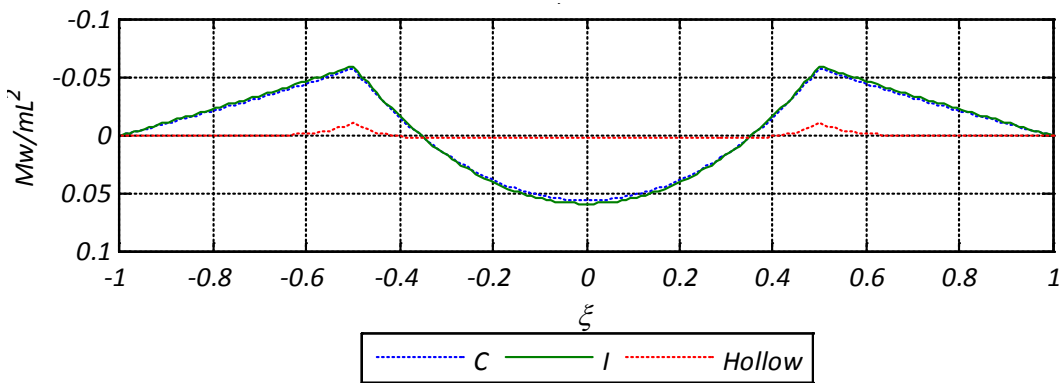


Figure 3.34– M_ω of a continuous three spans beam acted by uniform torque (analytical solution).

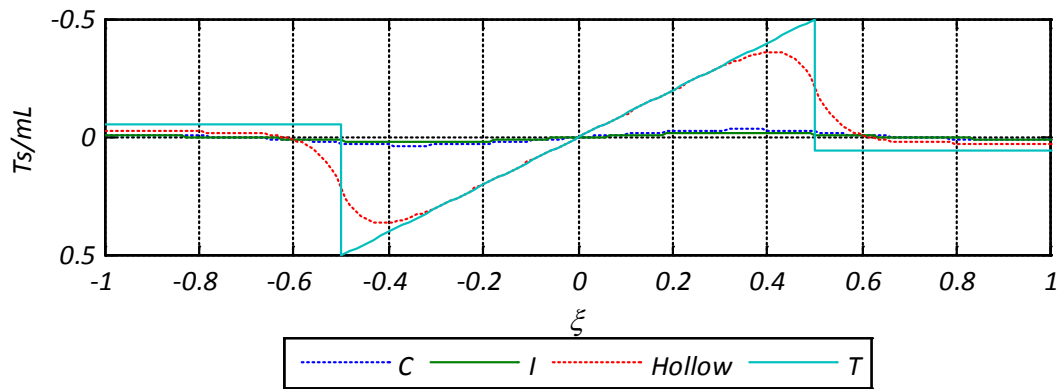


Figure 3.35 - Distribution of the torsion T_s and T of a continuous three spans beam acted by uniform torque (analytical solution).

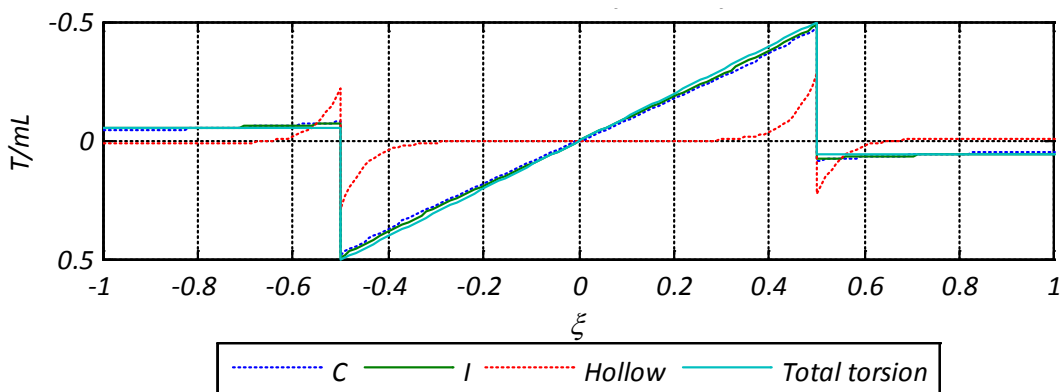


Figure 3.36 - Distribution of the torsion T_ω and T of a continuous three spans beam acted by uniform torque (analytical solution).

The figure 3.34 shows the warping moment normalized along the beam axes. In table 3.14 is illustrated the value of the redundant warping moment on the support section.

Table 3.14 - Dimensionless warping moment at supports.

Section type	Dimensionless warping moment at supports (X)
I-section	-0.597
C-section	-0.585
Hollow section	-0.019

As expectable, this results mean that the open sections have much more warping stiffness $EI_{\omega\omega}$ than the hollow sections and warping torsion absorb almost the totality of the total torque moment (figure 3.36).

3.3. Dynamic analysis

A structural-dynamic problem introduces a time-varying response of the system and the analysis has to take into account that internal forces in a general element must equilibrate not only the externally applied force but also the inertia forces resulting from the accelerations of the beam.

The physical properties of any linearly elastic structural system subjected to dynamic loads include mass, stiffness, damping and the external source of excitation or loading. When all these contributions are quantified it is possible to write an equation of motion in its general form

$$f_I + f_D + f_S = p(t) \quad (3.140)$$

This equation, written for a SDOF³ system, implies a relationship between inertial forces f_I , damping forces f_D , elastic forces f_S and applied loads $p(t)$. When the generalized displacement and its derivatives with respect to time are taken into account in the definitions of these forces, after substitution in the equation (3.140), the resultant equation of motion for the system can be written as follows

$$m\ddot{v} + c\dot{v} + kv = p(t) \quad (3.141)$$

This is the general form of a motion equation for a SDOF system. In the equation (3.141) m is the mass of the system, c is the damping of the system and k represents its stiffness.

There are three principal approaches to achieve mathematically this expression: the *direct equilibrium* of forces, the *virtual-work* analysis and the application of *Hamilton's principle*. This third way is a variational principle and will be used to define the equation of motion of the system analyzed.

The damping is not considered in the first approach for the formulation of dynamic equations, being the equation (3.141) simplified as follows

$$m\ddot{v} + kv = p(t) \quad (3.142)$$

After the derivation of these equations, some torsional vibration problems will be studied and compared with the analytical solutions, in order to evaluate warping influence in *free vibration* of a beam elements for different boundary conditions.

3.3.1. Equations of motion

The *variational principles* approach can also be used in dynamic (as in the static) for developing the equations of motion.

The potential energy density per unit length is expressed in terms of the generalized displacements and their derivatives by the functional $F(\eta, \eta', \varphi, \varphi', \varphi'', \xi_y, \xi_z, \xi'_y, \xi'_z, \xi''_y, \xi''_z)$ whereas the kinetic energy per unit length is defined by $C(\dot{\eta}, \dot{\xi}_y, \dot{\xi}_z, \dot{\varphi}, \dot{\xi}'_y, \dot{\xi}'_z, \dot{\varphi}')$. These two functional allow to define the dynamic problem in terms of a set of partial differential equations.

The solution for each generalized displacement satisfies the boundary conditions and respects the Hamilton's principle⁴

$$\int_{t_1}^{t_2} \delta(T - V)dt = \int_{t_1}^{t_2} \left(\frac{\partial T}{\partial q_i} \delta q_i + \frac{\partial T}{\partial \dot{q}_i} \delta \dot{q}_i + \frac{\partial T}{\partial \dot{q}'_i} \delta \dot{q}'_i - \frac{\partial V}{\partial q_i} \delta q_i - \frac{\partial V}{\partial q'_i} \delta q'_i - \frac{\partial V}{\partial q''_i} \delta q''_i \right) dt = 0 \quad (3.143)$$

³ SDOF-Single degree of freedom

⁴ See (Clough & Penzien, 1982).

where q_i is the generic i -generalized coordinate relative to the i -degree of freedom. Integrating the velocity dependent terms in eq. (3.143) by parts leads to

$$\int_{t_1}^{t_2} \frac{\partial T}{\partial \dot{q}_i} \delta \dot{q}_i dt = \left[\frac{\partial T}{\partial \dot{q}_i} \delta q_i \right]_{t_1}^{t_2} - \int_{t_1}^{t_2} \frac{\partial}{\partial t} \left(\frac{\partial T}{\partial \dot{q}_i} \right) \delta q_i dt \quad (3.144)$$

The same form of the eq.(3.144) is valid for solving the integral $\int_{t_1}^{t_2} \frac{\partial T}{\partial \dot{q}_i} \delta \dot{q}_i dt$. The boundary term of (3.144) is equal to zero for each coordinate, since $\delta q_i(t_1) = \delta q_i(t_2) = 0$ is the basic condition imposed to the variations. Substituting (3.144) in (3.143) follows that

$$\int_{t_1}^{t_2} \left(\frac{\partial T}{\partial q_i} \delta q_i - \frac{\partial}{\partial t} \left(\frac{\partial T}{\partial \dot{q}_i} \right) \delta q_i - \frac{\partial}{\partial t} \left(\frac{\partial T}{\partial \dot{q}_i'} \right) \delta q_i' - \frac{\partial V}{\partial q_i} \delta q_i - \frac{\partial V}{\partial q_i'} \delta q_i' - \frac{\partial V}{\partial q_i''} \delta q_i'' \right) dt = 0 \quad (3.145)$$

Integrating the $\delta q_i'$ and $\delta q_i''$ dependent terms in (3.145) by parts, as done for the equilibrium equations, all the terms will be multiplied by δq_i and a partial differential equation dependent in time and space will be obtained for each degree of freedom.

Note that if $T = 0$ and V is constant in time, (3.143) coincides with the theorem of *minimum potential energy*.

The potential energy and the kinetic energy refer to the elastic center (x_c, y_c) and to the shear center (y_a, z_a) , being the problem presented in its uncoupled form. Therefore, extension, bending and torsion can be treated separately, and all the coupling geometric quantities vanish.

Axial effects

The generalized displacement $\eta(x)$ describes the axial extension of the beam. The associated first variation of potential energy is defined in (3.101), while the kinetic energy can be written as follows

$$T(\dot{\eta}) = \int_0^L \frac{1}{2} \rho A \dot{\eta}^2 dx \quad (3.146)$$

where ρ is the mass per unit volume.

The equation (3.145) has been formulated considering the Hamilton principle. Thus, when the kinetic and potential energies are known, it can be applied directly and leads to

$$\int_{t_1}^{t_2} \int_0^L (-\rho A \ddot{\eta} \delta \eta - \eta' EA \delta \eta' + q_x \delta \eta) dx dt = 0 \quad (3.147)$$

Integrating by parts the second term, the following is obtained

$$- \int_{t_1}^{t_2} [\eta' EA \delta \eta]_0^L dt + \int_{t_1}^{t_2} \int_0^L (-\rho A \ddot{\eta} + \eta'' EA + q_x) \delta \eta dx dt = 0 \quad (3.148)$$

The first term represent the boundary virtual work of the axial force. In order to obtain a solution independent from the virtual displacement $\delta \eta$ it follows that

$$-\rho A \frac{\partial^2 \eta}{\partial t^2} + \frac{\partial^2 \eta}{\partial x^2} EA + q_x = 0 \quad (3.149)$$

which is the equation of motion for the extension problem of a finite length beam. The axial stiffness of the beam is supposed to be constant.

Bending

The bending problem is treated similarly to the axial effect problem. The associated kinetic energy is given by

$$T(\dot{\xi}_y, \dot{\xi}_z) = \int_0^L \frac{1}{2} \rho (I_{\alpha\beta} \dot{\xi}_\alpha' \dot{\xi}_\beta' + A \dot{\xi}_\alpha^2 - 2 \dot{\xi}_y S_z^A \dot{\varphi} + 2 \dot{\xi}_z S_y^A \dot{\varphi}) dx \quad (3.150)$$

where the repeated subscripts α and β imply summation over $\alpha = y, z$ and $\beta = y, z$. No subscript are used for the coupling terms involving S_z^A and S_y^A . Note that these quantities refer to the shear center (y_a, z_a) .

In this part it is considered that y, z axis are parallel to the principal axis and $I_{\alpha\beta} = 0$ if $\alpha \neq \beta$. In order to obtain the bending expression for (3.145) the terms involved will be calculated separately. The time derivatives are given from

$$\frac{\partial}{\partial t} \left(\frac{\partial T}{\partial \dot{q}_i} \right) \delta q_i + \frac{\partial}{\partial t} \left(\frac{\partial T}{\partial \dot{q}_i'} \right) \delta \dot{q}_i' = \int_0^L \frac{1}{2} \rho \left(2 I_{\alpha\alpha} \ddot{\xi}_\alpha' \delta \xi_\alpha' + 2 A \ddot{\xi}_\alpha \delta \xi_\alpha - 2 S_z^A \ddot{\varphi} \delta \xi_y + 2 S_y^A \ddot{\varphi} \delta \xi_z \right) dx \quad (3.151)$$

The first variation of $V(\xi_y, \xi_y', \xi_y'')$ is written as follows

$$\delta V(\xi_y) = \int_0^L (\xi_y'' \alpha EI_\alpha \delta \xi_y'' - (-m_\alpha \delta \xi_y' + q_\alpha \delta \xi_\alpha)) dx \quad (3.152)$$

The substitution of eq.(3.151) and eq.(3.152) in eq.(3.145) leads to

$$\begin{aligned} & \int_{t_1}^{t_2} \int_0^L \rho \left(I_{\alpha\alpha} \ddot{\xi}_\alpha' \delta \xi_\alpha' + A \ddot{\xi}_\alpha \delta \xi_\alpha - S_z^A \ddot{\varphi} \delta \xi_y + S_y^A \ddot{\varphi} \delta \xi_z \right) dx dt + \\ & + \int_{t_1}^{t_2} \int_0^L (\xi_y'' \alpha EI_\alpha \delta \xi_y'' + m_\alpha \delta \xi_y' - q_\alpha \delta \xi_\alpha) dx dt = 0 \end{aligned} \quad (3.153)$$

In order to obtain the equation of motion, the equation (3.153) is reformulated via integration by parts, where the derivatives $\delta \xi_\alpha'$ and $\delta \xi_y''$ are integrated:

$$\begin{aligned} & \int_{t_1}^{t_2} \left([\rho I_{\alpha\alpha} \ddot{\xi}_\alpha' \delta \xi_\alpha]_0^L + \int_0^L (-\rho I_{\alpha\alpha} \ddot{\xi}_\alpha'' \delta \xi_\alpha + \rho A \ddot{\xi}_\alpha \delta \xi_\alpha - \rho S_z^A \ddot{\varphi} \delta \xi_y + \rho S_y^A \ddot{\varphi} \delta \xi_z) dx \right) dt + \\ & + \int_{t_1}^{t_2} \left([EI_\alpha \xi_y'' \delta \xi_y']_0^L - [EI_\alpha \xi_y''' \delta \xi_y]_0^L + [m_\alpha \delta \xi_y]_0^L + \int_0^L ((EI_\alpha \xi_y'' \alpha)'' - m_\alpha' - q_\alpha) dx \right) \delta \xi_\alpha dt = 0 \end{aligned} \quad (3.154)$$

The boundary terms involving the distributed moment m_α and the bending moment M_α have already been identified for the equilibrium equations. The term containing the shear force V_α represents the virtual work of the inertial force. This term is constituted by three contributions written as follows,

$$V_\alpha = \rho I_\alpha \frac{\partial^2}{\partial t^2} \left(\frac{\partial \xi_\alpha}{\partial x} \right) - \frac{\partial}{\partial x} \left(EI_\alpha \frac{\partial^2 \xi_\alpha}{\partial x^2} \right) + m_\alpha, \quad \alpha = y, z \quad (3.155)$$

which represent the total force that produces work for the generalized displacement $\delta \xi_\alpha$. This force has a contribution due to the inertia of the beam element. The boundary term multiplied by $\delta \xi_\alpha'$ is the same of the static case defined by eq.(3.111).

The differential equations contained in the integral form of eq.(3.154) represent the solution for the flexural problem in the principal directions, for each arbitrary value of $\delta \xi_\alpha$, and can be written as follows

$$-\rho I_y \frac{\partial^2}{\partial x^2} \left(\frac{\partial^2 \xi_y}{\partial t^2} \right) + \rho A \left(\frac{\partial^2 \xi_y}{\partial t^2} \right) - \rho S_z^P \frac{\partial^2 \varphi}{\partial t^2} + \frac{\partial^2}{\partial x^2} \left(EI_y \frac{\partial^2 \xi_y}{\partial x^2} \right) - m_y' - q_y = 0 \quad (3.156)$$

$$-\rho I_z \frac{\partial^2}{\partial x^2} \left(\frac{\partial^2 \xi_z}{\partial t^2} \right) + \rho A \left(\frac{\partial^2 \xi_z}{\partial t^2} \right) + \rho S_y^P \frac{\partial^2 \varphi}{\partial t^2} + \frac{\partial^2}{\partial x^2} \left(EI_z \frac{\partial^2 \xi_z}{\partial x^2} \right) - m_z' - q_z = 0 \quad (3.157)$$

Substituting eq.(3.111) in eq.(3.155) and then eq.(3.155) in eq.(3.156) and eq.(3.157) the equation of motion for the bending problem are expressed as follows:

$$V_y = \frac{\partial M_y}{\partial x} + m_y + \rho I_y \frac{\partial^2 \xi_y'}{\partial t^2} \quad (3.158)$$

$$V_z = \frac{\partial M_z}{\partial x} + m_z + \rho I_z \frac{\partial^2 \xi_z'}{\partial t^2} \quad (3.159)$$

$$\frac{\partial V_y}{\partial x} + q_y - \rho A \left(\frac{\partial^2 \xi_y}{\partial t^2} \right) + \rho S_z^A \frac{\partial^2 \varphi}{\partial t^2} = 0 \quad (3.160)$$

$$\frac{\partial}{\partial x} V_z + q_z - \rho A \left(\frac{\partial^2 \xi_z}{\partial t^2} \right) - \rho S_y^A \frac{\partial^2 \varphi}{\partial t^2} = 0 \quad (3.161)$$

Torsion

For the formulation of the dynamic equations for the torsion problem a similar approach to that used for derive the governing bending equations will be used. The center of rotation considered is the shear centre. The kinetic energy due to the torsion is written as follows

$$T(\dot{\varphi}, \dot{\varphi}') = \int_0^L \frac{1}{2} \rho \left(I_{\omega\omega} \dot{\varphi}'^2 - 2 \xi_y^A S_z^A \dot{\varphi}' + I_z^A \dot{\varphi}'^2 + A \xi_z^2 + 2 \xi_z^A S_y^A \dot{\varphi}' + I_y^A \dot{\varphi}'^2 \right) dx \quad (3.162)$$

Considering the equation (3.145) by means of the functional $T(\dot{\varphi}, \dot{\varphi}')$ and $V(\varphi, \varphi', \varphi'')$, obtained in (3.115), after suitable rearrangements, the following expression of the Hamilton's principle is obtained

$$\begin{aligned} & \int_{t_1}^{t_2} \int_0^L \rho \left(I_{\omega\omega} \ddot{\varphi}' \delta\varphi' - S_z^A \xi_y^A \delta\varphi + S_y^A \xi_z^A \delta\varphi + (I_z^A + I_y^A) \ddot{\varphi} \delta\varphi \right) dx dt + \\ & \int_{t_1}^{t_2} \int_0^L \left(\varphi'' EI_{\omega\omega} \delta\varphi'' + \varphi' GK \delta\varphi' - m_\varphi \delta\varphi + b \delta\varphi' \right) dx dt = 0 \end{aligned} \quad (3.163)$$

Integration by parts of the derivatives $\delta\varphi'$ and $\delta\varphi''$ leads to

$$\begin{aligned} & \int_{t_1}^{t_2} \left([\rho I_{\omega\omega} \ddot{\varphi}' \delta\varphi]_0^L + \int_0^L \rho \left(-I_{\omega\omega} \ddot{\varphi}'' + (I_z^A + I_y^A) \ddot{\varphi} - S_z^A \xi_y^A + S_y^A \xi_z^A \right) \delta\varphi dx \right) dt + \\ & + \int_{t_1}^{t_2} \left([\varphi'' EI_{\omega\omega} \delta\varphi']_0^L - [(\varphi'' EI_{\omega\omega})' \delta\varphi]_0^L + [\varphi' GK \delta\varphi]_0^L + [b \delta\varphi]_0^L \right) dt + \\ & + \int_{t_1}^{t_2} \int_0^L \left((EI_{\omega\omega} \varphi'')'' - (GK \varphi')' - m_\varphi - b' \right) \delta\varphi dx dt = 0 \end{aligned} \quad (3.164)$$

The torsional moment is the boundary term that produce virtual work multiplied by $\delta\varphi$ and is given by

$$T = \rho I_{\omega\omega} \frac{\partial^2}{\partial t^2} \left(\frac{\partial \varphi}{\partial x} \right) - \frac{\partial}{\partial x} \left(EI_{\omega\omega} \frac{d^2 \varphi}{dx^2} \right) + \left(GK \frac{d\varphi}{dx} \right) + b \quad (3.165)$$

The first contribution on the right hand is due to the inertial torque per unit length of the beam. All the other boundary terms are already known and for the arbitrary rotation $\delta\varphi$, Hamilton's principle gives

$$\begin{aligned} & -\rho I_{\omega\omega} \frac{\partial^2}{\partial x^2} \left(\frac{\partial^2 \varphi}{\partial t^2} \right) + \rho (I_z^A + I_y^A) \frac{\partial^2 \varphi}{\partial t^2} - \rho S_z^A \frac{\partial^2 \xi_y}{\partial t^2} + \rho S_y^A \frac{\partial^2 \xi_z}{\partial t^2} + \frac{\partial^2}{\partial x^2} \left(EI_{\omega\omega} \frac{\partial^2 \varphi}{\partial x^2} \right) \\ & - \frac{\partial}{\partial x} \left(GK \frac{d\varphi}{dx} \right) - \frac{db}{dx} - m_\varphi = 0 \end{aligned} \quad (3.166)$$

Substituting (3.119) and (3.122) in (3.164) and then (3.165) in (3.166) the equations of motion for the torsional problem are given by:

$$T = \rho I_{\omega\omega} \frac{\partial^2}{\partial t^2} \left(\frac{\partial \varphi}{\partial x} \right) + \frac{\partial M_{\omega}}{\partial x} + T_s + b \quad (3.167)$$

$$\frac{dT}{dx} - \rho(I_z^A + I_y^A) \frac{\partial^2 \varphi}{\partial t^2} + \rho S_z^A \frac{\partial^2 \xi_y}{\partial t^2} - \rho S_y^A \frac{\partial^2 \xi_z}{\partial t^2} + m_{\varphi} = 0 \quad (3.168)$$

As shown by the (3.168), in the vibration problem, if all the inertial contributions are considered, bending and torsion are coupled through the terms S_z^A and S_y^A . In dynamic, the assumption of considering both shear center and elastic center do not allows to uncoupling bending and torsional motion, because rotation around (y_a, z_a) causes transverse displacements of the elastic center (figure 3.37).

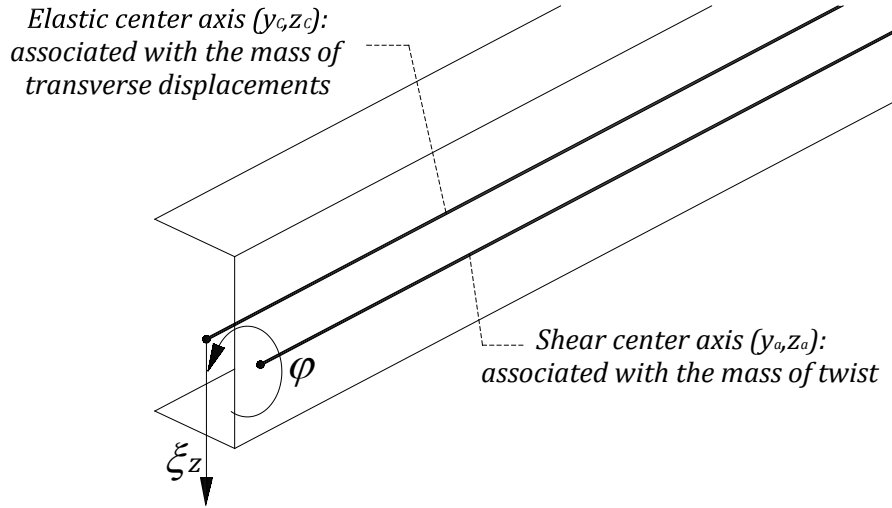


Figure 3.37 – Coupling between torsion and bending displacements for a C-beam.

A way to uncoupling torsion and bending of a beam is to consider shear center and elastic center at the same point, as will be done in the analysis of the practical problems in section 3.3.2.

3.3.2. Analysis of torsional free vibrations on thin-walled beams

The analysis of free torsional vibrations of thin-walled beams is analyzed for a simple case of an I-cross section. In this case, as already mentioned, the shear center and the elastic center coincide and the flexure of the beam is uncoupled from torsion (Gere, 1954).

The differential equation for torsional free vibrations has the following form

$$EI_{\omega\omega} \frac{\partial^4 \varphi}{\partial x^4} - GK \frac{\partial^2 \varphi}{\partial x^2} = \rho I_p \frac{\partial^2 \varphi}{\partial t^2} \quad (3.169)$$

where $I_p = I_z + I_y$ is the polar moment of inertia.

The general solution is obtained by *separation of variables* for different boundary conditions and for its exact determination see (Gere, 1954). The form of the twist rotation is written as follows

$$\varphi(x, t) = \phi(x)T(t) \quad (3.170)$$

where $\phi(x)$ is the shape function obtained from the static boundary conditions, and $T(t)$ is an harmonic function of the type

$$T(t) = A_n \cos p_n t + B_n \sin p_n t \quad (3.171)$$

Imposing the conditions of a *simply supported* beam (SS) on the shape function, illustrated in (3.136), the exact form of the fundamental frequencies of torsional vibration is found as follows (Gere, 1954)

$$(p_n)_{ss} = \frac{n\pi}{L^2} \sqrt{\frac{n^2\pi^2 EI_{\omega\omega} + L^2 GK}{\rho I_p}} \quad (3.172)$$

As illustrated from (3.172) the natural frequency is constituted by a term including the warping stiffness and a second contribution due to the Saint Venant torsional stiffness of the cross-section. If the first term vanishes, the frequency of the mode n is the same obtained from the classic beam's theory.

Others boundary conditions have been analyzed but the highly transcendental nature of the equations impose to obtain the solution only by lengthly trial-and error procedure (Gere, 1954).

Beam cross-sections

The numerical example illustrated by Gere has the characteristics reported in table 3.5.

Table 3.15 – Characteristics of the beam element analyzed by (Gere, 1954).

Beam cross-section	Length of the beam L	Torsional constant $\kappa = \sqrt{\frac{GK \cdot L^2}{EI_{\omega\omega}}}$
STANDARD WIDE-FLANGE BEAM 12 WF 45	6m (20 ft)	4

Example 3.4: Simply Supported beam of length L

The simply supported beam of figure 3.27 is studied.



Figure 3.38 – Simply supported beam analyzed by (Gere, 1954).

Using the exact solution for the problem, is possible to compare the effect on the natural frequencies of the first n -modes with or without warping by means of the parameter r

$$r = \frac{\text{Frequency with warping}}{\text{Freq. without warping}} = \sqrt{\frac{n^2\pi^2}{\kappa^2} + 1} \quad (3.173)$$

As shown by (3.173) this could be seen as the warping influence on the torsional frequency of a beam and depends by the torsional constant κ and the vibration mode n . The increasing of frequency is bigger for high modes, while it decrease for high values of κ , when torsion tends to be pure Saint Venant torsion.

In the figure it's possible to show the calculation of the ratio r for the first 8 vibration modes in a simply supported beam.

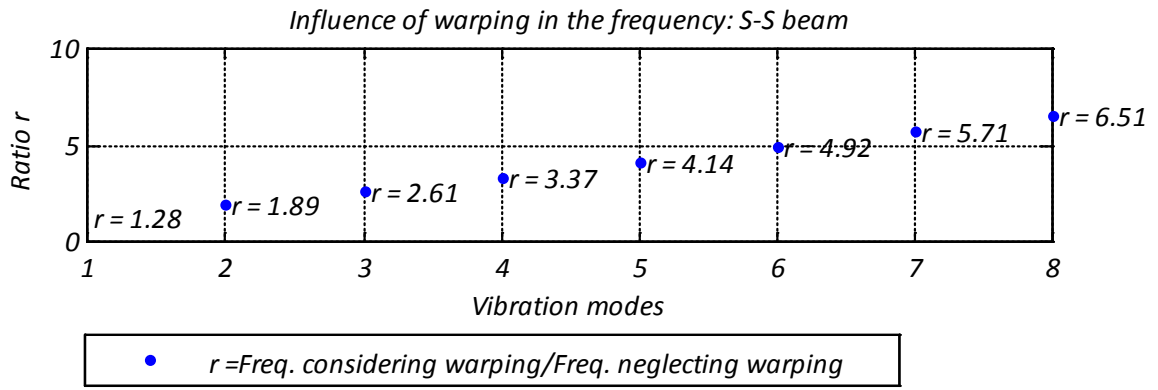


Figure 3.39 – Values of the ratio r for the first 8 torsional vibration modes.

4. FINITE ELEMENT APROXIMATION

The governing equations of thin-walled beams structural behavior are partial differential equations, being the corresponding analytical solutions difficult to obtain for an arbitrary cross-section.

The finite element method (FEM) is a numerical method that allows to solve partial differential equations approximately, and will be used in this chapter for solving the static and dynamic behavior of thin-walled beams.

The basic idea of FEM is to divide the beam into *finite elements* (finite element mesh) and obtain a numerical solution by approximating the governing variables (e.g. displacements) in order to verify the governing equations in a weak form.

For linear problems, the solution is obtained by solving a system of linear equations through a computer code implementation, made by MATLAB in this analysis.

In FEM method the development of a finite element involves three principal steps (Fish & Belytschko, 2007):

1. The knowledge of the *strong form*, which consists of the governing equations for the model and the boundary conditions formulation;
2. The *weak form*, which can be developed starting from the strong form through an integration by parts;
3. The *approximation functions*, by which a displacement field will be modeled using *shape functions* and *nodal displacements* vectors.

According to the Euler-Bernoulli theory a finite element has six *degrees of freedom* (DOF) for each end. In this case, due to the deformability of thin-walled beam elements out of their own plane, another degree of freedom is added representing the warping of the cross-section when it twists. This finite element with 7 DOF for each end is developed and used to solve structural problems on continuous beams loaded generically.

Combining the approximation functions introduced for first in section 4.1 with the weak form of a general differential equation it is possible to obtain the discrete finite element equations. In stress analysis these equations solve the equilibrium of a general structure. The discretization will involve the calculus of element matrices in order to describe the internal forces and the load acting upon the beam finite element. This is the purpose of section 4.2, where the problem of uncoupled torsion is solved as a first approach, being developed afterwards a beam element where coupled effect are considered.

In 4.3 an undamped vibration analysis is discretized by FEM method. In this case also inertial forces have to be considered in order to verify the equations of motion for each degree of freedom. The inertial forces should be described introducing an element mass matrix, which will be obtained for the uncoupled rotation of torsion and then in the general case, where coupled effect must be taken into account.

4.1. Beam displacements discretization

The introduction of approximations and their definition is one of the principal parts of the FEM development. The finite element can be convergent and the accuracy of a correctly developed FEM improves with mesh refinement, i.e. as the element size describing the problem decreases the solution tends to the exact solution. The two *necessary* conditions for convergence of the FEM are *continuity* and *completeness* (Fish & Belytschko, 2007).

Under these assumptions two *isoparametric* beam elements are introduced in order to calculate the *element stiffness matrix*, the *element mass matrix* and the *element external force matrix*. The key idea is to use the *shape functions* to represent *both the element geometry and the problem unknowns*, which in this case are displacements. Hence the name *isoparametric element*, often abbreviated to *iso-P element*.

4.1.1. Continuity

The choice of a function to describe a displacement field depends of the continuity required for the nodal degrees of freedom of the element nodes.

A function is called C^n function if its derivatives of order j for $0 \leq j \leq n$ exist and are continuous functions on the entire domain. A C^0 function is a linear function and is piecewise continuously differentiable, i.e. its first derivative is continuous except at selected points. So if a displacement is defined by a C^0 function, the strain, which corresponds to its derivative, is a C^{-1} function. This could be the case of the axial displacements, that allow a linear approximation and do not require any continuity of their derivatives.

If the continuity of an approximation function is required also for its derivatives it should be a C^1 function, which has not kinks or jumps as discontinuities. This function will be used in the next section for the approximation of *bending* and *torsional* displacements. The characteristics of C^{-1} , C^0 and C^1 functions are illustrated, in terms of smoothness in the table 4.1, taken from (Fish & Belytschko, 2007).

Table 4.1 – Smoothness of functions (Fish & Belytschko, 2007).

Smoothness	Kinks	Jumps	Comments
C^{-1}	Yes	Yes	Piecewise continuous
C^0	Yes	No	Piecewise continuously differentiable
C^1	No	No	Continuously differentiable

4.1.2. Approximation functions

Two-node linear element

Consider the simple one-dimensional element with two nodes as shown in figure 4.1. The approximation functions for this kind of element must be C^0 functions.

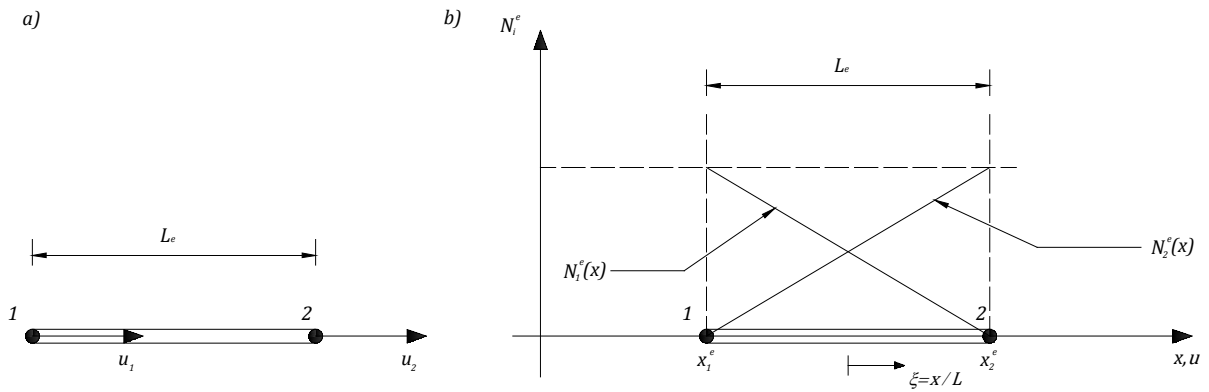


Figure 4.1 – Degrees of freedom and shape functions of the two node elements.

The global axis x passes through the bar axis and a non-dimensional coordinate $\xi = x/L$ is introduced, being $-1 \leq \xi \leq 1$. This parent domain allows to consider the Gauss quadrature in order to define polynomial functions that interpolate *weight functions* and *trial solutions*.

The relation between global and *natural* coordinates is written as follows

$$x = \frac{1}{2}(1 - \xi)x_1^e + \frac{1}{2}(1 + \xi)x_2^e = \mathbf{N}^e \cdot \mathbf{x}^e \quad (4.1)$$

where the vector $\mathbf{N}^e = [N_1^e \quad N_2^e] = \frac{1}{2}[(1 - \xi) \quad (1 + \xi)]$ represents the *element shape function* and $\mathbf{x}^e = \begin{bmatrix} x_1^e \\ x_2^e \end{bmatrix}$ represents the *global coordinates*.

The axial displacements of the bar, when one degree of freedom is considered for each end, are expressed in the same form of the global coordinates by the shape functions as follows

$$u^e = \mathbf{N}^e \cdot \mathbf{d}^e \quad (4.2)$$

being the vector of nodal displacements in axial direction defined as follows

$$\mathbf{d}^e = \begin{bmatrix} u_1^e \\ u_2^e \end{bmatrix} \quad (4.3)$$

It can be seen that the shape functions are linear in the element, as expected. This functions will be used for the approximation of the axial displacement field.

Two-node Euler-Bernoulli element

The element shown in figure 4.2 is an Euler-Bernoulli beam element, which requires continuous nodal displacement and rotation fields: this means that the *trial solution* and *weight function approximations* must be C^1 functions,

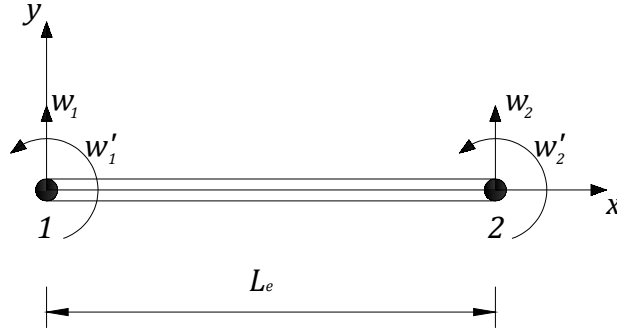


Figure 4.2 - Two-node Euler-Bernoulli element.

The displacements and their first derivatives at nodes must be degrees of freedom of the element and the class of functions generally used in this case are the Hermite polynomials, given by

$$H_1 = \frac{1}{4} (1 - \xi)^2 (2 + \xi) = \frac{1}{4} (2 - 3\xi + \xi^3) \quad (4.4)$$

$$H_2 = \frac{L_e}{8} (1 - \xi)^2 (1 + \xi) = \frac{1}{4} (1 - \xi - \xi^2 + \xi^3) \quad (4.5)$$

$$H_3 = \frac{1}{4} (1 + \xi)^2 (2 - \xi) = \frac{1}{4} (2 + 3\xi - \xi^3) \quad (4.6)$$

$$H_4 = \frac{L_e}{8} (1 + \xi)^2 (\xi - 1) = \frac{1}{4} (-1 - \xi + \xi^2 + \xi^3) \quad (4.7)$$

where

$$\xi = \frac{2x}{L_e} - 1, -1 \leq \xi \leq 1 \quad (4.8)$$

The shape functions are represented in (Fish & Belytschko, 2007). The displacement of the beam is defined as follows

$$w^e = \mathbf{H}^e \cdot \mathbf{u}^e \quad (4.9)$$

being the vector $\mathbf{u}^e = [w_1^e \quad w_1^{\prime e} \quad w_2^e \quad w_2^{\prime e}]$ the *displacement vector* and $\mathbf{H}^e = [H_1 \quad H_2 \frac{L_e}{2} \quad H_3 \quad H_4 \frac{L_e}{2}]$ the element interpolation function matrix.

Hence, Hermite polynomials will be used for describing bending and torsion with FEM discretization. Note that in the case of torsion these functions do not represent the deformed shape of the beam element when it twists, but they represent the values of the rotation and its first derivative.

4.2. The static formulation of the finite element

The differential equations obtained in chapter 3 describe the static problem in its *strong form* through the kinematics of the beam, the constitutive relation and the equilibrium equation, imposing the correct boundary conditions to the ends of the beam element. In section 4.2.1 a weak form will be developed starting from the strong form of the torsion differential equation. The development of weak forms for bending and axial differential equations are supposed to be already known.

The assembly of the seven degrees of freedom thin-walled beam element will be presented in section 4.2.2 with reference to two axes of reference as first approach: the elastic center and the shear center. Then the element will be based on the elastic center only and coupling terms will appear in the element fundamental matrices.

4.2.1. The formulation of a weak form for uncoupled torsion

In order to develop the finite element equations, the partial differential equations must be restated in an integral form called the *weak form*. The strong form can also be used to develop a finite element method, but very smooth trial solutions would be needed; such smooth trial solutions would be difficult to construct in more than one dimension.

In stress analysis the weak form is also known as *principle of virtual work* and it is a useful tool to approximate the displacement field with less smooth solutions and simplify the treatment of the boundary conditions. The weak form of the differential equations is equivalent to the governing equation and boundary conditions, i.e. the strong form (Fish & Belytschko, 2007).

From the strong form to the weak form for the torsion problem

The development of the weak form is accomplished as follows: the differential equation (3.118) is multiplied by a *weight function* $\phi(x)$ and then integrated over the corresponding domains, which gives:

$$\int_0^L \phi \left(\frac{d^2}{dx^2} \left(EI_{\omega\omega} \frac{d^2 \varphi}{dx^2} \right) - \frac{d}{dx} \left(GK \frac{d\varphi}{dx} \right) - \frac{db}{dx} - m_\varphi \right) dx = 0 \quad (4.10)$$

The arbitrariness of the weight function is crucial, as otherwise a weak form is not equivalent to the strong form. The equation (4.10) can now be rearranged and integrated by parts leading to the following

$$\begin{aligned} & \int_0^L \phi \left(\frac{d^2}{dx^2} \left(EI_{\omega\omega} \frac{d^2 \varphi}{dx^2} \right) \right) dx - \int_0^L \phi \left(\frac{d}{dx} \left(GK \frac{d\varphi}{dx} \right) \right) dx - \int_0^L \phi \left(\frac{db}{dx} \right) dx - \int_0^L \phi (m_\varphi) dx = \\ & \left[\phi \left(\frac{d}{dx} \left(EI_{\omega\omega} \frac{d^2 \varphi}{dx^2} \right) \right) \right]_0^L - \left[\frac{d\phi}{dx} \left(EI_{\omega\omega} \frac{d^2 \varphi}{dx^2} \right) \right]_0^L + \int_0^L \frac{d^2 \phi}{dx^2} \left(EI_{\omega\omega} \frac{d^2 \varphi}{dx^2} \right) dx - \left[\phi \left(GK \frac{d\varphi}{dx} \right) \right]_0^L \\ & + \int_0^L \frac{d\phi}{dx} \left(GK \frac{d\varphi}{dx} \right) dx - [\phi b]_0^L + \int_0^L \frac{d\phi}{dx} (b) dx - \int_0^L \phi m_\varphi dx = 0 \end{aligned} \quad (4.11)$$

Taking into account the boundary terms already derived in equation (3.117), the equation (4.11) can be written as follows

$$\int_0^L \frac{d^2 \phi}{dx^2} \left(EI_{\omega\omega} \frac{d^2 \phi}{dx^2} \right) dx + \int_0^L \frac{d\phi}{dx} \left(GK \frac{d\phi}{dx} \right) dx =$$

$$[\phi \bar{T}_\omega]_0^L - \left[\frac{d\phi}{dx} \bar{M}_\omega \right]_0^L + [\phi \bar{T}_S]_0^L + [\phi \bar{b}]_0^L - \int_0^L \frac{d\phi}{dx} (b) dx + \int_0^L \phi (m_\phi) dx \quad (4.12)$$

The above is an integral formulation of the mixed torsion differential equation (4.10) containing only second and first derivatives, which is called *weak form*. The terms in brackets represent the boundary conditions at the end points of the beam: the total torsion $\bar{T} = \bar{T}_\omega + \bar{T}_S + \bar{b}$ that produces work by ϕ , while the bimoment \bar{M}_ω gives its contribution to the virtual work by means of $-\frac{d\phi}{dx}$.

In solving a weak form, a set of admissible solutions $\phi(x)$, called *trial solutions*, is considered. The function that satisfy the equation (4.12) for all smooth $\phi(x)$ is stated as the solution of the equation.

Minimum potential energy

The equation (4.12) can also be obtained by considering the principle of *minimum potential energy*. This method has already been exposed in chapter 3. Considering eq.(3.116), the first variation of the potential energy can be expressed in terms of the weight function by substituting $w(x)$ with the virtual displacements $\delta\phi$ and considering the boundary terms, being written as follows:

$$\delta V(\phi) = \int_0^L \left(\frac{d^2 \phi}{dx^2} EI_{\omega\omega} \frac{d^2 \phi}{dx^2} + \frac{d\phi}{dx} GK \frac{d\phi}{dx} + b \frac{d\phi}{dx} - m_\phi \phi \right) dx - \left([\phi \bar{T}]_0^L - \left[\frac{d\phi}{dx} \bar{M}_\omega \right]_0^L \right) = 0 \quad (4.13)$$

Notice that in eq.(4.10) the concentrated loads were defined by means of volume forces, while in (4.13) the boundary terms are expressed directly.

The above, as already known, is the principle of virtual work, by which $\delta U = \delta W$. Thus, equation (4.13) corresponds to (4.12) after rearranging the terms, as considered by the variational principles. The coincidence of these two approaches will be useful in the next part of the analysis.

Discrete equations of the finite element

It is not required that the *weight functions* be approximated by the same interpolants that are used for the *trial solutions approximations*; however, for most problem it is advantageous to use the same approximation for these two kind of functions and the resulting method is called the Galerkin FEM. This method will be used and the weight functions and trial solution are written as follows

$$\varphi^e(x) = \mathbf{H}^e \cdot \mathbf{u}^e \quad (4.14)$$

$$\phi^e(x) = \mathbf{H}^e \cdot \boldsymbol{\phi}^e \quad (4.15)$$

The angle of twist φ is approximated in terms of Hermite's functions above described for an Euler-Bernoulli element. In fact, it has to be continuously differentiable and the dimensionless coordinate ξ is considered along the beam axis. Thus, the twist angle expression can be written as follows:

$$\varphi^e(\xi) = H_1\varphi_1 + H_2\frac{d\varphi_1}{d\xi} + H_3\varphi_2 + H_4\frac{d\varphi_2}{d\xi} \quad (4.16)$$

where the following applies

$$\frac{d\varphi_i}{d\xi} = \frac{d\varphi_i}{dx} \frac{L^e}{2} \quad (4.17)$$

being $\frac{L^e}{2}$ the jacobian of the beam element of length L taking into account the eq.(4.1). Substituting eq.(4.17) in the first and second derivatives of $\varphi(x)$ gives

$$\frac{d\varphi^e}{dx} = \frac{2}{L^e} \frac{d\varphi^e}{d\xi}; \quad \frac{d^2\varphi^e}{dx^2} = \frac{4}{L^{e2}} \frac{d^2\varphi^e}{d\xi^2} \quad (4.18)$$

Introducing the approximations of eq.(4.14) and eq.(4.15) and considering the jacobian into the eq.(4.12) gives

$$\begin{aligned} \boldsymbol{\phi}^{eT} \left\{ \int_{-1}^1 \left[\frac{16}{L^{e4}} \left(\frac{d^2\mathbf{H}^e}{d\xi^2} \right)^T EI_{\omega\omega} \left(\frac{d^2\mathbf{H}^e}{d\xi^2} \right) \right] \mathbf{u}^e \frac{L^e}{2} d\xi + \int_{-1}^1 \left[\frac{4}{L^{e2}} \left(\frac{d\mathbf{H}^e}{d\xi} \right)^T GK \left(\frac{d\mathbf{H}^e}{d\xi} \right) \right] \mathbf{u}^e \frac{L^e}{2} d\xi \right. \\ \left. - \int_{-1}^1 \mathbf{H}^{eT} m_{\varphi} \frac{L^e}{2} d\xi + \int_{-1}^1 \frac{2}{L^e} \left(\frac{d\mathbf{H}^e}{d\xi} \right)^T b \frac{L^e}{2} d\xi - \mathbf{H}^{eT} \bar{T}n|_{\Gamma^e} + \frac{2}{L^e} \left(\frac{d\mathbf{H}^e}{d\xi} \right)^T \bar{M}_{\omega}n|_{\Gamma^e} \right\} = 0 \end{aligned} \quad (4.19)$$

In equation (4.19) Γ^e represents the boundary nodes of the beam element and n is the normal vector: if $\xi = -1$ the n value is -1 , while $n = 1$ if $\xi = +1$.

\mathbf{K}_e represents the *stiffness matrix* of the element, which is given by

$$\begin{aligned} \mathbf{K}_e = \int_{-1}^1 \left[\frac{16}{L^{e4}} \left(\frac{d^2\mathbf{H}^e}{d\xi^2} \right)^T EI_{\omega\omega} \left(\frac{d^2\mathbf{H}^e}{d\xi^2} \right) \right] \mathbf{u}^e \frac{L^e}{2} d\xi + \int_{-1}^1 \left[\frac{4}{L^{e2}} \left(\frac{d\mathbf{H}^e}{d\xi} \right)^T GK \left(\frac{d\mathbf{H}^e}{d\xi} \right) \right] \mathbf{u}^e \frac{L^e}{2} d\xi \\ = \frac{EI_{\omega\omega}}{L^{e3}} \begin{bmatrix} 12 & 6L^e & -12 & 6L^e \\ & 4L^{e2} & -6L^e & 2L^{e2} \\ & & 12 & -6L^e \\ & & & 4L^{e2} \end{bmatrix} + \frac{GK}{30L^e} \begin{bmatrix} 36 & 3L^e & -36 & 3L^e \\ & 4L^{e2} & -3L^e & -L^{e2} \\ & & 36 & -3L^e \\ & & & 4L^{e2} \end{bmatrix} \end{aligned} \quad (4.20)$$

The vector \mathbf{f}_e is the *element external force matrix*, given by

$$\begin{aligned}
\mathbf{f}_e &= \int_{-1}^1 \mathbf{H}^{eT} m_\varphi \frac{L^e}{2} d\xi - \int_{-1}^1 \frac{2}{L^e} \left(\frac{d\mathbf{H}^e}{d\xi} \right)^T b \frac{L^e}{2} d\xi + \mathbf{H}^{eT} \bar{T} n|_{\Gamma^e} - \frac{2}{L^e} \left(\frac{d\mathbf{H}^e}{d\xi} \right)^T \bar{M}_\omega n|_{\Gamma^e} \\
&= \begin{bmatrix} m_\varphi \frac{L^e}{2} - b \\ m_\varphi \frac{L^{e2}}{12} \\ m_\varphi \frac{L^e}{2} + b \\ -m_\varphi \frac{L^{e2}}{12} \end{bmatrix} + \begin{bmatrix} -\bar{T}(-1) \\ -\bar{M}_\omega(-1) \\ \bar{T}(+1) \\ \bar{M}_\omega(+1) \end{bmatrix}
\end{aligned} \tag{4.21}$$

After considering the assembling of \mathbf{K}_e and \mathbf{f}_e , the expression for the entire structure is

$$\boldsymbol{\phi}^T \{ \mathbf{K} \mathbf{u} - \mathbf{f} \} = \boldsymbol{\phi}^T \{ \mathbf{r} \} = \mathbf{0} \tag{4.22}$$

Where \mathbf{r} is called *residual*. \mathbf{K} is the *global stiffness matrix* and \mathbf{f} is the *global external force matrix*. Note that this element can be used only if torsion is uncoupled from bending or extension of the beam element, as shown in figure 4.3.

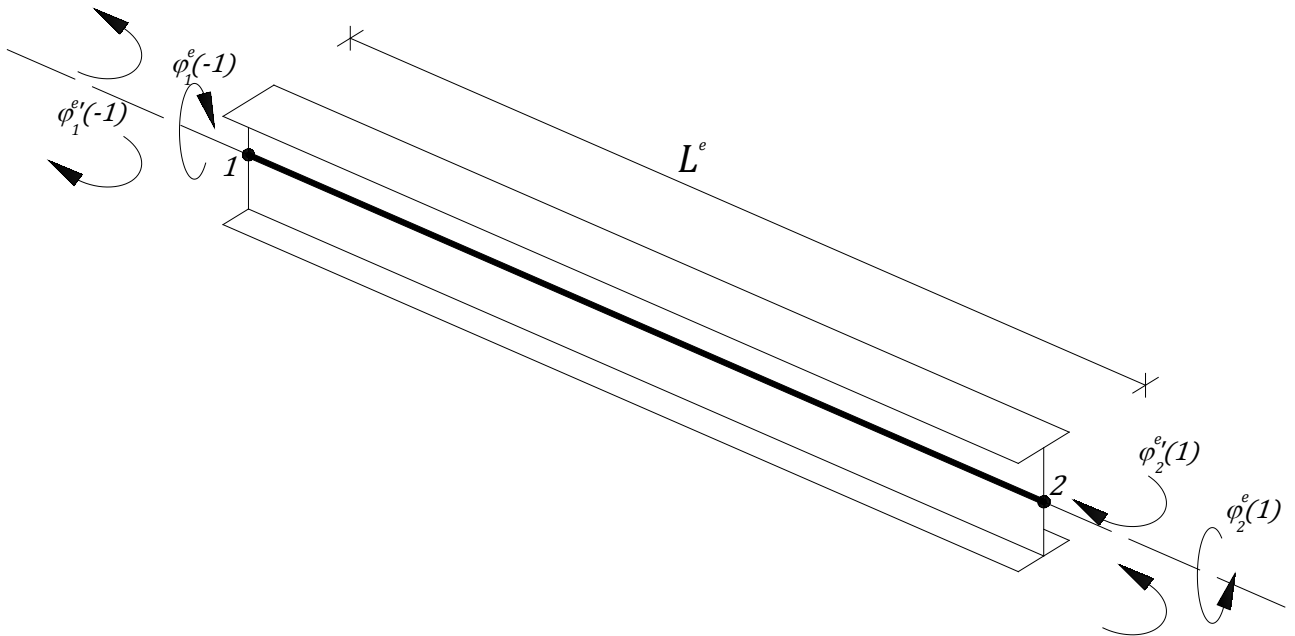


Figure 4.3 –Thin walled beam element subject to uncoupled torsion.

4.2.2. The thin-walled beam element considering an additional DOF of warping

When the shear center of a thin walled cross-section do not coincide with the elastic center, the torsion of a generally loaded beam element is coupled with its flexural behavior.

For these kind of problems a finite element with 7 DOF at each end of the element is developed. This element takes into account all the general displacements, in order to make an analysis of every thin-walled type of cross-section.

The development of a coupled generic formulation of a thin-walled beam element is approached by the *variational principles*.

As illustrated in the first part of this chapter, different types of approximation functions will be used for the interpolation of the beam element generalized displacements. These approximation functions are summarized in table 4.2. Note that N^e indicates linear interpolation functions for the element and H_i^e indicates polynomial Hermite's interpolations.

Table 4.2 – Displacement field and approximation functions.

Displacements	Smoothness required for the approximation	Displacement approximation functions	Nodal displacements vector
<i>Axial</i>	Piecewise continuously differentiable	$\eta^e(x) = N^e \cdot d^e$	$\mathbf{u}_x^e = \begin{bmatrix} u_1^e \\ u_2^e \end{bmatrix}$
<i>Bending</i>	Continuously differentiable	$\xi_y^e(x) = H_y^e \cdot \mathbf{u}_y^e$	$\mathbf{u}_y^e = [w_{y1}^e \quad w'_{y1} \quad w_{y2}^e \quad w'_{y2}]^T$
	Continuously differentiable	$\xi_z^e(x) = H_z^e \cdot \mathbf{u}_z^e$	$\mathbf{u}_z^e = [w_{z1}^e \quad w'_{z1} \quad w_{z2}^e \quad w'_{z2}]^T$
<i>Torsion</i>	Continuously differentiable	$\varphi^e(x) = H_\varphi^e \cdot \mathbf{u}_\varphi^e$	$\mathbf{u}_\varphi^e = [w_{\varphi1}^e \quad w'_{\varphi1} \quad w_{\varphi2}^e \quad w'_{\varphi2}]^T$

In section 4.2.1 it is illustrated that two alternative methods can be used to formulate the FEM discretization, the principle of virtual work or alternatively the minimum potential energy principle. This second approach is used in the sequel to obtain the discrete equations in a matrix format. The final displacement approximation could be considered as a vector as follows:

$$\begin{aligned} \boldsymbol{\zeta}^e(x) &= [\eta^e(x) \quad \xi_y^e(x) \quad -\xi_y'^e(x) \quad \xi_z^e(x) \quad \xi_z'^e(x) \quad \varphi^e(x) \quad -\varphi'^e(x)] \\ &= \left[N^e \quad H_y^e \quad -\frac{dH_y^e}{dx} \quad H_z^e \quad -\frac{dH_z^e}{dx} \quad H_\varphi^e \quad -\frac{dH_\varphi^e}{dx} \right] \begin{bmatrix} \mathbf{u}_x^e \\ \mathbf{u}_y^e \\ \mathbf{u}_z^e \\ \mathbf{u}_\varphi^e \\ \mathbf{u}_\varphi^e \end{bmatrix} \end{aligned} \quad (4.23)$$

This approximation, which is composed by 7 DOF, describes the beam displacement field. The corresponding element stiffness matrix is symmetric and constituted by 14 rows and 14 columns.

A first element stiffness matrix will be obtained considering two axes of reference for the displacements of the cross-section, according to the static governing equations already derived in chapter 3. Then a second

stiffness matrix will be illustrated considering the element axes coincident with the elastic center axis. This formulation will allow to define the displacement field, the stress distribution and the boundary conditions of the element as referred to the same axis. This aspect could have several advantages in the analysis of straight continuous beam elements with thin-walled section, i.e. complex frame structures and bridge models.

Axial effect

The first variation of the potential energy for a generic point P of the cross-section plan can be expressed as follows when axial effect is considered

$$\delta V(\delta\eta, \delta\eta') = \int_0^L E(A\eta'\delta\eta' - S^P_y \xi''_y \delta\eta' - S^P_z \xi''_z \delta\eta' - S^P_\omega \varphi'' \delta\eta') dx - \int_0^L q_x \delta\eta dx - [\bar{N}\delta\eta]_0^L = 0 \quad (4.24)$$

The equation (4.24) is equivalent to the *weak form* of the extension equilibrium with respect to a generic point P when coupling is considered between all the generalized displacements. The discretization of the equations according with (4.23) gives

- *Element stiffness matrix*

$$\begin{aligned} \mathbf{K}^e_\eta = & \int_{-1}^1 \left[\frac{4}{L^2} \left(\frac{d\mathbf{N}^e}{d\xi} \right)^T EA \left(\frac{d\mathbf{N}^e}{d\xi} \right) \right] \mathbf{u}_x^e \frac{L^e}{2} d\xi - \frac{1}{2} \int_{-1}^1 \left[\frac{8}{L^3} \left(\frac{d\mathbf{N}^e}{d\xi} \right)^T ES^P_y \left(\frac{d^2 \mathbf{H}_y^e}{d\xi^2} \right) \right] \mathbf{u}_y^e \frac{L^e}{2} d\xi \\ & - \frac{1}{2} \int_{-1}^1 \left[\frac{8}{L^3} \left(\frac{d\mathbf{N}^e}{d\xi} \right)^T ES^P_z \left(\frac{d^2 \mathbf{H}_z^e}{d\xi^2} \right) \right] \mathbf{u}_z^e \frac{L^e}{2} d\xi \\ & - \frac{1}{2} \int_{-1}^1 \left[\frac{8}{L^3} \left(\frac{d\mathbf{N}^e}{d\xi} \right)^T ES^P_\omega \left(\frac{d^2 \mathbf{H}_\varphi^e}{d\xi^2} \right) \right] \mathbf{u}_\varphi^e \frac{L^e}{2} d\xi = \\ & \frac{EA}{L^e} \begin{bmatrix} 1 & -1 \\ -1 & 1 \end{bmatrix} \mathbf{u}_x^e - \frac{ES^P_y}{2L^e} \begin{bmatrix} 0 & 1 & 0 & -1 \\ 0 & -1 & 0 & 1 \end{bmatrix} \mathbf{u}_y^e - \frac{ES^P_z}{2L^e} \begin{bmatrix} 0 & 1 & 0 & -1 \\ 0 & -1 & 0 & 1 \end{bmatrix} \mathbf{u}_z^e - \frac{ES^P_\omega}{2L^e} \begin{bmatrix} 0 & 1 & 0 & -1 \\ 0 & -1 & 0 & 1 \end{bmatrix} \mathbf{u}_\varphi \end{aligned} \quad (4.25)$$

- *External force vector*

$$\mathbf{f}^e_\eta = \int_{-1}^1 \mathbf{N}^{eT} q_x \frac{L^e}{2} d\xi + \mathbf{N}^{eT} \bar{N}n|_{\Gamma^e} = \begin{bmatrix} q_x \frac{L^e}{2} \\ \frac{L^e}{2} \\ q_x \frac{L^e}{2} \end{bmatrix} + \begin{bmatrix} -\bar{N}_1 \\ \bar{N}_2 \end{bmatrix} \quad (4.26)$$

where \bar{N}_1, \bar{N}_2 refer to the axial forces at the end nodes of the beam element and are positive if directed as the nodal displacements.

The internal forces that appear through the stiffness matrix are the effects of a general cross-section deformation. As shown in figure 4.4 the application of the axial force in a generic point P generates four different contributions: a uniform compression, bending in two directions and finally the warping of the section.

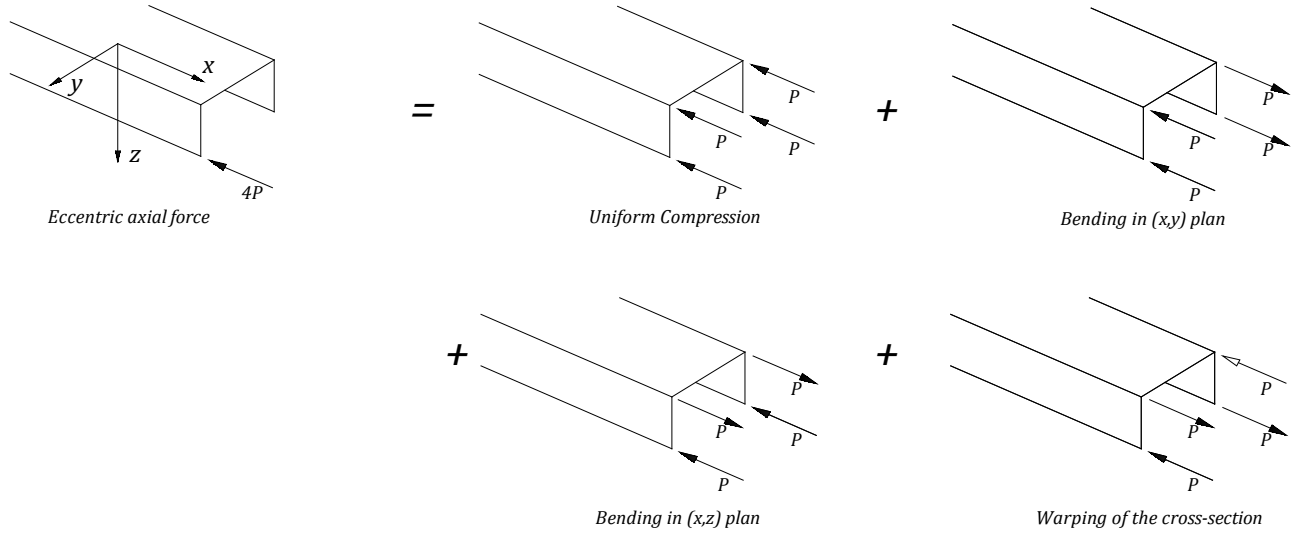


Figure 4.4 – Effects of the application of a general axial force on a thin walled beam (Cedolin, 1996).

Bending

As already done for the extension degree of freedom, the weak form is discretized starting from the first variation of the potential energy for bending in two directions

$$\begin{aligned} \delta V \left(\delta \xi_y, \delta \xi'_y, \delta \xi''_y \right) &= \int_0^L \left(-\delta \xi''_{\alpha} ES^P_{\alpha} \eta' + \delta \xi''_{\alpha} EI^P_{\alpha\beta} \xi''_{\beta} + \delta \xi''_{\alpha} EI^P_{\alpha\omega} \varphi'' + m_{\alpha} \delta \xi'_{\alpha} - q_{\alpha} \delta \xi_{\alpha} \right) dx \\ &\quad - [\delta \xi_{\alpha} \bar{V}_{\alpha}]_0^L + [\delta \xi'_{\alpha} \bar{M}_{\alpha}]_0^L \end{aligned} \quad (4.27)$$

The repeated subscripts α and β imply summation over $\alpha = y, z$ and $\beta = y, z$.

Considering for simplicity only the y -direction and admitting the same approximations for test functions and trial solutions, the discretized equation can be written as follows

- *Element stiffness matrix*

$$\begin{aligned} \mathbf{K}^e_{\xi_y} &= -\frac{1}{2} \int_{-1}^1 \left[\frac{8}{L^3} \left(\frac{d^2 \mathbf{H}_y^e}{d\xi^2} \right)^T ES^P_y \left(\frac{dN^e}{d\xi} \right) \right] \mathbf{u}_x^e \frac{L^e}{2} d\xi + \int_{-1}^1 \left[\frac{16}{L^4} \left(\frac{d^2 \mathbf{H}_y^e}{d\xi^2} \right)^T EI^P_y \left(\frac{d^2 \mathbf{H}_y^e}{d\xi^2} \right) \right] \mathbf{u}_y^e \frac{L^e}{2} d\xi + \\ &\quad \frac{1}{2} \int_{-1}^1 \left[\frac{16}{L^4} \left(\frac{d^2 \mathbf{H}_y^e}{d\xi^2} \right)^T EI^P_{yz} \left(\frac{d^2 \mathbf{H}_z^e}{d\xi^2} \right) \right] \mathbf{u}_z^e \frac{L^e}{2} d\xi + \frac{1}{2} \int_{-1}^1 \left[\frac{16}{L^4} \left(\frac{d^2 \mathbf{H}_y^e}{d\xi^2} \right)^T EI^P_{y\omega} \left(\frac{d^2 \mathbf{H}_{\varphi}^e}{d\xi^2} \right) \right] \mathbf{u}_{\varphi}^e \frac{L^e}{2} d\xi = \\ &\quad \frac{ES^P_y}{2L^e} \begin{bmatrix} 0 & 0 \\ 1 & -1 \\ 0 & 0 \\ -1 & 1 \end{bmatrix} \mathbf{u}_x^e + \frac{EI^P_y}{L^3} \begin{bmatrix} 12 & 6L^e & -12 & 6L^e \\ 6L^e & 4L^{e2} & -6L^e & 2L^{e2} \\ -12 & -6L^e & 12 & -6L^e \\ 6L^e & 2L^{e2} & -6L^e & 4L^{e2} \end{bmatrix} \mathbf{u}_y^e + \\ &\quad \frac{1}{2} \frac{EI^P_{yz}}{L^3} \begin{bmatrix} 12 & 6L^e & -12 & 6L^e \\ 6L^e & 4L^{e2} & -6L^e & 2L^{e2} \\ -12 & -6L^e & 12 & -6L^e \\ 6L^e & 2L^{e2} & -6L^e & 4L^{e2} \end{bmatrix} \mathbf{u}_z^e + \frac{1}{2} \frac{EI^P_{y\omega}}{L^3} \begin{bmatrix} 12 & 6L^e & -12 & 6L^e \\ 6L^e & 4L^{e2} & -6L^e & 2L^{e2} \\ -12 & -6L^e & 12 & -6L^e \\ 6L^e & 2L^{e2} & -6L^e & 4L^{e2} \end{bmatrix} \mathbf{u}_{\varphi}^e \end{aligned} \quad (4.28)$$

- External force vector

$$\mathbf{f}_{\xi y}^e = \int_{-1}^1 \mathbf{H}_y^e q_y \frac{L^e}{2} d\xi - \int_{-1}^1 \frac{2}{L^e} \left(\frac{d\mathbf{H}_y^e}{d\xi} \right) m_y \frac{L^e}{2} d\xi + \mathbf{H}_y^e \bar{V}_y n|_{\Gamma^e} - \left(\frac{d\mathbf{H}_y^e}{d\xi} \right) \bar{M}_y n|_{\Gamma^e} = \begin{bmatrix} q_y \frac{L^e}{2} - m_y \\ q_y \frac{L^e}{2} \\ q_y \frac{L^e}{2} + m_y \\ -q_y \frac{L^e}{2} \end{bmatrix} + \begin{bmatrix} -\bar{V}_y \\ -\bar{M}_y \\ \bar{V}_y \\ \bar{M}_y \end{bmatrix} \quad (4.29)$$

For the flexural plane (x, z) the same matrices are obtained and will be written in the complete stiffness matrix assembling.

Torsion

Uncoupled torsion has been already taken into account in its uncoupling form . When referred to the point P the first variation of potential energy is written as follows:

$$\delta V(\varphi) = \int_0^L \left(-\delta\varphi'' ES^P \omega \eta' + \delta\varphi'' I^P \omega_y \xi''_y + \delta\varphi'' I^P \omega_z \xi''_z + \delta\varphi'' EI^P \omega \omega \varphi'' + \delta\varphi' GK \varphi' + b \delta\varphi' - m_\varphi \delta\varphi \right) dx - ([\delta\varphi \bar{T}]_0^L - [\delta\varphi' \bar{M}_\omega]_0^L) \quad (4.30)$$

Substituting the FEM discretization and applying the Galerkin FEM to the discretization yields the following:

$$\begin{aligned} \mathbf{K}_\varphi^e &= -\frac{1}{2} \int_{-1}^1 \left[\frac{8}{L^e} \left(\frac{d^2 \mathbf{H}_\varphi^e}{d\xi^2} \right)^T ES^P \omega \left(\frac{d\mathbf{N}^e}{d\xi} \right) \right] \mathbf{u}_x^e \frac{L^e}{2} d\xi + \frac{1}{2} \int_{-1}^1 \left[\frac{16}{L^e} \left(\frac{d^2 \mathbf{H}_\varphi^e}{d\xi^2} \right)^T EI^P \omega_y \left(\frac{d^2 \mathbf{H}_y^e}{d\xi^2} \right) \right] \mathbf{u}_y^e \frac{L^e}{2} d\xi + \\ &\frac{1}{2} \int_{-1}^1 \left[\frac{16}{L^e} \left(\frac{d^2 \mathbf{H}_\varphi^e}{d\xi^2} \right)^T EI^P \omega_z \left(\frac{d^2 \mathbf{H}_z^e}{d\xi^2} \right) \right] \mathbf{u}_z^e \frac{L^e}{2} d\xi + \int_{-1}^1 \left[\frac{16}{L^e} \left(\frac{d^2 \mathbf{H}_\varphi^e}{d\xi^2} \right)^T EI^P \omega \omega \left(\frac{d^2 \mathbf{H}_\varphi^e}{d\xi^2} \right) \right] \mathbf{u}_\varphi^e \frac{L^e}{2} d\xi = \\ &-\frac{1}{2} \frac{ES^P \omega}{2L^e} \begin{bmatrix} 0 & 0 \\ 1 & -1 \\ 0 & 0 \\ -1 & 1 \end{bmatrix} \mathbf{u}_x^e + \frac{1}{2} \frac{EI^P \omega_y}{L^e} \begin{bmatrix} 12 & 6L^e & -12 & 6L^e \\ 6L^e & 4L^e & -6L^e & 2L^e \\ -12 & -6L^e & 12 & -6L^e \\ 6L^e & 2L^e & -6L^e & 4L^e \end{bmatrix} \mathbf{u}_y^e + \\ &\frac{1}{2} \frac{EI^P \omega_z}{L^e} \begin{bmatrix} 12 & 6L^e & -12 & 6L^e \\ 6L^e & 4L^e & -6L^e & 2L^e \\ -12 & -6L^e & 12 & -6L^e \\ 6L^e & 2L^e & -6L^e & 4L^e \end{bmatrix} \mathbf{u}_z^e + \frac{EI^P \omega \omega}{L^e} \begin{bmatrix} 12 & 6L^e & -12 & 6L^e \\ 6L^e & 4L^e & -6L^e & 2L^e \\ -12 & -6L^e & 12 & -6L^e \\ 6L^e & 2L^e & -6L^e & 4L^e \end{bmatrix} \mathbf{u}_\varphi^e + \\ &\frac{GK}{30L^e} \begin{bmatrix} 36 & 3L^e & -36 & 3L^e \\ 3L^e & 4L^e & -3L^e & -L^e \\ -36 & -3L^e & 36 & -3L^e \\ 3L^e & -L^e & -3L^e & 4L^e \end{bmatrix} \mathbf{u}_\varphi^e \end{aligned} \quad (4.31)$$

The external force matrix have already been written in eq.(4.21). Note that in the stiffness matrix the Saint Venant contribution does not depends on the point P.

Assembly of the uncoupled matrix of the element

The results obtained in the discretization of the equilibrium equations can be assembled for all the generalized displacements, allowing to write the element stiffness matrix.

It is convenient to write the elements of the vector of nodal displacements and the vector of associated nodal forces in the following order

$$\mathbf{d}^e = \begin{bmatrix} u_1^e \\ w_{y1}^e \\ w'_{y1}^e \\ w_{z1}^e \\ w'_{z1}^e \\ w_{\varphi 1}^e \\ w'_{\varphi 1}^e \\ u_2^e \\ w_{y2}^e \\ w'_{y2}^e \\ w_{z2}^e \\ w'_{z2}^e \\ w_{\varphi 2}^e \\ w'_{\varphi 2}^e \end{bmatrix}; \quad \mathbf{f}^e = \begin{bmatrix} q_x \frac{L^e}{2} \\ q_y \frac{L^e}{2} - m_y \\ q_y \frac{L^e}{12} \\ q_z \frac{L^e}{2} - m_z \\ q_z \frac{L^e}{12} \\ m_{\varphi} \frac{L^e}{2} - b \\ m_{\varphi} \frac{L^e}{12} \\ q_x \frac{L^e}{2} \\ q_y \frac{L^e}{2} + m_y \\ -q_y \frac{L^e}{12} \\ q_z \frac{L^e}{2} + m_z \\ -q_z \frac{L^e}{12} \\ m_{\varphi} \frac{L^e}{2} + b \\ m_{\varphi} \frac{L^e}{12} \end{bmatrix} + \begin{bmatrix} -\bar{N}_1 \\ -\bar{V}_{y1} \\ -\bar{M}_{y1} \\ -\bar{V}_{z1} \\ -\bar{M}_{z1} \\ -\bar{T}_1 \\ -\bar{M}_{\omega 1} \\ \bar{N}_2 \\ \bar{V}_{y2} \\ \bar{M}_{y2} \\ \bar{V}_{z2} \\ \bar{M}_{z2} \\ \bar{T}_2 \\ \bar{M}_{\omega 2} \end{bmatrix} \quad (4.32)$$

In order to simplify the discrete equations, the displacement field will be referred to the *elastic center* for axial effect and bending and to the *shear center* for the torsion as done for the equilibrium equations. This gives for the stiffness matrix

$$K_e = \begin{bmatrix} K^e_{\eta 1} \\ K^e_{\xi y 1} \\ K^e_{\xi z 1} \\ K^e_{\varphi 1} \\ K^e_{\eta 2} \\ K^e_{\xi y 2} \\ K^e_{\xi z 2} \\ K^e_{\varphi 2} \end{bmatrix} \quad (4.33)$$

$$= \begin{bmatrix} \frac{EA}{L^e} & 0 & 0 & 0 & 0 & 0 & 0 & 0 & -\frac{EA}{L^e} & 0 & 0 & 0 & 0 & 0 & 0 & 0 \\ 12 \frac{EI_y}{L^e} & 6 \frac{EI_y}{L^e} & 0 & 0 & 0 & 0 & 0 & 0 & -12 \frac{EI_y}{L^e} & 6 \frac{EI_y}{L^e} & 0 & 0 & 0 & 0 & 0 & 0 \\ 4 \frac{EI_y}{L^e} & 0 & 0 & 0 & 0 & 0 & 0 & 0 & -6 \frac{EI_y}{L^e} & 2 \frac{EI_y}{L^e} & 0 & 0 & 0 & 0 & 0 & 0 \\ 12 \frac{EI_z}{L^e} & 6 \frac{EI_z}{L^e} & 0 & 0 & 0 & 0 & 0 & 0 & 0 & 0 & -12 \frac{EI_z}{L^e} & 6 \frac{EI_z}{L^e} & 0 & 0 & 0 & 0 \\ 4 \frac{EI_z}{L^e} & 0 & 0 & 0 & 0 & 0 & 0 & 0 & 0 & 0 & -6 \frac{EI_z}{L^e} & 2 \frac{EI_z}{L^e} & 0 & 0 & 0 & 0 \\ 12 \frac{EI_{\omega\omega}}{L^e} + \frac{36 GK}{30 L^e} & 6 \frac{EI_{\omega\omega}}{L^e} + \frac{3 GK}{30} & 0 & 0 & 0 & 0 & 0 & 0 & -12 \frac{EI_{\omega\omega}}{L^e} - \frac{36 GK}{30 L^e} & 6 \frac{EI_{\omega\omega}}{L^e} + \frac{3 GK}{30} & 0 & 0 & 0 & 0 & 0 & 0 \\ 4 \frac{EI_{\omega\omega}}{L^e} + \frac{4 GK L^e}{30} & 0 & 0 & 0 & 0 & 0 & 0 & 0 & -6 \frac{EI_{\omega\omega}}{L^e} - \frac{3 GK}{30} & 2 \frac{EI_{\omega\omega}}{L^e} - \frac{1 GK L^e}{30} & 0 & 0 & 0 & 0 & 0 & 0 \\ \frac{EA}{L^e} & 0 & 0 & 0 & 0 & 0 & 0 & 0 & 0 & 0 & 0 & 0 & 0 & 0 & 0 & 0 \\ 12 \frac{EI_y}{L^e} & -6 \frac{EI_y}{L^e} & 0 & 0 & 0 & 0 & 0 & 0 & 0 & 0 & 0 & 0 & 0 & 0 & 0 & 0 \\ 4 \frac{EI_y}{L^e} & 0 & 0 & 0 & 0 & 0 & 0 & 0 & 0 & 0 & 0 & 0 & 0 & 0 & 0 & 0 \\ 12 \frac{EI_z}{L^e} & -6 \frac{EI_z}{L^e} & 0 & 0 & 0 & 0 & 0 & 0 & 0 & 0 & 0 & 0 & 0 & 0 & 0 & 0 \\ 4 \frac{EI_z}{L^e} & 0 & 0 & 0 & 0 & 0 & 0 & 0 & 0 & 0 & 0 & 0 & 0 & 0 & 0 & 0 \\ 12 \frac{EI_{\omega\omega}}{L^e} + \frac{36 GK}{30 L^e} & -6 \frac{EI_{\omega\omega}}{L^e} - \frac{3 GK}{30} & 0 & 0 & 0 & 0 & 0 & 0 & 0 & 0 & 0 & 0 & 0 & 0 & 0 & 0 \\ 4 \frac{EI_{\omega\omega}}{L^e} + \frac{4 GK L^e}{30} & 0 & 0 & 0 & 0 & 0 & 0 & 0 & 0 & 0 & 0 & 0 & 0 & 0 & 0 & 0 \end{bmatrix}$$

Symmetric

The 7 DOF element discretization have been completely defined and both nodal displacements and forces in (4.32) and in (4.33) refer to two different axes. The axis considered for the beam generalized displacements in order to uncoupling the effects of extension, bending and torsion are described in table 4.3,

Table 4.3 – Beam element displacements and corresponding axis of reference

Beam generalized displacements	Axis of reference
<i>Extension: $\delta\eta$</i>	<i>Elastic centre: (y_C, z_C)</i>
<i>Bending: $\delta\xi_y, \delta\xi'_y, \delta\xi_z, \delta\xi'_z$</i>	
<i>Torsion: $\delta\varphi, \delta\varphi'$</i>	<i>Shear centre: (y_A, z_A)</i>

The thin- walled beam element is represented by a generic example of a C-cross section in figure 4.5.

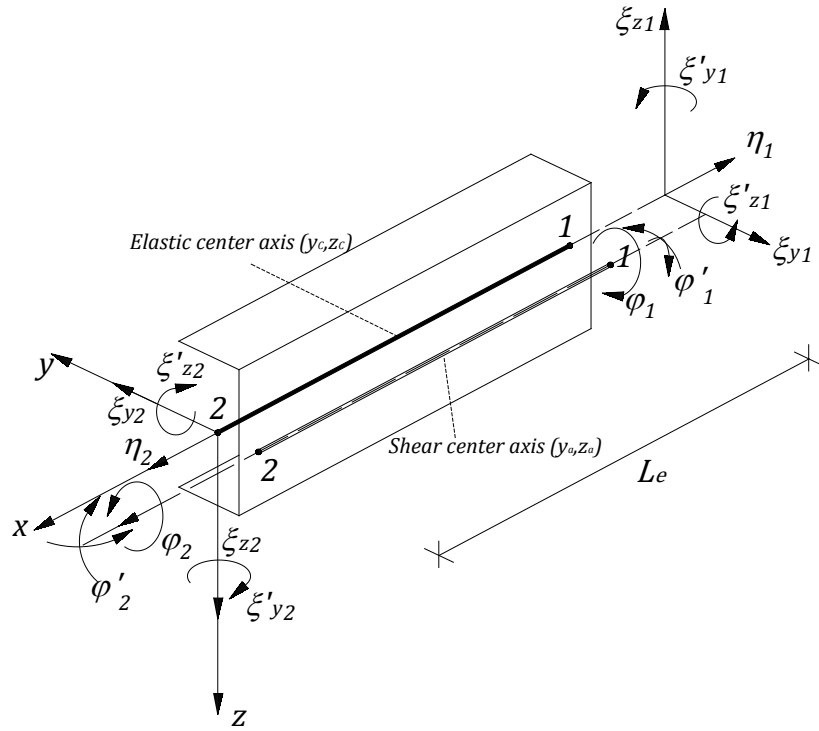


Figure 4.5 – Thin-walled C-beam element displacement referred to two axis.

Matrix of the element referred to the elastic center

The linear system defined by (4.32) and (4.33) describes the finite element approximation by means of two axis. Taking into account this model the boundary conditions for the thin walled beam must be imposed on two different axes according to the prescribed displacement of the general DOF.

The objective of the present analysis is to propose a discrete model in which only one axis is considered for the beam element in order to obtain a stress analysis for continuous spans beams, i.e. a straight multi-spans bridge deck. The axis chosen to describe the beam element is the elastic center: this means that kinematics, strain and stresses, expressed by means of \mathbf{K}^e , \mathbf{f}^e and \mathbf{d}^e , must refer to (y_c, z_c) and a coupling between axial effect, bending and torsion appears. Thus a sectorial coordinate ω_c and the relative warping parameter $I_{\omega\omega}^c$ referred to the elastic center axis will be considered in the sequel. The stiffness matrix obtained is written as follows:

$$K^e = \quad (4.34)$$

$$\left[\begin{array}{cccccccccccccccc}
 \frac{EA}{L^e} & 0 & 0 & 0 & 0 & 0 & -\frac{ES_{\omega}^C}{2L^e} & -\frac{EA}{L^e} & 0 & 0 & 0 & 0 & 0 & 0 & \frac{ES_{\omega}^C}{2L^e} \\
 12\frac{EI_y}{L^e{}^3} & 6\frac{EI_y}{L^e{}^2} & 0 & 0 & 6\frac{EI_{\omega y}}{L^e{}^3} & 3\frac{EI_{\omega y}}{L^e{}^2} & 0 & -12\frac{EI_y}{L^e{}^3} & 6\frac{EI_y}{L^e{}^2} & 0 & 0 & 0 & -6\frac{EI_{\omega y}}{L^e{}^3} & 3\frac{EI_{\omega y}}{L^e{}^2} \\
 4\frac{EI_y}{L^e} & 0 & 0 & 3\frac{EI_{\omega y}}{L^e{}^2} & 2\frac{EI_{\omega y}}{L^e} & 0 & -6\frac{EI_y}{L^e{}^2} & 2\frac{EI_y}{L^e} & 0 & 0 & 0 & 0 & -3\frac{EI_{\omega y}}{L^e{}^2} & \frac{EI_{\omega y}}{L^e} \\
 12\frac{EI_z}{L^e{}^3} & 6\frac{EI_z}{L^e{}^2} & 6\frac{EI_{\omega z}}{L^e{}^3} & 3\frac{EI_{\omega z}}{L^e{}^2} & 0 & 0 & 0 & -12\frac{EI_z}{L^e{}^3} & 6\frac{EI_z}{L^e{}^2} & -6\frac{EI_{\omega z}}{L^e{}^3} & 3\frac{EI_{\omega z}}{L^e{}^2} \\
 4\frac{EI_z}{L^e} & 3\frac{EI_{\omega z}}{L^e{}^2} & 3\frac{EI_{\omega z}}{L^e} & 0 & 0 & 0 & -6\frac{EI_z}{L^e{}^2} & 2\frac{EI_z}{L^e} & -3\frac{EI_{\omega z}}{L^e{}^2} & \frac{EI_{\omega z}}{L^e} \\
 12\frac{EI_{\omega\omega}}{L^e{}^3} + \frac{36GK}{30L^e} & 6\frac{EI_{\omega\omega}}{L^e{}^2} + \frac{3GK}{30} & 0 & -6\frac{EI_{\omega y}}{L^e{}^3} & 3\frac{EI_{\omega y}}{L^e{}^2} & -6\frac{EI_{\omega z}}{L^e{}^3} & 3\frac{EI_{\omega z}}{L^e{}^2} & -12\frac{EI_{\omega\omega}}{L^e{}^3} - \frac{36GK}{30L^e} & 6\frac{EI_{\omega\omega}}{L^e{}^2} + \frac{3GK}{30} \\
 4\frac{EI_{\omega\omega}}{L^e} + \frac{4GKL^e}{30} & \frac{ES_{\omega}^C}{2L^e} & -3\frac{EI_{\omega y}}{L^e{}^2} & \frac{EI_{\omega y}}{L^e} & -3\frac{EI_{\omega z}}{L^e{}^2} & \frac{EI_{\omega z}}{L^e} & -6\frac{EI_{\omega\omega}}{L^e{}^2} - \frac{3GK}{30} & 2\frac{EI_{\omega\omega}}{L^e} - \frac{1GKL^e}{30} \\
 \frac{EA}{L^e} & 0 & 0 & 0 & 0 & 0 & 0 & -\frac{ES_{\omega}^C}{2L^e} \\
 12\frac{EI_y}{L^e{}^3} & -6\frac{EI_y}{L^e{}^2} & 0 & 0 & 6\frac{EI_{\omega y}}{L^e{}^3} & -3\frac{EI_{\omega y}}{L^e{}^2} \\
 4\frac{EI_y}{L^e} & 0 & 0 & -3\frac{EI_{\omega y}}{L^e{}^2} & 2\frac{EI_{\omega y}}{L^e} \\
 12\frac{EI_z}{L^e{}^3} & -6\frac{EI_z}{L^e{}^2} & 6\frac{EI_{\omega z}}{L^e{}^3} & -3\frac{EI_{\omega z}}{L^e{}^2} \\
 4\frac{EI_z}{L^e} & -3\frac{EI_{\omega z}}{L^e{}^2} & 2\frac{EI_{\omega z}}{L^e} \\
 12\frac{EI_{\omega\omega}}{L^e{}^3} + \frac{36GK}{30L^e} & -6\frac{EI_{\omega\omega}}{L^e{}^2} - \frac{3GK}{30} & 4\frac{EI_{\omega\omega}}{L^e} + \frac{4GKL^e}{30}
 \end{array} \right]$$

Symmetric

In (4.34) both bending in (x, y) and (x, z) plane are coupled with non-uniform torsion of the thin-walled beam element (figure 4.6). For the C-cross section of the figure no coupling is considered in (x, y) plan because of the symmetry of the section with respect to the y -axis: the coupling between torsion and bending only appears in (x, z) plane.

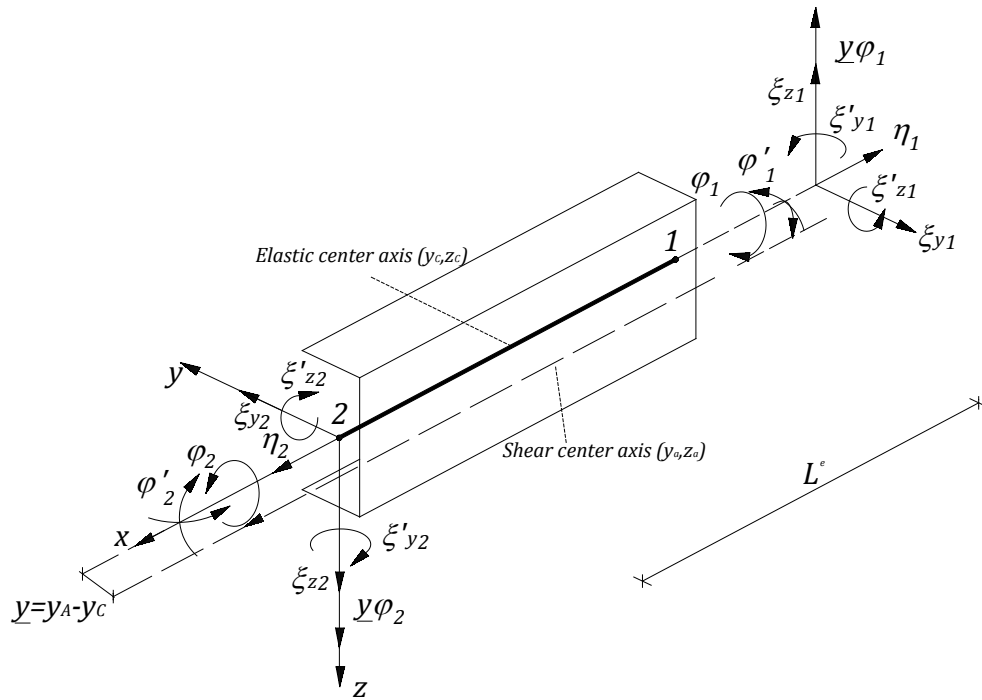


Figure 4.6 –Thin-walled C-beam element displacements described by the elastic center axis.

4.2.3. Selected load cases

In chapter 3 basic load cases of beams have been analyzed with particular attention to torsion. The mathematical solutions proposed by (Kollbrunner & Basler, 1969) can be approximated by the FEM discretization and the results will be illustrated in the sequel. The same cross section layouts of table 3.12 are used for modeling the beam elements and the number of finite elements utilized will be indicated for each load case. Then an indicator of the FEM convergence for this numerical example will be introduced considering the exact solution of Kollbrunner.

A comparison between the current analysis and the results obtained using the ABAQUS software will be developed for a simple numerical example and the results will be commented, in order to check the computer code implemented in the current analysis.

The study of some cross-section layouts cannot be done without considering the coupled effect between torsion and bending of the beam element. This is the case of an open bridge deck section where the torsional displacements are illustrated and compared with a closed box deck section. The response to torsion displacements depends generally from the cross-section type and differences will be plotted for open and closed cross-sections.

Example 4.1: Simply Supported beam acted by uniform torque

The simply supported beam of the example 3.1 is analyzed by a discretization of 60 elements per beam. The characteristics of the cross-section layouts are summarized in the table 4.4, where also the axis of the finite element is specified.

Table 4.4 – Cross-section layout characteristics.

Cross-section	Characteristics	Axis of reference for the FEM analysis
Closed hollow section	$b = 100 \text{ mm}; h = 360 \text{ mm};$ $t = t_w = t_f = 14 \text{ mm};$ $\kappa_{Hollow \text{ sec.}} = 19.89$	Elastic center (coincident with the shear center)
Channel cross Section	$b = 100 \text{ mm}; h = 360 \text{ mm};$ $t = t_w = t_f = 14 \text{ mm};$ $\kappa_{C \text{ sec.}} = 1.5$	Shear center
I cross Section	$b = b_{f1} = b_{f2} = 170 \text{ mm}; h = 360 \text{ mm};$ $t_f = 12.7 \text{ mm}, t_w = 8 \text{ mm};$ $\kappa_{I \text{ sec.}} = 1.19$	Elastic center (coincident with the shear center)

The coordinate system considered is represented in figure 4.7.

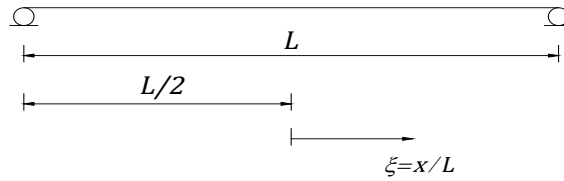


Figure 4.7 – Non-dimensional coordinate system.

The boundary conditions are described in table 4.5.

Table 4.5 – Boundary conditions of the beam.

Coordinate	Static boundary prescribed	Kinematic boundary prescribed
$\xi = -0.5$	$M_\omega(-0.5) = 0$	$\varphi(-0.5) = 0$
$\xi = +0.5$	$M_\omega(+0.5) = 0$	$\varphi(+0.5) = 0$

The results in terms of displacements and internal forces are obtained solving the linear system composed by eq.(4.20) and eq.(4.21) and are represented in the figure 4.8,figure 4.9,figure 4.10 and figure 4.11 where the normalized $\varphi, \varphi', M_\omega, T$ distributions along the beam axis are depicted (Dotted line: FEM model; Continuous line: analytical solution).

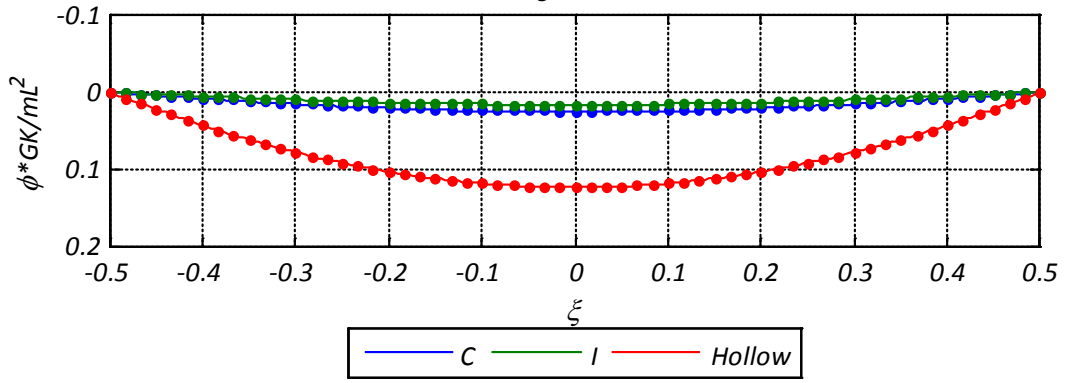


Figure 4.8 – ϕ value of a S-S beam acted by uniform torque (FEM solution).

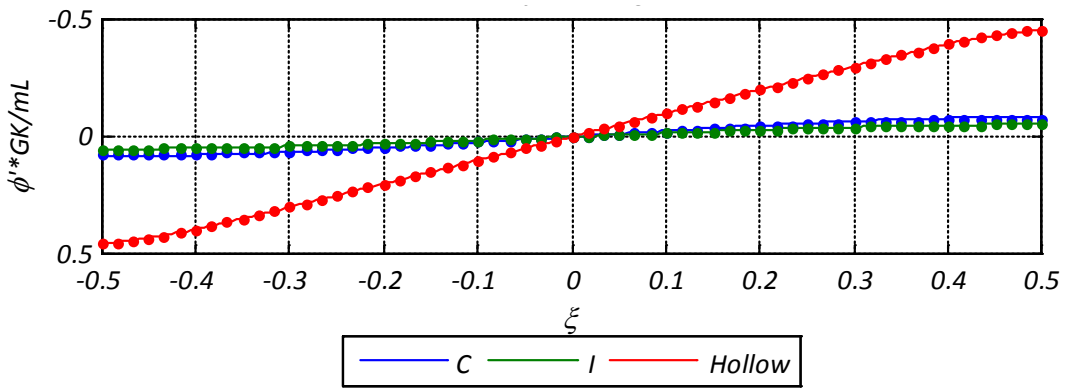


Figure 4.9 – ϕ' value of a S-S beam acted by uniform torque (FEM solution).

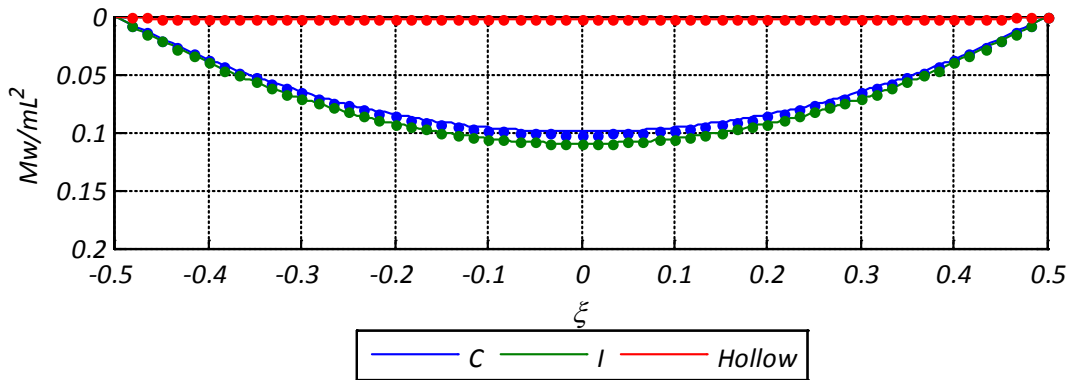


Figure 4.10 – M_ω of a S-S beam acted by uniform torque (FEM solution).

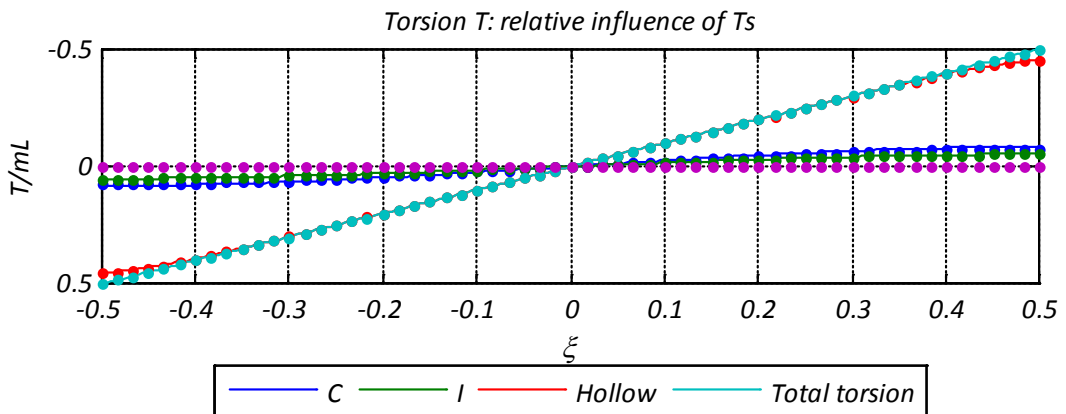


Figure 4.11 – Torsion T of a S-S beam acted by uniform torque (FEM solution).

Example 4.2: Concentrated load on a simply supported beam

In this example, the exact solution of the load case 3.2 will be approximated by the FEM for obtain the twist rotation of the beam, its first derivative, the warping moment and the relatives contributions of torsion. The same coordinate system of figure 4.7 for the same cross-section layouts is used and the boundary conditions for the problem are written in table 4.5. figure 4.12, figure 4.13, figure 4.14 and figure 4.15 show the results obtained(Dotted line: FEM model; Continuous line: analytical solution).

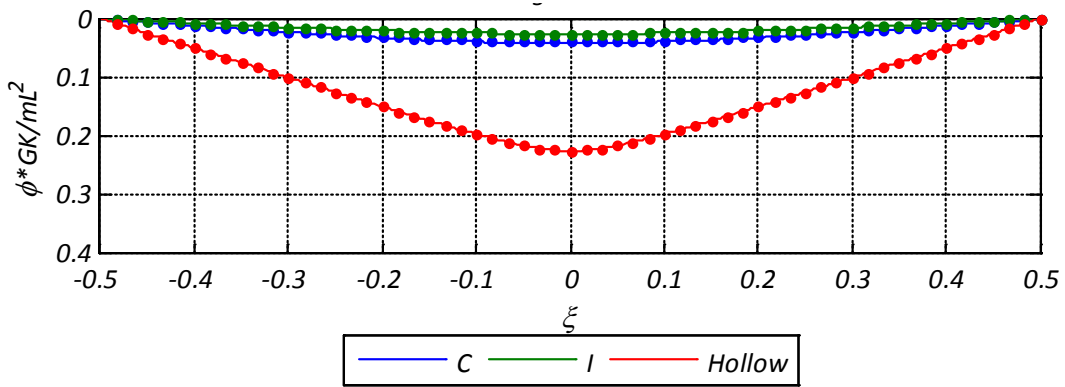


Figure 4.12 – ϕ value of a S-S beam acted by concentrated torque (FEM solution).

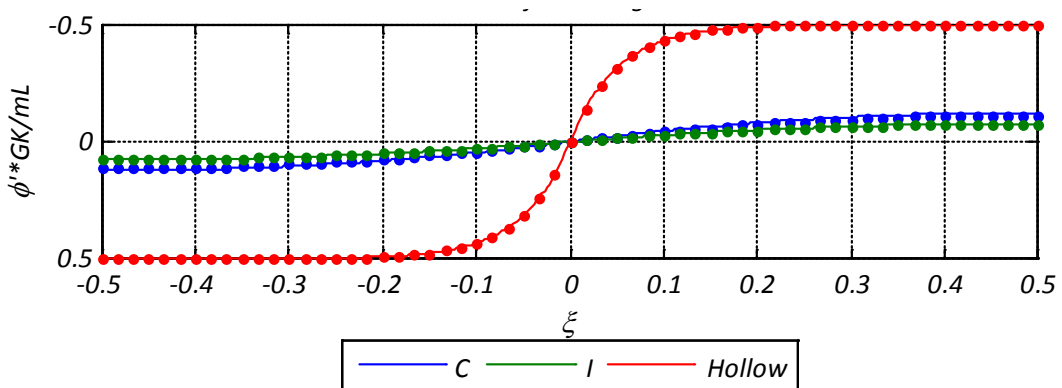


Figure 4.13 – ϕ' value of a S-S beam acted by concentrated torque (FEM solution).

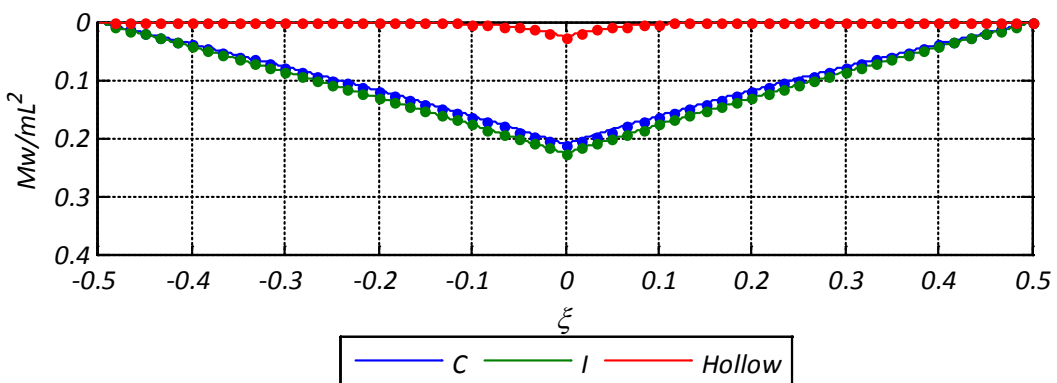


Figure 4.14- M_{ω} of a S-S beam acted by concentrated torque (FEM solution).

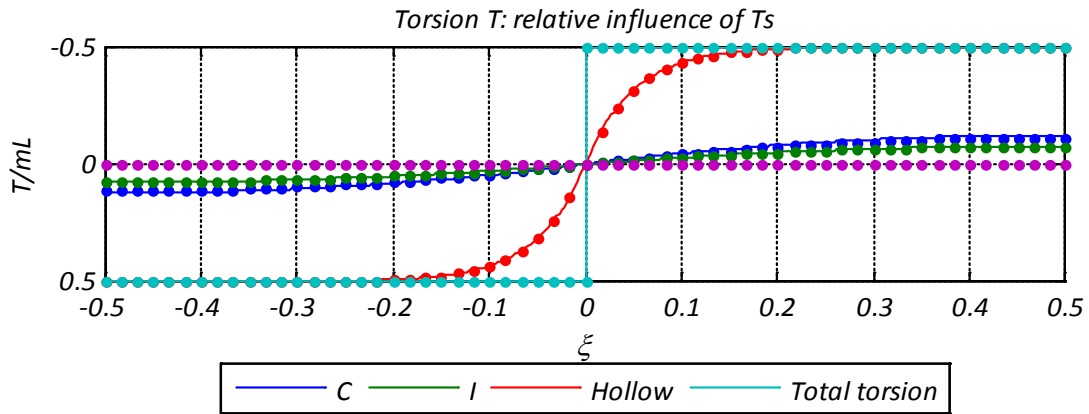


Figure 4.15 - Torsion T of a S-S beam acted by concentrated torque (FEM solution).

Example 4.3: Three continuous spans acted by uniform torque

In this case, as done in the example 3.3, a three continuous spans beam is considered and the approximation of the FEM method refer to the following coordinate system (figure 4.16).

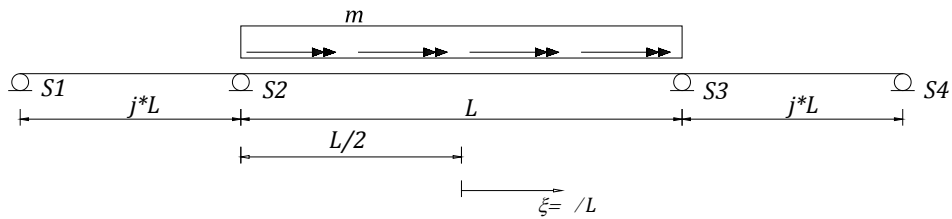


Figure 4.16 - Coordinate system of the three continuous spans beam.

Table 4.6 Shows the discretization considered for each span of the continuous beam.

Table 4.6 - FEM discretization for the continuous three spans beam.

Span	Number of finite element per span	Element length (according to isoparametric coordinates)
Central span $[L]$	120	8.33E-03
Lateral span $[j * L]$	60	

Note that the element size is the same as the element number varies for each span. The boundary conditions are written in table 4.7.

Table 4.7 - Boundary conditions of the three continuous spans beam.

Nodal coordinate	Kinematic conditions prescribed
$S1(\xi = -1.0)$	$\varphi(S1) = 0$
$S2(\xi = -0.5)$	$\varphi(S2) = 0$
$S3(\xi = +0.5)$	$\varphi(S3) = 0$
$S4(\xi = +1.0)$	$\varphi(S4) = 0$

In figure 4.17, figure 4.18, figure 4.19 and figure 4.20 the results are shown considering 60 finite elements in the approximation of the solution. Note that dimensionless functions are shown attempting to (Kollbrunner &

Basler, 1969) in order to be independent from the geometry of the problem(Dotted line: FEM model; Continuous line: analytical solution).

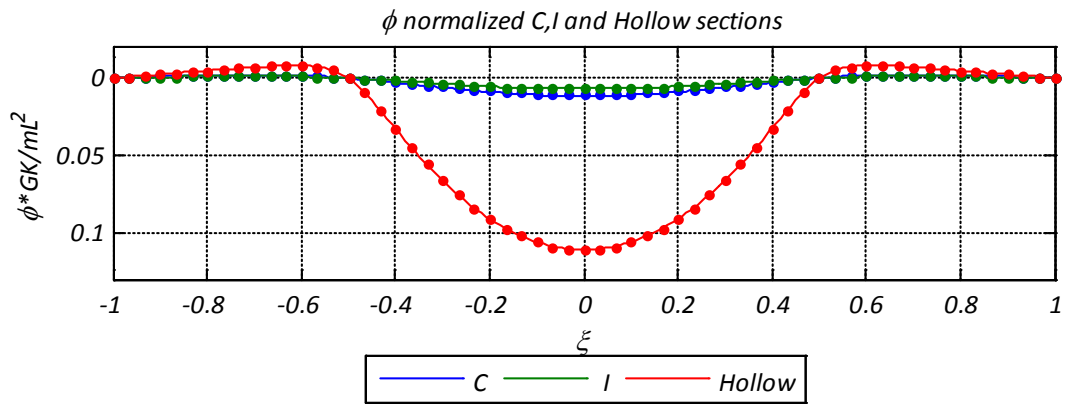


Figure 4.17 - ϕ value of a T-C-S⁵ beam acted by uniform torque (FEM solution).

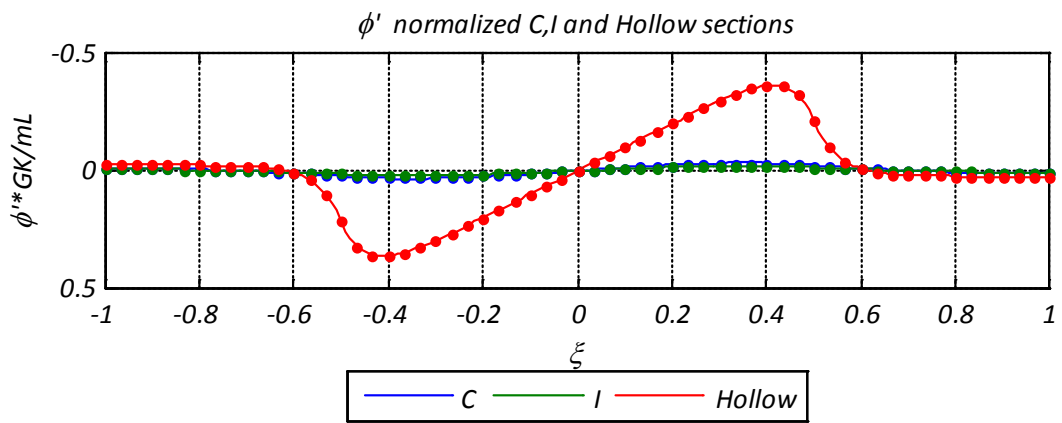


Figure 4.18 - ϕ' value of a T-C-S beam acted by uniform torque (FEM solution).

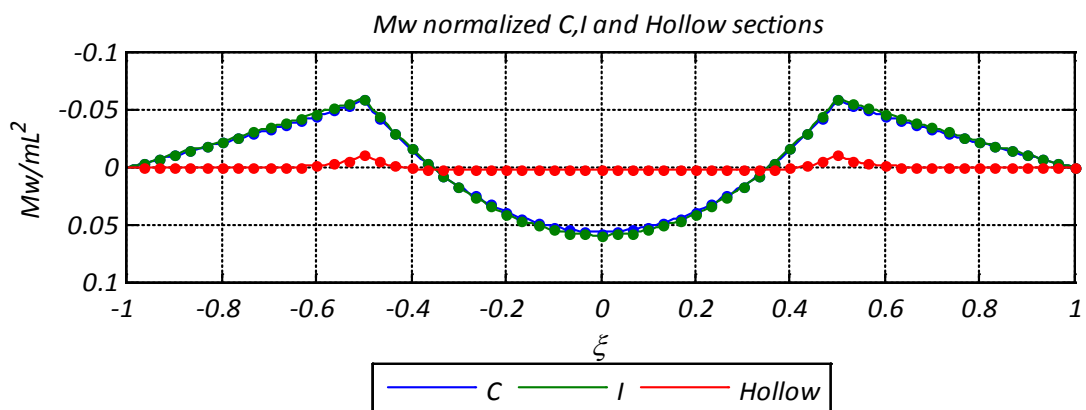


Figure 4.19 - M_{ω} of a T-C-S beam acted by uniform torque (FEM solution).

⁵ Three continuous spans.

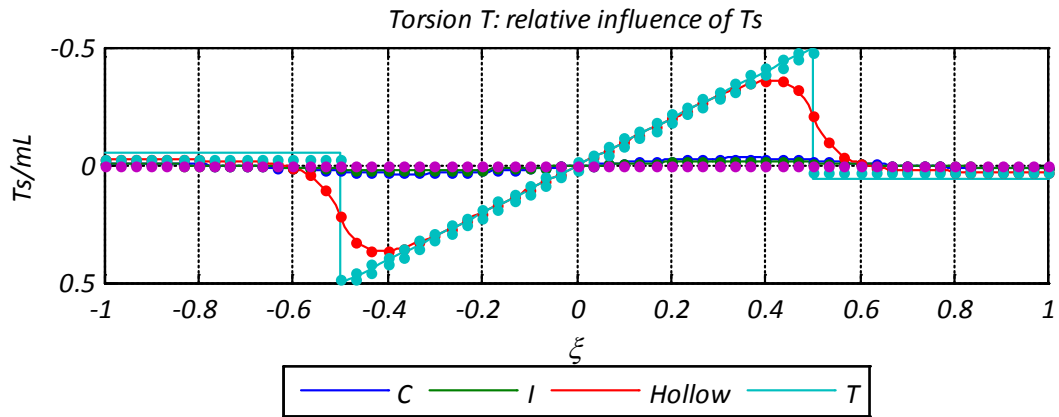


Figure 4.20 – Torsion T of a T-C-S beam acted by uniform torque (FEM solution).

Example 4.4: Convergence of the FEM discretization

With the FEM approximation the results obtained for a load case must be compared with the analytical results. For this reason it is useful to include a parameter allowing to estimate the error in the finite element solution. The rate of *convergence* of this approximated solution can be observed increasing the number of elements, according to the *refinement* type h .

The example 4.3 of a continuous three-spans beam is considered as an example, where 240 elements are used for the analysis of the entire beam. The table 4.8 shows the error variation of $M_\omega/(mL^2)$ at the internal support S2 (see figure 4.16) taking into account a different element length for each approximation, which correspond to consider every FEM mesh with a different number of elements. The total number of elements used in modeling the entire beam is shown in the table, while the number of elements used for the discretization of the central span is half of the total number of elements.

Table 4.8 – Decrease of the relative error of $M_\omega/(mL^2)$ for different finite element meshes.

Element size	12.5E-02 (8 Elem.)	8.33E-02 (12 Elem.)	6.25E-02 (16 Elem.)	5E-02 (20 Elem.)	1.25-02 (80 Elem.)	8.33E-03 (120 Elem.)	4.17E-03 (240 Elem.)	Exact value
$M_\omega/(mL^2)(S2)$	0.0286	0.0386	0.0437	0.0468	0.0564	0.0575	0.0586	0.0597
Relative Error	001%	000%	000%	000%	000%	000%	000%	

The values of the normalized warping moment can be represented as a function of the number of elements used for the discretization of the central span. This function is represented in figure 4.21 where a semi-logarithmic scale is used for the mid-span number of elements.

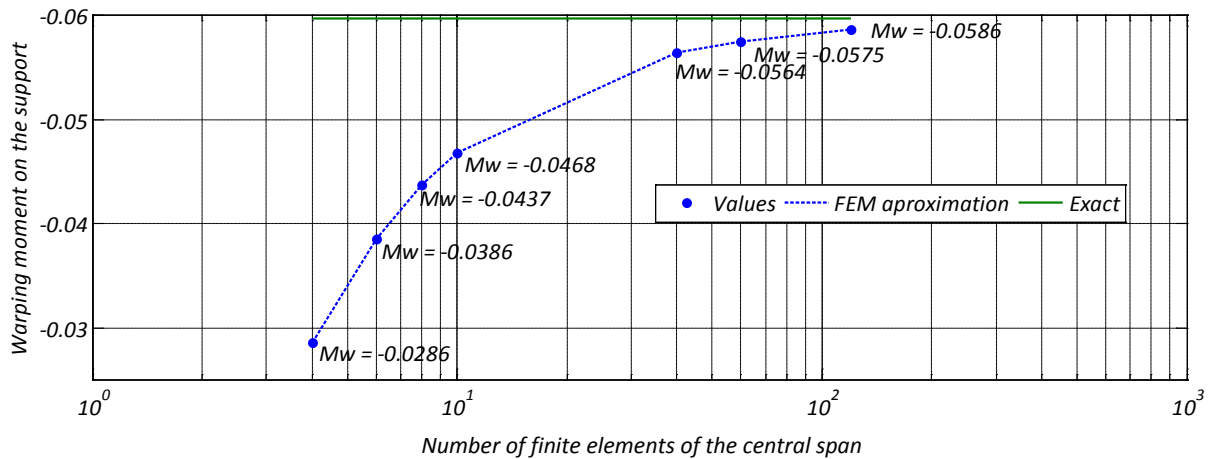


Figure 4.21 – Convergence of the M_{ω} value as function of the mesh refinement.

The analytical value of the normalized warping moment is -0.597 and the analysis performed in the example 4.3 leads to a good approximation of the solution. Note that the warping moment according to the eq.(3.139) is mathematically described by hyperbolic functions and in the finite element model Hermite polynomials were adopted.

Example 4.5: Comparative study between ABAQUS model and current analysis

The software ABAQUS has in its library (Hibbit, 2007) a 7 DOF beam element to perform the analysis of open thin-walled beam cross-sections. This type of element can be used for the study of thin-walled beams, whenever warping cannot be neglected. The characteristics for the element B310S (Hibbit, 2007) are sketched in Figure 4.22.

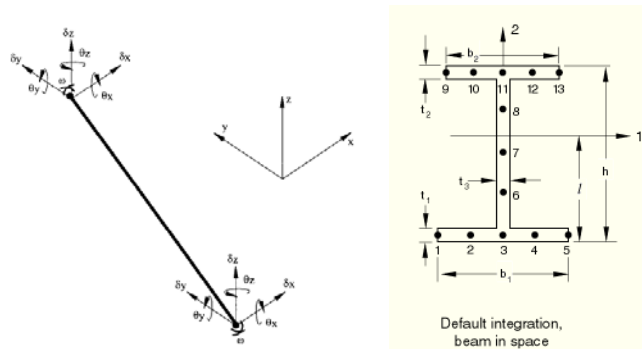


Figure 4.22 – ABAQUS element B310S and integration points for I-beam section.

In this case the FEM approximation will be checked for the three load cases performed above and I-section. The characteristics of the section and the ABAQUS element are illustrated in table 4.9. The table 4.10 shows the results obtained for each load case and estimates the relative error between the two analysis methods, using for the ABAQUS simulation the same number of elements. The normal tension σ_x is calculated at the extreme point of the I-section flange, i.e. the point number 1 in the I-section presented by figure 4.22.

Table 4.9 – Characteristics of the beam Elements loaded.

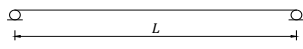
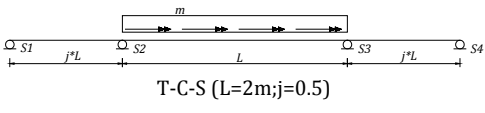
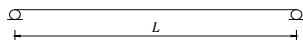
STATIC CHARACTERISTICS						
BOUNDARY CONDITION	LOADING	SECTION	$I\omega\omega$ [m^6]	ELEMENT (ABAQUS)	Nº of elements	Nº integration points for the cross-section
 S-S (L=2m)	Uniform torque distributed	I-Section	3.14E-07	B310S	60	13
 T-C-S (L=2m;j=0.5)	Uniform torque distributed acting upon the middle span				240	
 S-S (L=2m)	Concentrated moment at midspan				60	

Table 4.10 – Comparison of results between current model and ABAQUS element.

Load case	ROTATION φ (max)			BICURVATURE φ'' (max)			BIMOMENT $M\omega$ (max) [N.m]			σ_{xx} (max) [kPa]		
	ABAQUS	Current analysis	ERROR	ABAQUS	Current analysis	ERROR	ABAQUS	Current analysis	ERROR	ABAQUS	Current analysis	ERROR
S-S (uniform load)	2.80E-03	2.80E-03	0.14%	6.59E-03	6.60E-03	0.12%	434.10	436.00	0.45%	2.04E+07	2.05E+07	0.44%
T-C-S (load on the central span)	1.24E-03	1.20E-03	-3.42%	3.56E-03	3.50E-03	-1.55%	234.10	233.70	-0.17%	1.10E+07	1.10E+07	-0.17%
SS (Concent. load)	2.25E-03	2.20E-03	-2.38%	6.67E-03	6.80E-03	2.00%	439.00	448.60	2.20%	2.07E+07	2.11E+07	2.19%

It can be verified from the table 4.10 that the relative error between the present analysis and the ABAQUS beam element does not exceed 3.5% in terms of the angle of twist φ value and that the approximation of normal stress depends directly from the warping moment value.

This check could be considered as a FEM model indicator for its numerical implementation and the accuracy performed leads to a good approximation of the ABAQUS results.

Example 4.6: Coupled behavior of typical bridge cross-sections

A continuous three-spans beam is analyzed as a structural model of a highway bridge deck. The longitudinal model of the numerical example is represented in figure 4.23.

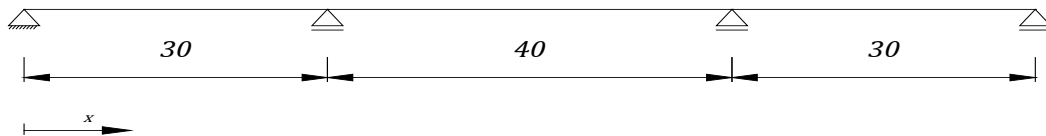


Figure 4.23 - Longitudinal model of a bridge numerical example.

This practical example is analyzed taking into account two cross-section layouts: the *closed box section* represented by figure 4.24, which is typically used for these structural solutions, and a *double-T cross-section*, which is represented in figure 4.25.

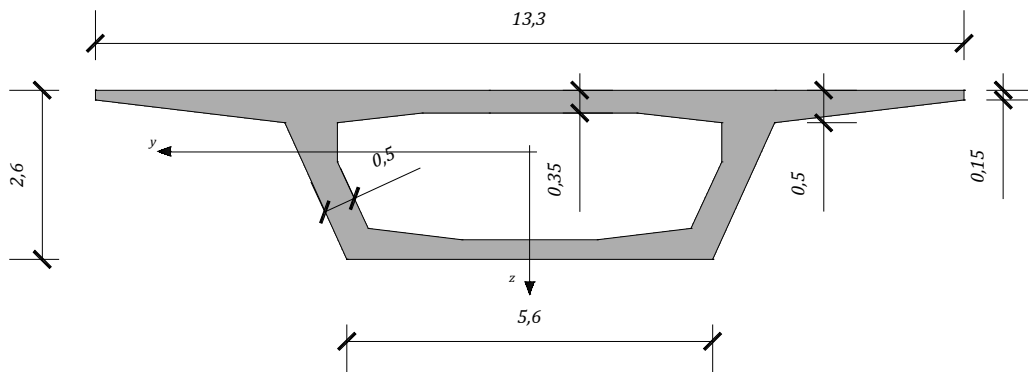


Figure 4.24 - Box-section of the bridge deck.

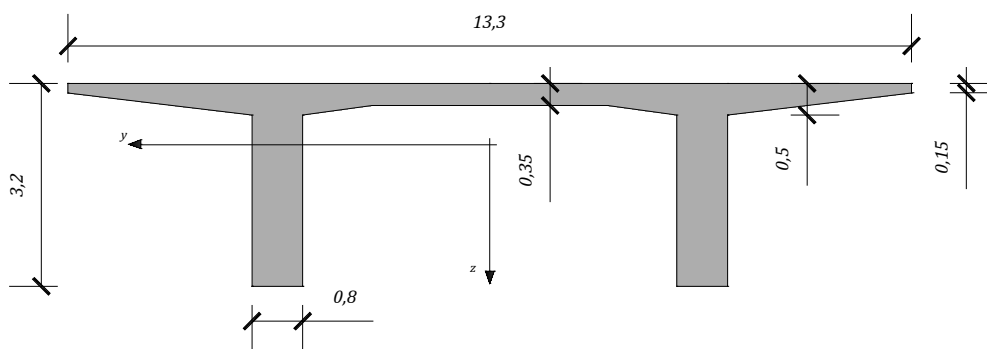
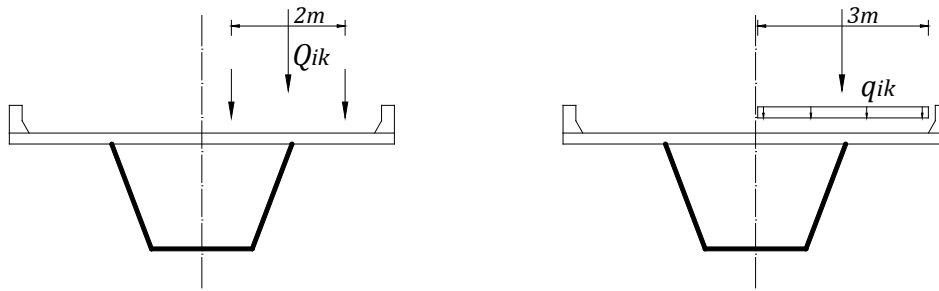


Figure 4.25 - Double-T section of the bridge deck.

The loading on a bridge section, according to EN 1991-2, can be considered as an eccentric line load applied in the z-direction. This vertical type of load generates *bending* and *torsion* of the deck, as represented in figure 4.26.



Tandem Load

Lane Load

Figure 4.26 – Lane model for general types of vertical loads.

The cross-sections represented are compared as two possible structural solutions for the bridge design. For this reason have been chosen considering approximately the same moment of inertia I_z in the flexural plan (x, z) obtained in relation to the elastic center. The bending characteristics of the two cross-section are given in the table 4.11.

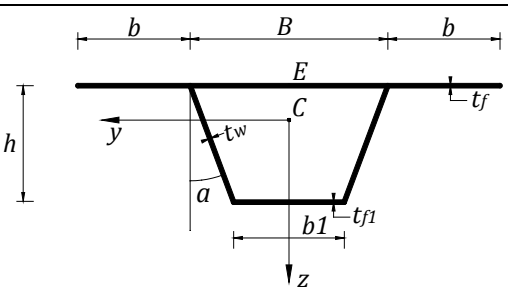
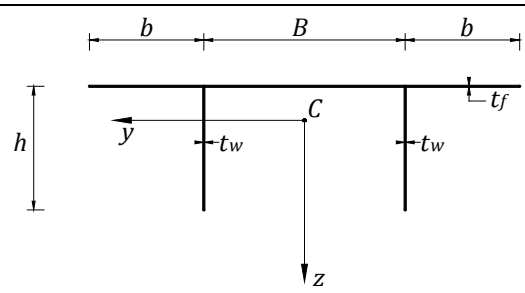
Table 4.11 – Flexural characteristics of the bridge deck cross-sections.

Cross-section layout	Height h [m]	Slenderness λ of the mid-span	Moment of inertia I_z [m⁴]
Box	2.6	10.8	8.10
Double-T	3.2	8.75	8.99

The slenderness of the bridge section is defined by the ratio $\lambda = \frac{L}{h}$, being $L = 0.7 * L_0$ and L_0 the length of the central span.

The geometry of the referred cross-sections are defined by the respective mid-line, being the correspondent dimensions given in table 4.12.

Table 4.12 – Section properties of the bridge cross-sections.

	Box Section	Double-T Section
		
$B[m]$	7.30	6.65
$b[m]$	3.00	3.33
$t_w[m]$	0.50	0.80
$t_f[m]$	0.35	0.35
$t_{f1}[m]$	0.30	-
α	23°	-
$h[m]$	2.28	3.03

The torsional behavior of the two different cross-sections, as already presented, is described by the calculation of the non-dimensional parameter κ , which involves both material and section properties and also the geometry of the structure through the mid-span length L_i . These quantities are listed in table 4.13.

Table 4.13 – Cross-section properties and torsion parameters.

	Box section	Double-T Section
$E [GPa]$	33.00	
$G [GPa]$	13.75	
$K [m^4]$	17.14	1.17
$I_{\omega\omega} [m^4]$	12.04	110.14
$L_i [m]$	40.00	
κ	30.86	2.66

The elastic modulus E and the shear modulus G corresponds to a concrete class C30/37 considered for the bridge deck. All the coordinate distributions of the cross-section, which were used to define the properties summarized in table 4.13 are presented in the annex A.

By applying the constitutive law to Saint Venant torsion (3.122), the ratio between the torsion parameters of the two sections can be obtained:

$$\frac{K_{box\ section}}{K_{open\ section}} = \frac{\varphi'_{Box\ section}}{\varphi'_{open\ section}} = 14.65 \quad (4.35)$$

The K magnitude greatly exceeds that of the open sections, being the GK value the first source of torsional stiffness for all the compact solid and hollow sections.

In the sequel it will be considered the loading represented in figure 4.27 and figure 4.28 adopting $P_z = 1$ and $e = 1$.

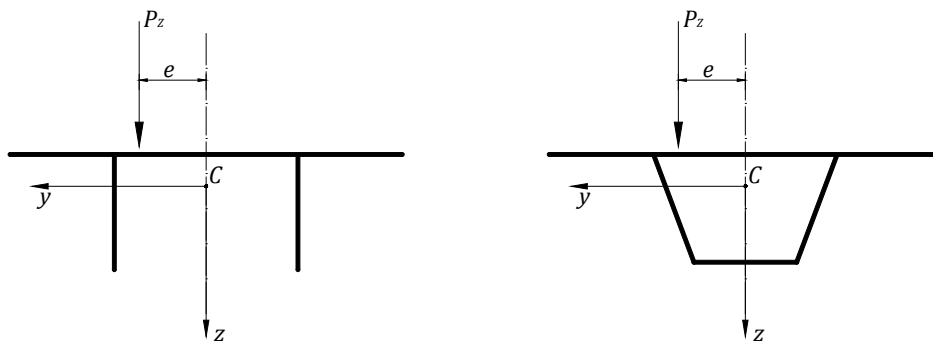


Figure 4.27 - Loading in the cross-section plane.

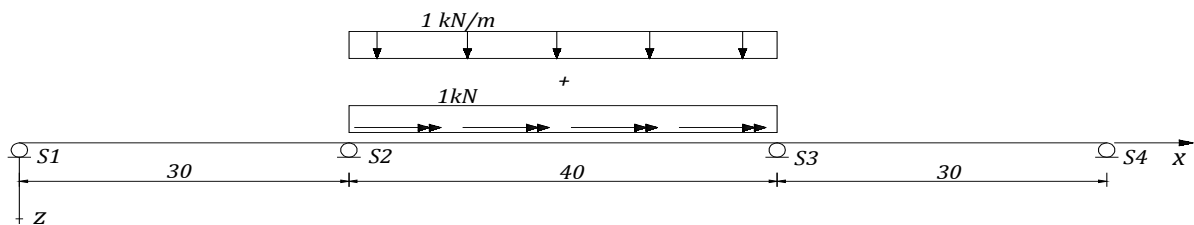


Figure 4.28 -Loading in the longitudinal direction.

As a first approach only the double-T section will be analyzed. This section is asymmetric with respect to y -axis and an additional y -displacement due to torsion will appear when twist is considered in the elastic center, as illustrated in figure 4.29. This effect is the same shown in figure 4.6 when the finite element have been assembled considering the elastic center axis for reference.

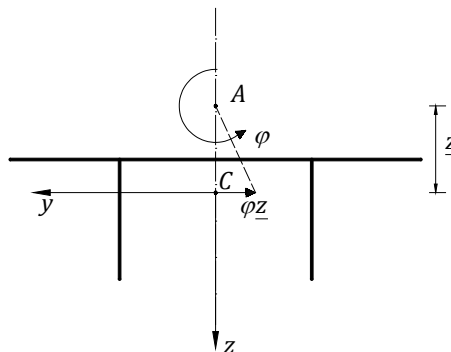


Figure 4.29 - Coupling effect between torsion and transversal displacement.

The displacement field due to the loading represented in figure 4.28 is obtained by using the FEM model, being the coupling effect illustrated in figure 4.29 considered by using the element stiffness matrix (4.34).

The boundary prescriptions for FEM model are listed in table 4.14.

Table 4.14 – Boundary displacement fixed at nodes.

Nodal coordinate	Boundary conditions prescribed
$S1(x = 0)$	$u_y(S1) = u_z(S1) = \varphi(S1) = 0$
$S2(x = 30\text{ m})$	$u_y(S2) = u_z(S2) = \varphi(S2) = 0$
$S3(x = 70\text{ m})$	$u_y(S3) = u_z(S3) = \varphi(S3) = 0$
$S4(x = 100\text{ m})$	$u_y(S4) = u_z(S4) = \varphi(S4) = 0$

The results are presented in figure 4.30 for the transversal displacements and the twist.

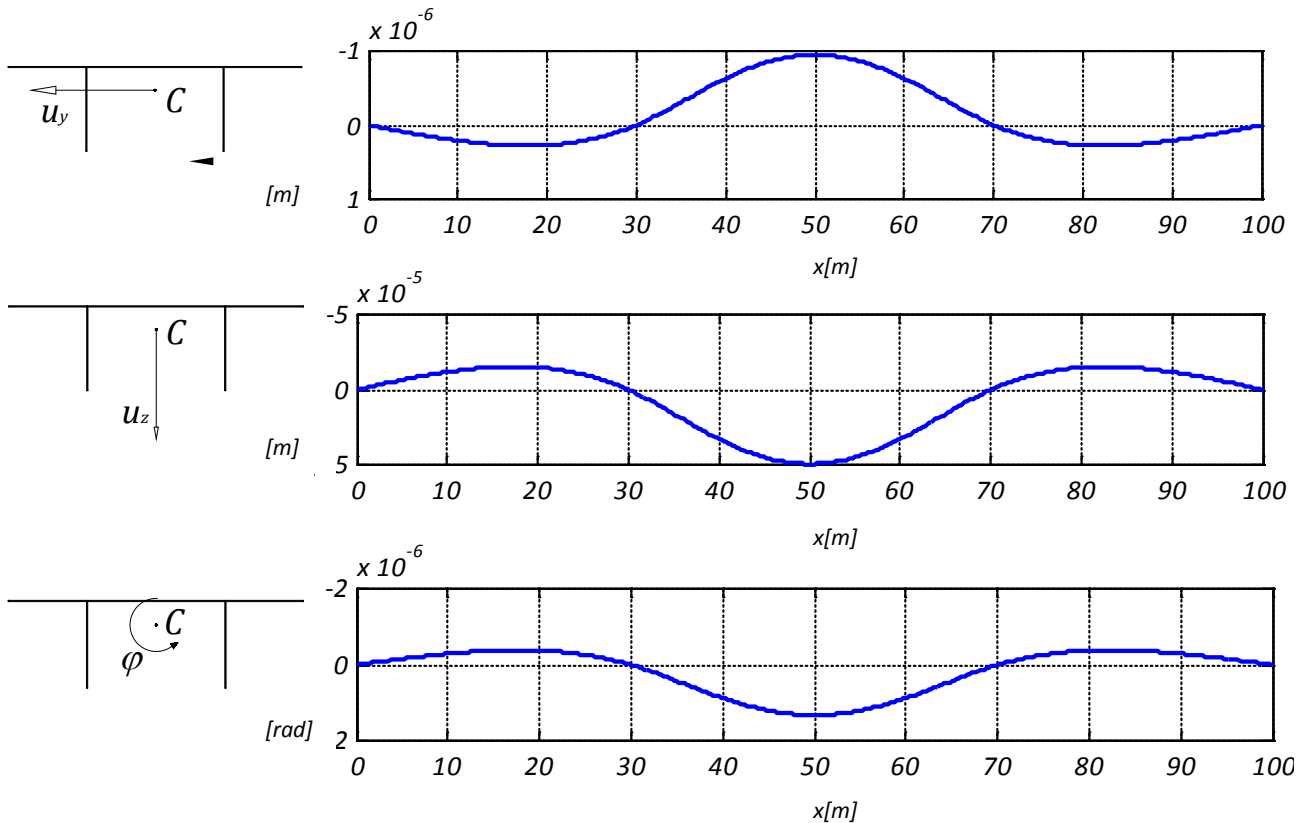


Figure 4.30 – Displacements and rotation of the bridge model with double-T section (FEM model).

As already mentioned, there are no bending displacements in (x, y) plane but the twist around the shear center generates a transversal displacement u_y of the elastic center axis, as shown in figure 4.30.

In terms of internal forces, the shear diagram and bending moments in (x, z) plane are represented in figure 4.31. The torsion moment and the *bimoment* distribution along the beam axis are represented in figure 4.32.

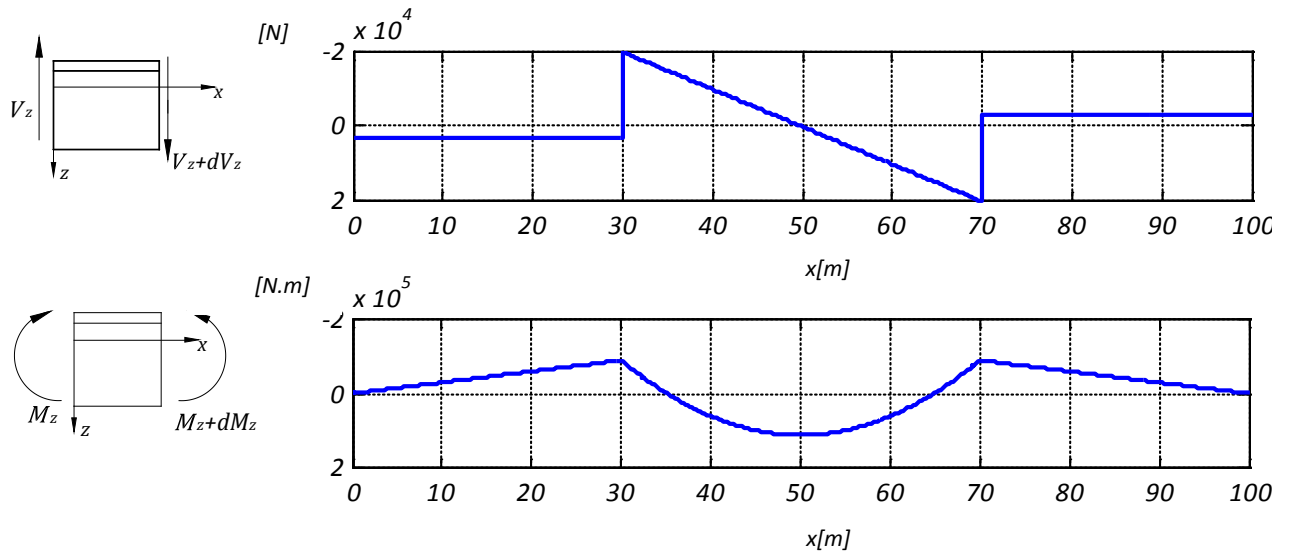


Figure 4.31 – Shear force V_z and bending moment M_z along the elastic center axis.

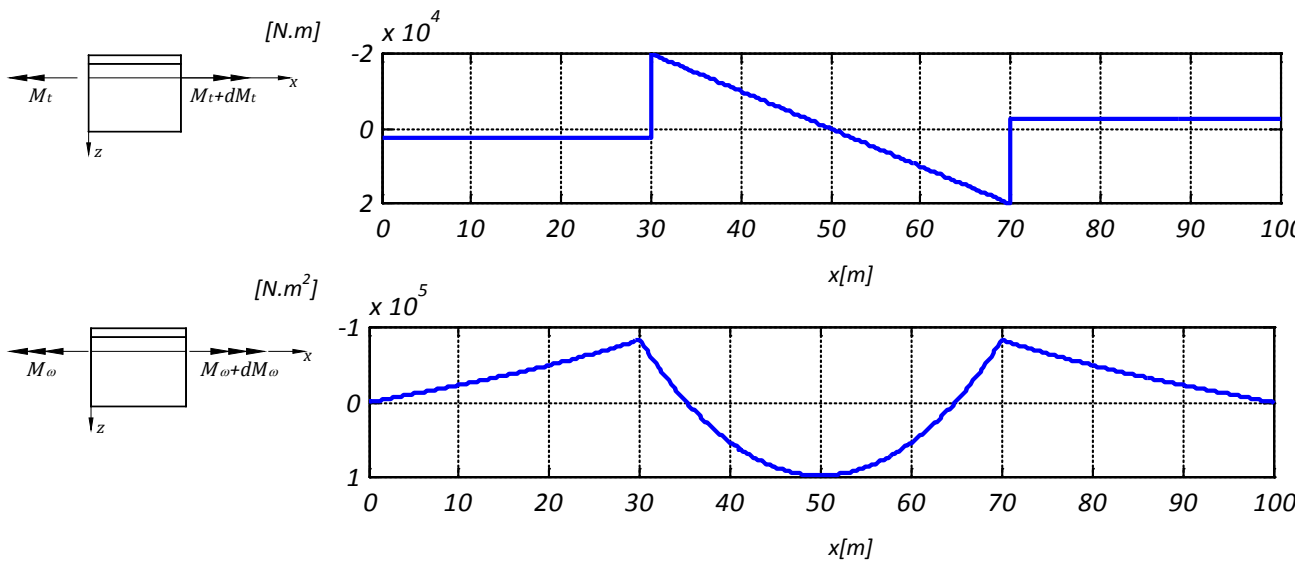


Figure 4.32 – Torsion moment M_t and warping moment M_ω along the elastic center axis.

A comparison between the double-T section analyzed and the box section, considering the warping effect, can be described by showing the different torsional behavior. The φ -rotation of the box section compared between box-section and double-T section is shown in figure 4.33, while is represented in figure 4.34 the Saint Venant torsion $T_S = \varphi'GK$ along the bridge axis for the same two examples of deck section.

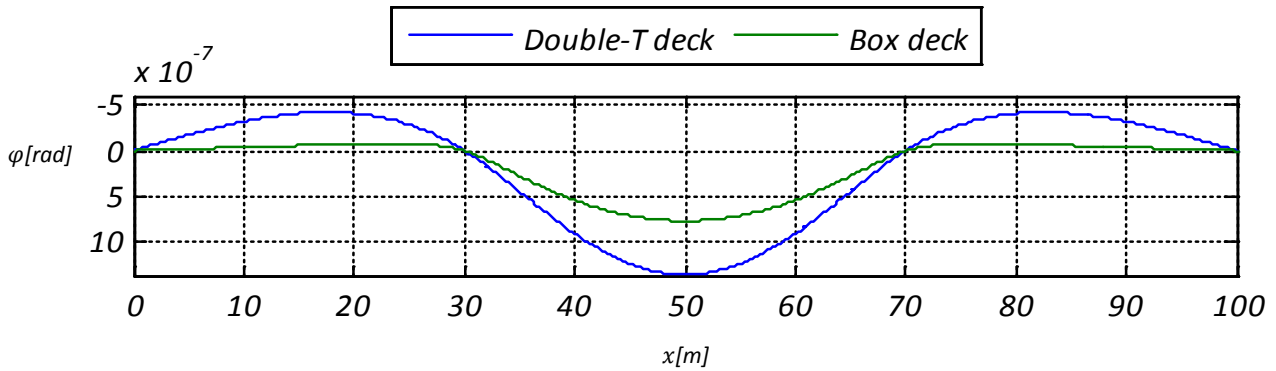


Figure 4.33 - Twist values along the beam axis for the double-T section and for the Box section.

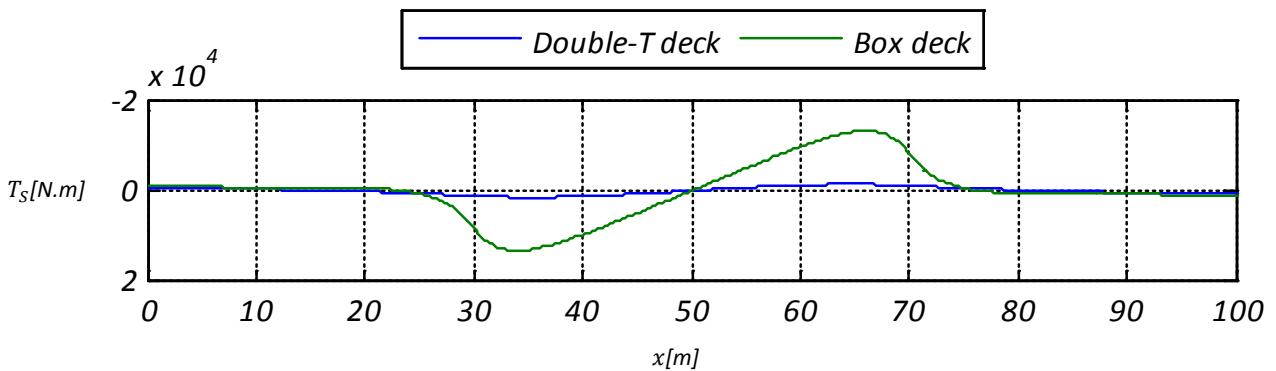


Figure 4.34 – Saint Venant torsion contribution for the double-T section and for the Box section.

It can be observed that as expectable the Saint Venant contribution to the total torsion of the bridge is almost the totality.

Notice that when coupled effect is considered, the value of the warping parameter used is referred to the elastic center and is $I_{\omega\omega}^C$. The coupling is expressed by the terms in the stiffness matrix involving $I_{y\omega}^C$. Details of calculus about these quantities are also illustrated in the Annex 1.

Example 4.7: Torsion behavior and accuracy of the solutions

The problem of mixed torsion have been examined by three load cases and an approximation have been proposed for the analysis of thin-walled beams. The effect of warping for more cross-section layouts can be evaluated in order to present general results and classify typical section behaviors with respect to torsion.

A dimensionless presentation of the results can be done if the warping moments $M_{\omega}(\kappa)$ are compared with the warping moment $M_{\omega}(\kappa = 0)$ when only warping torsion is considered. Results between 1 and 0 of the ratio $M_{\omega}(\kappa)/M_{\omega}(\kappa = 0)$ indicate the torsion response of beam-elements loaded by uniform or concentrated torque.

The graph demonstrate that within large regions of small and large κ -values one torsional component may be neglected as opposed to the other without appreciable error. The results obtained by the FEM for the loading and beams presented in examples 4.1,4.2 and 4.3 are represented in figure 4.35 by a semi-logarithmic scale.

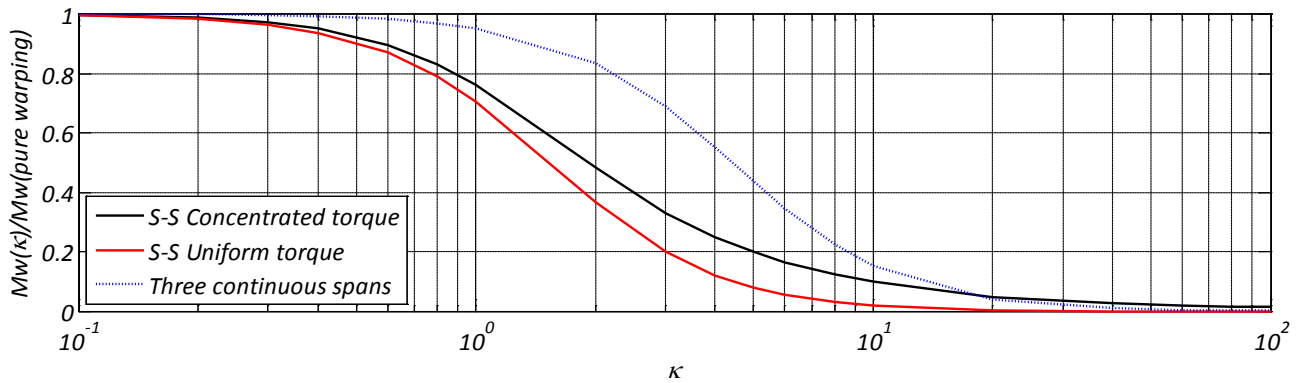


Figure 4.35 – Warping torsion influence in torsion response for different κ -values (FEM solution).

The same representation have been done by (Kollbrunner & Basler, 1969) by the approximation of the solutions for small κ -values. The figure 4.35 shows basically that more local variation of bicurvature implies more influence on warping response. In fact, when the S-S beam is loaded by the concentrated torque the warping influence is higher than the one calculated considering an uniformly distributed torque. This effect is more important for the three continuous spans beam (blue line), which is the case of the bridge models that will be considered.

Several considerations can be concluded from the last example on the bridge deck's cross-section:

- κ -values smaller than 1 correspond to cross-sections that can be analyzed for pure warping torsion only. Generally, cold formed profiles or open bridge cross-sections, with steel floor slabs reinforced by ribs, belong to this group.
- κ -values between 1 and 10 correspond to open sections subjected to *mixed torsion*. In this cases both Saint Venant torsion and warping torsion should be taken into account as done by the FEM model presented in the current analysis. The commercial I-Section and C-Section analyzed in the first three examples of this chapter and the open bridge section of the example 4.6 belong to this group.
- Cross-sections with κ -values bigger than 10 have a torsional behavior essentially composed only by the Saint Venant contribution. This is the case of the hollow section of the examples 4.1, 4.2, 4.3 and of the bridge box section. The Saint Venant part of the torsion response dominates and warping effect can be neglected.

4.3. The dynamic formulation of the finite element

In the static formulation of the developed finite element a weak form have been derived according to the variational principles. The FEM model is used in the sequel for solving the problem of vibration, where the MDOF⁶ system is described by a generic form of the *algebraic* equations:

$$\mathbf{M}\ddot{\mathbf{v}} + \mathbf{C}\dot{\mathbf{v}} + \mathbf{K}\mathbf{v} = \mathbf{p}(\mathbf{t}) \quad (4.36)$$

The equation of motion is composed by the fundamental element matrices of the structural system: the mass matrix \mathbf{M} , the stiffness matrix \mathbf{K} and the damping matrix \mathbf{C} . The equations of motion for a *freely vibrating* undamped system can be obtained by omitting the damping matrix and the applied load from (4.36), yielding the following equation:

$$\mathbf{M}\ddot{\mathbf{v}} + \mathbf{K}\mathbf{v} = \mathbf{0} \quad (4.37)$$

The element stiffness matrix for the FEM model has already been obtained.

An element mass matrix will be deduced in section 4.3.1 for the uncoupled problem of torsion by taking into account the kinetic energy of the beam element. The coupling between generalized displacements for asymmetric sections can be taken into account, being a general element mass matrix obtained through variational principles in section 4.3.2 for a 7 DOF beam element. This matrix will refer, as already done for the stiffness matrix, to the elastic centre axis of the beam element.

When all the matrices in eq. (4.37) are known and assembled for the system analyzed, the discrete equation can be solved by a *frequency analysis*: frequency equations of the system are polynomial equations that allow to obtain for each DOF a mode of vibration. The mode shapes and the mode frequency are the solution of an eigenvalues equation that will be solved by FEM model in 4.3.3.

In the analysis of thin walled beam section examples of uncoupled vibration will be shown in the selected cases 4.3.4 and also coupled examples of free vibration in thin-walled element analysis will be compared.

4.3.1. The formulation of a weak form for the uncoupled torsion

The variational principles have been applied for the static case in order to obtain a system of discrete and linear equations. The equivalent in dynamics is the application of the Hamilton's principle. The differential equations for uncoupled torsion is defined by (3.169) and the terms in this equation refer to the shear center A . If the shear centre S coincides with the elastic center C the bending of the beam is uncoupled from its torsion. This consideration gives the following equation

$$-\rho I_{\omega\omega} \frac{\partial^2}{\partial x^2} \left(\frac{\partial^2 \varphi}{\partial t^2} \right) + \rho (I_z^A + I_y^A) \frac{\partial^2 \varphi}{\partial t^2} + \frac{\partial^2}{\partial x^2} \left(EI_{\omega\omega} \frac{\partial^2 \varphi}{\partial x^2} \right) - \frac{\partial}{\partial x} \left(GK \frac{d\varphi}{dx} \right) - \frac{db}{dx} - m_\varphi = 0 \quad (4.38)$$

Notice that in the equation (3.169), which was studied by (Gere, 1954) and presented in chapter 3, is neglected the inertial contribution of warping displacement, while in the present work all the parcels will be considered. This equation can be multiplied by the virtual rotation ϕ , called weight function, and then integrated on the domain of the element (as already done in static): this gives the weak form. Alternatively, the principle of Hamilton can be used and, considering the boundary terms out of the integral, gives

⁶ Multi-degrees of freedom.

$$\int_{t_1}^{t_2} \int_0^L \rho (I_{\omega\omega} \ddot{\phi}' \phi' + I_p^A \ddot{\phi} \phi) dx dt + \int_{t_1}^{t_2} \int_0^L (\varphi'' EI_{\omega\omega} \phi'' + \varphi' GK \phi' - m_\varphi \phi + b \phi') dx dt - \int_{t_1}^{t_2} \left([\phi \bar{T}]_0^L - \left[\frac{d\phi}{dx} \bar{M}_\omega \right]_0^L \right) dt = 0 \quad (4.39)$$

where $I_p^A = (I_z^A + I_y^A)$ is the polar moment of inertia. Applying the Galerkin FEM to the functions in eq.(4.39) a discrete linear equation can be expressed: the first term defines the *mass element matrix* while all the other terms of (4.39) have already been presented. The approximation functions are the Hermite polynomials and the separation of variables made by (4.14) and (4.15) allow to refer the time derivatives of the functions $\varphi(x, t)$ and $\phi(x, t)$ to the nodal displacement vectors $\cdot \mathbf{u}^e$ and $\cdot \boldsymbol{\phi}^e$. In fact, notice that if the time-depending terms are omitted the equation (4.39) corresponds to the (4.13).

The substitution of the approximation functions in (4.39) gives

$$\begin{aligned} \boldsymbol{\phi}^{eT} \left\{ \int_{-1}^1 \left[\frac{4}{L^2} \left(\frac{d\mathbf{H}^e}{d\xi} \right)^T \rho I_{\omega\omega} \left(\frac{d\mathbf{H}^e}{d\xi} \right) \right] \ddot{\mathbf{u}}^e \frac{L^e}{2} d\xi + \int_{-1}^1 [\mathbf{H}^{eT} \rho I_p^A \mathbf{H}^e] \ddot{\mathbf{u}}^e \frac{L^e}{2} d\xi \right. \\ \left. + \int_{-1}^1 \left[\frac{16}{L^4} \left(\frac{d^2 \mathbf{H}^e}{d\xi^2} \right)^T EI_{\omega\omega} \left(\frac{d^2 \mathbf{H}^e}{d\xi^2} \right) \right] \mathbf{u}^e \frac{L^e}{2} d\xi + \int_{-1}^1 \left[\frac{4}{L^2} \left(\frac{d\mathbf{H}^e}{d\xi} \right)^T GK \left(\frac{d\mathbf{H}^e}{d\xi} \right) \right] \mathbf{u}^e \frac{L^e}{2} d\xi \right. \\ \left. - \int_{-1}^1 \mathbf{H}^{eT} m_\varphi \frac{L^e}{2} d\xi + \int_{-1}^1 \frac{2}{L^e} \left(\frac{d\mathbf{H}^e}{d\xi} \right)^T b \frac{L^e}{2} d\xi - \mathbf{H}^{eT} \bar{T} n|_{r^e} + \frac{2}{L^e} \left(\frac{d\mathbf{H}^e}{d\xi} \right)^T \bar{M}_\omega n|_{r^e} \right\} = 0 \end{aligned} \quad (4.40)$$

The linear equation expressed by (4.40) refers to the simple case in which shear center and elastic center points coincide, which occurs for the I-Beam of Figure 4.3. Note that the coincidence between these two points implies that $I_p^A = I_p = I_y + I_z$.

The first and second terms constitute the contribution of the *inertia forces* and their integration over the parent domain yields the *consistent mass matrix* that is written as follows:

$$\begin{aligned} \mathbf{M}_e = \int_{-1}^1 \left[\frac{4}{L^2} \left(\frac{d\mathbf{H}^e}{d\xi} \right)^T \rho I_{\omega\omega} \left(\frac{d\mathbf{H}^e}{d\xi} \right) \right] \ddot{\mathbf{u}}^e \frac{L^e}{2} d\xi + \int_{-1}^1 [\mathbf{H}^{eT} \rho I_p^A \mathbf{H}^e] \ddot{\mathbf{u}}^e \frac{L^e}{2} d\xi \\ = \frac{\rho I_{\omega\omega}}{30L^e} \begin{bmatrix} 36 & 3L^e & -36 & 3L^e \\ & 4L^{e2} & -3L^e & -L^{e2} \\ & & 36 & -3L^e \\ & & & 4L^{e2} \end{bmatrix} + \frac{\rho I_p L^e}{420} \begin{bmatrix} 156 & 22L^e & 54 & -13L^e \\ & 4L^{e2} & 13L^e & -3L^{e2} \\ & & 156 & -22L^e \\ & & & 4L^{e2} \end{bmatrix} \end{aligned} \quad (4.41)$$

After considering the assembling of \mathbf{M}_e , \mathbf{K}_e and \mathbf{f}_e over the entire number of beam elements the expression of the discrete equation is given by:

$$\boldsymbol{\phi}^T \{ \mathbf{M} \dot{\mathbf{u}} + \mathbf{K} \mathbf{u} - \mathbf{f} \} = \boldsymbol{\phi}^T \{ \mathbf{r} \} = \mathbf{0} \quad (4.42)$$

where \mathbf{r} is the *residual*.

4.3.2. The element mass matrix considering an additional DOF of warping

The discretization of the equation of motion for a generic problem, where coupled inertial effects are considered, requires the knowledge of a consistent mass matrix for the thin-walled beam element. The displacement field is approximated by the function listed in table 4.2, which corresponds to a set of 7 generalized displacements at each end of the derived finite element. The stiffness matrix \mathbf{K}_e and the internal forces vector \mathbf{f}_e have already been defined and the objective of this part is to derive the mathematical formulation of the element mass matrix \mathbf{M}_e . The approach will be similar to the one used in the formulation of the stiffness matrix. A first element mass matrix will be obtained considering two axes of reference for the displacements of the cross-section, according to the equations of motion already derived in chapter 3. Then, a second mass matrix will be derived considering the element axis coincident with the elastic center axis.

Axial effect

The Hamilton principle for a generic point P of the cross-section plane is applied considering the generalized displacement η . The kinetic energy per unit length of the axial effect is given by

$$T(\dot{\eta}) = \frac{1}{2} \rho (A\dot{\eta}^2 - S^P_y \dot{\eta} \dot{\xi}_y' - S^P_z \dot{\eta} \dot{\xi}_z' - S^P_\omega \dot{\eta} \dot{\varphi}') \quad (4.43)$$

The equation (4.43) can be substituted in eq.(3.145) in order to obtain, after suitable rearrangements, the following

$$\begin{aligned} & \int_{t_1}^{t_2} \frac{1}{2} \rho \int_0^L (2A\dot{\eta} - S^P_y \dot{\xi}_y' - S^P_z \dot{\xi}_z' - S^P_\omega \dot{\varphi}') \delta\eta dx dt \\ & + \int_{t_1}^{t_2} \int_0^L E (A\eta' \delta\eta' - S^P_y \xi_y'' \delta\eta' - S^P_z \xi_z'' \delta\eta' - S^P_\omega \varphi'' \delta\eta') dx dt \\ & - \int_{t_1}^{t_2} \int_0^L q_x \delta\eta dx dt - \int_{t_1}^{t_2} [\bar{N} \delta\eta]_0^L = 0 \end{aligned} \quad (4.44)$$

The first term represents the contribution of mass and after substituting the displacement approximation functions, it allows to obtain the mass matrix as follows

$$\begin{aligned} \mathbf{M}_e^e \boldsymbol{\eta} &= \int_{-1}^1 [\mathbf{N}^{eT} \rho A \mathbf{N}^e] \dot{\mathbf{u}}_x^e \frac{L^e}{2} d\xi - \frac{1}{2} \int_{-1}^1 \left[\frac{2}{L^e} \mathbf{N}^{eT} \rho S^P_y \left(\frac{d\mathbf{H}_y^e}{d\xi} \right) \right] \dot{\mathbf{u}}_y^e \frac{L^e}{2} d\xi \\ & - \frac{1}{2} \int_{-1}^1 \left[\frac{2}{L^e} \mathbf{N}^{eT} \rho S^P_z \left(\frac{d\mathbf{H}_z^e}{d\xi} \right) \right] \dot{\mathbf{u}}_z^e \frac{L^e}{2} d\xi - \frac{1}{2} \int_{-1}^1 \left[\frac{2}{L^e} \mathbf{N}^{eT} \rho S^P_\omega \left(\frac{d\mathbf{H}_\varphi^e}{d\xi} \right) \right] \dot{\mathbf{u}}_\varphi^e \frac{L^e}{2} d\xi \\ & = \frac{\rho A L^e}{6} \begin{bmatrix} 2 & 1 \\ 1 & 2 \end{bmatrix} \dot{\mathbf{u}}_x^e - \frac{\rho S^P_y}{24} \begin{bmatrix} -6 & L^e & 6 & -L^e \\ -6 & -L^e & 6 & L^e \end{bmatrix} \dot{\mathbf{u}}_y^e - \frac{\rho S^P_z}{24} \begin{bmatrix} -6 & L^e & 6 & -L^e \\ -6 & -L^e & 6 & L^e \end{bmatrix} \dot{\mathbf{u}}_z^e \\ & - \frac{\rho S^P_\omega}{24} \begin{bmatrix} -6 & L^e & 6 & -L^e \\ -6 & -L^e & 6 & L^e \end{bmatrix} \dot{\mathbf{u}}_\varphi^e \end{aligned} \quad (4.45)$$

Also the mass contribution of the axial displacements involves coupling between axial effect, bending and torsion. The first term is the consistent mass matrix of the finite element considering axial displacement, while the other terms are the off-diagonal terms of the mass matrix. Note that the sum of all the terms in the first matrix is $\rho A L^e$, which is the total mass of the beam, while the sum of the other masses is 0 given of the fact that the displacement field considered correspond to the flexural and torsional degrees of freedom.

Bending

As already done for the beam's extension, the variational principle is imposed and only the displacement ξ_y is considered for the moment. The corresponding expression of the kinetic energy is given by

$$T(\dot{\xi}_y, \dot{\xi}_y') = \frac{1}{2} \rho (-S_y^P \dot{\xi}_y' \dot{\eta} + I_y^P \dot{\xi}_y'^2 + I_{yz}^P \dot{\xi}_y' \dot{\xi}_z' + I_{y\omega}^P \dot{\xi}_y' \dot{\varphi}' + A \dot{\xi}_y'^2 - \dot{\xi}_y S_z^P \dot{\varphi}) \quad (4.46)$$

Substituting the kinetic energy per unit length (4.46) in (3.145) and rearranging the terms gives

$$\begin{aligned} & \int_{t_1}^{t_2} \frac{1}{2} \rho \int_0^L (-S_y^P \ddot{\eta} + 2I_y^P \ddot{\xi}_y' + I_{yz}^P \ddot{\xi}_z' + I_{y\omega}^P \ddot{\varphi}') \delta \xi_y' dx dt + \int_{t_1}^{t_2} \frac{1}{2} \rho \int_0^L (2A \dot{\xi}_y' - S_z^P \dot{\varphi}) \delta \xi_y dx dt \\ & + \int_{t_1}^{t_2} \frac{1}{2} \int_0^L (-\delta \xi_y'' E S_y^P \eta' + 2\delta \xi_y'' E I_{yz}^P \xi_z'' + \delta \xi_y'' E I_y^P \xi_y'' + \delta \xi_y'' E I_{y\omega}^P \varphi'') dx dt \\ & - \int_{t_1}^{t_2} \int_0^L (-m_y \delta \xi_y' + q_y \delta \xi_y) dx dt - \int_{t_2}^{t_1} \left([\delta \xi_y \bar{V}_y]_0^L - [\delta \xi_y' \bar{M}_y]_0^L \right) = 0 \end{aligned} \quad (4.47)$$

Considering the same approximations for test functions and trial solutions (Galerkin approach) the discretized equation in y -direction of the mass matrix gives

$$\begin{aligned} \mathbf{M}_{\xi_y}^e &= -\frac{1}{2} \int_{-1}^1 \left[\frac{2}{L^e} \left(\frac{d\mathbf{H}_y^e}{d\xi} \right)^T \rho S_y^P \mathbf{N}^e \right] \ddot{\mathbf{u}}_x^e \frac{L^e}{2} d\xi + \int_{-1}^1 \left[\frac{4}{L^{e2}} \left(\frac{d\mathbf{H}_y^e}{d\xi} \right)^T \rho I_y^P \left(\frac{d\mathbf{H}_y^e}{d\xi} \right) \right] \ddot{\mathbf{u}}_y^e \frac{L^e}{2} d\xi + \\ & \int_{-1}^1 \left[\mathbf{H}_y^{eT} \rho A \mathbf{H}_y^e \right] \ddot{\mathbf{u}}_y^e \frac{L^e}{2} d\xi + \frac{1}{2} \int_{-1}^1 \left[\frac{4}{L^{e2}} \left(\frac{d\mathbf{H}_y^e}{d\xi} \right)^T \rho I_{yz}^P \left(\frac{d\mathbf{H}_z^e}{d\xi} \right) \right] \ddot{\mathbf{u}}_z^e \frac{L^e}{2} d\xi + \\ & \frac{1}{2} \int_{-1}^1 \left[\frac{4}{L^{e2}} \left(\frac{d\mathbf{H}_y^e}{d\xi} \right)^T \rho I_{y\omega}^P \left(\frac{d\mathbf{H}_\varphi^e}{d\xi} \right) \right] \ddot{\mathbf{u}}_\varphi^e \frac{L^e}{2} d\xi - \frac{1}{2} \int_{-1}^1 \left[\mathbf{H}_y^{eT} \rho S_z^P \mathbf{H}_\varphi^e \right] \ddot{\mathbf{u}}_\varphi^e \frac{L^e}{2} d\xi = \\ & -\frac{\rho S_y^P}{24} \begin{bmatrix} -6 & L^e & 6 & -L^e \\ -6 & -L^e & 6 & L^e \end{bmatrix}^T \ddot{\mathbf{u}}_x^e + \frac{\rho I_y^P}{30L^e} \begin{bmatrix} 36 & 3L^e & -36 & 3L^e \\ & 4L^{e2} & -3L^e & -L^{e2} \\ & & 36 & -3L^e \\ & & & 4L^{e2} \end{bmatrix} \ddot{\mathbf{u}}_y^e + \\ & \frac{\rho A L^e}{420} \begin{bmatrix} 156 & 22L^e & 54 & -13L^e \\ & 4L^{e2} & 13L^e & -3L^{e2} \\ & & 156 & -22L^e \\ & & & 4L^{e2} \end{bmatrix} \ddot{\mathbf{u}}_y^e + \frac{1}{2} \frac{\rho I_{yz}^P}{30L^e} \begin{bmatrix} 36 & 3L^e & -36 & 3L^e \\ & 4L^{e2} & -3L^e & -L^{e2} \\ & & 36 & -3L^e \\ & & & 4L^{e2} \end{bmatrix} \ddot{\mathbf{u}}_z^e + \\ & \frac{1}{2} \frac{\rho I_{y\omega}^P}{30L^e} \begin{bmatrix} 36 & 3L^e & -36 & 3L^e \\ & 4L^{e2} & -3L^e & -L^{e2} \\ & & 36 & -3L^e \\ & & & 4L^{e2} \end{bmatrix} \ddot{\mathbf{u}}_\varphi^e - \frac{1}{2} \frac{\rho S_z^P}{420} \begin{bmatrix} 156 & 22L^e & 54 & -13L^e \\ & 4L^{e2} & 13L^e & -3L^{e2} \\ & & 156 & -22L^e \\ & & & 4L^{e2} \end{bmatrix} \ddot{\mathbf{u}}_\varphi^e \end{aligned} \quad (4.48)$$

For the flexural plane (x, z) a similar form is obtained and will be written in the final form of the mass matrix.

Torsion

Torsion has already been taken into account in its uncoupling form. When referred to the generic point P the kinetic energy of torsion per unit length is given by

$$T(\dot{\varphi}, \dot{\varphi}') = \frac{1}{2} \rho \left(-S_{\omega}^P \dot{\eta}' + I^P_{\omega y} \dot{\varphi}' \dot{\xi}'_y + I^P_{\omega z} \dot{\varphi}' \dot{\xi}'_z + I^P_{\omega \omega} \dot{\varphi}'^2 - \dot{\xi}'_y S_z^P \dot{\varphi} + \dot{\xi}'_z S_y^P \dot{\varphi} + (I_z^P + I_y^P) \dot{\varphi}^2 \right) \quad (4.49)$$

The application of the Hamilton principle implies that the following applies:

$$\begin{aligned} & \int_{t_1}^{t_2} \frac{1}{2} \rho \int_0^L \left((-S_{\omega}^P \dot{\eta}' + I^P_{\omega y} \dot{\varphi}' \dot{\xi}'_y + I^P_{\omega z} \dot{\varphi}' \dot{\xi}'_z + 2I^P_{\omega \omega} \dot{\varphi}') \delta \varphi' + (-\dot{\xi}'_y S_z^P + \dot{\xi}'_z S_y^P + 2(I_z^P + I_y^P) \dot{\varphi}) \delta \varphi \right) dx dt \\ & + \int_{t_1}^{t_2} \int_0^L \left(-\delta \varphi'' ES_{\omega}^P \eta' + \delta \varphi'' EI^P_{\omega y} \xi''_y + \delta \varphi'' EI^P_{\omega z} \xi''_z + \delta \varphi'' EI^P_{\omega \omega} \varphi'' \right. \\ & \left. + \delta \varphi' GK \varphi' + b \delta \varphi' - m_{\varphi} \delta \varphi \right) dx dt - \int_{t_1}^{t_2} ([\delta \varphi \bar{T}]_0^L - [\delta \varphi' \bar{M}_{\omega}]_0^L) dt = 0 \end{aligned} \quad (4.50)$$

Considering the approximations for the displacement field, in the context of the FEM formulation, substituted in the first integral of (4.50) gives for the mass matrix

$$\begin{aligned} \mathbf{M}^e_{\varphi} &= -\frac{1}{2} \int_{-1}^1 \left[\frac{2}{L^e} \left(\frac{d\mathbf{H}_{\varphi}^e}{d\xi} \right)^T \rho S_{\omega}^P \mathbf{N}^e \right] \ddot{\mathbf{u}}_x^e \frac{L^e}{2} d\xi + \frac{1}{2} \int_{-1}^1 \left[\frac{4}{L^{e2}} \left(\frac{d\mathbf{H}_{\varphi}^e}{d\xi} \right)^T \rho I^P_{\omega y} \left(\frac{d\mathbf{H}_y^e}{d\xi} \right) \right] \ddot{\mathbf{u}}_y^e \frac{L^e}{2} d\xi \\ & - \frac{1}{2} \int_{-1}^1 \left[\mathbf{H}_{\varphi}^{eT} \rho S_z^P \mathbf{H}_y^e \right] \ddot{\mathbf{u}}_y^e \frac{L^e}{2} d\xi + \frac{1}{2} \int_{-1}^1 \left[\frac{4}{L^{e2}} \left(\frac{d\mathbf{H}_{\varphi}^e}{d\xi} \right)^T \rho I^P_{\omega z} \left(\frac{d\mathbf{H}_z^e}{d\xi} \right) \right] \ddot{\mathbf{u}}_z^e \frac{L^e}{2} d\xi \\ & + \frac{1}{2} \int_{-1}^1 \left[\mathbf{H}_{\varphi}^{eT} \rho S_y^P \mathbf{H}_z^e \right] \ddot{\mathbf{u}}_z^e \frac{L^e}{2} d\xi + \int_{-1}^1 \left[\frac{4}{L^{e2}} \left(\frac{d\mathbf{H}_{\varphi}^e}{d\xi} \right)^T \rho I^P_{\omega \omega} \left(\frac{d\mathbf{H}_{\varphi}^e}{d\xi} \right) \right] \ddot{\mathbf{u}}_{\varphi}^e \frac{L^e}{2} d\xi \\ & + \int_{-1}^1 \left[\mathbf{H}_{\varphi}^{eT} \rho (I_z^P + I_y^P) \mathbf{H}_{\varphi}^e \right] \ddot{\mathbf{u}}_{\varphi}^e \frac{L^e}{2} d\xi \\ & = -\frac{\rho S_{\omega}^P}{24} \begin{bmatrix} -6 & L^e & 6 & -L^e \\ -6 & -L^e & 6 & L^e \end{bmatrix}^T \ddot{\mathbf{u}}_x^e + \frac{1}{2} \frac{\rho I^P_{\omega y}}{30L^e} \begin{bmatrix} 36 & 3L^e & -36 & 3L^e \\ 4L^{e2} & -3L^e & 36 & -L^e \\ & & & 4L^{e2} \end{bmatrix} \ddot{\mathbf{u}}_y^e \\ & - \frac{1}{2} \frac{\rho S_z^P L^e}{420} \begin{bmatrix} 156 & 22L^e & 54 & -13L^e \\ & 4L^{e2} & 13L^e & -3L^{e2} \\ & & 156 & -22L^e \\ & & & 4L^{e2} \end{bmatrix} \ddot{\mathbf{u}}_y^e + \frac{1}{2} \frac{\rho I^P_{\omega z}}{30L^e} \begin{bmatrix} 36 & 3L^e & -36 & 3L^e \\ 4L^{e2} & -3L^e & 36 & -L^e \\ & & & 4L^{e2} \end{bmatrix} \ddot{\mathbf{u}}_z^e \\ & + \frac{1}{2} \frac{\rho S_y^P L^e}{420} \begin{bmatrix} 156 & 22L^e & 54 & -13L^e \\ & 4L^{e2} & 13L^e & -3L^{e2} \\ & & 156 & -22L^e \\ & & & 4L^{e2} \end{bmatrix} \ddot{\mathbf{u}}_z^e + \frac{\rho I^P_{\omega \omega}}{30L^e} \begin{bmatrix} 36 & 3L^e & -36 & 3L^e \\ 4L^{e2} & -3L^e & 36 & -L^e \\ & & & 4L^{e2} \end{bmatrix} \ddot{\mathbf{u}}_{\varphi}^e \\ & + \frac{\rho (I_z^P + I_y^P)}{420} \begin{bmatrix} 156 & 22L^e & 54 & -13L^e \\ & 4L^{e2} & 13L^e & -3L^{e2} \\ & & 156 & -22L^e \\ & & & 4L^{e2} \end{bmatrix} \ddot{\mathbf{u}}_{\varphi}^e \end{aligned} \quad (4.51)$$

Assembly of the consistent mass matrix

In order to simplify the discrete equations, the displacement field will be referred to the *elastic center* for axial effect and bending and to the *shear center* for the torsion as done for the equilibrium equations. The same assumption has been used in the first formulation of the stiffness element matrix and thus the mass matrix can be assembled in a systematic way that gives

$$M_e = \begin{bmatrix} M^e_{\eta 1} \\ M^e_{\xi y 1} \\ M^e_{\xi z 1} \\ M^e_{\varphi 1} \\ M^e_{\eta 2} \\ M^e_{\xi y 2} \\ M^e_{\xi z 2} \\ M^e_{\varphi 2} \end{bmatrix} = \quad (4.52)$$

$$\begin{bmatrix} \frac{\rho AL^e}{3} & 0 & 0 & 0 & 0 & 0 & 0 & \frac{\rho AL^e}{6} & 0 & 0 & 0 & 0 & 0 & 0 & 0 & 0 & 0 & 0 \\ \frac{36 \rho I_y}{30 L^e} + \frac{156}{420} \rho AL^e & \frac{3}{30} \rho I_y + \frac{22}{420} \rho AL^e & 0 & 0 & 0 & 0 & 0 & 0 & -\frac{36 \rho I_y}{30 L^e} + \frac{54}{420} \rho AL^e & \frac{3}{30} \rho I_y - \frac{13}{420} \rho AL^e & 0 & 0 & 0 & 0 & 0 & 0 & 0 & 0 \\ \frac{4}{30} \rho I_y L^e + \frac{4}{420} \rho AL^e & 0 & 0 & 0 & 0 & 0 & 0 & 0 & -\frac{3}{30} \rho I_y + \frac{13}{420} \rho AL^e & -\frac{1}{30} \rho I_y L^e - \frac{3}{420} \rho AL^e & 0 & 0 & 0 & 0 & 0 & 0 & 0 & 0 \\ \frac{36 \rho I_z}{30 L^e} + \frac{156}{420} \rho AL^e & \frac{3}{30} \rho I_z + \frac{22}{420} \rho AL^e & 0 & 0 & 0 & 0 & 0 & 0 & -\frac{36 \rho I_z}{30 L^e} + \frac{54}{420} \rho AL^e & \frac{3}{30} \rho I_z - \frac{13}{420} \rho AL^e & 0 & 0 & 0 & 0 & 0 & 0 & 0 & 0 \\ \frac{4}{30} \rho I_z L^e + \frac{4}{420} \rho AL^e & 0 & 0 & 0 & 0 & 0 & 0 & 0 & -\frac{3}{30} \rho I_z + \frac{13}{420} \rho AL^e & -\frac{1}{30} \rho I_z L^e - \frac{3}{420} \rho AL^e & 0 & 0 & 0 & 0 & 0 & 0 & 0 & 0 \\ \frac{36 \rho I_{\omega\omega}}{30 L^e} + \frac{156}{420} \rho I_p^A L^e & \frac{3}{30} \rho I_{\omega\omega} + \frac{22}{420} \rho I_p^A L^e & 0 & 0 & 0 & 0 & 0 & 0 & -\frac{36 \rho I_{\omega\omega}}{30 L^e} + \frac{54}{420} \rho I_p^A L^e & \frac{3}{30} \rho I_{\omega\omega} - \frac{13}{420} \rho I_p^A L^e & 0 & 0 & 0 & 0 & 0 & 0 & 0 & 0 \\ \frac{4}{30} \rho I_{\omega\omega} L^e + \frac{4}{420} \rho I_p^A L^e & 0 & 0 & 0 & 0 & 0 & 0 & 0 & -\frac{3}{30} \rho I_{\omega\omega} + \frac{13}{420} \rho I_p^A L^e & -\frac{1}{30} \rho I_{\omega\omega} L^e - \frac{3}{420} \rho I_p^A L^e & 0 & 0 & 0 & 0 & 0 & 0 & 0 & 0 \\ \frac{\rho AL^e}{3} & 0 & 0 & 0 & 0 & 0 & 0 & 0 & 0 & 0 & 0 & 0 & 0 & 0 & 0 & 0 & 0 & 0 \\ \frac{36 \rho I_y}{30 L^e} + \frac{156}{420} \rho AL^e & -\frac{3}{30} \rho I_y - \frac{22}{420} \rho AL^e & 0 & 0 & 0 & 0 & 0 & 0 & 0 & 0 & 0 & 0 & 0 & 0 & 0 & 0 & 0 & 0 \\ \text{Symmetric} & \frac{4}{30} \rho I_y L^e + \frac{4}{420} \rho AL^e & 0 & 0 & 0 & 0 & 0 & 0 & 0 & 0 & 0 & 0 & 0 & 0 & 0 & 0 & 0 & 0 \\ \frac{36 \rho I_z}{30 L^e} + \frac{156}{420} \rho AL^e & -\frac{3}{30} \rho I_z - \frac{22}{420} \rho AL^e & 0 & 0 & 0 & 0 & 0 & 0 & 0 & 0 & 0 & 0 & 0 & 0 & 0 & 0 & 0 & 0 \\ \frac{4}{30} \rho I_z L^e + \frac{4}{420} \rho AL^e & 0 & 0 & 0 & 0 & 0 & 0 & 0 & 0 & 0 & 0 & 0 & 0 & 0 & 0 & 0 & 0 & 0 \\ \frac{36 \rho I_{\omega\omega}}{30 L^e} + \frac{156}{420} \rho I_p^A L^e & -\frac{3}{30} \rho I_{\omega\omega} - \frac{22}{420} \rho I_p^A L^e & 0 & 0 & 0 & 0 & 0 & 0 & 0 & 0 & 0 & 0 & 0 & 0 & 0 & 0 & 0 & 0 \\ \frac{4}{30} \rho I_{\omega\omega} L^e + \frac{4}{420} \rho I_p^A L^e & 0 & 0 & 0 & 0 & 0 & 0 & 0 & 0 & 0 & 0 & 0 & 0 & 0 & 0 & 0 & 0 & 0 \end{bmatrix}$$

The beam mass described by the matrix is located in two different points of the cross-section. Hence, the inertia forces are uncoupled each others (Friberg, 1985). The element is defined as shown in figure 4.36.

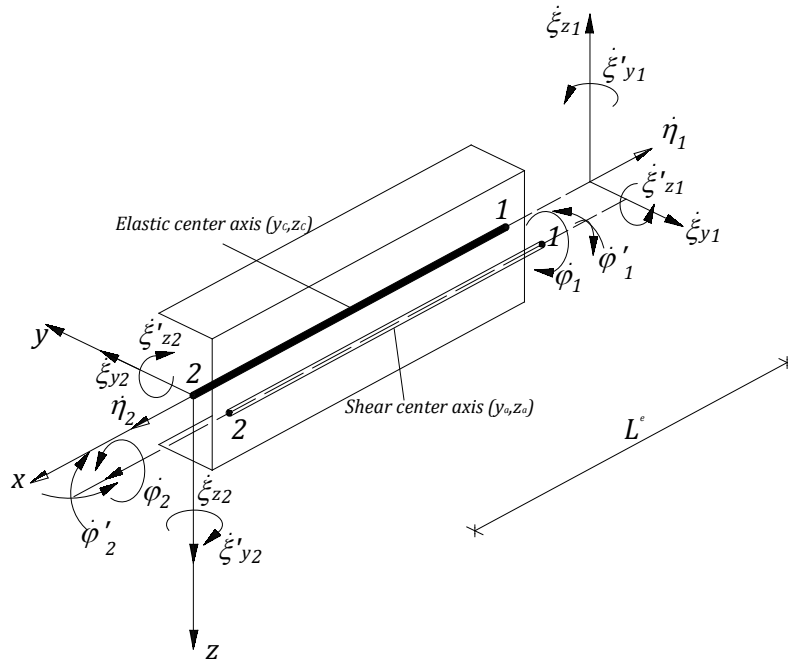
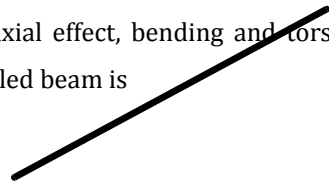


Figure 4.36 –Thin-walled C-beam element and uncoupled kinematic field.

In the current analysis, the finite element will be derived referring the all governing equations to the elastic center, which as a consequence will produce a coupling between axial effect, bending and torsion. The mass matrix considering (y_c, z_c) as reference for the kinetic of the thin-walled beam is



$M_e =$

(4.53)

$\frac{\rho AL^e}{3}$	0	0	0	0	$\frac{6}{24}\rho S^C_{\omega}$	$-\frac{1}{24}\rho S^C_{\omega}L^e$	$\frac{\rho AL^e}{6}$	0	0	0	0	$-\frac{6}{24}\rho S^C_{\omega}$	$\frac{1}{24}\rho S^C_{\omega}L^e$
$\frac{36\rho I_y}{30L^e} + \frac{156}{420}\rho AL^e$	$\frac{3}{30}\rho I_y + \frac{22}{420}\rho AL^{e2}$	0	0	0	$\frac{18\rho I^C_{yw}}{30L^e}$	$\frac{3}{60}\rho I^C_{yw}$	0	$-\frac{36\rho I_y}{30L^e} + \frac{54}{420}\rho AL^e$	$\frac{3}{30}\rho I_y - \frac{13}{420}\rho AL^{e2}$	0	0	$-\frac{18\rho I^C_{yw}}{30L^e}$	$\frac{3}{60}\rho I^C_{yw}$
$\frac{4}{30}\rho I_yL^e + \frac{4}{420}\rho AL^{e3}$	0	0	0	$\frac{3}{60}\rho I^C_{yw}$	$\frac{4}{60}\rho I^C_{yw}L^e$	0	$-\frac{3}{30}\rho I_y + \frac{13}{420}\rho AL^{e2} - \frac{1}{30}\rho I_yL^e - \frac{3}{420}\rho AL^{e3}$	0	0	0	0	$-\frac{3}{60}\rho I^C_{yw}$	$-\frac{1}{60}\rho I^C_{yw}L^e$
$\frac{36\rho I_z}{30L^e} + \frac{156}{420}\rho AL^e$	$\frac{3}{30}\rho I_z + \frac{22}{420}\rho AL^{e2}$	0	0	$\frac{18\rho I^C_{zw}}{30L^e}$	$\frac{3}{60}\rho I^C_{zw}$	0	0	0	0	$-\frac{36\rho I_z}{30L^e} + \frac{54}{420}\rho AL^e$	$\frac{3}{30}\rho I_z - \frac{13}{420}\rho AL^{e2}$	$-\frac{18\rho I^C_{zw}}{30L^e}$	$\frac{3}{60}\rho I^C_{zw}$
$\frac{4}{30}\rho I_zL^e + \frac{4}{420}\rho AL^{e3}$	0	0	0	$\frac{3}{60}\rho I^C_{zw}$	$\frac{4}{60}\rho I^C_{zw}L^e$	0	0	0	0	$-\frac{3}{30}\rho I_z + \frac{13}{420}\rho AL^{e2} - \frac{1}{30}\rho I_zL^e - \frac{3}{420}\rho AL^{e3}$	$-\frac{3}{60}\rho I^C_{zw}$	$-\frac{1}{60}\rho I^C_{zw}L^e$	
$\frac{36\rho I_{\omega\omega}}{30L^e} + \frac{156}{420}\rho I_p^AL^e$	$\frac{3}{30}\rho I_{\omega\omega} + \frac{22}{420}\rho I_p^AL^{e2}$	0	0	$\frac{6}{24}\rho S^C_{\omega}$	$-\frac{18\rho I^C_{yw}}{30L^e}$	$\frac{3}{60}\rho I^C_{yw}$	$-\frac{18\rho I^C_{zw}}{30L^e}$	$\frac{3}{60}\rho I^C_{zw}$	$-\frac{36\rho I_{\omega\omega}}{30L^e} + \frac{54}{420}\rho I_p^AL^e$	$\frac{3}{30}\rho I_{\omega\omega} - \frac{13}{420}\rho I_p^AL^{e2}$	0	$-\frac{36\rho I_{\omega\omega}}{30L^e} + \frac{54}{420}\rho I_p^AL^e$	$\frac{3}{30}\rho I_{\omega\omega} - \frac{13}{420}\rho I_p^AL^{e2}$
$\frac{4}{30}\rho I_{\omega\omega}L^e + \frac{4}{420}\rho I_p^AL^{e3}$	$\frac{1}{24}\rho S^C_{\omega}L^e$	0	0	$-\frac{3}{60}\rho I^C_{yw}$	$-\frac{1}{60}\rho I^C_{yw}L^e$	$-\frac{3}{60}\rho I^C_{zw}$	$-\frac{1}{60}\rho I^C_{zw}L^e$	$-\frac{3}{30}\rho I_{\omega\omega} + \frac{13}{420}\rho I_p^AL^{e2} - \frac{1}{30}\rho I_{\omega\omega}L^e - \frac{3}{420}\rho I_p^AL^{e3}$	0	0	0	$-\frac{3}{30}\rho I_{\omega\omega} + \frac{13}{420}\rho I_p^AL^{e2} - \frac{1}{30}\rho I_{\omega\omega}L^e - \frac{3}{420}\rho I_p^AL^{e3}$	$-\frac{3}{60}\rho I^C_{zw}L^e$
$\frac{\rho AL^e}{3}$	0	0	0	0	0	0	0	0	0	$-\frac{6}{24}\rho S^C_{\omega}$	$-\frac{1}{24}\rho S^C_{\omega}L^e$	$-\frac{6}{24}\rho S^C_{\omega}$	$-\frac{1}{24}\rho S^C_{\omega}L^e$
$\frac{36\rho I_y}{30L^e} + \frac{156}{420}\rho AL^e$	$-\frac{3}{30}\rho I_y - \frac{22}{420}\rho AL^{e2}$	0	0	0	0	0	0	0	0	$\frac{18\rho I^C_{yw}}{30L^e}$	$-\frac{3}{60}\rho I^C_{yw}$	$\frac{18\rho I^C_{yw}}{30L^e}$	$-\frac{3}{60}\rho I^C_{yw}$
<i>Symmetric</i>	0	0	0	0	0	0	0	0	0	$-\frac{3}{60}\rho I^C_{yw}$	$\frac{4}{60}\rho I^C_{yw}L^e$	$-\frac{3}{60}\rho I^C_{yw}$	$\frac{4}{60}\rho I^C_{yw}L^e$
0	0	0	0	0	0	0	0	0	0	$\frac{36\rho I_z}{30L^e} + \frac{156}{420}\rho AL^e$	$-\frac{3}{30}\rho I_z - \frac{22}{420}\rho AL^{e2}$	$\frac{36\rho I^C_{zw}}{30L^e}$	$-\frac{3}{30}\rho I^C_{zw}$
0	0	0	0	0	0	0	0	0	0	$\frac{4}{30}\rho I_zL^e + \frac{4}{420}\rho AL^{e3}$	0	$-\frac{3}{30}\rho I^C_{zw}$	$\frac{4}{30}\rho I^C_{zw}L^e$
0	0	0	0	0	0	0	0	0	0	$\frac{4}{30}\rho I_zL^e + \frac{4}{420}\rho AL^{e3}$	0	$-\frac{3}{30}\rho I^C_{zw}$	$\frac{4}{30}\rho I^C_{zw}L^e$
0	0	0	0	0	0	0	0	0	0	0	0	$\frac{36\rho I_{\omega\omega}}{30L^e} + \frac{156}{420}\rho I_p^AL^e$	$-\frac{3}{30}\rho I_{\omega\omega} - \frac{22}{420}\rho I_p^AL^{e2}$
0	0	0	0	0	0	0	0	0	0	0	0	$\frac{4}{30}\rho I_{\omega\omega}L^e + \frac{4}{420}\rho I_p^AL^{e3}$	$-\frac{3}{30}\rho I_{\omega\omega}L^e - \frac{3}{420}\rho I_p^AL^{e3}$

The element defined by (4.52) is exemplified in figure 4.37 by a C-beam.

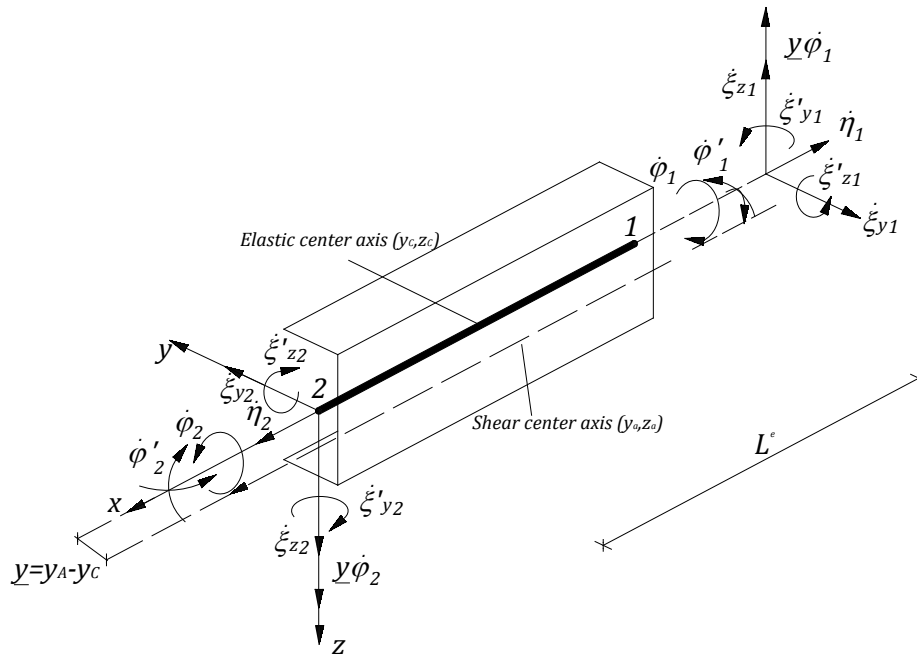


Figure 4.37 - Thin-walled C-beam element and coupled kinematic field.

4.3.3. The undamped free-vibration

In the discussion presented in chapter 3 the dynamical behavior of a beam element has been investigated by a set of SDOF systems represented by single differential equations.

However, in general, the dynamic response of a structure cannot be described adequately by a SDOF model. In fact, the structure dynamics behavior can be described only in terms of more than one degree of freedom. In the development of the equations of motion for the MDOF beam finite element, which is object of this analysis, all the discretized equation will refer to the structural-property matrices of motion of a general system.

The motion of a beam element have been defined by general displacements of a set of discrete points on the beam and the corresponding equation of motion, treated in chapter 3 for selected points of the cross-section plane. These equations can be written for each axis reference by expressing the dynamic equilibrium of the effective forces associated with each degree of freedom. When the force vectors are presented in matrix form, the MDOF equivalent of (3.140) is written as follows:

$$\mathbf{f}_I + \mathbf{f}_D + \mathbf{f}_S = \mathbf{f}(t) \quad (4.54)$$

where the subscripts indicate inertia, damping and elastic forces, while $\mathbf{f}(t)$ is the externally applied load for each degree of freedom.

In the next part, the *undamped* free-vibration motion will be considered. This means that $\mathbf{f}_D = \mathbf{0}$ and, in general, for civil structures the damping influence is relatively low.

Mode shapes and mode frequencies

The problem of vibration analysis for a MDOF system consists of obtaining the conditions under which (4.37) will allow motions to occur. By analogy with the behavior of SDOF systems, it can be assumed that the free-vibration motion is simple harmonic, which may be expressed for a MDOF system as (Clough & Penzien, 1982)

$$\mathbf{v}(t) = \hat{\mathbf{v}} \sin(pt + \theta) \quad (4.55)$$

where $\hat{\mathbf{v}}$ represents the shape of the system, p is the radian frequency and θ is a phase angle.

When the second time derivative of (4.55) is taken, the accelerations in free vibration are given by

$$\ddot{\mathbf{v}} = -p^2 \hat{\mathbf{v}} \sin(pt + \theta) = -p^2 \mathbf{v} \quad (4.56)$$

Substituting (4.55) and (4.53) into (4.37) gives

$$-p^2 \mathbf{M} \hat{\mathbf{v}} \sin(pt + \theta) + \mathbf{K} \hat{\mathbf{v}} \sin(pt + \theta) = \mathbf{0} \quad (4.57)$$

in which $\mathbf{0}$ is a zero vector. The equation (4.57) may be written as follows:

$$[\mathbf{K} - p^2 \mathbf{M}] \hat{\mathbf{v}} = \mathbf{0} \quad (4.58)$$

A nontrivial solution for this set of simultaneous equations is possible only when

$$\|\mathbf{K} - p^2 \mathbf{M}\| = 0 \quad (4.59)$$

The equation (4.59) is called *frequency equation* of the system and is an equation of N th degree in the frequency parameter p^2 for a system having N degrees of freedom. The N roots of this equation represent the frequencies of the N modes of vibration, which are possible in the system. The modes are sorted by ascending values of frequency; thus the first mode is the one having the lowest frequency and so on. The vector made up of the entire set of modal frequencies, arranged in sequence, will be called *frequency vector* \mathbf{p} and is written as follows

$$\mathbf{p} = \begin{bmatrix} p_1 \\ p_2 \\ \vdots \\ p_N \end{bmatrix} \quad (4.60)$$

When the frequencies of vibration are obtained by (4.59) a new matrix can be defined by subtracting $p_n^2 \mathbf{M}$ from the stiffness matrix, which yields

$$\mathbf{E}^n = \mathbf{K} - p_n^2 \mathbf{M} \quad (4.61)$$

Since it depends on the frequency, it is different for each mode. The equation (4.58) is satisfied identically and the amplitude of the vibrations is indeterminate, but the shape of the vibrating system can be obtained by solving for all the displacements in terms of any coordinate.

With this process the shape of the N vibration modes can be found and the square matrix made up of the N mode shapes will be represented by

$$\boldsymbol{\phi} = \begin{bmatrix} \phi_{11} & \dots & \phi_{1N} \\ \phi_{21} & \dots & \phi_{2N} \\ \vdots & \dots & \vdots \\ \phi_{N1} & \dots & \phi_{NN} \end{bmatrix} \quad (4.62)$$

This means that the vibration analysis of a structural system is a form of eigenvalue problem of matrix-algebra theory: the *modal frequencies* are the eigenvalues and the *mode shapes* are the eigenvectors. Note that this matrix consists of N independent modal vectors, thus it is nonsingular and can be inverted.

The vibrating shapes have special properties that are useful in structural-dynamics analysis: the orthogonality relationships. For a detailed exposition of these properties and for their demonstration see (Clough & Penzien, 1982). The orthogonality conditions can be expressed as follows

$$\boldsymbol{\phi}_m^T \mathbf{M} \boldsymbol{\phi}_n = 0 \quad m \neq n \quad (4.63)$$

$$\boldsymbol{\phi}_m^T \mathbf{K} \boldsymbol{\phi}_n = 0 \quad m \neq n \quad (4.64)$$

Where m, n are two different modes of a structural system. These conditions show that the vibrating shapes are orthogonal with respect to the stiffness matrix as well as to the mass.

Normal coordinates

The mode shapes constitute N independent displacement patterns, the amplitude of which may serve as generalized coordinates to express any type of displacement. Thus, a much more useful representation of the displacements can be provided by the free-vibration mode shapes.

Any displacement vector \mathbf{v} for the structure can be developed by superposing suitable amplitudes of the modes of vibration. For any modal component $\hat{\mathbf{v}}_n$, the displacements are given by the mode-shape vector $\boldsymbol{\phi}_n$ multiplied by the modal amplitude Y_n ; thus

$$\hat{\mathbf{v}}_n = \boldsymbol{\phi}_n Y_n \quad (4.65)$$

Then the total displacement is obtained as a sum of the modal components as follows:

$$\mathbf{v} = \sum_{n=1}^N \boldsymbol{\phi}_n Y_n = \boldsymbol{\Phi} \mathbf{Y} \quad (4.66)$$

The mode-shape matrix serves to transform the generalized coordinates \mathbf{Y} into the cartesian coordinates \mathbf{v} .

In order to evaluate any arbitrary normal coordinate Y_n , the equation (4.66) can be multiplied by the product of the transpose of the corresponding modal vector and the mass matrix $\boldsymbol{\phi}_n^T \mathbf{M}$. This gives

$$\boldsymbol{\phi}_n^T \mathbf{M} \mathbf{v} = \boldsymbol{\phi}_n^T \mathbf{M} \boldsymbol{\Phi} \mathbf{Y} \quad (4.67)$$

The right-hand side of this equation can be expanded in a series where all the terms vanish except that corresponding to $\boldsymbol{\phi}_n$ because of the orthogonality property (4.63). This consideration leads to

$$\boldsymbol{\phi}_n^T \mathbf{M} \mathbf{v} = \boldsymbol{\phi}_n^T \mathbf{M} \boldsymbol{\phi}_n Y_n \quad (4.68)$$

which allows to obtain the modal amplitudes as follows:

$$Y_n = \frac{\boldsymbol{\phi}_n^T \mathbf{M} \mathbf{v}}{\boldsymbol{\phi}_n^T \mathbf{M} \boldsymbol{\phi}_n} \quad (4.69)$$

Y_n represents the participation of the n -vibration mode in the global response of the structure. The *modal participation factor* allows to establish the vibration influence of each degree of freedom in a particular mode.

4.3.4. Examples

The analysis presented deals with the free-torsional vibrations of thin-walled beams with open cross-section in which the shear center can or not coincide with the elastic center. An I-Beam will be analyzed by the FEM model and torsional vibrations will be studied in their uncoupled form for different boundary prescriptions. The vibration modes will be derived directly with the corresponding modal frequency.

The results obtained will be compared with the case in which warping of the section is neglected for different boundary conditions and for different vibration modes. Note that the case of a cross-section which does not warp is a limiting case of the general problem.


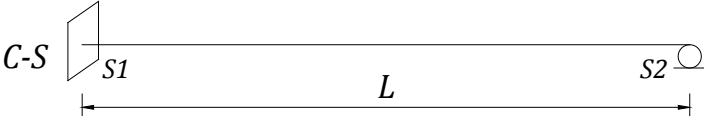
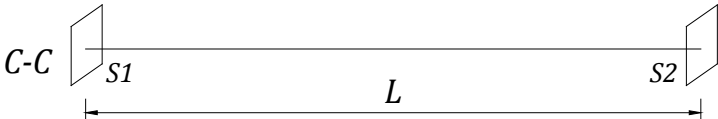
Example 4.8: Free-torsional vibration of bars with thin-walled open cross-section

Boundary conditions

The standard wide-flange beam 12 WF 45 studied by (Gere, 1954) and presented in table 3.5 will be analyzed. In (Gere, 1954) the formulas for the principal torsional frequencies and for the mode shapes are obtained for a simply supported bar, while the frequency equation solutions for other conditions of support are presented in graphical form. This is due to the high transcendental form of the equations in their analytic solution.

The current analysis with FEM will obtain the solution of the free-vibration problem for the boundary conditions listed in table 4.15.

Table 4.15 – Boundary conditions of the bar (S-S⁷,C-S⁸,C-C⁹).

S1	Support conditions	S2
$\varphi = 0$		$\varphi = 0$
$M_\omega = 0$		$M_\omega = 0$
$\varphi = 0$		$\varphi = 0$
$\varphi' = 0$		$\varphi = 0$
$\varphi = 0$		$\varphi = 0$
$\varphi' = 0$		$\varphi' = 0$

The theoretical analysis made in the example 3.4 shows the influence of warping in increasing the beam frequency. This effect is expectable since warping increases the stiffness of the bar against twisting and can be verified separating the different contributions of the element stiffness matrix (4.20) as follows

$$\mathbf{K}^e = \mathbf{K}_{EI_{\omega\omega}}^e + \mathbf{K}_{GK}^e \quad (4.70)$$

The element mass matrix (4.41) for the uncoupled problem also can be seen as summation of two contributions, thus

$$\mathbf{M}^e = \mathbf{M}_{I_{\omega\omega}}^e + \mathbf{M}_{I_p}^e \quad (4.71)$$

The mass considered by (Gere, 1954) is the contribution due to the polar inertia I_p , being the inertial effect related to the warping through $I_{\omega\omega}$ neglected by (Gere, 1954). Thus, the element mass matrix considered for

⁷ Simply Supported.

⁸ Clamped and Supported.

⁹ Clamped and Clamped.

reproducing the values of ratio r given in eq.(3.173) consists of only the contribution $M_{I_p}^e$. The denominator of r is obtained considering $K^e = K_{GK}^e$.

The ratio r between frequencies will be calculated for the first 8 vibration modes and is shown in figure 4.38, figure 4.39 and figure 4.40 for a discretization of 60 elements per beam. Notice that the results represented by figure 4.38 are the same of those obtained in figure 3.39 with the analytical expression. The length of the beam is assumed to be the same of the one considered by Gere (Length $L = 6m(20 ft)$ with $\kappa = 4$).

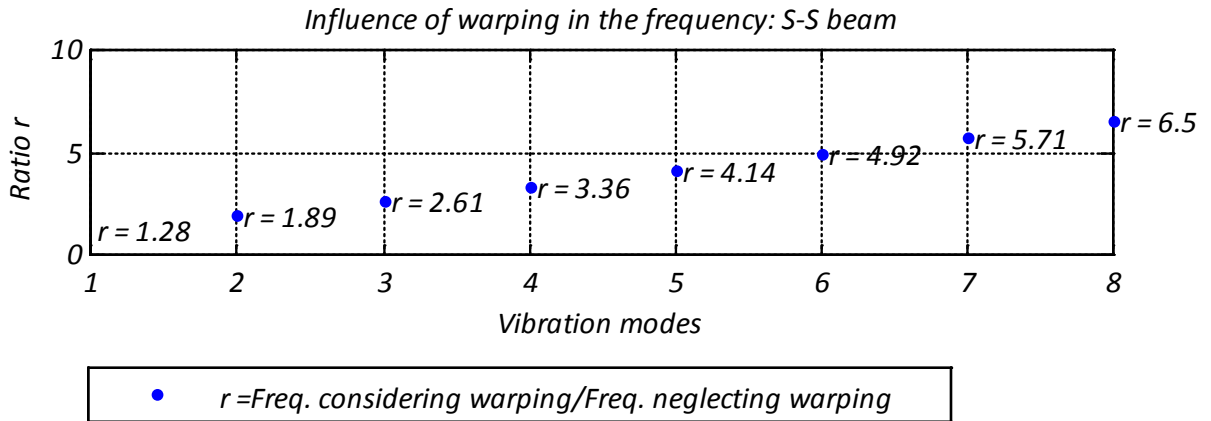


Figure 4.38 - Ratio r for 8 vibration modes in a S-S beam. Solution obtained by the presented model.

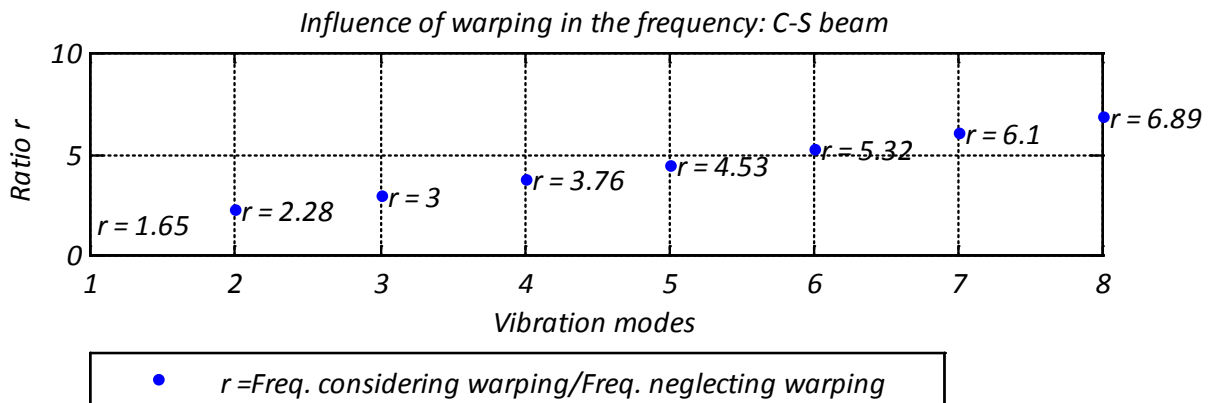


Figure 4.39 - Ratio r for 8 vibration modes in a C-S beam. Solution obtained by the presented model.

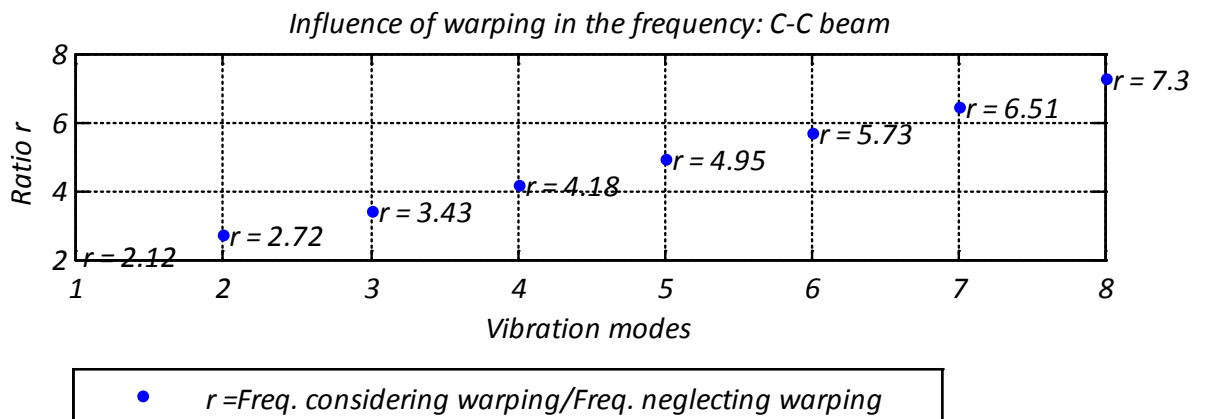


Figure 4.40 - Ratio r for 8 vibration modes in a C-C beam. Solution obtained by the presented model.

The results of the presented model (figure 4.38) compared with those analytical represented by figure 3.39 allow to state that the solutions obtained are the same for the free torsional-vibration of a S-S bar is considered. As expectable when the extreme are clamped the increase of frequency is higher because of the warping restraining imposed from the supports. Note that FEM approximation allows to make free vibration analysis of supported bars for which the exact solution is not known. This is possible because the FEM is based on algebraic equations making part of a linear system that can be easily solved by a computer code.

Example 4.9: Influence of warping for different boundary conditions

The example 4.8 shown that the warping of an open cross-section has an important role in increasing the frequency of a beam. A non-dimensional indicator of the frequency increase can be expressed by the ratio between the frequency of a generally supported beam and the frequency of a S-S beam. In the analysis performed by Gere the results were shown in a graphic form and only the denominator was calculated exactly in (3.172).

FEM approximation allows to obtain the following non-dimensional quantity

$$\frac{p}{p_{SS}}(\kappa) \tag{4.72}$$

where p_{SS} is the frequency of the S-S beam. This ratio is calculated by solving the eigenvalue problem for all the boundary conditions listed in table 4.15. The variation of this value is presented as a function of the dimensionless parameter κ for a single vibration mode, in order to explore all the cross-sections types. Note that the graphs are expressed in a semi-logarithmic scale.

The results for the first four modes of vibration are exposed in figure 4.41, figure 4.42, figure 4.43 and figure 4.44. The arrow indicates the increasing of the restriction and tends to the condition of both element ends clamped.

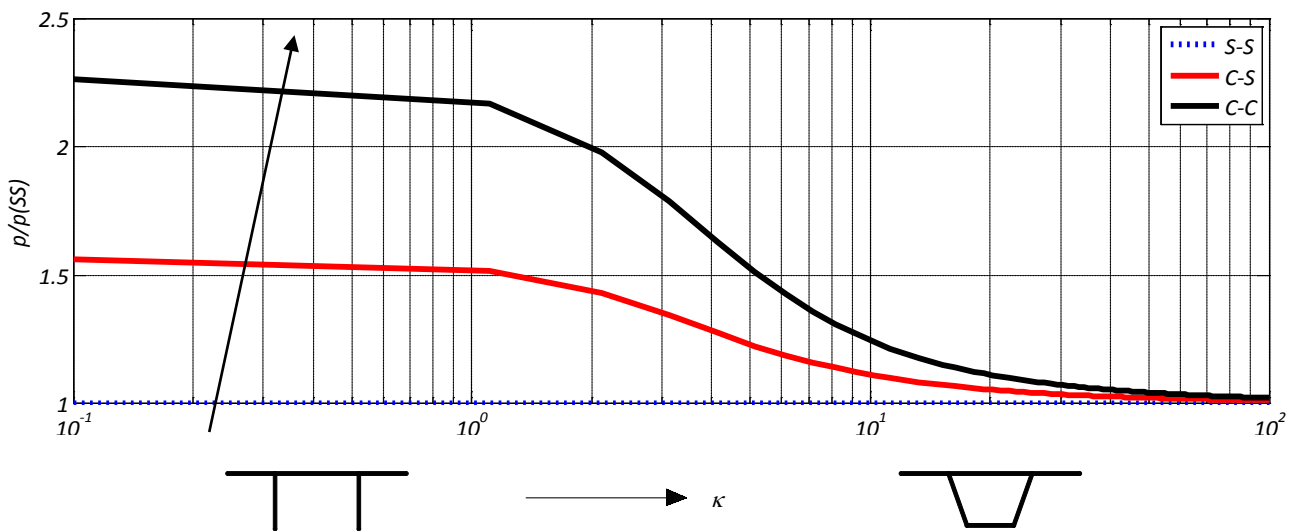


Figure 4.41 - Influence of boundary conditions on the 1st mode frequency.

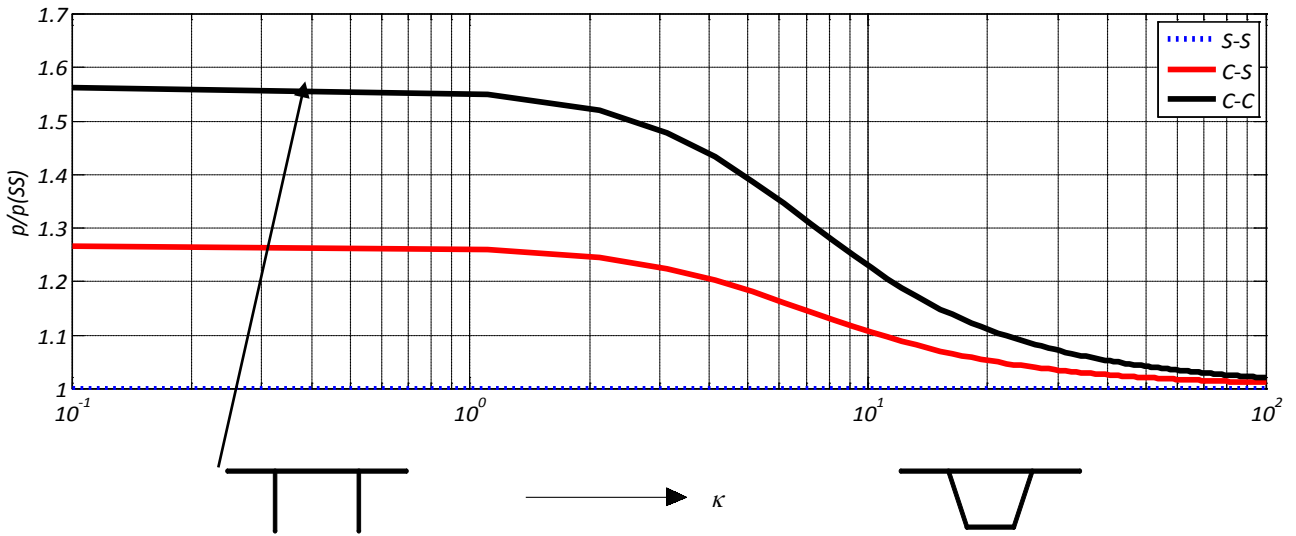


Figure 4.42 - Influence of boundary conditions on the 2nd mode frequency.

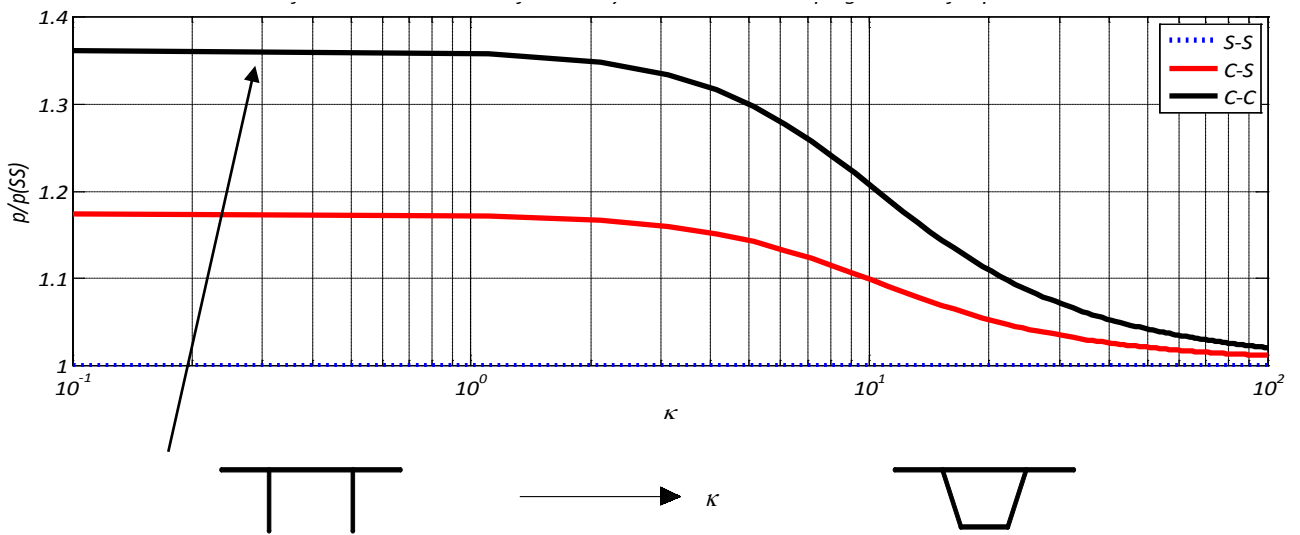


Figure 4.43- Influence of boundary conditions on the 3rd mode frequency.

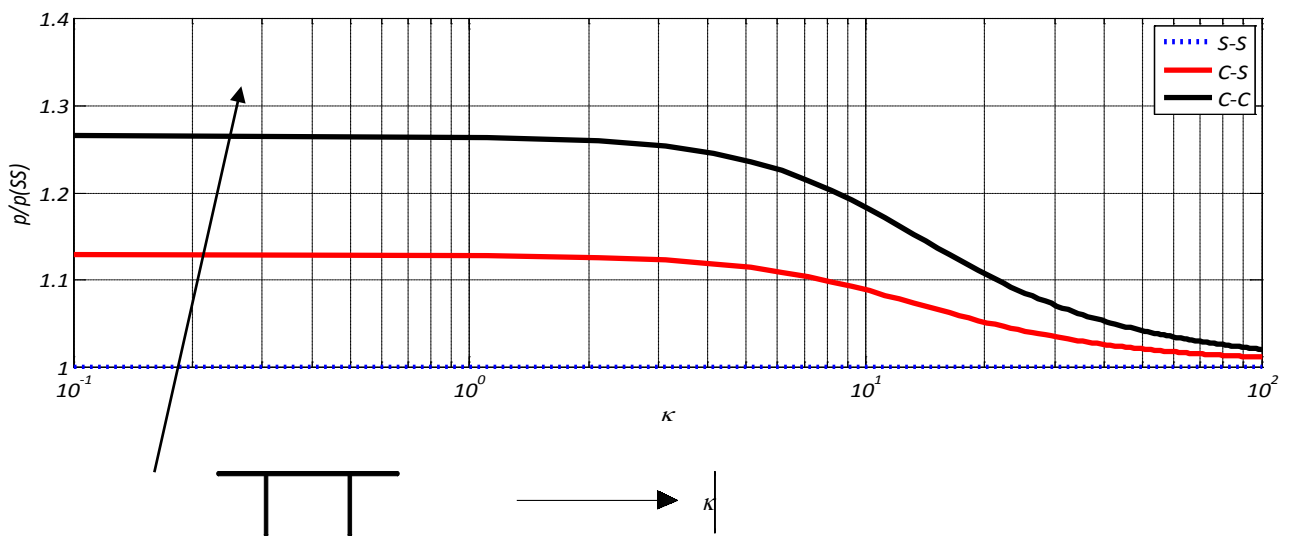


Figure 4.44 - Influence of boundary conditions on the 4th mode frequency.

Notice that, as expectable, for lower κ -values the increase of the frequency is more evident and by restraining warping in both ends, the ratio reaches values of 230% for the first vibration mode.

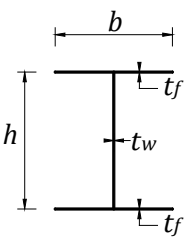

When the torsion response of the section tends to pure Saint Venant torsion ($\kappa > 15$) the value of $p/p_{SS}(\kappa)$ is low and the warping influence on increasing the frequency is not so high. These conclusions prove that the results obtained are more relevant for open thin-walled cross-sections, being the boundary conditions of warping restrained an important factor to be accounted, which greatly increases the vibration frequency of these beam-like elements. The increasing of the modal frequency for higher vibration modes is smaller, even for the cases of pure warping torsion, because these modes have higher frequency values the effect of restraining warping affects less the stiffness as the modal frequency increases.

Example 4.10: Modal analysis of a Simply Supported beam

The equation of motion expressed by the FEM model neglecting the damping and the applied loads allows to obtain the vibration modes and the frequency modal values. The simply-supported beam of the example 4.1 is considered and the torsional vibration modes will be calculated solving the linear system of the eigenvalue problem (4.59) using the element mass matrix (4.41) and the element stiffness matrix (4.20) calculated for the uncoupled problem of torsion.

The I-steel beam already seen in static is analyzed. Characteristics of the cross-section layout and length of the simply supported beam are expressed in table 4.16.

Table 4.16 – Characteristics of the steel beam cross-section layout and bar length.

Cross-section		$b[mm]$	170.0
		$h[mm]$	360.0
		$t_w[mm]$	8.0
		$t_f[mm]$	12.7
Support conditions		$L[mm]$	2000

The first 6 vibration modes with the relative mode frequency are exposed in table 4.17.

Table 4.17 – Torsional vibration modes for a simply supported I-beam.

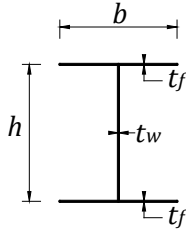
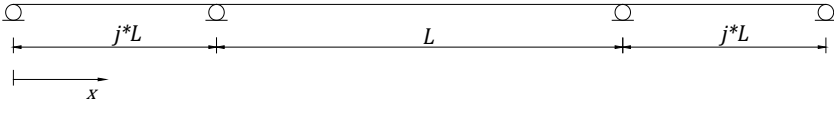
1	Modal frequency [Hz]	93.9	2	Modal frequency [Hz]	349.8
3	Modal frequency [Hz]	752.8	4	Modal frequency [Hz]	1274.9
5	Modal frequency [Hz]	1887.0	6	Modal frequency [Hz]	2562.8

Notice that the vibration shapes refer to the φ - values and do not represent the deformed shape of the beam as happen for flexural displacements.

Example 4.11: Modal analysis of a three continuous spans beam

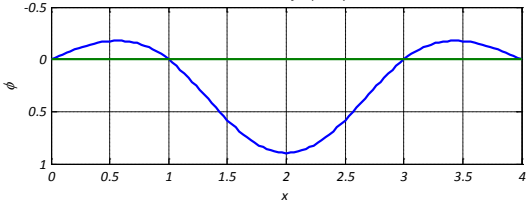
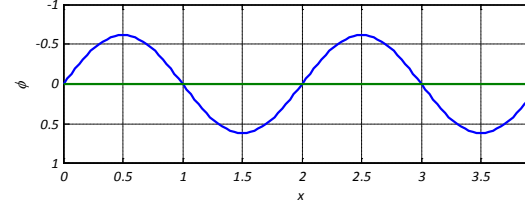
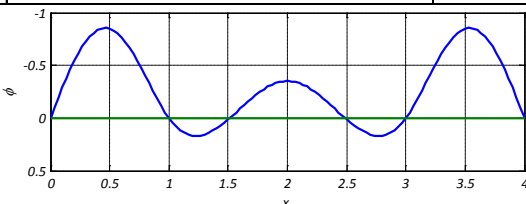
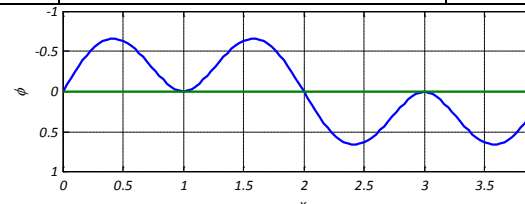
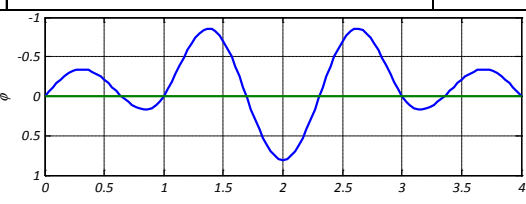
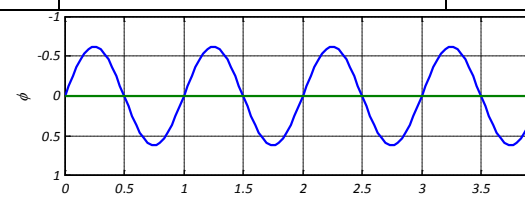
With the same FEM model used in the example 4.10 a three continuous spans steel beam in its free and undamped motion is analysed. The cross-section details and the span dimensions are summarized in table 4.18.

Table 4.18 - Characteristics of the cross-section layout and span lengths.

Cross-section		$b[mm]$	170.0
		$h[mm]$	360.0
		$t_w[mm]$	8.0
		$t_f[mm]$	12.7
Support conditions		$L[mm]$	2000
		j	0.5

In table 4.19 are illustrated the first 6 vibration modes of the three-continuous spans beam with the respective modal frequency obtained by solving the eigenvalue equation of the undamped motion.

Table 4.19 - Torsional vibration modes for a three continuous spans I-beam.

					
1	Modal frequency [Hz]	142.7	2	Modal frequency [Hz]	359.7
					
3	Modal frequency [Hz]	452.8	4	Modal frequency [Hz]	556.9
					
5	Modal frequency [Hz]	939.1	6	Modal frequency [Hz]	1420.2

Example 4.12: Comparative study with ABAQUS

A comparative study with ABAQUS is presented in this example. The modal frequency for the two last examples 4.10 and 4.11 will be set as an indicator obtained from an ABAQUS model. The ABAQUS element used for modeling the beam section is the B310S (ABAQUS users manual version 6.7, 2007) and the results are shown in Table 4.21 for the first 6 vibration modes of the simply supported beam. Notice that the same example is developed by using the exact frequency expression obtained in (Gere, 1954) by the eq.(3.172). The results obtained by the developed model coincide with the analytical results, while lower values of modal frequencies are obtained through the ABAQUS model.

In Table 4.22 the same comparison is developed for the continuous beam. The table 4.20 shows the characteristics of the element and of the cross-section considered. The boundary conditions and the number of finite elements used is also indicated.

Table 4.20 – Characteristics of the cross-sections and structural systems compared.

FREE VIBRATION ANALYSIS				
Boundary Conditions	Cross-section	$I\omega\omega$ [m]	ABAQUS element	Nº of elements
SS (L=2m)	I-Section	3.14E-07	B310S	60
T-C-S (L=2m;j=0.5)				240

Table 4.21 – Mode vibration frequencies for the S-S beam and relative errors compared with ABAQUS.

Vibration mode	1	2	3	4	5	6	SS (L=2m)
Modal frequency [Hz]	94.5	359.7	801.6	1420.2	2215.6	3187.7	Exact (Gere)
	93.9	349.8	752.8	1274.9	1887.0	2562.8	ABAQUS
	94.5	359.7	801.6	1420.2	2215.6	3187.7	The developed model
	0.32%	1.90%	4.32%	7.45%	11.10%	15.10%	Error (AB.)

Table 4.22 – Mode vibration frequencies for the T-C-S beam and relative errors compared with ABABUS.

Vibration mode	1	2	3	4	5	6	SS (L=2m)
Modal frequency [Hz]	140.0	355.8	445.0	523.5	851.7	1279.5	ABAQUS
	142.3	356.4	448.2	550.9	918.9	1370.0	The developed model
	1.6%	0.17%	0.71%	4.97%	7.31%	6.6%	Error

The frequency values obtained by the ABAQUS software are lower than those calculated using the presented model for both the S-S beam and the continuous beam. This is probably due to different considerations in the formulation of the beam model B310S about the stiffness of the element. This results mean that lower values of modal stiffness are considered by the software ABAQUS if compared with those considered in the presented formulation.

5. ANALYSIS OF DYNAMIC RESPONSE TO MOVING LOADS

The present chapter deals with the linearized modal analysis of combined flexural-torsional vibration of multi-span beams with monosymmetric cross-sections, due to an eccentric moving load of constant magnitude.

After thoroughly investigating the free vibrations of the structure, the dynamic analysis of beams which correspond to a common bridge layout, its forced motions under the aforementioned loading type are studied. The vibration of the beam-like elements will be examined only during the period of the load moving along the structure. Once the load departs from the structure, it begins to vibrate in free motion. The attenuation of the motion it is greatly affected by the damping characteristics of both the structure and the material.

In the section 5.1 the method of vibration analysis by superposing the vibration modes will be described, while the section 5.2 deals with the presentation of the numerical methods solving the problem of the dynamic structural response. The section 5.3 illustrates a numerical example, where two bridge section are compared in their dynamical response to a moving load.

5.1. The procedure of mode superposition

The *mode-superposition method* of dynamic analysis is based on the normal-coordinate transformation, which changes the set of N coupled equations of motion of a MDOF system into a set of N uncoupled equations. The method can be used to evaluate the response of any linear structure for which the displacements have been expressed for each degree of freedom as a linear combination of modal amplitudes and mode shapes.

The procedure is described by the following steps:

- Description of the dynamic equilibrium of the system by the *equation of motion*;
- Determination of the *mode shape* and *frequency analysis* by solving the eigenvalue problem;
- Transformation of the equation of motion in the generalized system. All the properties of the structure will be expressed in terms of modal coordinates;
- Obtainment of the *uncoupled equations of motion* for each vibration mode;
- Expression of the modal response to the loading: the amplitude for each mode is time-dependent for the assigned load and a general response could be obtained by the Duhamel integral;
- Displacement response in *geometric coordinates*, when the amplitude at time t is known;
- Evaluation of the *elastic force* response in the structure directly from its displacements;

These steps will be considered in the next and through the computer code developed the problem of a system loaded by a concentrated force will be solved in order to obtain its response for different displacements and conditions.

5.1.1. Uncoupled equations of motion with damping

The orthogonality properties of the normal coordinates may now be used to simplify the equations of motion of the MDOF system. The general form of the dynamic equations for the damped system is written as follows

$$\mathbf{M}\ddot{\mathbf{v}} + \mathbf{C}\dot{\mathbf{v}} + \mathbf{K}\mathbf{v} = \mathbf{f}(t) \quad (5.1)$$

Introducing the normal coordinate expression (4.66) and its time derivatives and premultiplying by the transpose of the n th mode-shape vector $\boldsymbol{\phi}_n^T$ leads to

$$\boldsymbol{\phi}_n^T \mathbf{M} \boldsymbol{\phi}_n \ddot{Y}_n + \boldsymbol{\phi}_n^T \mathbf{C} \boldsymbol{\phi}_n \dot{Y}_n + \boldsymbol{\phi}_n^T \mathbf{K} \boldsymbol{\phi}_n Y_n = \boldsymbol{\phi}_n^T \mathbf{f}(t) \quad (5.2)$$

In the equation (5.2) the orthogonality conditions (4.63) and (4.64) are taken into account and it has been assumed that the corresponding orthogonality conditions applies to the damping matrix considering that

$$\boldsymbol{\phi}_m^T \mathbf{C} \boldsymbol{\phi}_n = 0 \quad (5.3)$$

The assembling of a damping matrix where the orthogonality conditions are considered will be shown later.

The equation (5.2) can be written in terms of normalized coordinates as follows

$$M_n \ddot{Y}_n + C_n \dot{Y}_n + K_n Y_n = F_n(t) \quad (5.4)$$

Where the structural properties matrices are also expressed in terms of normal modal coordinates.

The procedure described above can be used to obtain an independent SDOF equation for each mode of vibration of the structure. Thus the use of the normal coordinates allows to transform the equations of motion from a set of N simultaneous differential equations, which are coupled by the off-diagonal terms in the mass and stiffness matrices, to a set of N independent normal-coordinate equations.

Conditions for damping orthogonality

It has been assumed that the normal-coordinate transformation in (5.3) allows to uncouple the damping forces in the same way that it uncouples the inertia and elastic forces. This is possible if the vibration mode shapes in the damped system are the same of the undamped mode shapes. Rayleigh showed that a damping matrix proportional to the mass and stiffness matrix satisfies this conditions. Hence, it can be written as follows

$$\mathbf{C} = c_1 \mathbf{M} + c_2 \mathbf{K} \quad (5.5)$$

This formula respect the orthogonality conditions. c_1 and c_2 represent two arbitrary proportionality factors that could be obtained solving the following system where two vibration modes are considered:

$$\begin{bmatrix} \xi_m \\ \xi_n \end{bmatrix} = \frac{1}{2} \begin{bmatrix} \frac{1}{p_m} & p_m \\ \frac{1}{p_n} & p_n \end{bmatrix} \begin{bmatrix} c_1 \\ c_2 \end{bmatrix} \quad (5.6)$$

where p_m, p_n are the frequencies that correspond to the m th and n th vibration mode of the structure, while ξ_m, ξ_n are the corresponding damping coefficients. If more vibration modes are considered, see (Clough & Penzien, 1982) for detailed information about the procedure. In this case the values of the Rayleigh constants can be obtained by

$$\begin{bmatrix} c_1 \\ c_2 \end{bmatrix} = 2 \frac{p_m p_n}{p_n^2 - p_m^2} \begin{bmatrix} p_n & -p_m \\ -\frac{1}{p_n} & \frac{1}{p_m} \end{bmatrix} \begin{bmatrix} \xi_m \\ \xi_n \end{bmatrix} \quad (5.7)$$

A numerical representation of the curve that describes the variation of the damping coefficients as a function of the modal frequency will be shown in the next numerical example. Note that the frequency values should be

chosen by considering only the significant frequency values for the structural response, being the frequency interval recommended by the Eurocodes for civil engineering structures.

5.1.2. Modal response to loading

The general dynamic response of a structure when subjected to moving loads has been studied by many authors in its analytical form and for a more detailed treatment of the argument see (Fryba, 1999). When the case of a constant vertical force moving at constant speed on a simply supported beam is considered, the external load $f(x, t)$ is obtained as a function of its position by the Dirac function.

For the analysis of the forced lateral-torsional vibrations, a similar approach is used, but when coupling between bending and torsion is considered the exact formulation in terms of differential equations are difficult to solve. In fact, a limited number of examples considering simply supported conditions have been treated in literature (Michaltos, Sarantithou, & Sophianopoulos, 2003).

The FEM model developed in chapter 4 allows to solve the equation (5.2) for a MDOF system when the external load vector and the damping matrix are considered. When the vibration modes and the modal response at time t for the n -mode $Y_n(t)$ are known, the displacement expressed in cartesian coordinates can be obtained.

Displacement and elastic force response in geometric coordinates

The amplitude is known for each mode when the modal response $Y_n(t)$ has been obtained. Considering the transformation in (4.66) the displacements can be expressed in geometric coordinates as follows:

$$v(t) = \phi_1 Y_1 + \phi_2 Y_2 + \dots + \phi_n Y_n + \dots \quad (5.8)$$

This merely represents the superposition of the modal contributions. When the displacement history of the structure is obtained, it represents the basic measure of its response to dynamic loadings.

In considering the moving load as a concentrated force eccentrically applied, as shown in figure 5.1, the following assumption are adopted (Fryba, 1999)

1. The mass of the moving load is small compared with the mass of the beam; this means that only the *gravitational effects* of the load are considered;
2. The load moves at a constant speed, from left to right;
3. At the instant of the force arrival, the beam model is at rest, i.e. possesses neither deflection nor velocity.

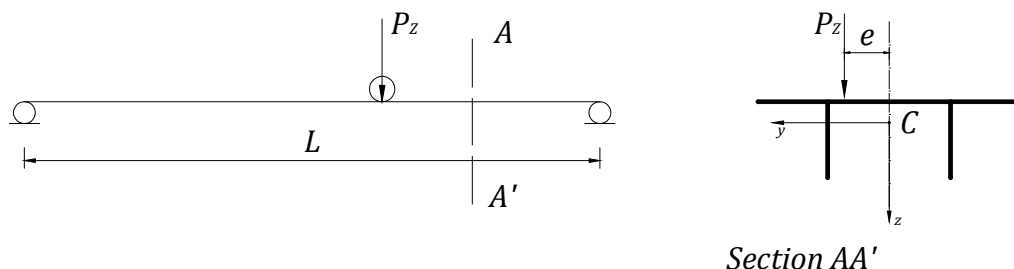


Figure 5.1 – Example of supported beam element acted by a constant and eccentric moving load.

For more details about the theoretical solutions, in terms of differential equation of motion, for this kind of problem, see (Fryba, 1999) or (Michaltos, Sarantithou, & Sophianopoulos, 2003).

5.2. Numerical modeling of dynamical response

When the structural system is discretized in finite beam elements a numerical integration method must be applied in order to find the displacement field according to the FEM method. Firstly, damping is considered using the Rayleigh method after the stiffness and mass matrices have been assembled. Then, an externally applied load vector for each time instant is needed: the time-variation of the load position will be accounted by means of an interpolations for the load intensity. Both damping matrix and externally applied load vector will be obtained as shown by the section 5.2.1.

The system of MDOF equation can finally be written in terms of modal coordinates as described by (5.4), in order to obtain a set of independent SDOF modal equation. The equation can be solved using a time-step integration method: the Newmark method will be used in this case. When the time amplitudes of every modes are known the response of the structure is completely defined and all the effects related with the displacement filed could be calculated.

5.2.1. Element property matrices

The element mass matrix and the stiffness matrix are known for the beam element being assembled when the structural properties and the boundary conditions are known. When these matrices are known, the free-vibration analysis of the structure can be simulated by the numerical FEM model, while the analysis of forced vibrations requires the knowledge of the damping matrix and of the external load matrix.

The damping matrix depends directly from the stiffness matrix and the mass matrix of the structure when Rayleigh's assumption is considered. The external load matrix is time-dependent and will be calculated by a suitable approximation of the load intensity at time t for each joint of the beam.

Damping matrix

The two constants of the equation (5.7) can be calculated directly for the structural system when the eigenvalue problem has been solved. The damping coefficient that should be considered for the n and m -vibration mode can be deduced by experimental results obtained monitoring the dynamic response of real bridges, as shown in figure 5.2.

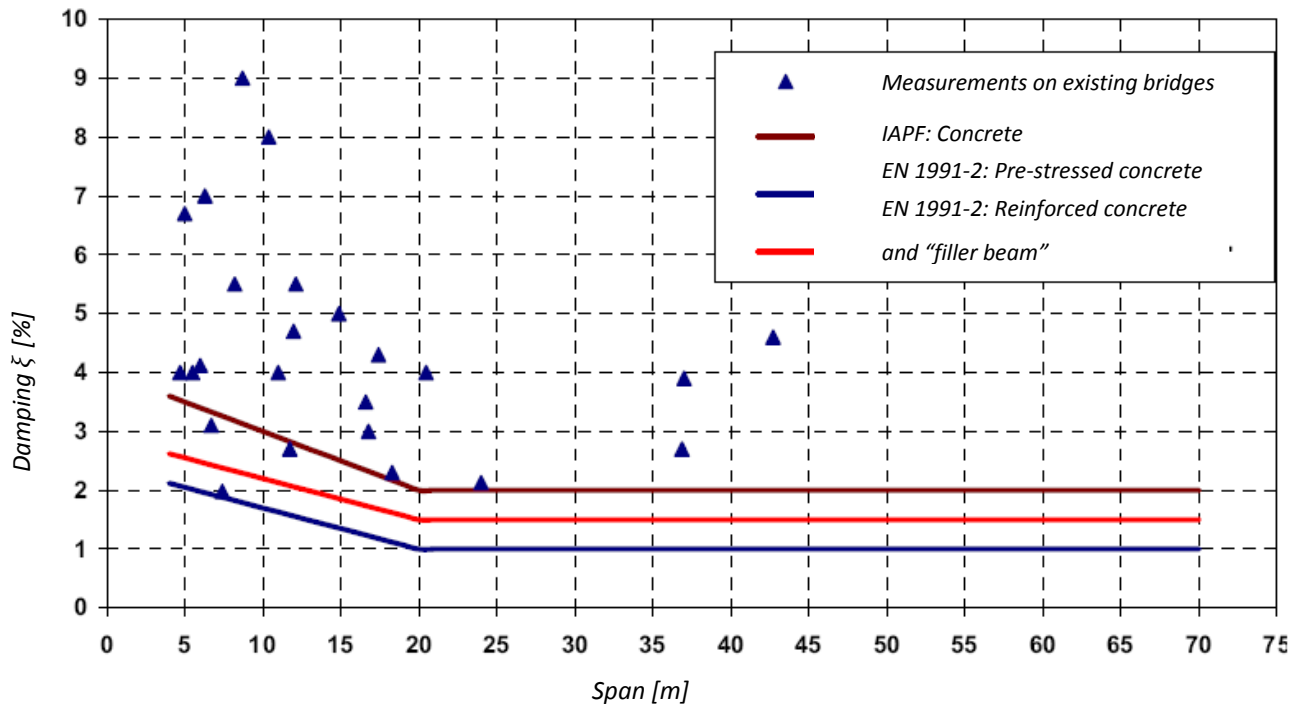


Figure 5.2 – Experimental values of the damping coefficient for different bridge spans. (Cunha, 2007).

When the constants c_1 and c_2 are known, the Rayleigh expression (5.6) can be used in order to obtain the damping matrix C .

Vector of nodal forces

The vector of externally applied nodal forces $f(t)$ that appears in (5.1) should be calculated for the whole time interval of the load acting. This vector contains the nodal *intensity* of the generalized load type $I(t)$ multiplied by the load value when the load is acting on the element j , between the joints i and $i + 1$. A vertical load P_z is applied eccentrically moving at constant speed v : this means that both nodal vertical force and applied torque should be taken into account when the load vector is assembled, as shown in figure 5.3.

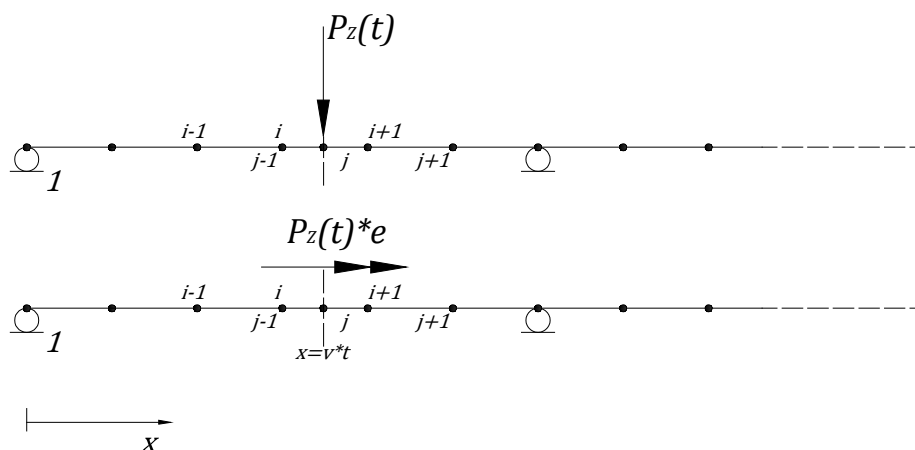


Figure 5.3 – Applied loads on a supported beam along x -direction.

The load intensity per joint can be obtained as follows

$$P_z^i(t) = I^i(t) * P_z \quad (5.9)$$

$$P_z^i(t) * e = I^i(t) * P_z * e \quad (5.10)$$

The time variation of $I^i(t)$ is approximated by a linear interpolation as shown in figure 5.4. Alternatively, the intensity could be interpolated by Hermite functions, as done for the displacement field. However, the problem of the time intensity of the load can be approximated by increasing the time steps.

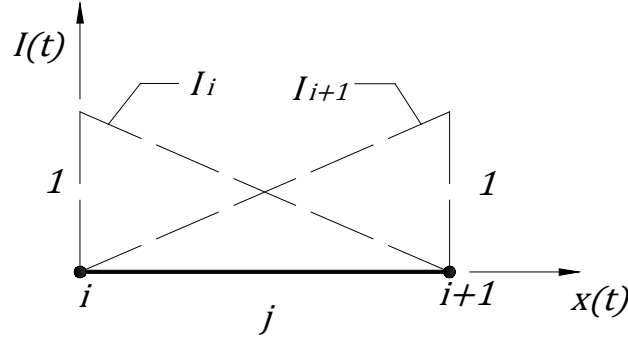


Figure 5.4 – Linear interpolation for the time intensity at time t.

Note that the sum of all the nodal loads contained in the vector $f(t)$ considering the selected generalized displacement must be equal to the load P_z or $P_z * e$.

5.2.2. Time-stepping Newmark's method

Several methods are known for the integration of the equation (5.1), differing in the approach and in the stability of the solutions obtained. One of the most used is the Newmark method of numerical integration. This is a so-called *time-stepping method* because the response in terms of displacement is obtained starting from the previous step results. Then the velocity and acceleration fields depend on the displacements calculated for the same time-step and from the previous step.

An hypothesis is necessary as a first approach about the variation of the acceleration field between t and $t + \Delta t$. With this assumption the method solves the equation of motion in terms of displacements.

Basis of the Newmark method

As already mentioned the Newmark method considers for the acceleration field a constant variation. This implies that

$$\dot{v}(t + \Delta t) = \dot{v}(t) + \int_0^{\Delta t} \ddot{v}(\tau) d\tau = \dot{v}(t) + (1 - \gamma)\Delta t \ddot{v}(t) + \gamma \Delta t \ddot{v}(t + \Delta t) \quad (5.11)$$

$$v(t + \Delta t) = v(t) + \int_0^{\Delta t} \dot{v}(\tau) d\tau = v(t) + \Delta t \dot{v}(t) + \left(\frac{1}{2} - \beta\right) \Delta t^2 \ddot{v}(t) + \beta \Delta t^2 \ddot{v}(t + \Delta t) \quad (5.12)$$

Newmark assumes that $\gamma = 1/2$ and $\beta = 1/4$ in (5.11) and (5.12), respectively, for the assumption above mentioned (Chopra, 1995). The values of $\dot{v}(t + \Delta t)$ and $\ddot{v}(t + \Delta t)$ can be obtained from these equations and after being substituted in the general equation of motion (5.1), the expression for calculate the displacements can be expressed as follows

$$\bar{K}v(t + \Delta t) = \bar{f}(t, t + \Delta t) \quad (5.13)$$

where

$$\bar{\mathbf{K}} = \frac{\mathbf{M}}{\beta\Delta t^2} + \frac{\gamma\mathbf{C}}{\beta\Delta t} + \mathbf{K} \quad (5.14)$$

$$\begin{aligned} \bar{\mathbf{f}}(t, t + \Delta t) = & \mathbf{f}(t + \Delta t) + \mathbf{M} \left(\frac{\mathbf{v}(t)}{\beta\Delta t^2} + \frac{\dot{\mathbf{v}}(t)}{\beta\Delta t} + \left(\frac{1}{2\beta} - 1 \right) \ddot{\mathbf{v}}(t) \right) \\ & + \mathbf{C} \left(\frac{\gamma}{\beta\Delta t} \mathbf{v}(t) + \left(\frac{\gamma}{\beta} - 1 \right) \dot{\mathbf{v}}(t) + \Delta t \left(\frac{\gamma}{2\beta} - 1 \right) \ddot{\mathbf{v}}(t) \right) \end{aligned} \quad (5.15)$$

The values of $\dot{\mathbf{v}}(t + \Delta t)$ and $\ddot{\mathbf{v}}(t + \Delta t)$ can be calculated in a second phase as functions of the displacement $\mathbf{v}(t + \Delta t)$ or imposing the dynamic equilibrium.

Stability of the method and time step

The constant variation of the acceleration assumption, which is the basis of the Newmark method, provides an efficient step-by-step integration procedure as long as a short time increment is used. Usually, the time increment required to achieve an adequate accuracy of the significant response is not unreasonably short considering that the Newmark method is an *unconditionally stable* step-by-step method.

In the next numerical example it will be considered for the time step that

$$\Delta t \leq \frac{T_1}{100} \quad (5.16)$$

where T_1 is the fundamental period of vibration of the structure $T_1 = 1/f_1$ expressed in [s]. Different values of Δt can be considered to improve the precision of the solution obtained.

5.3. Numerical example

The described modal superposition method can be seen as the method for assembly the solution of a structural N -degrees of freedom system in terms of displacements through the solution of a set of N independent SDOF partial differential equations, written in terms of modal coordinates. A numerical example of a three-spans bridge is presented in the following section. The geometry in the longitudinal direction is the same of the example 4.6 represented in figure 4.23, being considered the bridge decks represented in figure 4.24 and figure 4.25 for comparison purposes. The bridge deck properties are described in Table 4.12.

5.3.1. Actions on the bridge and structural properties

In railway bridge design there are two essential types of loads involved, the *general actions* and the *rail traffic actions*.

The *general actions* acting on structures are defined in the EN 1991 (Part 1) and they include the so-called quasi-permanent loads (Parts 1-1 to 1-6) and the accidental actions (1-7) acting as static loads.

The *rail traffic actions* with all the action effects are described by the EN 1991 (Part 2). The rail traffic loads are proposed by alternative models for railway loadings, being the dynamical and centrifugal effects considered specifically.

In the design of bridges for high speed trains all these loads must be taken into account and the present analysis considers only a simplified model. The track structure interaction should be considered but it will not be the object of the present study.

The general actions considered are the densities and the self-weight of imposed loads for railway bridges and are shown in Table 5.1.

Table 5.1 – General actions of the railway bridge.

Action	Load magnitude
Self-weight per unit volume (C30/37) [kN/m^3]	25
Permanent loads [kN/m]	85

Note that the permanent loads presented in Table 5.1 include:

- *Ballast;*
- *Track + Sleepers;*
- *Post and catenary;*
- *Concrete blocks for posts;*

The concentrated vertical force P_z considered as railway action has a magnitude of 1000 kN and an eccentricity of 2.5 m . A layout type of the bridge cross-section is proposed as an example in figure 5.5 for a closed box section.

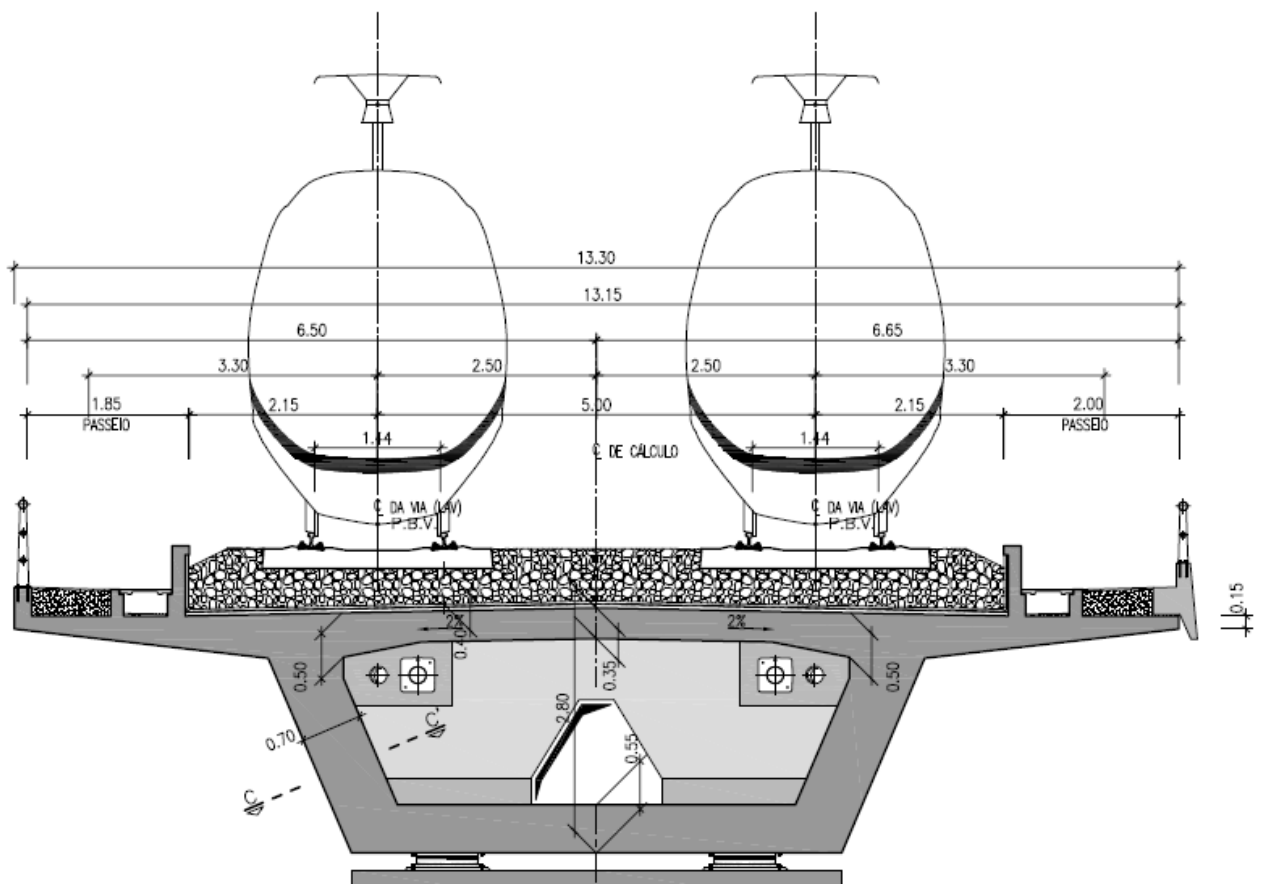


Figure 5.5 – Bridge layout of the cross-section and sketch of the actions considered.

The structural properties of the bridge decks analyzed are summarized in table 4.13 and the concrete type considered is the C30/37.

5.3.2. Undamped free-vibration analysis

The undamped free-vibration analysis is performed considering the FEM model of the structure and by the numerical solution of the corresponding eigenvalue problem is possible to obtain the vibration modes and the respective modal frequencies. The free-vibrating undamped motion refers to both open and closed bridge cross-section.

Not all the vibration modes will be considered as relevant for the analysis: the EN 1990-A2 refers that the frequencies until 30 Hz should be considered in the dynamic analysis of the bridge.

Note that the mass of the bridge is defined by the general actions specified in Table 5.1 and the element stiffness and mass matrices used are illustrated by the equations (4.34) and (4.53), respectively.

Open section

For the open double-T bridge section the modal vibration analysis and respective modal frequency are listed in table 5.2.

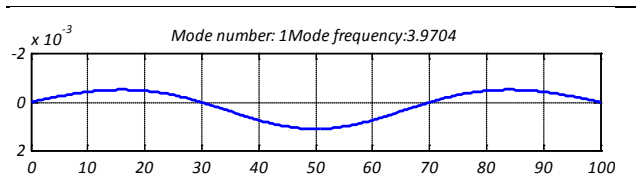
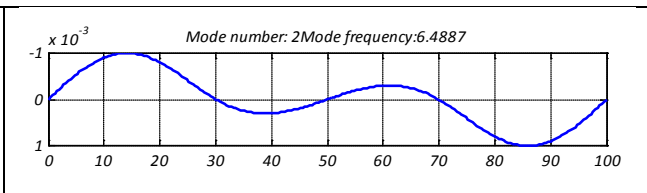
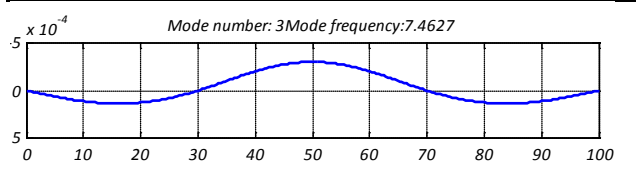
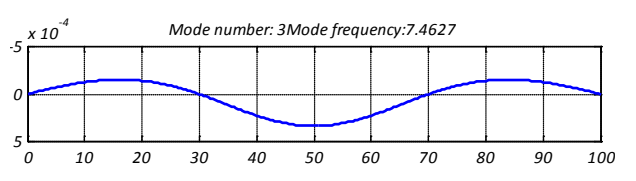
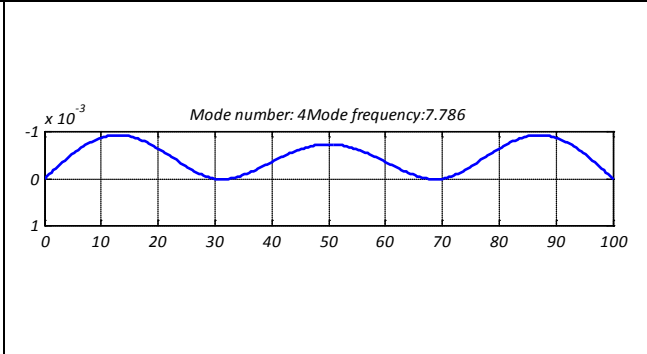
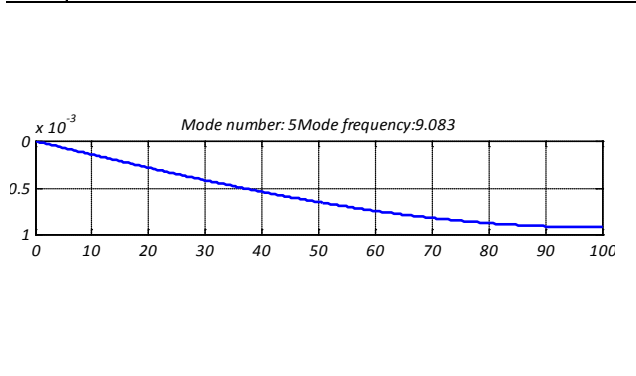
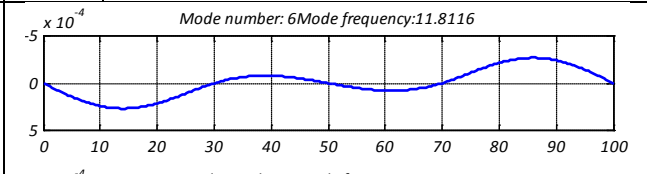
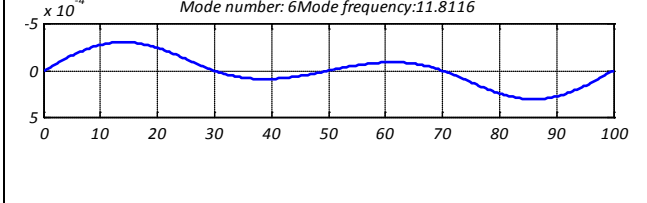
Table 5.2 – Undamped vibration modes and respective modal frequencies for the double-T bridge section.

Mode number	Frequency [Hz]	Major modal participation
1	3.97	<i>Bending motion in (x,z) plan</i>
2	6.49	<i>Bending motion in (x,z) plan</i>
3	7.46	<i>Coupled lateral (y)- torsional (φ) motion</i>
4	7.79	<i>Bending motion in (x,z) plan</i>
5	9.08	<i>Axial motion</i>
6	11.81	<i>Coupled lateral (y)- torsional (φ) motion</i>
7	13.96	<i>Coupled lateral (y)- torsional (φ) motion</i>
8	14.84	<i>Bending motion in (x,z) plan</i>
9	16.53	<i>Coupled lateral (y)- torsional (φ) motion</i>
10	22.51	<i>Bending motion in (x,z) plan</i>
11	24.55	<i>Bending motion in (x,z) plan</i>
12	26.03	<i>Coupled lateral (y)- torsional (φ) motion</i>
13	26.33	<i>Coupled lateral (y)- torsional (φ) motion</i>
14	27.25	<i>Axial motion</i>
15	31.71	<i>Coupled lateral (y)- torsional (φ) motion</i>

As expectable, the first two modes are flexural modes and only the third mode is a torsional mode. Note that torsion and displacement in the vertical direction are uncoupled, while the y-displacement is coupled with the twist rotation. Note also that the higher frequencies correspond to much lateral-torsional vibration modes.

The vibration modes for the double-T bridge section are shown in table 5.3 until the 6th mode. Notice that when the lateral-torsional modes are considered, they cannot be shown by a single graph. In fact, the mode shape is defined by the coupling between the lateral and torsional displacements and both must be represented (modes 3 and 6).

Table 5.3 – Vibration modes for the double-T bridge section (frequencies in [Hz]).

 <p>Mode number: 1 Mode frequency: 3.9704</p>	 <p>Mode number: 2 Mode frequency: 6.4887</p>
<p>1 Bending motion in (x,z) plan</p>	<p>2 Bending motion in (x,z) plan</p>
 <p>Mode number: 3 Mode frequency: 7.4627</p>  <p>Mode number: 3 Mode frequency: 7.4627</p>	 <p>Mode number: 4 Mode frequency: 7.786</p>
<p>3 Coupled lateral (y)- torsional (φ) motion</p>	<p>4 Bending motion in (x,z) plan</p>
 <p>Mode number: 5 Mode frequency: 9.083</p>	 <p>Mode number: 6 Mode frequency: 11.8116</p>  <p>Mode number: 6 Mode frequency: 11.8116</p>
<p>5 Axial motion</p>	<p>6 Coupled lateral (y)- torsional (φ) motion</p>

Notice that the lateral-torsional vibration modes of the continuous beam have different shapes if compared with those obtained in table 4.19 because of the different proportionality between the lateral and the central span. The ratio used in the case of table 5.3 is commonly used in real bridge models.

Closed section

The closed-section, which has the properties represented in Table 4.12, have been analyzed in order to obtain the main vibration modes for the same structure layout, being the results for the first 16 modes with the respective frequencies represented in table 5.4.

Table 5.4 – Undamped vibration modes and respective modal frequencies for the box bridge section.

Mode number	Frequency [Hz]	Major modal participation
1	3.79	<i>Bending motion in (x,z) plan</i>
2	6.19	<i>Bending motion in (x,z) plan</i>
3	7.43	<i>Bending motion in (x,z) plan</i>
4	9.08	<i>Axial motion</i>
5	12.05	<i>Coupled lateral (y)- torsional (φ) motion</i>
6	14.16	<i>Bending motion in (x,z) plan</i>
7	15.37	<i>Coupled lateral (y)- torsional (φ) motion</i>
8	16.12	<i>Coupled lateral (y)- torsional (φ) motion</i>
9	16.54	<i>Coupled lateral (y)- torsional (φ) motion</i>
10	21.50	<i>Bending motion in (x,z) plan</i>
11	23.44	<i>Bending motion in (x,z) plan</i>
12	24.56	<i>Coupled lateral (y)- torsional (φ) motion</i>
13	26.02	<i>Coupled lateral (y)- torsional (φ) motion</i>
14	27.25	<i>Axial motion</i>
15	29.52	<i>Coupled lateral (y)- torsional (φ) motion</i>
16	30.70	<i>Bending motion in (x,z) plan</i>

As can be verified from the table 5.4, also in the case of closed section, the first three modes correspond to the bending in the vertical plane, while the first lateral-torsional motion mode only appears as the 5th vibration mode.

5.3.3. Forced-vibrations analysis and mode-superposition procedure

In the current analysis the dynamic response of the bridge structure will be obtained by the modal superposition method. The vibration of the system is forced by a moving load P_z with magnitude of 1000kN travelling at constant speed. The vertical load is applied eccentrically and the eccentricity value is 2.5m, which is considered according to the tracks position (figure 5.5). The influence of damping is considered for the two sections studied and for each one of them a damping matrix will be obtained considering the orthogonality conditions.

Conditions for damping orthogonality

The damping matrix is obtained considering the undamped mode frequencies and the orthogonality property of the Rayleigh method.

Two different cross-section layouts are compared and for this reason two different damping matrices will be calculated. The bridge has a 40m central span length and considering the coefficient results for existing bridges represented in figure 5.2 a damping ratio 0.01 (1%) will be adopted for the 1st and for the 6th bending modes in the vertical plan. This allows to define numerically the Rayleigh coefficients c_1 and c_2 described in the equation (5.7) as shown in table 5.5.

Table 5.5 – Rayleigh coefficients for the bridge cross-sections considered.

Section type	Mode frequency [<i>rad/s</i>]	Damping coefficient	Rayleigh constants
Double-T section	24.95	1%	$c_1 = 0.4295$
	154.25	1%	$c_2 = 0.00011$
Box girder section	23.79	1%	$c_1 = 0.4097$
	147.28	1%	$c_2 = 0.00012$

The modal damping coefficients are a function of the circular modal frequencies and their distribution curves are represented in figure 5.6 and figure 5.7 for the double-T bridge section and for the box girder section, respectively.

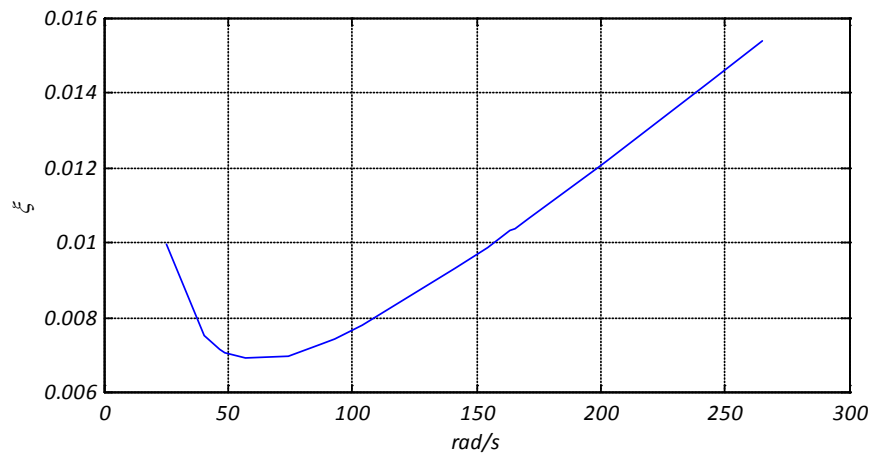


Figure 5.6 – Damping coefficients variation for the double-T bridge section.

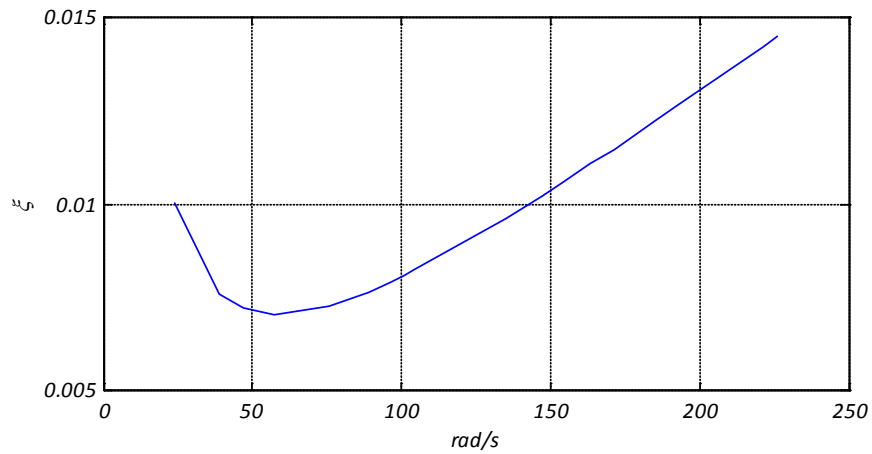


Figure 5.7 – Damping coefficients variation for the box girder bridge section.

Comparison of results

The vertical bending motion of the bridge obtained for the double-T section using the developed FEM model can be compared with the exact results for the simply supported bridge layout showed in figure 5.8.

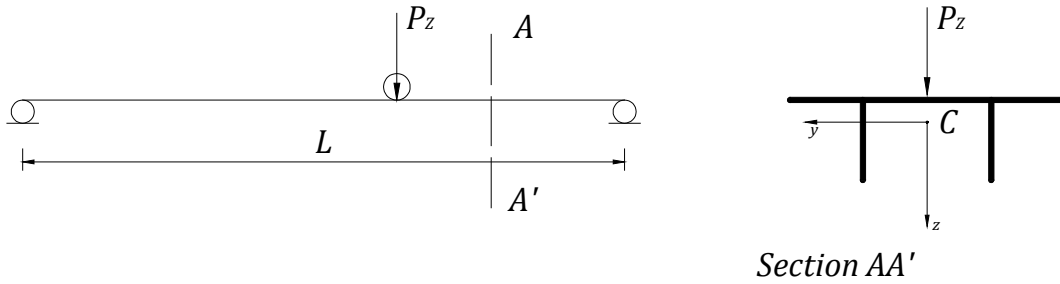


Figure 5.8 – Layout of the simply supported beam and moving load.

The bridge cross-section of the analysis is the double-T section, which properties are given in table 4.12, being the length considered for the span $L = 40m$.

At a first approach the undamped motion of the bridge will be considered. The mid-span dimensionless vertical displacement can be obtained as a function of the considered j -vibration mode and of the corresponding dimensionless velocity, given as follows

$$\alpha = \frac{p}{p_{(j)}} = \frac{v}{v_{cr}} \quad (5.17)$$

where $p_{(j)} = \frac{\pi^4 E I_z}{L^2} j^4$ is the circular frequency of the j -vibration mode, p is the load frequency, v is the load velocity and $v_{cr} = \frac{2f_{(j)}L}{j}$ is the critical structure velocity, defined for the first mode as $v_{cr} = 2f_{(1)}L$ for $f_{(j)} = \frac{p_{(j)}}{2\pi}$.

For $\alpha \neq j$ and considering only the first vibration mode ($j = 1$), the dimensionless displacement at mid-span ($x = L/2$) gives

$$\frac{u_z(x, t)}{u_{z0}} = \sin \frac{\pi}{2} \frac{1}{(1 - \alpha^2)} (\sin pt - \alpha \sin p_{(1)}t) \quad (5.18)$$

where $u_{z0} = \frac{P_z L^3}{48 E I_z}$ is the static displacement of the simply supported beam.

For $\alpha = j = 1$ the displacement is given as follows

$$\frac{u_z(x, t)}{u_{z0}} = \frac{1}{2} (\sin pt - pt \cos pt) \sin \frac{\pi}{2} \quad (5.19)$$

The results for three characteristics values of α are shown in figure 5.9, figure 5.10 and figure 5.11, where the values obtained from the developed model are successfully compared with the results obtained by (Fryba, 1999). In table 5.6 is listed the fundamental frequency, the period and the time interval Δt used for the Newmark integration.

Table 5.6 – Properties of the simply supported beam-like bridge discretization.

$f_{(1)}$ [Hz]	3.5
$T_{(1)}$ [s]	0.29
Δt [s]	0.003
Number of finite elements	100

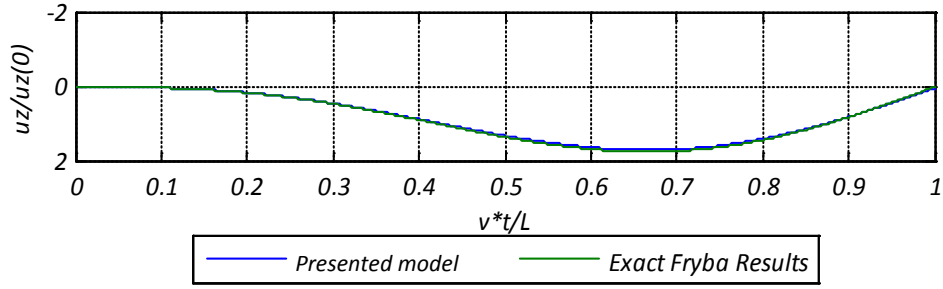


Figure 5.9 – Mid-span dimensionless displacement comparison ($\alpha = 0.5$).

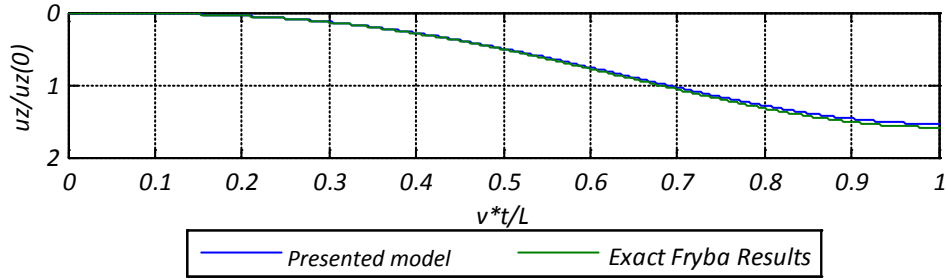


Figure 5.10 – Mid-span dimensionless displacement comparison ($\alpha = 1$).

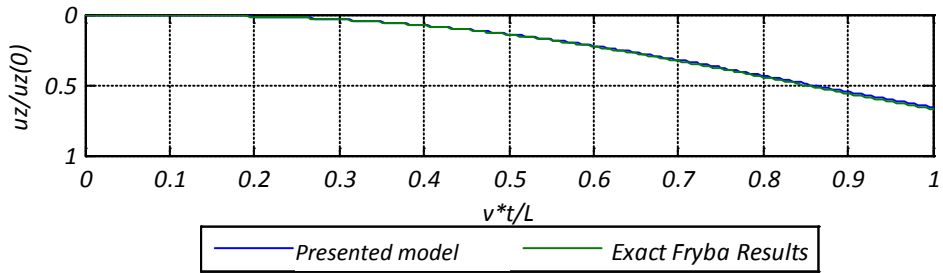


Figure 5.11 – Mid-span dimensionless displacement comparison ($\alpha = 2$).

As can be verified from figure 5.9, 5.10, 5.11, 5.12 the results obtained from the developed FEM model are in an excellent agreement with the exact results obtained by (Fryba, 1999).

If light damping is considered, as generally happens for the civil engineering structures, the next dimensionless quantity is defined as follows

$$\beta = \frac{p_b}{p_{(1)}} \quad (5.20)$$

where $p_b = p \cdot \xi$ is the circular frequency of damping of the beam, being ξ the damping coefficient.

The coefficient of the equation (5.20) defines the damping effect and $\beta = 1$ will be taken into account in this comparison.

For $\alpha \neq j$ and considering only the first vibration mode ($j = 1$), the dimensionless displacement at mid-span ($x = L/2$) gives

$$\frac{u_z(x, t)}{u_{z0}} = \sin \frac{\pi}{2} \frac{1}{(1 - \alpha^2)} (\sin pt - \alpha e^{(-p_b t)} \sin p_{(1)} t) \quad (5.21)$$

For $\alpha = j = 1$ the dimensionless value of the vertical displacement is given as follows

$$\frac{u_z(x, t)}{u_{z0}} = \frac{1}{2} \left[e^{(-p_b t)} \sin pt - \frac{1}{\beta} \cos pt (1 - e^{-p_b t}) \right] \sin \frac{\pi}{2} \quad (5.22)$$

The results for the damped motion are shown in figure 5.12, figure 5.13 and figure 5.14 for $\alpha = 0.5, 1, 2$.

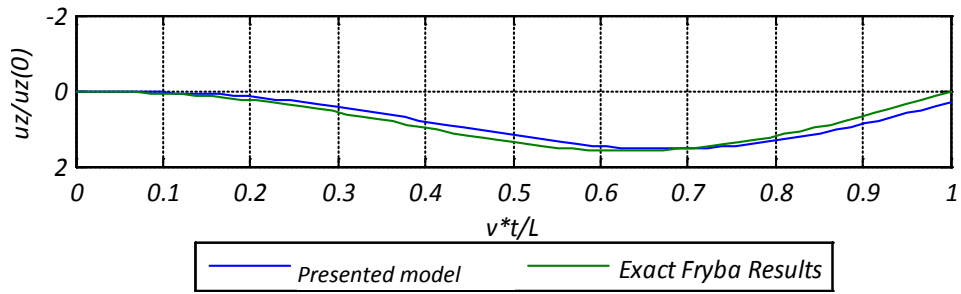


Figure 5.12 - Mid-span dimensionless displacement comparison ($\alpha = 0.5, \beta = 0.1$).

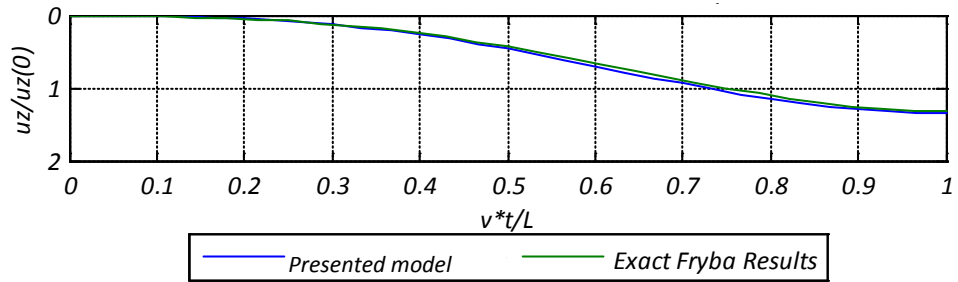


Figure 5.13 - Mid-span dimensionless displacement comparison ($\alpha = 1, \beta = 0.1$).

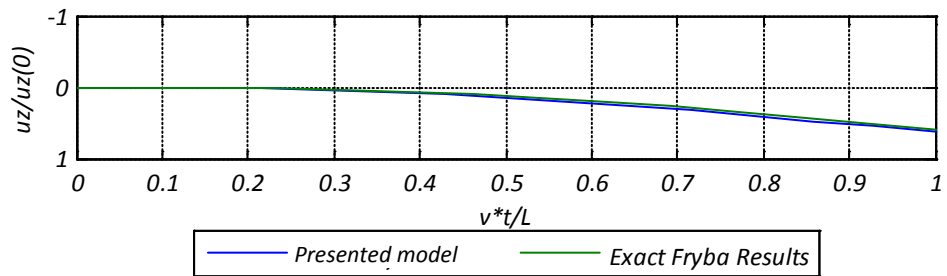


Figure 5.14 - Mid-span dimensionless displacement comparison ($\alpha = 2, \beta = 0.1$).

Also in the case in which light damping is considered ($\beta \ll 1$) the accuracy of the results obtained by using the mode superposition method is sufficiently good. Note that the same quantities listed in table 5.6 are used in the approximation of the current analysis. The effect of damping in this case is not so influent in terms of normalized displacements, being the influence lines obtained with $\beta = 0.1$ similar to the obtained considering the undamped motion.

Analysis of the three-span bridge dynamic response

The three spans bridge model with the two cross-section sketched in Figure 5.15 is analysed. The cross-section dimensions are represented in table 4.12. This section deals with the study of the dynamic response of the beam-like bridge decks when acted by a vertical and eccentric moving load also shown in Figure 5.15. The load magnitude is considered constant in time and space and the load motion is assumed to be at a constant speed.

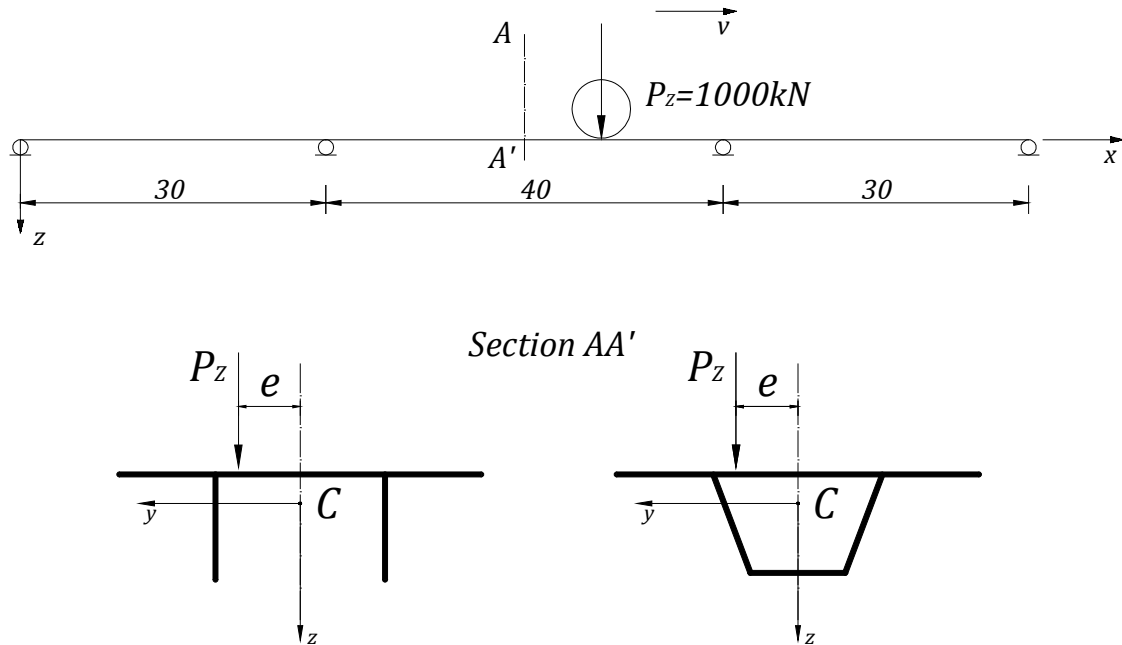


Figure 5.15 – Longitudinal beam-like model (a) and layout of the cross-section analyzed (b).

The eccentricity considered in the numerical example is also constant and its value is fixed to $e = 2.5\text{m}$ because the distance between the vertical axis and the train tracks is imposed from the bridge deck section type (figure 5.5).

The dynamic behavior of the beam-like bridge is investigated for a set of five different speed values of the load, considering a maximum speed of 350 km/h that corresponds to a design speed of 420 km/h for high speed railway bridges. The velocity values considered as an example to obtain influence lines are shown in Table 5.7.

Table 5.7 – Set of train velocities considered.

Train velocities [km/h]
200
250
300
350
420

The dynamic influence of the following kinematic quantities will be analyzed:

- Vertical displacement u_z at mid-span (section AA' of figure 5.15)
- Horizontal transversal displacement u_y at mid-span (section AA' of figure 5.15)
- Twist angle φ at mid-span (section AA' of figure 5.15)

The results in terms of the dynamic influence lines for the mid-span (AA') displacements are represented in figure 5.16, figure 5.17 and figure 5.18 for the double-T open bridge section. Note that the numerical parameters used in the current analysis relative to the time integration and the FEM model are detailed in table 5.8.

Table 5.8 – Parameters considered for the numerical simulation of the current analysis.

Number of finite elements	Lateral span L=30m	75
	Middle-span L=40m	100
	Lateral span L=30m	75
Time integration interval	$\Delta t [s] = T_{(1)}/200$	
Vibration modes considered	Double-T section	15
	Box Girder section	16

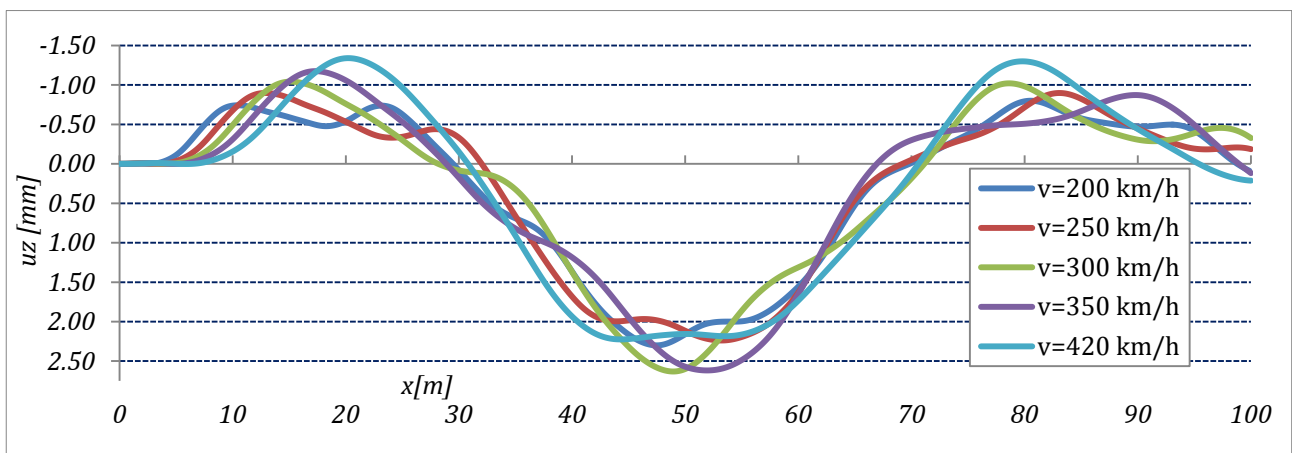


Figure 5.16 – Dynamic influence lines of the displacement u_z at the section AA' (double-T section).

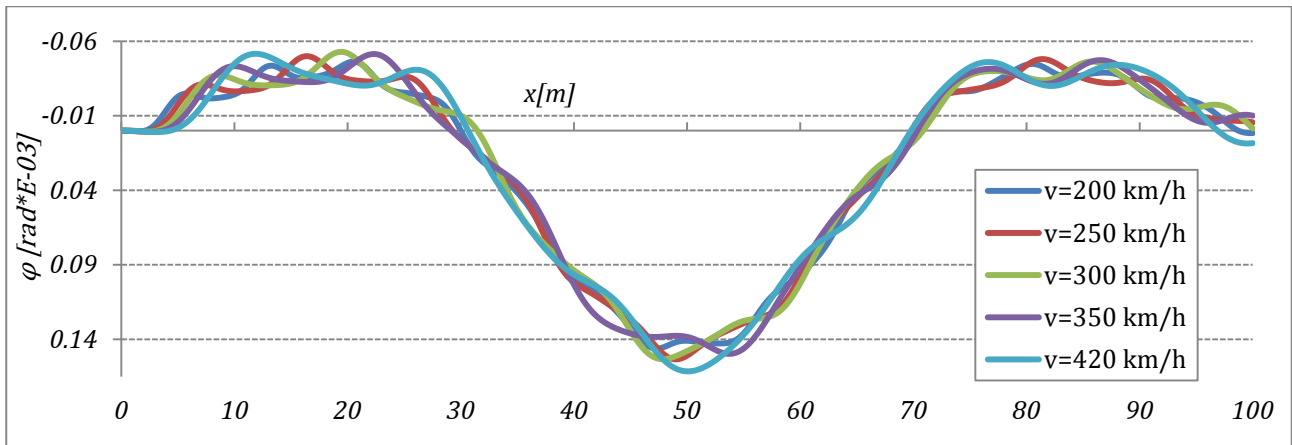


Figure 5.17 - Dynamic influence lines of the twist φ at the section AA' (double-T section).

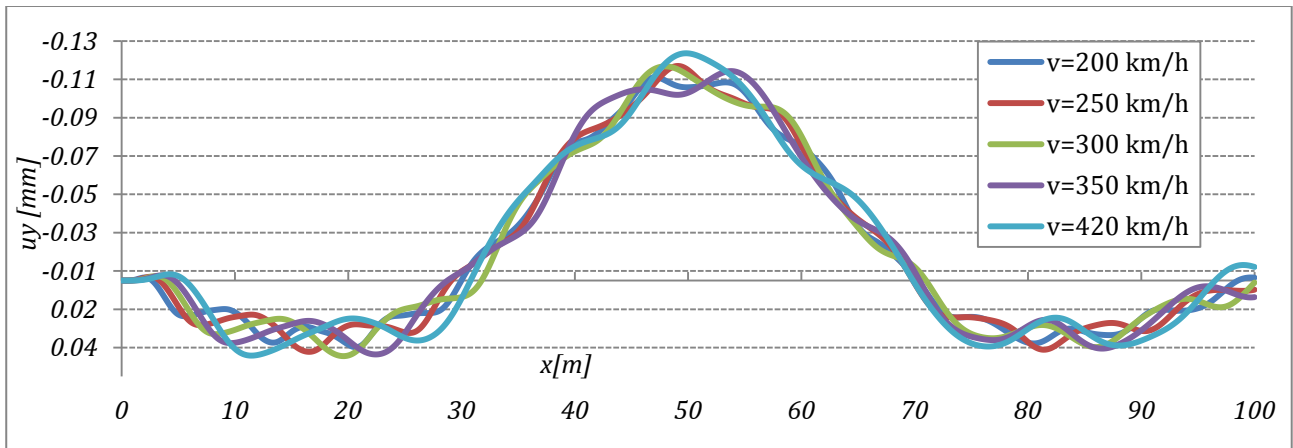


Figure 5.18 - Dynamic influence lines of the displacement u_y at the section AA' (double-T section).

The dynamic influence lines can be seen as an index of the flexibility of a structure when subjected to a moving load in the considered direction. The maximum mid-span vertical displacement is obtained for speed values of 300 km/h and 350 km/h.

Notice the different behavior of the bridge horizontal displacement (figure 5.18) and the twist angle (figure 5.17) from the vertical displacements (figure 5.16). In fact, the u_y and φ influence lines present functions with much more oscillations, due to the higher frequencies of the respective vibration modes, if are compared with the vertical displacement u_z , which has a modal contribute with lower frequency.

The effect of warping characterizes the torsional response of the double-T section shape as represented in figure 5.17, where significant variations of the twist angle values at the section AA' result from different load positions along the beam axis.

Table 5.8 shows the limit to the number of vibration modes analyzed considering a maximum frequency of 30 Hz. This assumption reduces the influence of the numerical noise in the results obtained for the model in analysis.

The figure 5.19, figure 5.20 and figure 5.21 represent the functions obtained for the displacements u_z , u_y and for the rotation φ , respectively, when the box girder section is considered

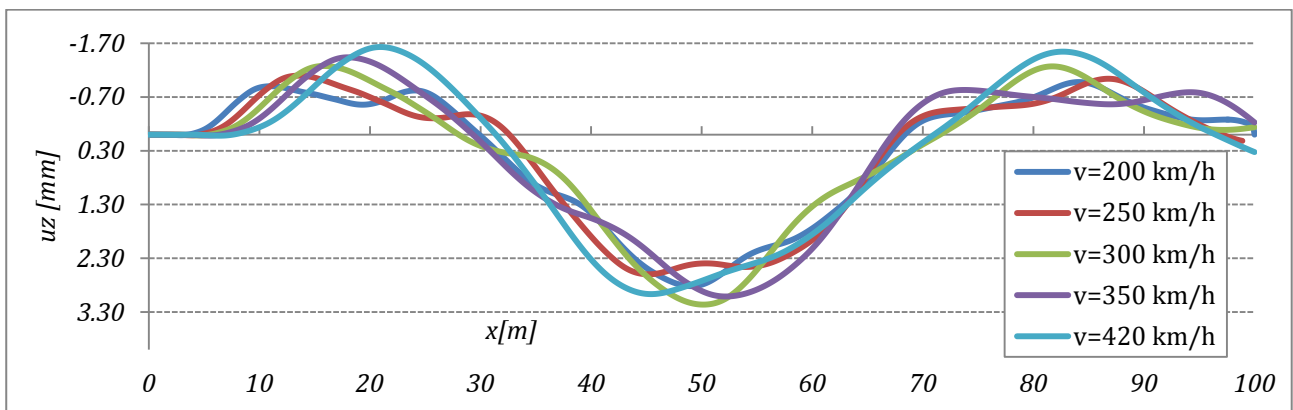


Figure 5.19 - Dynamic influence lines of the displacement u_z at the section AA' (box girder section)..

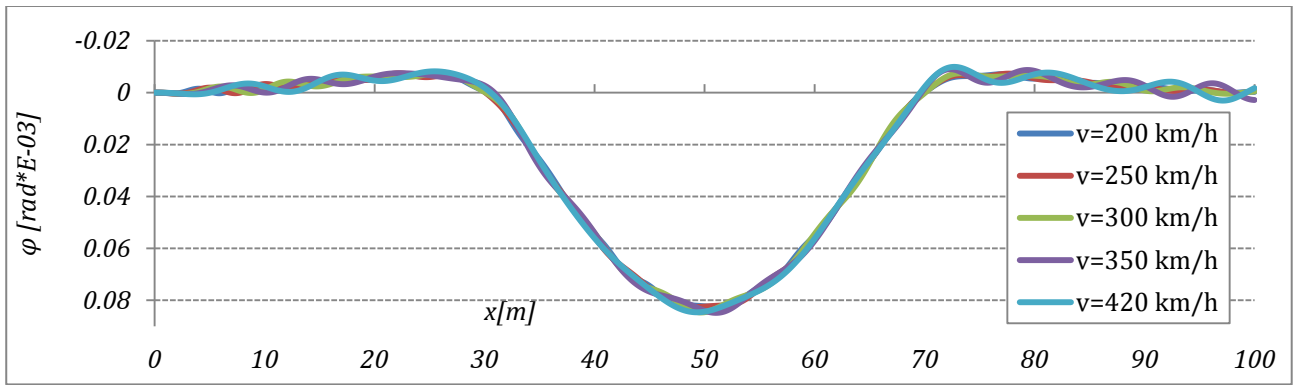


Figure 5.20 - Dynamic influence lines of the twist φ at the section AA' (box girder section).

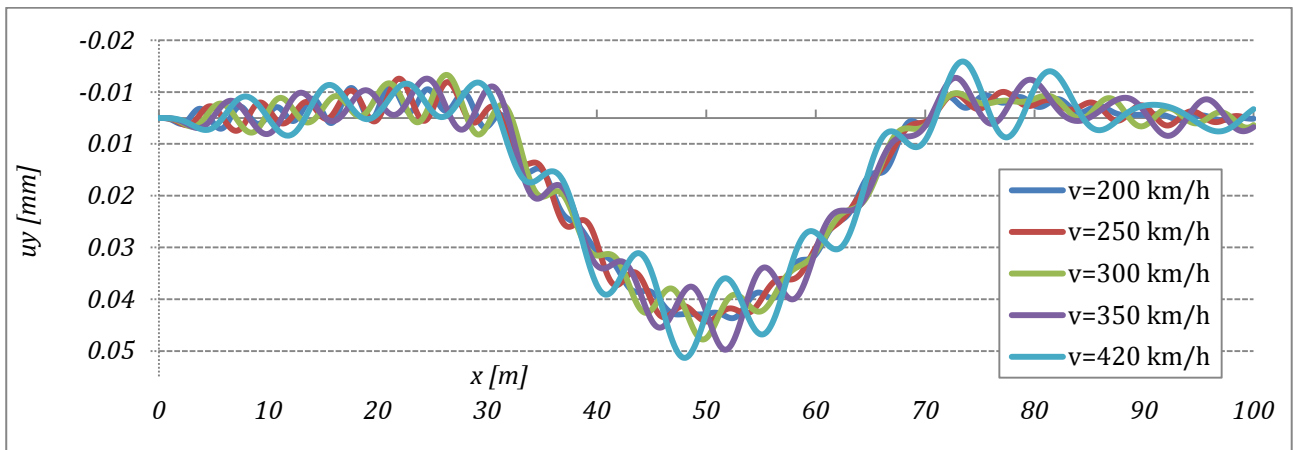


Figure 5.21 - Dynamic influence lines of the displacement u_y at the section AA' (box girder section).

The vertical deflections of the box section are similar to those obtained for the open section, being the inertia of these sections in vertical plan of the same order of magnitude (Figure 5.19). The figure 5.22 presents a further comparison between the two cross-sections for the vertical displacement influence lines.

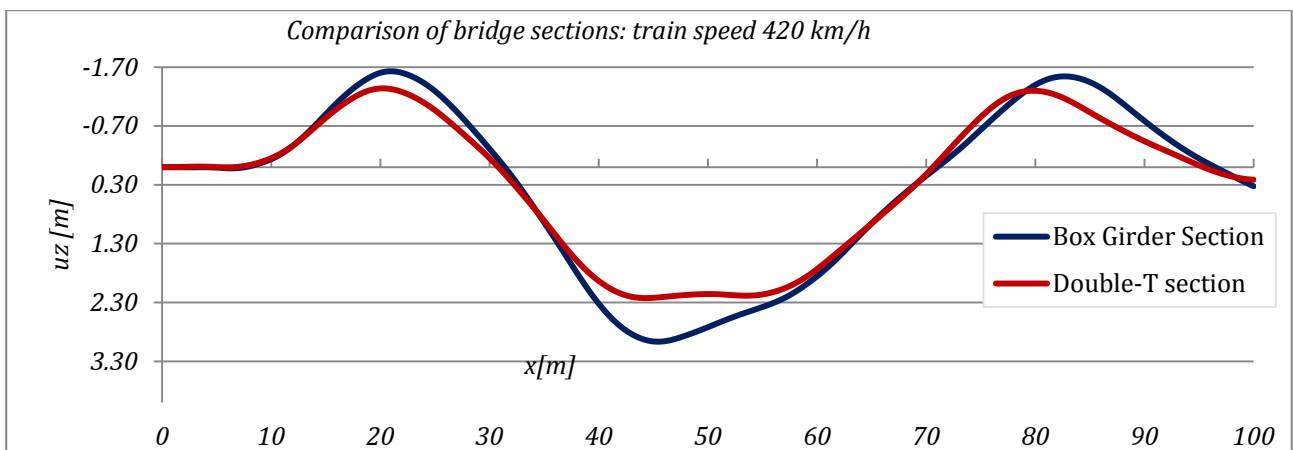


Figure 5.22 - Displacement u_z for the two bridge sections analyzed (load speed: 420 km/h).

The torsional response represented by the influence line of figure 5.20 allows to conclude that a box girder has much more torsional stiffness when compared with the double-T section. In fact, figure 5.20 shows that the dynamic influence line tends to the static influence line for the twist of the section. The horizontal displacements (figure 5.21) of the box girder sections are less important, in terms of the respective magnitude, if compared with those of the double-T section. The response in the horizontal direction presents a different sign of the u_y if

compared to that of the open bridge section. This effect is probably due to the consideration of the shear strain included in the sectorial coordinate, according to (Benscoter, 1954): for the box-girder section layout the shear centre assumes a different position, being the sign of $(z_c - z_a)$ opposite to that of the open double-T section. This different effect on the horizontal displacement of the two section-types analyzed is shown by figure 5.23 for the fixed value of maximum train speed analyzed: $v=420$ km/h.

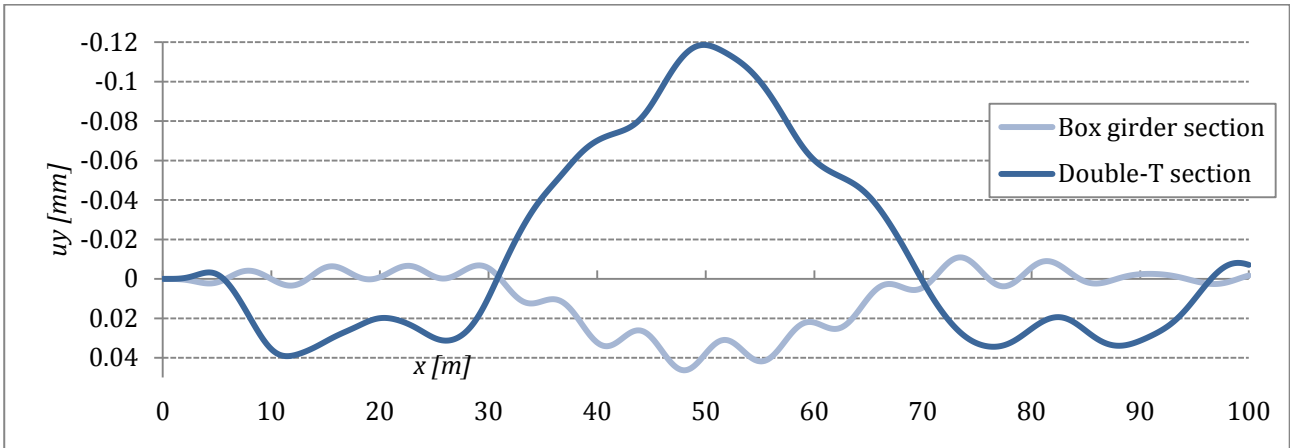


Figure 5.23 – Horizontal displacements of the bridge cross-section (load speed: 420 km/h).

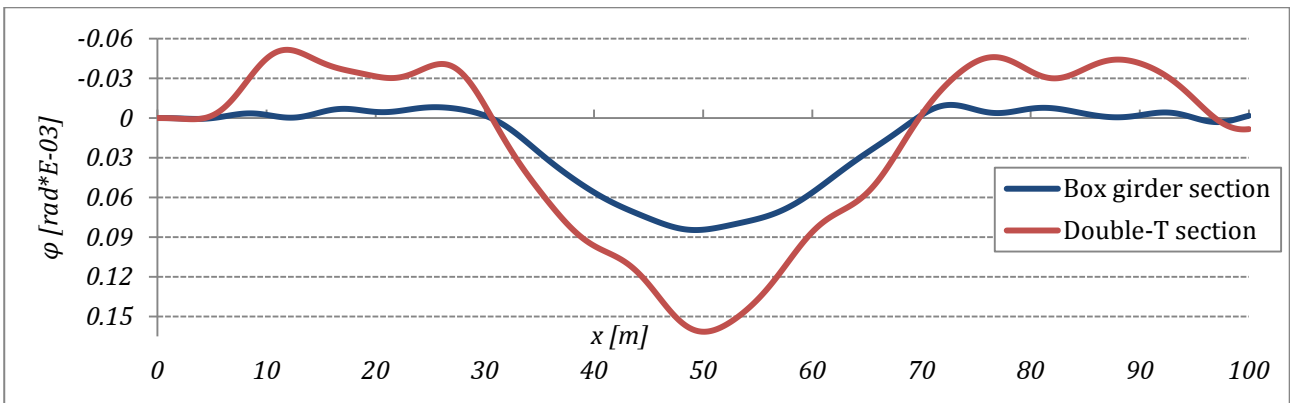


Figure 5.24 - Twist of the bridge sections (load speed: 420 km/h).

The torsional response is completely different for the two section types (Figure 5.24). As expectable, the closed section twist only reaches high values for the loading positioned at the central span, while the open section, more affected by warping, presents high values of rotation for a load located at the external spans.

The maximum displacement and twist rotation φ at the section AA' can also be plotted as functions of the load speed values. These curves are shown in figure 5.25 and figure 5.26 for the double-T and for the box girder bridge sections.

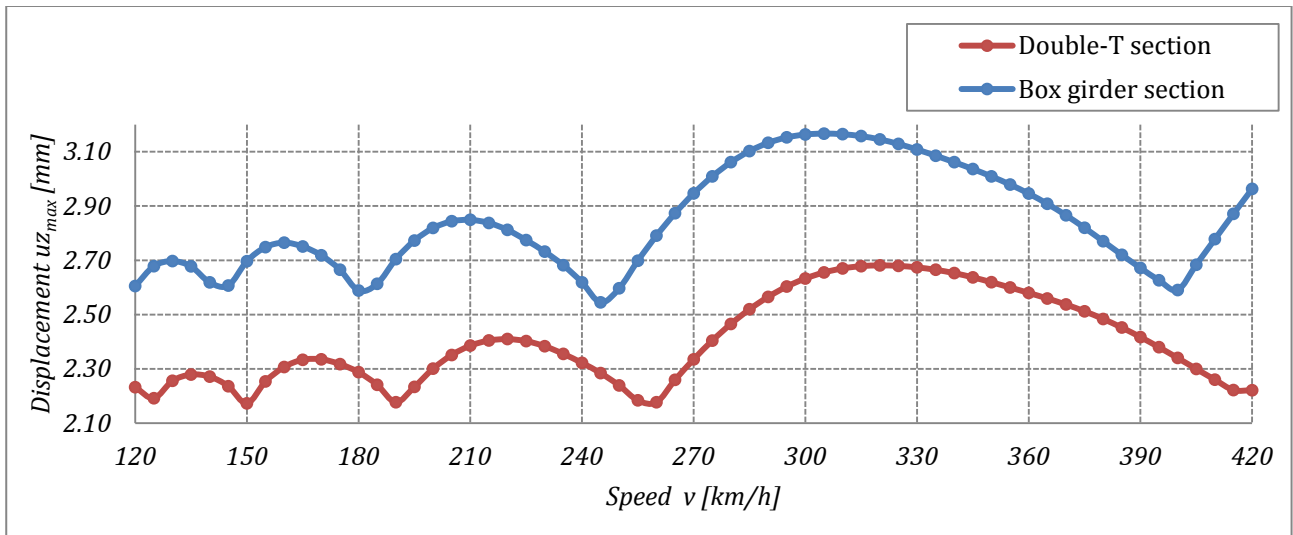


Figure 5.25 – Maximum vertical deflection of the section AA' for various speed values.

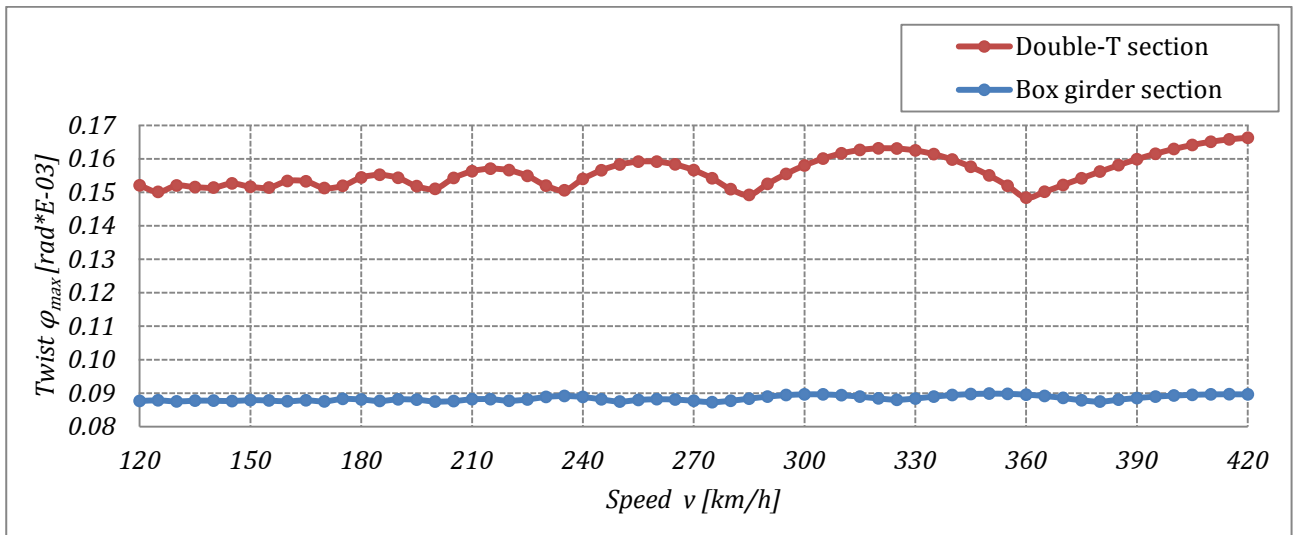


Figure 5.26 – Maximum twist rotation of the section AA' for various speed values.

The maximum values of the displacements u_z of figure 5.25 are similar in terms of maximum values, being the maximum displacements shown in table 5.9 The shapes of the functions are the same because both bending stiffness and response of the sections are similar. The figure 5.25 represents how the speed load influences the vertical deflection: this dynamic effect, well-known as *resonance*, depends from the characteristic of both structure and excitation velocity.

Table 5.9 – Maximum displacement values for some characteristic velocities.

Speed [km/h]		130	160	210	305	420
$u_{z,max}$ [mm]	Double-T	2.26	2.31	2.39	2.66	2.22
	Box Girder	2.70	2.76	2.85	3.17	2.94

Table 5.10 – Maximum twist values for some characteristic velocities.

Speed [km/h]		185	215	255	320	420
φ_{max} [rad*E-03]	Double-T	0.15	0.15	0.15	0.16	0.16
	Box Girder	0.08	0.08	0.08	0.08	0.08

The figure 5.26 presents the values of the φ_{max} at mid-span (AA') and, as expected, the results for the different sections are much more different from each other than those obtained for the vertical displacement response. Consequently for the box girder section the speed value of the moving load rather affect the maximum twist at the section AA'. The angle of torsion is constant for any speed values. On the other hand, the φ_{max} value for the double-T section is variable with the velocity as seen for the vertical displacements and the maximum rotation value is obtained at 420 km/h (see table 5.10). The resonance is appreciably also at 325 km/h and 255 k/h: note that at these velocities the vertical deflection has the minimum value.

A last example is presented: the double-T section illustrated by table 4.12 will be analyzed taking into account the warping of the cross-section and then neglecting this deformation in order to show the influence of warping deformation for open bridge sections. The vertical displacement of the generic point P will be calculated. This point corresponds to the track's position and has eccentricity $e = 2.5m$ as represented by figure 5.27.

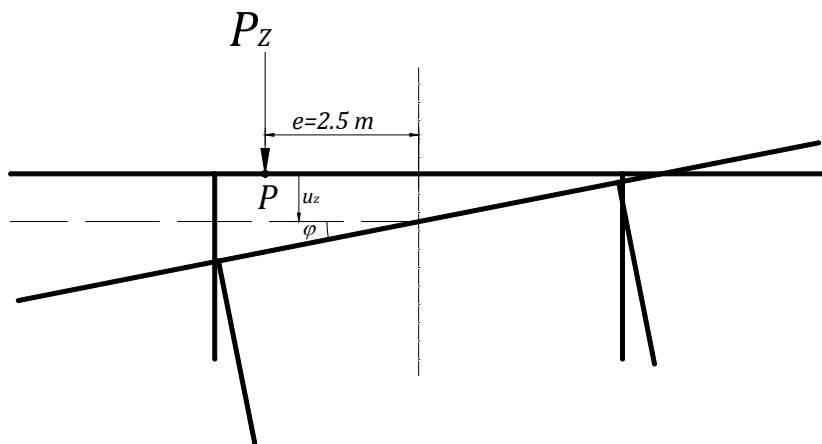


Figure 5.27 – Displacement of the point P of the double-T section.

The displacement of the point P is obtained as follows:

$$u_z^P(x, t) = u_z^C(x, t) + e * \varphi(x, t) \tag{5.23}$$

where u_z^C is the contribution of the vertical displacement of the elastic center, e is the eccentricity and φ is the twist angle of the section. The influence line of the displacement u_z^P is represented by figure 5.28 for a constant velocity of 300 km/h and $P_z = 1000kN$.

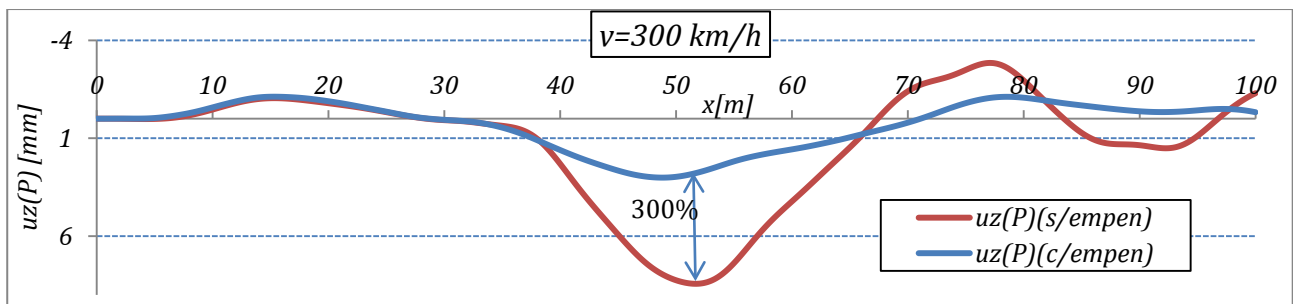


Figure 5.28 – Dynamic influence line of the displacement u_z^P .

The figure 5.28 shows that the maximum value of the twist angle obtained by neglecting the warping of the cross-section is 300% higher than the value obtained considering it. This confirms that the primary source of torsion resistance, in the case of open sections, is the warping stiffness and the error in estimating the dynamic displacements is greatly affected by its consideration.

6. CONCLUSIONS AND FINITE DEVELOPMENTS

6.1. General remarks

The introduction of this thesis stated that the main objective of this work was to investigate one-dimensional thin-walled beam-like structures for arbitrary geometry of the cross-section, loading cases and boundary conditions and to enable an accurate representation of the widest range possible of behaviors in static and dynamics.

The analysis performed in this work is focused on the consideration of the torsional response of both open and closed cross-sections of thin-walled beams. For this reason a finite element model with seven degrees of freedom for each end has been formulated and implemented through a numerical code.

The target was reached; all the designed and developed models gave satisfactory results and were conclusive. The work has provided important information that enhances the understanding of structural problems and the fundamental physical principles that underlie them related to the cross-section warping. The model that has been presented allows a simplified analysis of straight thin-walled beam with arbitrary boundary conditions and generally loaded, both in statics and dynamics. The major propose is the application of this beam element to the analysis of bridges, in particular in the analysis to moving loads.

6.1. Conclusions

Starting from the governing differential equations of the axial, bending and torsional effects and considering the Euler Bernoulli and Vlasov thin-walled beam theories, a finite element formulation has been developed according to variational principles.

The whole beam element with arbitrary thin-walled cross-section was represented by its elastic center axis and Hermite polynomials were used as approximation functions of the displacement field. For this discrete element the stiffness and mass matrices and the vector of external loads were derived without neglecting terms.

In statics, basic examples of generally loaded beams with different cross-sectional behaviors have been presented for the understanding of the influence of warping in the displacement field and stress analysis. The exact results obtained by (Kollbrunner & Basler, 1969) have been simulated in order to check the accuracy of the obtained solution. Also a comparison with ABAQUS has been performed in order to check the stiffness method developed in the work.

The focus of these comparisons has been based on the following aspects:

- The consideration of a C, I and hollow cross-section;
- Two types of simply supported structures: a simply supported beam and a three continuous spans beam;
- Two types of loading: a concentrated and an uniformly distributed torque.

A study of convergence has been presented for the finite element model developed by increasing the elements of the mesh until it was reached a sufficiently good approximation. Also two sections, a double-T and a closed box, of a three-span bridge layout have been studied, being the lateral-torsional response obtained in terms of displacements and forces.

In dynamics, the following three structural behaviors have been investigated:

- The free torsional vibrations of generally supported beams. In this case, the results have been compared with those obtained by (Gere, 1954) for I-sections and the influence of warping and boundary conditions in the modal frequency values is studied;
- The forced vibrations of generally supported beams acted by a moving vertical load at constant velocity. The results have been compared with the exact solution of (Fryba, 1999) for the simple case of a load acting in the vertical plane without eccentricity;
- The effect of an eccentric vertical load in the lateral-torsional and flexural response of a straight beam with continuous spans. The bridge sections considered were a double-T girder and a box girder with two lanes.

The modal superposition method has been used in order to obtain the structural response and obtain dynamic influence lines for the thin-walled beams analyzed. In dynamics, the comparison between the two cross-sections mentioned has been performed. The bridge model response confirmed that the warping deformation greatly affects its behavior when the open section is considered.

The differences in terms of twist angle and lateral displacements, obtained for a set of different load speeds, between the box section and the open section has allowed to verify that warping is fundamental to a correct analysis of these structural element types.

6.2. Future developments

As already known from the Saint Venant theory, the closed sections warp much less than open thin walled sections and for this reason the classic Euler-Bernoulli beam element neglects the warping deformability. Therefore these elements are commonly used by the most known structural software such SAP, or ADINA.

Other simulation codes, such the ANSYS or the ABAQUS, allow to use elements with seven degrees of freedom, but the use of these tools are more adequate to the study of buckling and connection problems and its understanding is not so simple at a first approach.

The presented model could be considered as the first step tending to a more complete formulation accounting for several aspects that have not yet been considered, listed as follows:

- The addition of the Benscoter's consideration of the distortion in the degrees of freedom of the finite element, which is an important aspect in the analysis of box girder bridge sections;
- The variation of the cross-section height along the beam axis, important specially for the analysis of open bridge sections because of the high values of the hogging moments on the bearing sections;
- The consideration of curved bridges in plane, with arbitrary types of cross-sections;
- The compatibility with the Eurocodes relative to the rail traffic model that should be considered as traffic loads. This aspect involves the consideration of load models more complex than the simple load considered by the analysis, i.e. the load models for real trains(HSLM¹⁰ model);
- Consideration of track-structure interactions that must be taken into account according to the EN 1991-2.

¹⁰ High Speed Load Model.

- The consideration of support conditions defined at the real point of their applications, i.e. the bearings of a real multi-span bridges at the pier sections.

7. References

- 1) Attard, N. a. (1987). A direct method of evaluating the warping properties of thin-walled open and closed profiles. *Thin-Walled Structures*, 351-364.
- 2) Benscoter, S. (1954). A theory of torsion bending for multicell beams. *Journal of Applied Mechanics*, 25-34.
- 3) Cedolin, L. (1996). *Torsione e taglio di travi a parete sottile*. Milano: Edizioni Cusl.
- 4) Chopra, A. (1995). *Dynamics of Structures- Theory and application to the Earthquake Engineering*. Berkeley: Prentice Hall,Inc.
- 5) Clough, R., & Penzien, J. (1982). *Dynamics of structures*. McGraw-Hill.
- 6) Cunha, R. (2007). Dinâmica de Pontes em Viga Caixão em Linhas Ferroviárias de Alta Velocidade (Master Thesis). FEUP. (p-40). *Dinâmica de Pontes em Viga Caixão em Linhas Ferroviárias de Alta Velocidade (Master Thesis)*. FEUP. (p-40). Porto.
- 7) Ferreira, A. (2010). *Problemas De Elementos Finitos em Matlab*. Lisbon: Fundação Calouste Gulbenkian.
- 8) Fish, J., & Belytschko, T. (2007). *A First Course In Finite Elements*. John Wiley & Sons Ltd.
- 9) Friberg, P. (1985). Beam element matrices derived from Vlasov's theory of open thin-walled elastic beams . *International Journal for Numerical Methods in Engineering* , 1206-1218.
- 10) Fryba, L. (1999). Simply supported beam subjected to a moving constant force. In L. Fryba, *Vibration of Solids and Structures under Moving Loads (third edition)* (pp. 13-56). Prague: Thomas Telford Ltd.
- 11) Gere, J. (1954). Torsional Vibrations of Beams of Thin-Walled Open Section. *Journal Of Applied Mechanics*, 381-387.
- 12) Hibbit, K. a. (2007). *ABAQUS users manual version 6.7*. U.S.A., U.S.A.
- 13) Kollbrunner, C., & Basler, K. (1969). Torsion in Structures: An Engineering Approach. In C. Kollbrunner, & K. Basler, *Kollbrunner,C.F.;Basler,K.* (pp. 158-200). Springer.
- 14) Manzoni, G. (2001). Analisi Generalizzata di Strutture composte da Aste in Parete Sottile. *Tesi di laurea in ingegneria edile*. Milano, Italia.
- 15) Michaltos, G., Sarantithou, E., & Sophianopoulos, D. (2003). Flexural-torsional vibration of simply supported open cross-section steel beams under moving loads. *Journal of Sound and Vibrations*, 480-494.
- 16) Murray, N. (1984). *Introduction to the theory of Thin-walled Structures*. Oxford: Oxford University Press.
- 17) Okeil, A., & S., E.-T. (2004). Warping stresses in curved box girder bridges:case study. . *Journal of Bridge Engineering* , 487-496.
- 18) Prokić, A. (2002). Stiffness method of thin-walled beams with closed cross-section. *Computers and Structures*, 40-51.
- 19) Prokić, A. (2003). On triply coupled vibrations of thin-walled beams with arbitrary cross-section. *Journal of Sound and Vibration*, 723-737.
- 20) Prokić, A., & Lukić, D. (2007). Dynamic analysis of thin-walled closed-section beams . *Journal of Sound and Vibration*, 963-980.
- 21) Saadé, K., Espion, B., & Warzée, G. (2003). Non-uniform torsional behavior and stability of thin-walled elastic beams with arbitrary cross sections. *Thin-Walled Structures*, 857-881.

- 22) Shakourzadeh, H., Guo, Y., & Batoz, J. (1993). A torsion bending element for thin-walled beams with open and closed cross-sections. *Computers and Structures*, 1045-1054.
- 23) Vlasov, V. (1961). *Thin-walled elastic bars (english transl.)*. Jerusalem.

ANNEX 1

In the Annex 1 the cross-section cartesian and sectorial coordinates for the layouts analyzed are represented referred to the elastic center of the section. The sectorial coordinates are calculated by using the classic approach. In alternative, the direct method described in section 3.1.3 can be used : in this case the evaluation of the warping parameter and of the warping distribution involves two steps:

- i) the application of the direct method in order to obtain the shear center location, the warping function distribution and the warping parameter;
- ii) the use of the formulae described in section 3.1.2 in order to transfer these parameters to the elastic center reference.

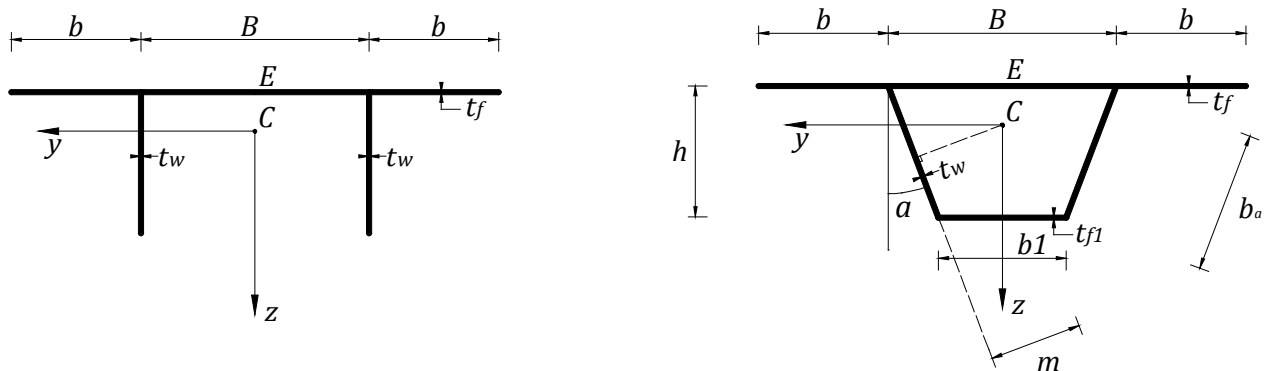


Figure A.0.1 – Cross-section layouts

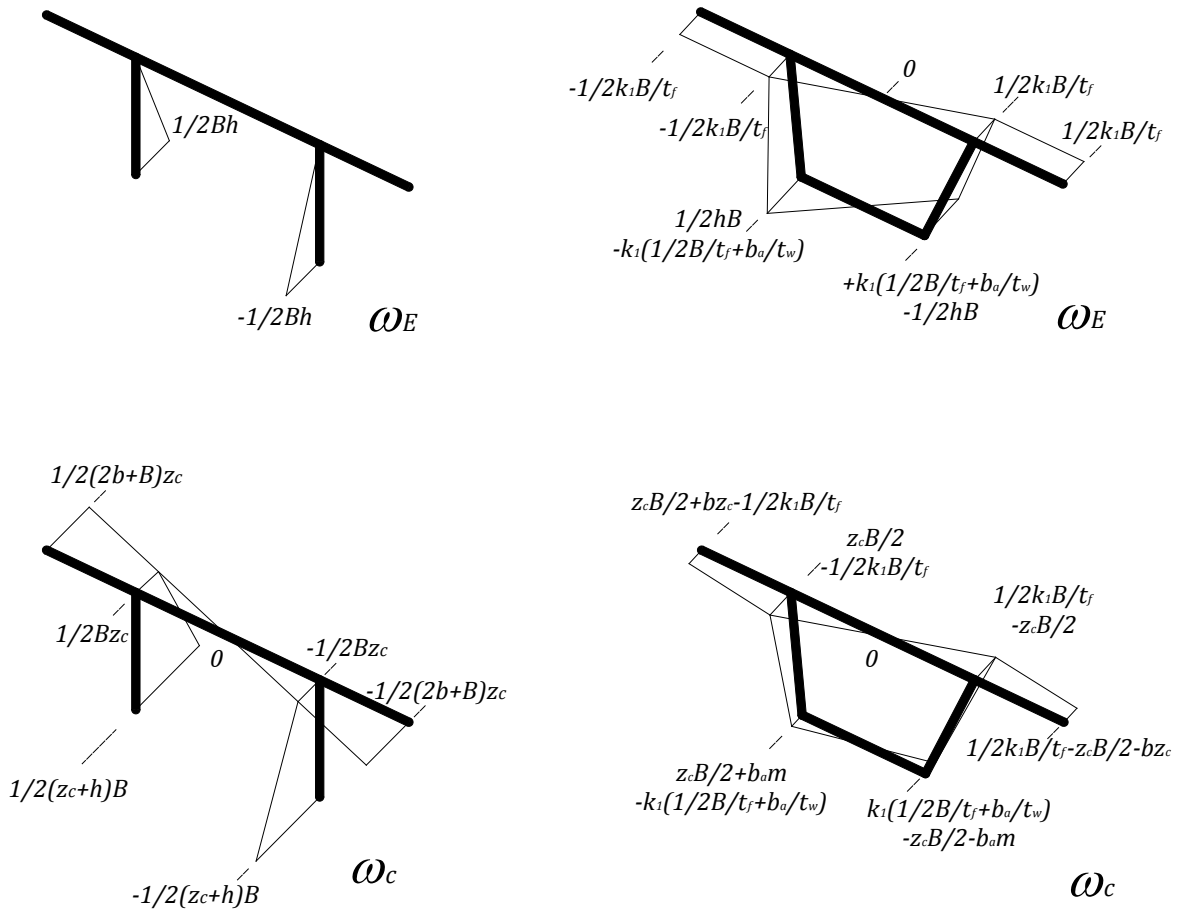


Figure A.0.2 – Sectorial coordinate for the open and closed cross-sections.

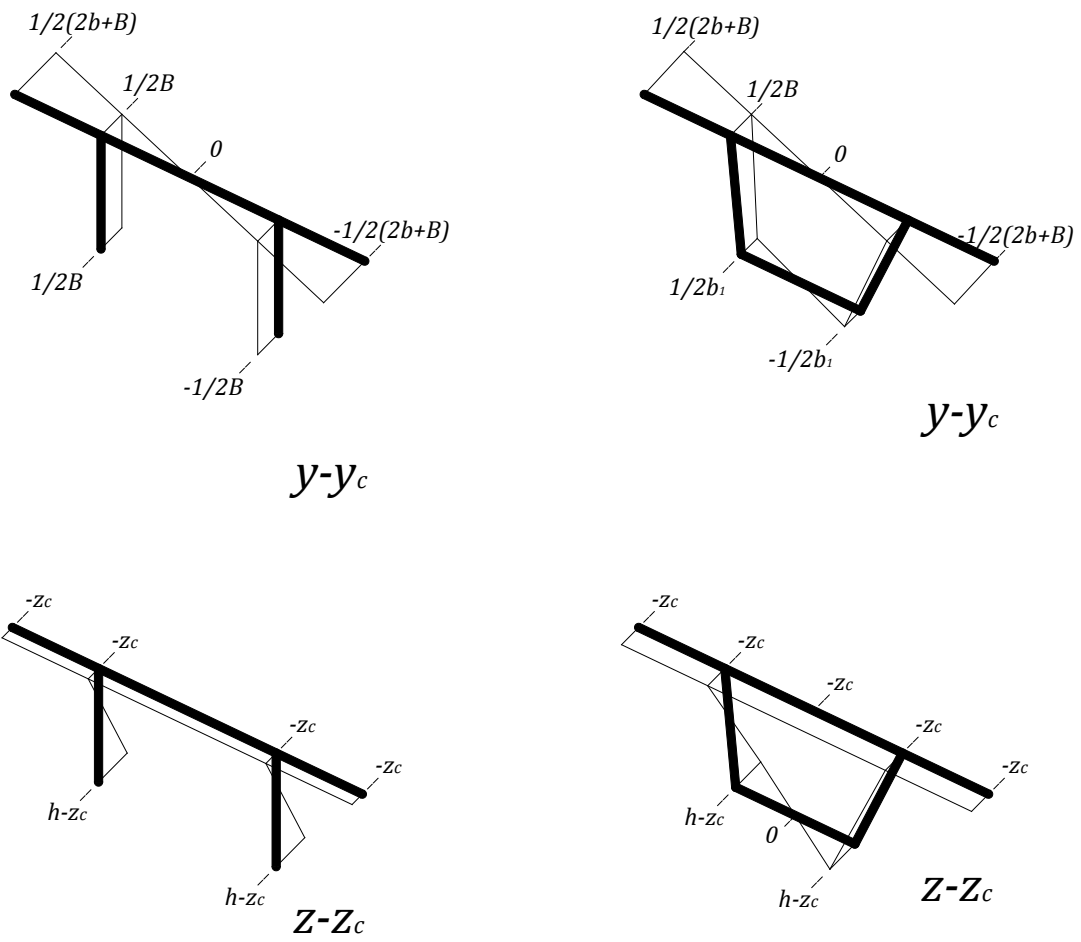


Figure A.0.3 – Cartesian coordinates referred to the elastic center.